IDENTIFYING GENETIC VARIANTS IMPLICATED IN PERRAULT SYNDROME FOR IMPROVED HEARING LOSS DIAGNOSIS AND THERAPEUTICS

A thesis submitted to The University of Manchester for the degree of
Doctor of Philosophy
in the Faculty of Biology, Medicine and Health

2017

Leigh A.M. Demain

School of Biological Sciences

Contents

Word Count -58,134

Figures

Tables

Abbreviations

aaRS - Aminoacyl-tRNA synthetase

ABR - Auditory brain stem response testing

ADP- Adenosine diphosphate

AOSCA - Infantile onset spinocerebellar ataxia

APS - Ammonium persulphate

ARSAL - Autosomal recessive spastic ataxia with leukoencephalopathy

ATP- Adenosine triphosphate

bp - Base pairs

BSA - Bovine serum albumin

C. elegans - Caenorhabditis elegans

CLPP - Caseinolytic mitochondrial matrix peptidase proteolytic subunit

DAP3 - Death associated protein 3

DBP – D-bifunctional protein

dbSNP – Single nucleotide polymorphism database

DMEM - Dulbecco's modified eagle medium

Drp1 - Dynamin related protein 1

EDTA - Ethylenediaminetetraacetic acid

ERAL1 - Era-Like 1

EVS – Exome variant server

ExAC - Exome aggregation consortium

FBS - Foetal bovine serum

FSH – Follicle stimulating hormone

FWF - Austrian Science Fund

HSMN – Hereditary sensory motor neuropathy

HUPRA - Hyperuricemia, pulmonary hypertension, renal failure in infancy and alkalosis syndrome

IHC - Inner hair cell

IU - International units

kb - Kilobases

LB - Luria-Bertani

LBSL - Leukoencephalopathy with brain stem and spinal cord involvement and lactate elevation

LH – Luteinising hormone

LTBL - Leukoencephalopathy with thalamus and brainstem involvement and high lactate

MEM -minimal essential medium

MIM – Mendelian inheritance in man

Mitonuclear communication - Mitochondrial and nuclear communication

Mitoribosome - Mitochondrial ribosome

MLASA - Myopathy, lactic acidosis, and sideroblastic anaemia syndrome

MRC - Medical Research Council

MRI - Magnetic resonance imaging

MRPS29 – Mitochondrial ribosomal protein S29

Mt – Mitochondrial

MtDNA - Mitochondrial DNA

MTDPS7 - Mitochondrial DNA depletion syndrome 7

mtLeuRS - Mitochondrial leucyl aminocyl tRNA synthetase

mtRNase P - Mitochondrial RNase P

NGS – Next generation sequencing

NHS - National Health Service

NIDCD - National Institute on Deafness and Other Communication Disorders

NIH - National Institutes of Health

NOP14 - Nucleolar protein 14

OD - Optical density

OHC - Outer hair cell

OXPHOS - Oxidative phosphorylation

P9 – Position nine

PBS - Phosphate buffered saline

PCA - Phenol:chloroform:isoamyl

PEOA3 - Progressive external ophthalmoplegia, autosomal dominant, 3

PKA - Cyclic AMP-dependant kinase

PMSF - Phenylmethanesulfonyl fluoride

POI – Primary ovarian insufficiency

Pre-tRNA - Precursor-tRNA

PRORP - Proteinaceous RNase P

PX - Postnatal day X (where X is the number of days after birth)

qPCR – Quantitative PCR

SD - Synthetic defined

SDS- Sodium dodecyl sulfate

SNAP25 - Synaptosome-associated protein 25

SNHL – Sensorineural hearing loss

SNP – Single nucleotide polymorphism

TAE - Tris base, acetic acid, EDTA

TBE -Tris, Borate, EDTA

TE - Tris , EDTA

TEMED - Tetramethylethylenediamine

TSH - Thyroid stimulating hormone

UHSM – University Hospital of South Manchester

VLCFA - Very long chain fatty acid

Wt – Wild type

YPD - Yeast extract peptone dextrose

Abstract

Identifying genetic variants implicated in Perrault syndrome for improved hearing loss diagnosis and therapeutics. Leigh A. M. Demain; The University of Manchester, Doctor of Philosophy, 2017.

Perrault syndrome is a rare autosomal recessive condition characterised by sensorineural hearing loss affecting both sexes and premature ovarian insufficiency in 46, XX females. Some affected individuals present with neurological features such as ataxia, neuropathies and intellectual disability. To date six genes which cause Perrault syndrome have been identified; *HSD17B4, HARS2, LARS2, CLPP*, *C10orf2* and *ERAL1*. In many cases the genetic cause of Perrault syndrome is unknown.

We used whole exome sequencing to identify the genetic basis of Perrault syndrome in nine affected families. In six families we identified variants in known Perrault syndrome genes and highlighted a genotype-phenotype link between the variant *LARS2* c.1565C>A p.(T522N) and low frequency sensorineural hearing loss. We also found marfanoid habitus in Perrault syndrome is not genotype specific. In three families we identified putative pathogenic variants in three novel Perrault syndrome genes; *PRORP*, *NOP14* and *DAP3*.

Investigation of novel Perrault genes revealed a defect of mitochondrial translation is the likely pathogenic mechanism in the case of Perrault syndrome caused by variants in *PRORP,* but data from a patient with Perrault syndrome caused by *DAP3* showed that this is unlikely to be the mechanism in all cases. PRORP is a subunit of mitochondrial RNase P, a mitochondrial tRNA processing complex. The variant in the affected family, PRORP p.A485V, reduced mitochondrial tRNA processing by 40% resulting in accumulation of unprocessed RNA transcripts and a defect of mitochondrial translation in patient fibroblasts. DAP3 is an essential subunit of the mitochondrial ribosome. In the proband with the variant DAP3 p.C395Y, which is *in trans* to a large deletion, there was no defect of mitochondrial translation seen in fibroblasts. The variant DAP3 p.C395Y likely affects a non-ribosomal role of DAP3 indicating a different Perrault Syndrome pathology to that of Perrault syndrome caused by defects of PRORP. NOP14 localises to the nucleolus and functions in ribosome biogenesis but our data suggests NOP14 may have a mitochondrial function. Haploinsufficiency of NOP14 in yeast causes the slow loss of mitochondria and we saw a distinct non-nucleolar localisation of Nop14 in the mouse organ of Corti.

Perrault syndrome shows large genetic and phenotypic heterogeneity. We have identified three novel Perrault syndrome genes and shed some light on the molecular pathology of Perrault syndrome.

Declaration

No work referred to in this thesis, which has been attributed to the author, has been submitted in support of an application for another degree or qualification of this or any other university or other institute of learning. Work attributed to Liam M. Jones and Robyn Bell has been submitted to the University of Manchester in support of applications towards a Master of Science and Bachelor of Science degree respectively. Work attributed to Stephanie Oerum has been submitted to the University of Oxford in support of a Doctorate of Philosophy. Additional work attributed to listed co-authors may have been submitted in support of an application for another degree or qualification of this or another university or other institute of learning.

Copyright Statement

i. The author of this thesis (including any appendices and/or schedules to this thesis) owns certain copyright or related rights in it (the “Copyright”) and he/she has given The University of Manchester certain rights to use such Copyright, including for administrative purposes.

ii. Copies of this thesis, either in full or in extracts and whether in hard or electronic copy, may be made only in accordance with the Copyright, Designs and Patents Act 1988 (as amended) and regulations issued under it or, where appropriate, in accordance with licensing agreements which the University has from time to time. This page must form part of any such copies made.

iii. The ownership of certain Copyright, patents, designs, trademarks and other intellectual property (the “Intellectual Property”) and any reproductions of copyright works in the thesis, for example graphs and tables (“Reproductions”), which may be described in this thesis, may not be owned by the author and may be owned by third parties. Such Intellectual Property and Reproductions cannot and must not be made available for use without the prior written permission of the owner(s) of the relevant Intellectual Property and/or Reproductions.

iv. Further information on the conditions under which disclosure, publication and commercialisation of this thesis, the Copyright and any Intellectual Property and/or Reproductions described in it may take place is available in the University IP Policy (seehttp://documents.manchester.ac.uk/DocuInfo.aspx?DocID=24420), in any relevant Thesis restriction declarations deposited in the University Library, The University Library’s regulations (seehttp://www.library.manchester.ac.uk/about/regulations/) and in The University’s policy on Presentation of Theses.

Acknowledgements

I would like to express my gratitude to my supervisory team; Prof. William Newman, Dr Raymond O'Keefe, Dr Thomas Friedman and Prof. Kevin Munro for all their guidance and support. I would like to thank Prof. William Newman for allowing me to join his lab and for all of his input into the experimental design and manuscripts. I would like to thank Dr Raymond O'Keefe for teaching me many of the laboratory techniques used to produce this thesis and for all his input into the experimental design. I would like to thank Dr Thomas Friedman for giving me the opportunity and funding to work in his lab at the NIH and for showing so much enthusiasm about this project. I am grateful to Prof. Kevin Munro for all his support and for providing an audiologist perspective on this work.

I must thank all of my collaborators for their hard work. Their expert input and data have allowed this work to progress in a way I could not have achieved alone. I would like to express special thanks to the members of the Zschocke lab, the Taylor lab and the Yue lab for providing both excellent data and discussion. I am very grateful to all of the clinicians for choosing to collaborate with us and providing such detailed medical evaluation of the patients.

Special thanks must go to members of the Newman, O'Keefe and Friedman Labs, all of whom were a pleasure to work with and unwaveringly generous with their time and expertise. I would like to thank Jill Urqhart and James O'Sullivan for their help with whole exome data, Inna Belyantseva and Melanie Barzik for all the time they spent teaching me how to perform immunohistochemistry and immunocytochemistry and Glenda Beaman, Helen Byers and Rahat Perveen for all their help organising experiments.

Finally I would like to thank the patients for their participation and Action on Hearing Loss for providing funding without either of which this research would not have been possible.

Rationale for Journal Format

The body of work comprising this thesis is presented in journal format with each experimental chapter prepared as an individual paper suitable for submission to a peer reviewed publication. Chapter 3 and chapter 4 have been published in Clinical Genetics (*Clin Genet,* 91(2)**,** 302-312) and Clinical Dysmorphology (*Clin Dysmorphol,* 26(4)**,** 200-204) respectively. Chapter 5 is available on the pre-print server biorxiv (http://www.biorxiv.org/content/early/2017/07/25/168252). Chapters 6 and 7 have been prepared as journal format papers but have not been submitted for publication.

This thesis represents an investigation into the genetic and molecular cause of Perrault syndrome in 12 families. We identified variants in known genes in six families and in three families we identified putative pathogenic variants in novel Perrault syndrome genes. In three additional families the genetic cause of Perrault syndrome could not be determined. The different experimental approaches to investigate the variants in known genes and in each individual novel gene meant that the chapters form naturally around the case studies and in this way provide a more linear story for each chapter than traditional format.

Chapter 3 and chapter 4 comprise studies of families with causative variants identified in known Perrault syndrome genes. In chapter 3 we identified five families with variants in *HDS17B4*, *LARS2*, *CLPP* and *C10orf2*. In chapter 4 we present a single family with a known Perrault syndrome variant in *LARS2* and a phenotype not previously seen in association with the variant. These chapters introduce the genotypic and phenotypic heterogeneity of Perrault syndrome and present data for the existence of novel Perrault syndrome genes. They also highlight some of the unresolved questions around Perrault syndrome.

Three novel Perrault syndrome genes were identified over the course of this project. The characterisation of these genes took different routes depending on the function of the gene.

In chapter 5 we identified a novel Perrault syndrome gene, *PRORP*, in a large consanguineous family. We used patient dermal fibroblasts and an *in vitro* assay to characterise a defect of mitochondrial translation in the affected individuals.

In chapter 6 we identified a homozygous variant in *NOP14* as the cause of Perrault syndrome in a single family. We used *Saccharomyces cerevisiae* as a model organism to study this variant. We found NOP14 is required for normal mitochondrial function in yeast. Future work will focus on identifying the function of NOP14 in mitochondria and assessing variant effect on this function.

In chapter 7 we found a rare variant in *DAP3 in trans* to a large deletion. Investigating the variant in *Saccharomyces cerevisiae* proved difficult as the loss of the DAP3 yeast orthologue causes rapid and irretrievable loss of mitochondria. Patient cells did not show a defect of mitochondrial translation and future work will focus on identifying the effect of the variant on alternate function of DAP3.

The chapters presented in this thesis are unified by the study of the genetic and molecular pathology of Perrault syndrome. Although the chapters have a unifying theme the different experimental approach necessary in each chapter and meant that journal format was the most appropriate format for this thesis.

Author Contributions

A number of collaborators contributed to the data presented in this thesis. My contributions and those of collaborators are detailed below for each experimental chapter.

Chapter 3: Expanding the genotypic spectrum of Perrault syndrome.

Clin Genet, 91(2), 302-312.

Leigh A. M. Demain, Jill E. Urquhart, James O'Sullivan, Simon G. Williams, Sanjeev S. Bhaskar, Emma M. Jenkinson, Charles M. Lourenco, Arvid Heiberg, Simon H. Pearce, Stavit A. Shalev, Wyatt W. Yue, Sabrina Mackinnon, Kevin J. Munro, Ruth Newbury-Ecob, Kristen Becker, Min Jeong Kim, Raymond T. O' Keefe, William G. Newman.

I identified the variants in *LARS2* and *HSD17B4* and performed the confirmation and genetic characterisation of all variants. I prepared the manuscript under the guidance of W.G.N.

J.E.U identified the variants in C10orf2 and CLPP and performed autozygosity mapping. Whole exome sequencing was performed by J.E.U and J.O. with bioinformatic analysis by S.G.W and S.S.B. Clinical characterisation of patients was performed by C.M.L., A.H., S.H.P., S.A.S., R.N-E, K.B. and M.J.K. Protein modelling was performed by W.W.Y. and S.M. All authors reviewed and commented upon the manuscript.

Chapter 4: Marfanoid habitus is a nonspecific feature of Perrault syndrome.

Clin Dysmorphol, 26(4)**,** 200-204.

Zerkaoui, M., Demain, L. A. M., Cherkaoui Jaouad, I., Ratbi, I., Amjoud, K., Urquhart, J. E., O'Sullivan, J., Newman, W. G. & Sefiani, A.

I identified the variant in *LARS2* and performed the confirmation of the variant. I provided the review of cases of Perrault syndrome caused by *LARS2* in table 1 and prepared figure 1. I prepared the manuscript equally with M.Z. under the guidance of W.G.N and A.S.

Whole exome sequencing was performed by J.E.U and J.O. Clinical characterisation of patients was performed by M.Z., I.C.J., I.R., K.A. and A.S. All authors reviewed and commented upon the manuscript.

Chapter 5: A homozygous variant in mitochondrial RNase P subunit PRORP is associated with Perrault syndrome characterized by hearing loss and primary ovarian insufficiency

bioRxiv.

Irit Hochberg, Leigh A. M. Demain, Jill E. Urquhart, Albert Amberger, Andrea J. Deutschmann, Sandra Demetz, Kyle Thompson, James O'Sullivan, Inna A. Belyantseva, Melanie Barzik, Simon G. Williams, Sanjeev S. Bhaskar, Emma M. Jenkinson, Nada AlSheqaih, Zeev Blumenfeld, Sergey Yalonetsky, Stephanie Oerum, Walter Rossmanith, Wyatt W. Yue, Johannes Zschocke, Robert W. Taylor, Thomas B. Friedman, Kevin J. Munro, Raymond T. O'Keefe, William G. Newman.

I confirmed and genetically characterised the variant in *PRORP*. I prepared the material for, performed and analysed the results of tRNA processing assays under the guidance of R.T.O. I performed the localisation of PRORP in the mouse organ of Corti under the guidance of I.A.B. I prepared the manuscript under the guidance of W.G.N and R.T.O.

Clinical characterisation of patients was performed by I.H., Z.B. and S.Y. J.E.U. identified the variant and performed Autozygosity mapping. Whole exome sequencing was performed by J.E.U. and J.O. with bioinformatic analysis of whole exome data by S.G.W. and S.S.B. N.A. performed screening in ethnic controls. A.A., A.J.D., S.D. and J.Z. performed analysis of mitochondrial RNase P levels in patient fibroblasts, northern blots of mitochondrial RNA and rescue experiments. K.T. and R.W.T. performed analysis of the OXPHOS complexes in patient fibroblasts. Protein modelling and analysis of protein stability was performed by S.O and W.W.Y. All authors reviewed and commented upon the manuscript.

Chapter 6: Biallelic Variants in Nucleolar protein NOP14 are associated with Perrault syndrome and highlight NOP14 is important for mitochondrial homeostasis

Leigh A. M. Demain, Jill E. Urquhart, James O'Sullivan, Liam M. Jones, Walid Omara, Inna A. Belyantseva, Melanie Barzik, Simon G. Williams, Sanjeev S. Bhaskar, Emma M. Jenkinson, Thomas B. Friedman, Kevin J. Munro, Raymond T. O'Keefe, William G. Newman.

I confirmed and genetically characterised the variant, and performed conservation mapping. I prepared the plasmid pRS-STE5-Nop14 and transformed it into the YPH501_NOP14Δ yeast strain under the guidance of R.T.O. I prepared the plasmid Nop14-EGFP and performed the immunocytochemistry in HeLa cells under the guidance of M.B. I performed the localisation of Nop14 in the mouse organ of Corti and gene gun transfections under the guidance of I.A.B. I prepared the manuscript under the guidance of W.G.N and R.T.O.

J.E.U. identified the variant and performed Autozygosity mapping. Whole exome sequencing was performed by J.E.U. and J.O with bioinformatic analysis of whole exome data by S.G.W. and S.S.B. Characterisation of the strain BY4743 and production and characterisation of the strain YPH501_NOP14Δ were performed by W.O. and L.M.J.

Chapter 7: Variants in mitochondrial ribosomal protein DAP3 are causative of Perrault syndrome without a defect of mitochondrial translation

Leigh A. M. Demain, Jill E. Urquhart, James O'Sullivan, Jamie M. Ellingford, Christian Beetz, Liam M. Jones, Robyn Bell, Inna A. Belyantseva, Melanie Barzik, Monika Olahova, Ruth Glasgow, Simon G. Williams, Sanjeev S. Bhaskar, Emma M. Jenkinson, Robert W. Taylor, Thomas B. Friedman, Kevin J. Munro, Raymond T. O'Keefe, William G. Newman.

I confirmed and genetically characterised the missense variant. I performed conservation mapping and predicted variant consequence. I prepared the plasmid Dap3-EGFP and performed the immunocytochemistry in HeLa cells under the guidance of M.B. I performed the localisation of Dap3 in the mouse organ of Corti and gene gun transfections under the guidance of I.A.B. I prepared the manuscript under the guidance of W.G.N and R.T.O.

The missense variant in DAP3 was identified by E.J. Whole exome sequencing was performed by J.E.U and J.O'S with bioinformatic analysis of whole exome data by S.G.W

and S.S.B. The whole exome read depth analysis was performed by J.M.E and confirmation of the deletion by C.B. DAP3 yeast experiments were performed by W.O., L.M.J, R.B, and R.T.O. Analysis of patient fibroblasts was performed by M.O., R.G. and R.W.T.

Chapter 1: Introduction

1.1 Perrault syndrome overview

In 1951 Perrault described a case of two sisters with Turner syndrome and hearing loss (Perrault et al. 1951). In further studies it was noted that these sisters had a 46,XX karyotype, which is not consistent with Turner syndrome (Josso 1963). Upon review of four families affected by hearing loss in both sexes and ovarian dysgenesis in 46,XX karyotype females Pallister and Opitz (1979) termed this condition Perrault Syndrome (MIM 233400) (Online Mendelian Inheritance in Man OMIM®).

Perrault syndrome is a rare autosomal recessive genetic disorder (Pallister and Opitz 1979). In Europe a rare disease or disorder is defined as one that affects less than 1 in 2000 people. A disorder can be classed as rare and have approximately 246,000 affected individuals in Europe (European Commission DG Health & Consumers 2014). Perrault Syndrome has fewer than 100 affected families reported in literature worldwide (Geethalakshmi et al. 2015), therefore is a very rare condition.

Perrault syndrome is characterised by sensorineural hearing loss (SNHL) in both sexes and ovarian dysfunction in 46,XX karyotype females (Pallister and Opitz 1979). Neurological features such as ataxia, neuropathies and intellectual disability have also been reported in some affected individuals (Gottschalk et al. 1996;Fiumara et al. 2004). The syndrome is both clinically and genetically heterogeneous. Symptoms vary in severity even within affected families (Newman et al. 2014). To date there have been six genes identified as causative genes for Perrault syndrome *HSD17B4* (MIM 233400) (Pierce et al. 2010), *HARS2* (MIM 614926) (Pierce et al. 2011), *LARS2* (MIM 615300) (Pierce et al. 2013), *CLPP* (MIM 614129) (Jenkinson et al. 2013), *C10orf2* (MIM 616138) (Morino et al. 2014) and *ERAL1* (MIM 607435) (Chatzispyrou et al. 2017). The latter five genes function in mitochondrial translation suggesting that at least some cases of Perrault syndrome are caused by a defect of mitochondrial translation. In many Perrault syndrome families the genetic causes of the syndrome are unknown. Some of these families have been screened for variants in known Perrault genes, but no causative variants were found (Jenkinson et al. 2012;Kim et al. 2013;Demain et al. 2017b). These families may contain variants in novel Perrault syndrome genes.

1.2 The clinical aspects of Perrault syndrome

Two presentations are required for a clinical diagnosis of Perrault Syndrome: sensorineural hearing loss, which is not sex biased; and primary ovarian insufficiency in a 46,XX karyotype female (Pallister and Opitz 1979). In addition some patients have reported additional clinical features, most commonly neurological (Fiumara et al. 2004;Gottschalk et al. 1996). These neurological features may include ataxia, intellectual disability, nystagmus and hereditary sensory motor neuropathy (Gottschalk et al. 1996;Morino et al. 2014). A diagnosis of Perrault syndrome can be difficult to achieve, especially in males and pre-pubertal females, without the presence of another affected family member. Males and pre-pubertal females will present with non-syndromic hearing loss and in many cases the diagnosis of Perrault syndrome relies on the presentation of primary ovarian insufficiency (Newman et al. 2014). Recently there have been cases of Perrault syndrome diagnosed from genetic data rather than clinical features (Ahmed et al. 2015;Demain et al. 2017b). This type of diagnosis is likely to become more common as next generation sequencing is routinely applied as a diagnostic tool.

1.2.1 Sensorineural hearing loss

Hearing loss is the most common sensory deficit in humans with 1 in every 1000 children in the U.K. born with a disabling permanent childhood hearing loss. By adolescence the prevalence of permanent hearing impairment is 2 in 1000. (Fortnum et al. 2001). Sensorineural hearing loss (SNHL) is associated with dysfunction of the inner ear in comparison to conductive hearing loss, which is caused by dysfunction of the outer and/or middle ear (Kochhar et al. 2007). Causes of SHNL include genetic and environmental causes or a combination of both factors. It is estimated that in developed countries genetic factors cause as much as 50% of SNHL. The genetic causes of SNHL are highly heterogeneous and present as both syndromic cases, which include associated additional clinical features; and non-syndromic cases, in which hearing loss is the only presentation (Kochhar et al. 2007). The genetic causes of hearing loss include all modes of inheritance and in some cases syndromic and non-syndromic hearing loss may result from different variants in the same gene (Smith et al. 2017).

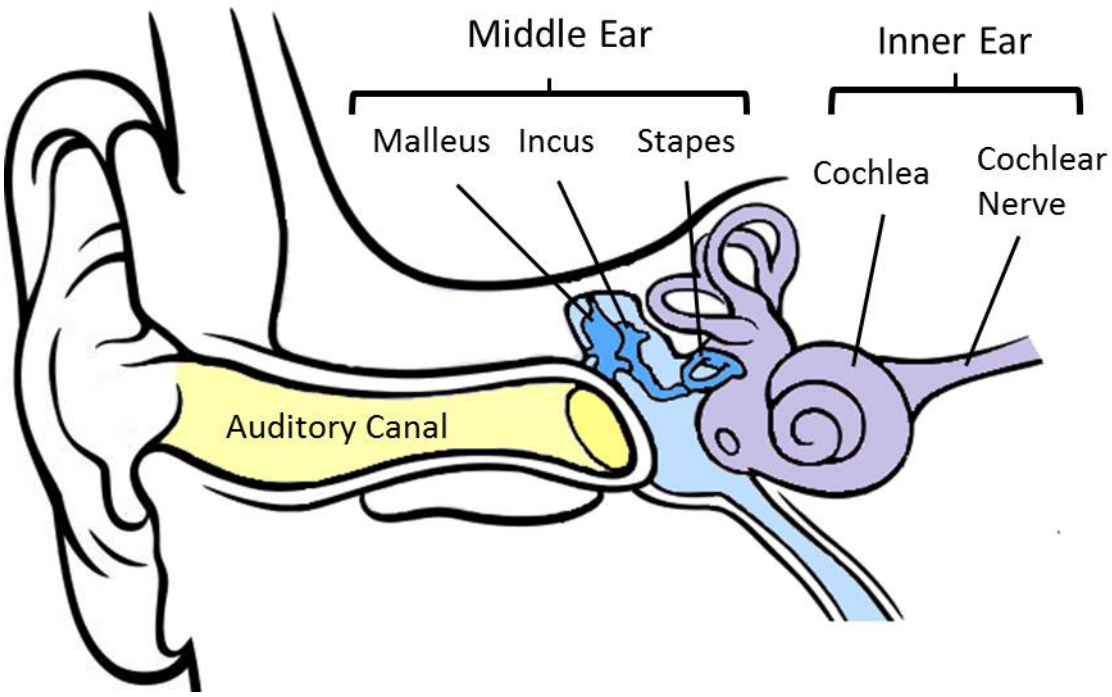

Figure 1.1. Anatomy of the ear.

Sensorineural loss is due to impairment or damage of the structures of the inner ear, specifically the cochlea or the cochlear nerve (Kochhar et al. 2007). Image adapted from Chittka and Brockmann (2005).

The receptor organ for hearing, the organ of Corti, is located in the cochlea (Pujol et al. 2016b) (Fig 1.2). The organ of Corti contains two types of mechanosensory hair cells responsible for detecting sound, inner hair cells which are the primary sound detector cells and outer hair cells which modulate the signal improving frequency detection (Pujol et al. 2016a). The hair cells are arranged as three rows of outer hair cells and a single row of inner hair cells positioned on the basilar membrane (Pujol et al. 2016b) (Fig. 1.2). Sound is transmitted to the inner ear via the vibration of the tympanic membrane (eardrum) and ossicles (malleus, incus and stapes) of the middle ear. The stapes vibrates against the oval window of the cochlea and causes movement of the perilymph fluid within. The movement of the fluid within the scala tympani causes movement in the basilar membrane and subsequent movement of stereocilia on the apical surface of the hair cells (Pujol et al. 2016b). The movement of the stereocilia opens ion channels which allows potassium from the potassium rich endolymph to enter the hair cells, causing them to become depolarised and release neurotransmitter to the auditory nerves (Pujol

et al. 2016a). Defects in different functional aspects of the organ of Corti, including mechanoelectric transduction and ion homeostasis, can lead to SNHL (Eisen and Ryugo 2007).

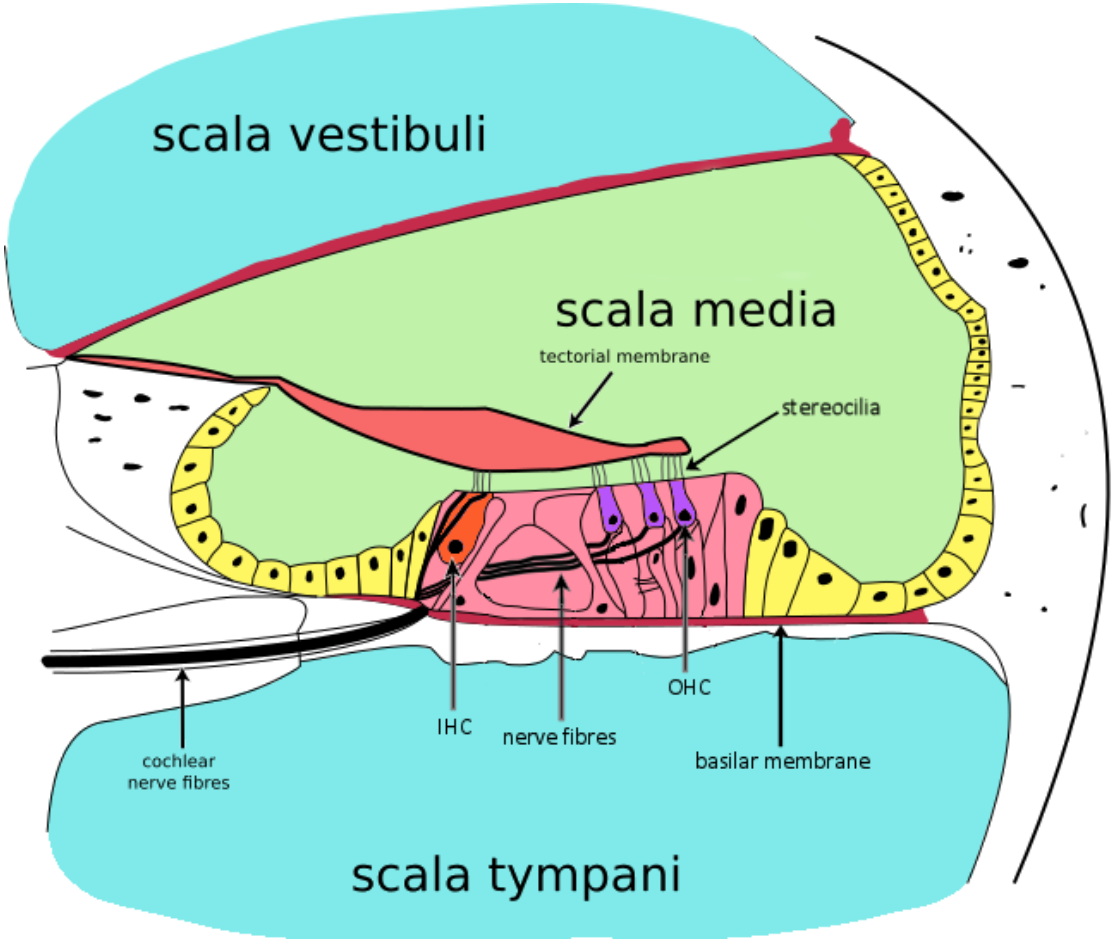

Figure 1.2. The organ of Corti.

A cross section of the cochlea showing the organ of Corti. OHC, outer hair cell. IHC, inner hair cell. Adapted from Cochlea-crosssection.png: The original uploader was Oarih at English Wikipedia derivative work: Fred the Oyster [CC-BY-SA-3.0 (http://creativecommons.org/licenses/by-sa/3.0/) or GFDL (http://www.gnu.org/copyleft/fdl.html)], via Wikimedia Commons.

To detect hearing loss in older children and adults pure tone audiometry testing is performed (Smith et al. 2017). Pure tone audiometry involves an audiometer producing sounds at different frequencies and volumes with the individual being tested confirming,

usually by pressing a button, when they hear a sound. Two types of pure tone audiometry are employed, air conduction audiometry and bone conduction audiometry. In air conduction audiometry the audiometer delivers sound via air, the way the subject would normally detect sound. The level of hearing (or threshold) as determined by air conduction audiometry is known as the air threshold. In bone conduction testing the sound is transmitted by a probe placed on the mastoid bone, effectively bypassing the middle ear. The minimum level of hearing recorded from bone conduction testing is known as the bone threshold (Smith et al. 2017). The thresholds for each tested frequency are recorded on a specialised graph known as an audiogram (Fig. 1.3) (Hearing Link. 2017). On audiograms hearing loss is split into 4 categories mild (21-40dB), moderate (41-70dB), severe (71- 95 dB) and profound (greater than 96 dB) (Fig. 1.3) (Action on Hearing Loss 2017). When used in conjunction pure tone audiometry and bone conduction tests can help distinguish between middle ear (conductive) hearing loss and the inner ear hearing loss (SNHL). A similar hearing threshold on both bone and air tests is indicative of SNHL while a significantly lower threshold on bone conduction tests is indicative of conductive hearing loss (Hearing Link. 2017). Additional physiological tests may be performed to determine the etiology of hearing loss in the affected individual (Smith et al. 2017). Auditory brain stem response (ABR) testing assesses the function of the cochlea and auditory nerves by using surface electrodes to record electrophysiological response from the auditory brainstem and nerves in response to click stimuli. ABR testing is used as the primary tool to detect hearing loss in infants, in which pure tone audiometry is not suitable (Smith et al. 2017). Immittance testing (also known as tympanometry) assesses function of the middle ear by applying pressure to the tympanic membrane. Immittance testing assesses middle ear pressure, tympanic membrane flexibility and ossicle mobility. (Smith et al. 2017).

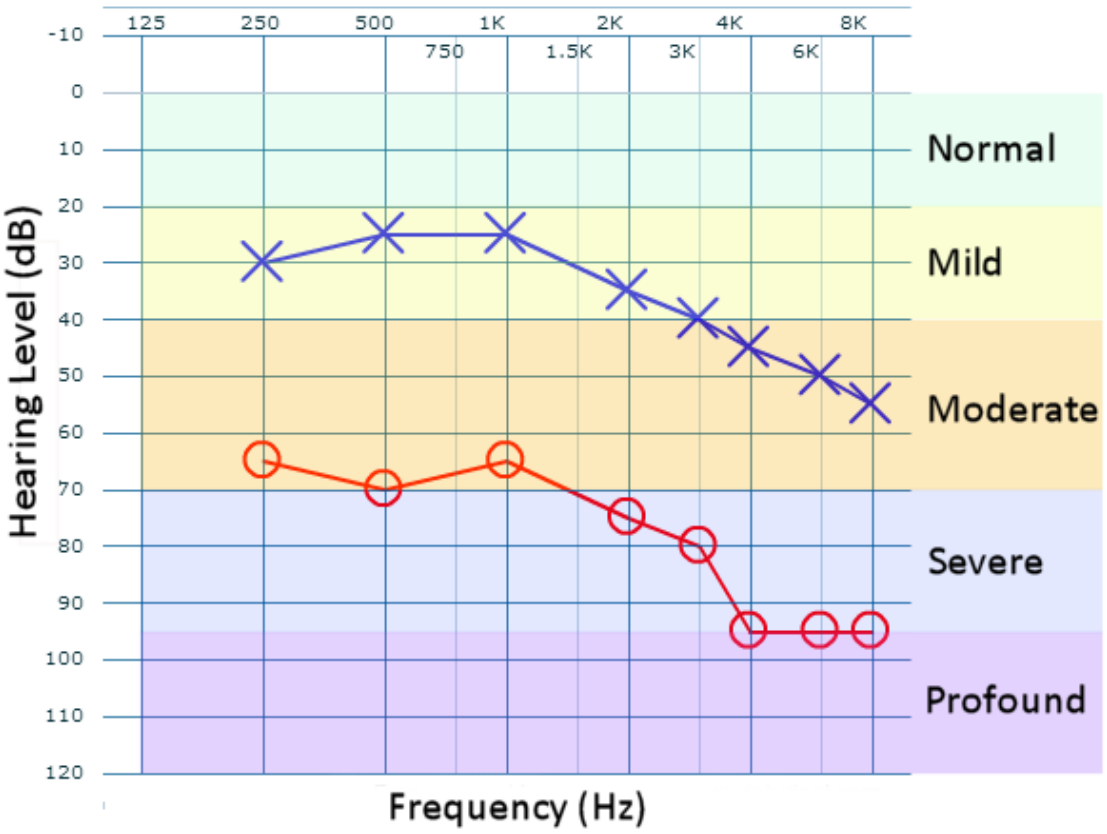

Figure 1.3. Example audiogram.

Example of an audiogram of a patient with a mild to moderate loss in the left ear and moderate to profound loss in the right ear with both ears having a more severe loss at high frequencies (Action on Hearing Loss 2017). The left ear is represented by crosses and the right by circles. Only the air threshold is shown. Audiogram created using Audgen software (http://audsim.com/audgen/AudGen.html).

SNHL is typically the earliest detected clinical feature of Perrault syndrome and is heterogeneous in both onset age and severity. Severity ranges from mild to profound with onset from congenital (pre-lingual) to post-lingual (Newman et al. 2014). The average age of hearing loss diagnosis in people affected by Perrault syndrome is eight years of age (Marlin et al. 2008). The oldest reported age of the onset of hearing loss was 31 years of age (Pallister and Opitz 1979). The hearing loss is normally bilateral, present in both affected males and females (Newman et al. 2014), and can be progressive (Pallister and Opitz 1979). The audiometric nature of the hearing loss shows the same clinical

heterogeneity as the other aspects of the syndrome. Pallister and Opitz (1979) noted that affected members of a large family had hearing loss which was severe at higher frequencies with some milder hearing loss at the mid-level frequencies. In contrast Laercio et al. (1992) described two sisters with flat type curve audiograms where hearing loss was similar across all frequencies. Some affected individuals have been noted as having a distinctive upwards sloping audiogram with hearing impairment more severe at lower frequencies (Pierce et al. 2013). This low frequency hearing loss appears to be associated with a variant in a single Perrault syndrome gene, *LARS2* (Pierce et al. 2013;Demain et al. 2017b). These upwards sloping audiograms may prove useful as an early indicator of possible Perrault syndrome in the absence of other clinical aspects of the condition (Newman et al. 2014) and may help to narrow the scope of genetic investigations.

The pathology of hearing loss in Perrault syndrome is currently unknown but recently two studies have shed some light on a possible pathology. Nishio et al. (2017) conducted a study of gene expression of hearing loss associated genes in the mouse organ of Corti. Four genes associated with Perrault syndrome (*HSD17B4*, *HARS2*, *LARS2* and *CLPP*) were found to be expressed at much higher levels in the neurons of the spiral ganglion than in other parts of the organ of Corti. The spiral ganglion connects auditory input from the hair cells to the central auditory system in the brain (Nishio et al. 2017). In a pair of sisters with Perrault syndrome, due to variants in *C10orf2*, there was atrophy of the auditory nerve and the authors theorised that the defect in this case was localised to the synapses of the hair cells and auditory nerve (Oldak et al. 2017). The area of defect localisation suggests that hearing loss in some cases of Perrault syndrome may be due to a defect of the auditory neurons rather than the sensory organ. Often in depth analysis of the hearing loss phenotype required to differentiate between an auditory neuropathy and sensory hearing loss is not performed and in most cases of Perrault syndrome the pathology of the hearing loss remains unresolved.

1.2.2 Ovarian dysfunction

The second defining clinical aspect of Perrault syndrome is primary ovarian insufficiency (POI). POI is classed as cessation of the correct function of the ovaries before 40 years of

age and may also be referred to as premature ovarian failure (Rebar 2009). In practice there is a wide range of ovarian dysfunction associated with Perrault syndrome, from severe ovarian dysgenesis with absent or streak gonads to milder POI. Women affected by Perrault syndrome present with either primary or secondary amenorrhea, as a consequence of POI, and may lack secondary sexual characteristics (Newman et al. 2014).

In women affected by Perrault syndrome POI is accompanied by hypergonadotropic hypogonadism (Newman et al. 2014). Hypergonadotropic hypogonadism is characterised by high levels of gonadotropin hormones, follicle stimulating hormone (FSH) and luteinising hormone (LH), and low levels of oestrogen. The ovaries are small, streak or absent in patients with hypergonadotropic hypogonadism (Aittomäki et al. 1995). High levels of gonadotropins are produced because of the absence of an ovarian negative feedback loop. The ovaries are absent or non-responsive to gonadotropins and fail to produce appropriate levels of oestrogen. Oestrogen supresses the production of gonadotropins, so without oestrogen the levels of FSH and LH remain high (Fig. 1.4). Hypergonadotropic hypogonadism indicates a defect of the ovaries rather than the thyroid gland, which may also cause hypogonadism (Aittomäki et al. 1995). Gonadotropins and oestrogen are measured by immunoassays and quantified using international units (IU), a measure against a standard reference (Rebar 2009). Rebar (2009) suggests test results where levels of FSH are above 30mIU/ml and levels of oestrogen are below 50pg/ml in a woman with amenorrhea can be indicative of POI. In contrast Aiman and Smentek (1985) recommend levels of FSH and LH be above 50mIU/ml for a diagnosis of POI.

The phenotypic range of ovarian dysfunction is such that while many individuals affected by Perrault syndrome present with primary amenorrhea or secondary amenorrhea in their teens or early twenties there has been a recorded case of an affected individual having sufficient ovarian function to have two children before the onset of secondary amenorrhea (Jenkinson et al. 2013).

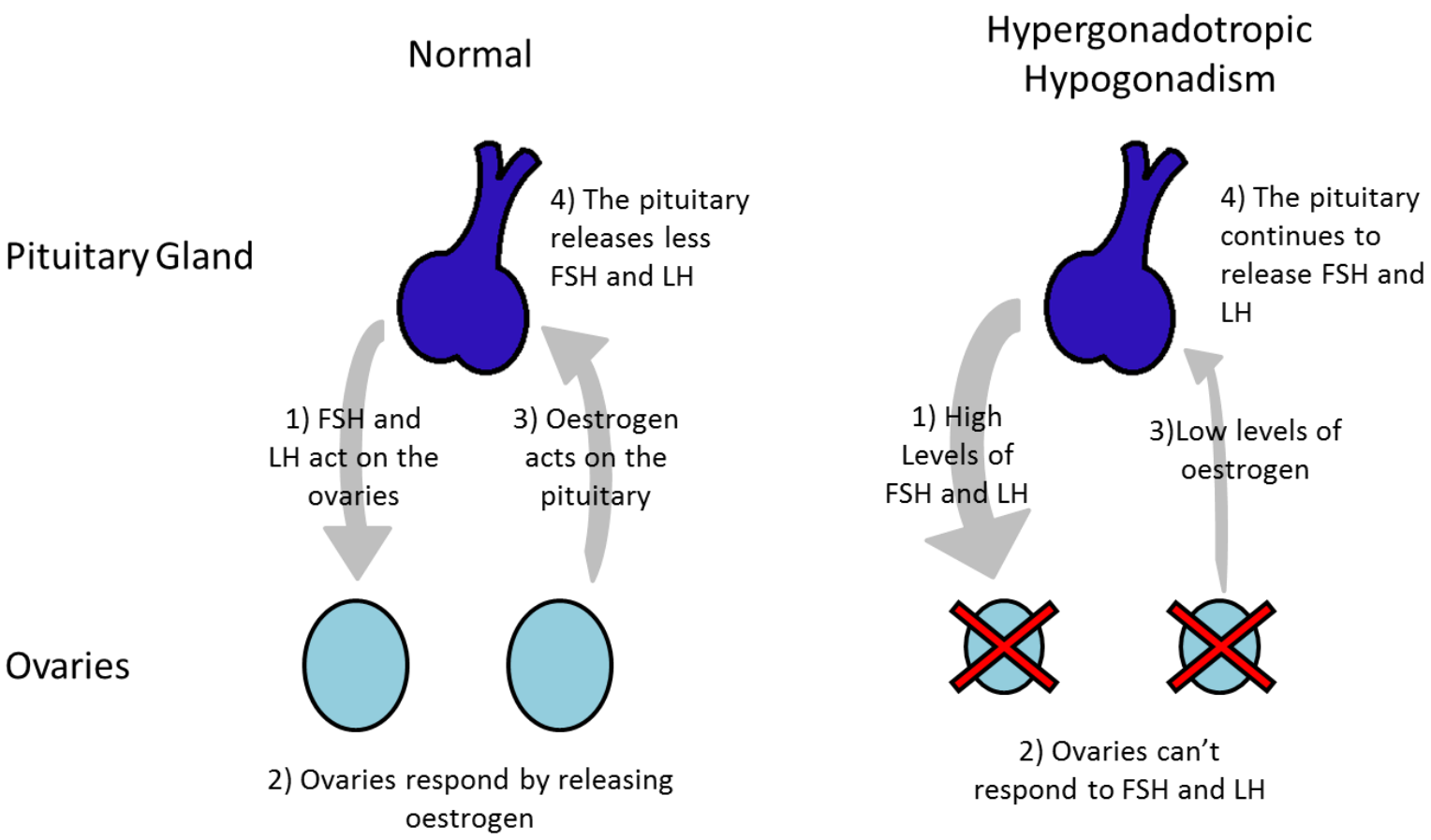

Figure 1.4. The ovarian negative feedback loop in hypergonadotropic hypogonadism.

The ovaries are small, streak or absent in patients with hypergonadotropic hypogonadism (Aittomäki et al. 1995). FSH – Follicle stimulating hormone, LH – Luteinising hormone.

It is the absence of puberty or the presentation of secondary amenorrhea that often leads to the diagnosis of Perrault syndrome. POI should be accompanied by a 46,XX karyotype for a diagnosis of Perrault syndrome. Karyotyping is essential to eliminate the differential diagnosis of Ulrich Turner syndrome (Newman et al. 2014). Women with Turner syndrome present with ovarian dysfunction (Gravholt 2004) and 60% of affected women also have some degree of hearing loss (Morimoto et al. 2006). The karyotype in women with Turner syndrome is 45,X or 45,X/46,XX mosaicism (Morimoto et al. 2006).

The pathology of primary ovarian insufficiency in Perrault syndrome is unknown. During ovarian development the number of oocytes peak at approximately 7 million at week 20 of the developing embryo. After this peak oocytes are continuously depleted via atresia to approximately 300,000 at menarche (Ramalho-Santos and Amaral 2013). It has been suggested that this depletion may select against oocytes with poor functioning mitochondria. As individuals with Perrault syndrome may have mitochondrial dysfunction over depletion of the ovarian follicles selecting against poor functioning mitochondria could be responsible for the POI in Perrault syndrome patients (Pierce et al. 2011). The fact that one patient with Perrault syndrome had children (Jenkinson et al. 2013), plus cases of secondary amenorrhea, suggest that the ovaries can develop some function before the onset of POI. The suggested mechanism of ovarian dysfunction where the ovarian follicles are subject to excessive apoptosis selecting against mitochondrial dysfunction (Pierce et al. 2011) would explain the apparent difference in gonadal dysfunction between male and female patients in Perrault syndrome.

1.2.3. Additional features of Perrault syndrome

Additional clinical features have been reported in some cases of Perrault syndrome. These features are most commonly neurological and may include: ataxia, hereditary sensory motor neuropathy, epilepsy, nystagmus, and intellectual disability (Fiumara et al. 2004;Morino et al. 2014;Gottschalk et al. 1996).

Neurological features are not present in every case of Perrault syndrome which resulted in the proposal that Perrault syndrome be split into 2 classifications, Type I and Type II. Type I would represent the classical Perrault syndrome with no additional neurological features. Type II would encompass patients with the additional features (Fiumara et al.

2004). There is a large clinical heterogeneity in the Perrault syndrome case studies reported in the literature, both between and within families. However in three families with Perrault syndrome due to variants in *CLPP* the presentation of neurological features segregated with the specific variant (Jenkinson et al. 2013). Where no neurological features were reported some affected individuals were young at the time of the report and it is possible neurological features may become apparent with age.

Morphological features have been reported in association with Perrault syndrome. Marfanoid habitus has been noted in some cases of Perrault syndrome.(Ameen and Pinninti 2012;Kim et al. 2013). Arachnodactyly (Lerat et al. 2016) and high arched palate have also been reported as clinical features (Nishi et al. 1988). Arachnodactyly and high arched palate may represent a milder clinical presentation of the marfanoid habitus phenotype (Zerkaoui et al. 2017). Short stature has also been reported (Jenkinson et al. 2013;Pierce et al. 2010).

To date, there is no clear genotype- phenotype correlation of neurological or morphological features (Newman et al. 2014).

1.3 The molecular aspects of Perrault syndrome

Biallelic variants in six genes have been associated with Perrault syndrome: *HSD17B4* (Pierce et al. 2010)*, HARS2* (Pierce et al. 2011)*, LARS2* (Pierce et al. 2013)*, CLPP* (Jenkinson et al. 2013)*, C10orf2* (Morino et al. 2014) and *ERAL1* (Chatzispyrou et al. 2017). The latter five of these genes function in mitochondrial translation and evidence is increasing that at least some cases of Perrault syndrome are associated with mitochondrial dysfunction (Chatzispyrou et al. 2017).

1.3.1 *HSD17B4*

HSD17B4 was the first gene to be associated with Perrault syndrome. Two sisters were investigated to determine the genetic cause of Perrault syndrome (Pierce et al. 2010). The sisters had been previously clinically characterised by McCarthy and Opitz (1985) with a further study to review their progression conducted by Fiumara et al. (2004). Both sisters had ovarian failure, little to no pubertal development, a 46,XX karyotype and moderate to severe bilateral SNHL. The sisters also had neurological features including weakness of

the lower limbs, pes cavus and ataxia (McCarthy and Opitz 1985;Fiumara et al. 2004). The neurological presentations were progressive in both siblings and more severe in the elder sister. The neurological presentations were initially thought to be limited to the elder sister and to be static (McCarthy and Opitz 1985), but Fiumara et al. (2004) showed this to be false in their case review.

Whole exome sequencing was performed on the elder sister and identified compound heterozygous variants in *HSD17B4*; c.650A>G p.(Tyr217Cys) a paternally inherited missense variant and c.1704T>A p.(Tyr568*) a maternally inherited nonsense variant. These variants were confirmed in the younger affected sibling using Sanger sequencing. (Pierce et al. 2010).

The gene *HSD17B4* encodes D-bifunctional protein (DBP), which is localised to the peroxisome. It is involved in two steps of the β oxidation of fatty acids via the function of separate dehydrogenase and hydratase domains (de Launoit and Adamski 1999). Variants in the *HSD17B4* gene are more commonly associated with the syndrome DBP deficiency. DBP deficiency is a severely life limiting condition with affected individuals rarely surviving beyond two years of age. The clinical presentations include: hypotonia, seizures, hearing and vision loss, myelination defects and failure to achieve developmental milestones (Ferdinandusse et al. 2006a). DBP deficiency is classified based on the enzyme function affected. Type I is deficiency of both the hydratase and dehydrogenase domains, Type II is deficiency of the hydratase domain and Type III is deficiency of the dehydrogenase domain. It was noted that while DBP deficiency classifications do not differ in clinical presentation they may have a predictive effect on lifespan (Ferdinandusse et al. 2006a).

Expression analysis of the variant transcripts in the affected sisters showed reduced p.(Tyr568*) levels in comparison to wild type transcripts. DBP levels were assayed in the mother and younger sibling. The expression of the full length protein and the dehydrogenase domain was reduced in the mother and further reduced in the younger sister. It was suggested that a combination of nonsense mediated decay of the p.(Tyr568*) transcript and reduced levels of the missense protein p.(Tyr217Cys) would account for the reduced protein levels in the affected individuals. As a result of these

findings the two sisters were tentatively classified as having a Type II DBP deficiency, suggesting there is clinical overlap between DBP deficiency and Perrault syndrome. Six additional Perrault syndrome families were screened for variants in *HSD17B4,* but no variants of significance were found (Pierce et al., 2010).

A second case of Perrault syndrome due to variants in *HSD17B4* was identified by Demain et al. (2017b). The affected female was of Brazilian descent and from a non-consanguineous family with unaffected parents and an unaffected brother. The proband presented with severe to profound SNHL with a small uterus and ovaries and a hypergonadotropic hypogonadism. The proband also displayed progressive ataxia and a mild intellectual disability. Very long chain fatty acid (VLCFA) analysis was normal in this individual. VLCFA levels are elevated in infantile cases of DBP deficiency (Ferdinandusse et al. 2006b). Whole exome sequencing performed on the proband identified biallelic compound heterozygous variants in *HSD17B4*; c.46G>A, p.(Gly16Ser) which was inherited maternally and c.244G>T, p.(Val82Phe) which was inherited paternally (Demain et al. 2017b). Both of these variants are situated in the dehydrogenase domain of DBP. p.(Gly16Ser) has been predicted to disrupt cofactor binding in DBP and is a known pathogenic variant associated with DBP deficiency (Ferdinandusse et al. 2006a). In contrast p.(Val82Phe) is a novel variant and was predicted to cause a small rearrangement which may mildly disrupt co-factor binding. It was theorised that the combination of the known pathogenic variant and the hypomorphic variant reduced DBP activity below a threshold to cause the Perrault syndrome phenotype in the proband but with function not impaired enough to cause DBP deficiency (Demain et al. 2017b). The discovery of a variant known to cause DBP deficiency in this Perrault syndrome patient further reinforces the overlap between Perrault syndrome and DBP deficiency.

McMillan et al. (2012) identified two brothers with what they describe as DBP type IV deficiency. They define this as "[DBP deficiency] due to compound heterozygous variants affecting two different domains of DBP but associated with a relatively milder clinical and biochemical phenotype"(McMillan et al. 2012). The two affected patients presented with moderate to severe bilateral SNHL, ataxia, pes cavus, sensorimotor neuropathy and retinal atrophy. These symptoms were milder in the younger brother. The older brother had developed normally but the younger brother had not achieved puberty by the age of

14 years. The authors of the paper make the argument for re-classifying the two sisters from Pierce et al. (2010) as DBP deficient type IV (McMillan et al. 2012).

Lines et al. (2014) identified a family affected by DBP deficiency type IV. The family consisted of two affected females and one affected male. The clinical presentations in these patients included SNHL, ataxia, demyelinating motor neuropathy and intellectual disability. Ovarian failure was seen in the affected females from this family. Ovarian dysfunction had not been seen previously in DBP deficiency and was one of the clinical presentations alongside the absence of the classical biochemical indicators of DBP deficiency that defined the original clinical case for classifying the sisters from Pierce et al. (2010) as having Perrault syndrome.

The gene *HSD17B4* has also been associated with POI independently of DBP deficiency (Pyun et al. 2012). In a comparison of 98 women with POI and 218 control women, all of Korean ethnicity, a haplotype of *HSD17B4* was found to be protective against POI and an epistatic interaction between a single nucleotide polymorphism (SNP) in *HSD17B4* and a SNP in thyroglobulin were found to be a risk factor for POI (Pyun et al. 2012). It is possible given the molecular data and the emergence of DBP deficiency type IV cases that the affected individuals from Pierce et al. (2010) and Demain et al. (2017b) may be reclassified as having a type IV DBP deficiency and not Perrault syndrome.

1.3.2 *HARS2*

Variants in the gene *HARS2*, encoding mitochondrial histidyl-tRNA synthetase, were identified by Pierce et al. (2011) to be the likely cause of Perrault syndrome in a large non-consanguineous family of European ancestry. There were 11 siblings in the family of which five were affected, three females and two males. All of the affected siblings had bilateral SNHL which varied in severity and age of onset. The three affected female siblings had ovarian dysgenesis and a 46,XX karyotype. The affected male siblings had normal pubertal development and gonadal function. All members of the family had normal intelligence and no neurological presentations were noted (Pallister and Opitz 1979). The clinical presentations were consistent with the proposed Perrault syndrome type I classification.

The size of the affected family allowed for the use of genome wide linkage analysis in the identification of novel variants. A region with a high linkage score was identified and sequenced using Sanger sequencing. In this region of linkage two novel variants in the *HARS2* gene were identified as being the most likely cause of Perrault syndrome in the family. The affected individuals were compound heterozygous for two variants in *HARS2*, the paternally inherited *HARS2* c.598C > G p.(Leu200Val) and the maternally inherited *HARS2* c.1102G >T p.(Val368Leu). The paternally inherited variant c.598C > G p.(Leu200Val) also resulted in an alternate splice site causing a deletion of 12 codons from the *HARS2* transcript (Pierce et al. 2011).

Aminoacyl-tRNA synthetases (aaRS) are enzymes with important functions in nuclear and mitochondrial protein synthesis. They catalyse the addition of the appropriate amino acid to the corresponding tRNA molecule and so are vital components of the translational machinery (Konovalova and Tyynismaa 2013). All but two aaRS, glycyl-tRNA synthetase (encoded by *GARS*) and lysyl-tRNA synthetase (encoded by *KARS*), are encoded by separate genes for nuclear and mitochondrial functions. Genes encoding mitochondrial proteins are identified by the 2 at the end of their gene name. *HARS2* encodes mitochondrial histidyl-tRNA synthetase and is responsible for the addition of histidine to the appropriate tRNA molecule for mitochondrial translation (Diodato et al. 2014a). There are a number of syndromes and pathologies associated with variants in mitochondrial aaRS genes, many of which produce neurological symptoms. Table 1.1 outlines some of these conditions but is not an exhaustive list. Of particular note in reference to Perrault syndrome are variants in *NARS2* which cause non-syndromic hearing loss (Simon et al. 2015) and variants in *AARS2* which can cause leukoencephalopathy and POI (Dallabona et al. 2014)

.

Gene	Protein	Syndrome or Condition	Clinical Presentations	Reference
DARS2	Mitochondrial aspartyl-tRNA synthetase	Leukoencephalopathy with brain stem and spinal cord involvement and lactate elevation (LBSL)	Slowly progressive cerebellar ataxia, spasticity, cerebellar and dorsal column dysfunction	(Scheper et al. 2007)
RARS2	Mitochondrial arginyl-tRNA synthetase	Pontocerebellar hypoplasia	Mitochondrial encephalopathy, seizures, hypotonia, microcephaly, failure to thrive	(Edvardson et al. 2007)
YARS2	Mitochondrial tyrosyl-tRNA synthetase	Myopathy, lactic acidosis, and sideroblastic anaemia syndrome (MLASA)	Progressive exercise intolerance, sideroblastic anaemia, some cases of intellectual disability	(Riley et al. 2010)
SARS2	Mitochondrial seryl-tRNA synthetase	Hyperuricemia, pulmonary hypertension, renal failure in infancy and alkalosis (HUPRA) Syndrome	Hyperuricemia, metabolic alkalosis, pulmonary hypertension, progressive renal failure	(Belostotsky et al. 2011)
AARS2	Mitochondrial alanyl-tRNA synthetase	Infantile mitochondrial cardiomyopathy	Hypertrophic cardiomyopathy, hypotonia, developmental delay	(Götz et al. 2011)
		Leukoencephalopathy with POI	Leukoencephalopathy, ataxia, spasticity, cognitive decline, POI	(Dallabona et al. 2014)
MARS2	Mitochondrial methionyl-tRNA synthetase	Autosomal recessive spastic ataxia with leukoencephalopathy (ARSAL)	Cerebellar ataxia, spasticity, dystonia, scoliosis, cognitive impairment	(Bayat et al. 2012)
FARS2	Mitochondrial phenylalanyl-tRNA synthetase	Fatal infantile alpers encephalopathy	Mitochondrial encephalopathy, epilepsy, lactic acidemia, severe progressive cerebral atrophy	(Elo et al. 2012)
EARS2	Mitochondrial glutamyl–tRNA synthetase	Leukoencephalopathy with thalamus and brainstem involvement and high lactate (LTBL)	Elevated lactate levels, hypotonia, spasticity, failure to reach or loss of developmental milestones, seizures	(Steenweg et al. 2012)
VARS2	Mitochondrial valyl tRNA-synthetase	Mitochondrial encephalopathy	Developmental delay, microcephaly, seizures	(Diodato et al. 2014b)
NARS2	Mitochondrial asparaginyl-tRNA Synthetase	Non-syndromic hearing loss	Pre-lingual, profound SNHL	(Simon et al. 2015)
		Hearing loss and Leigh syndrome	Hearing loss, epilepsy, laryngomalacia, pharyngeal hypotonia, legions in the brainstem and thalamus	
TARS2	Mitochondrial threonyl tRNA-synthetase	Mitochondrial encephalopathy	Hypotonia, elevated lactate levels, developmental delay	(Diodato et al. 2014b)

Table 1.1. Conditions associated with variants in mitochondrial aaRS genes.

From the crystal structures of *HARS2* prokaryotic orthologues it was predicted both the c.598C > G p.(Leu200Val) and c.1102G >T variants would alter packing interactions in the protein and consequently may decrease the histidine binding affinity of the active site. In functional studies the alternate transcript of c.598C > G p.(Leu200Val) was poorly expressed in both 293T cells and bacterial cells leading to the conclusion that the transcript was unstable. Studies in yeast using *HARS2* orthologues showed that p.Leu200Val provided almost wild type aminoacylation activity with p.Val368Leu showing reduced aminoacylation activity. The combination of the reduced activity of p.(Val368Leu) and the reduced functional transcripts for p.(Leu200Val) may have reduced histidine aminoacylation below the level required for the normal function of mitochondria causing the Perrault syndrome phenotype in these individuals. Functional studies in *C.elegans* implicated *HARS2* as a causative agent for infertility via mechanisms relating to cell apoptosis (Pierce et al. 2011).

Recently two additional families were identified as having Perrault syndrome due to variants in *HARS2*. Using a next generation sequencing (NGS) panel comprising 35 hearing loss genes, including five Perrault syndrome genes (*HSD17B4, HARS2, LARS2, CLPP* and *C10orf2*), Lerat et al. (2016) identified two unrelated individuals with Perrault syndrome. Both affected individuals were from consanguineous families and were homozygous for the same variant *HARS2* c.1010A>G p.(Tyr337Cys). Both female probands were from the same region in Morocco and share a haplotype suggesting a founder effect. Both affected individuals have a similar phenotype of profound SNHL with onset before 3 years of age and secondary amenorrhea presenting at 25 and 26 years of age respectively. Neither proband has any neurological phenotypes but both have hypothyroidism (Lerat et al. 2016), which is not commonly associated with Perrault syndrome but has been previously reported (Demain et al. 2017b). These individuals have a very similar phenotype which could be due not only to the same Perrault syndrome variant but also to the similar genetic background.

The males in the family reported by Pierce et al. (2011) were fertile. There were no affected males in the additional two families with Perrault syndrome due to variants in *HARS2* (Lerat et al. 2016). It has been proposed that apoptosis leading to cochlear degeneration and excessive apoptosis in the ovarian follicles, selecting against poor

functioning mitochondria, is responsible for the SNHL and ovarian dysfunction of Perrault syndrome due to *HARS2* variants (Pierce et al. 2011). This mechanism may account for the apparent disparity in gonadal development and function between males and females affected by Perrault syndrome.

1.3.3 *LARS2*

Initially variants in the *LARS2* gene were found to be associated with Perrault syndrome in two families (Pierce et al. 2013). Family 1, who were consanguineous and of Palestinian descent, consist of a female proband and her two affected brothers. There were no unaffected siblings in family 1. All siblings were diagnosed with bilateral SNHL between 3-5 years of age. The brothers had a distinctive upsloping audiogram present bilaterally which in the proband was present in one ear only with mild hearing loss in the other ear. The proband had primary amenorrhea with no ovaries visible on an ultrasound examination, raised levels of gonadotropins and a 46,XX karyotype. There were no pubertal delays reported in the brothers and no intellectual or neurological abnormalities were reported in any members of the family. Family 2 is non-consanguineous and of Slovenian ancestry. The proband is an only child with: severe hearing loss; secondary amenorrhea, which presented at 19 years of age; and high levels of FSH. No ultrasound data was available for the proband of family 2. This family also reported no neurological symptoms (Pierce et al. 2013).

Whole exome sequencing identified three novel variants in the *LARS2* gene which were proposed to be causative of Perrault syndrome in these families. All 3 affected siblings in family 1 were homozygous for the missense variant *LARS2* c.1565C>A p.(Thr522Asn). The proband in family 2 was compound heterozygous for the paternally inherited frameshift variant *LARS2* c.1077delT p.(Ile360PhefsTer15) and maternally inherited *LARS2* c.1886C>T p.(Thr629Met) missense variant (Pierce et al. 2013).

LARS2 encodes mitochondrial leucyl-tRNA synthetase which is responsible for the addition of leucine to the appropriate tRNA molecule in mitochondrial translation. As with mitochondrial histidyl-tRNA synthetase, mitochondrial leucyl-tRNA synthetase is an essential component for mitochondrial translation (Diodato et al. 2014a). The importance of the mitochondrial aaRS enzymes is underscored by the fact that none of the disease

causing variants in mitochondrial aaRS enzymes result in a full loss of function suggesting that some residual function in these enzymes is a pre-requisite for life (Konovalova and Tyynismaa 2013).

The protein produced as a result of the variant in family 1, p.(Thr522Asn), was predicted to have reduced aminoacylation efficiency. Functional studies in yeast showed that p.(Thr522Asn) has reduced aminoacylation activity in comparison to wild type mitochondrial leucyl-tRNA synthetase (Pierce et al. 2013). It has since been demonstrated that the variant p.Thr522Asn has a 9 fold reduced aminoacylation efficiency compared to human wild type mitochondrial leucyl-tRNA synthetase (Riley et al. 2015). The variant *LARS2* c.1077delT is predicted to yield a non-functioning protein missing vital domains. Functional tests have shown that c.1077delT is unable to rescue mitochondrial function in yeast mutants in which the *LARS2* orthologue *NAM2* was deleted. The second variant in family 2, p.(Thr629Met), showed near wild type aminoacylation activity in functional tests. It was predicted that the combination of the 2 variants reduces the enzyme function below a threshold level and produces a Perrault syndrome phenotype in the proband of family 2 (Pierce et al. 2013).

There have been multiple additional reports of individuals with Perrault syndrome due to variants in *LARS2*. The phenotypes and genotypes of all the individuals with Perrault syndrome due to *LARS2* to date, including the cases detailed in Pierce et al. (2013), are presented in more detail in Table 1.2.

Two siblings, one female and one male were found to be compound heterozygous for biallelic variants in *LARS2* by Solda et al. (2016). The family were non-consanguineous and of Italian descent, comprising two affected and two unaffected siblings. Both affected siblings presented with congenital profound SNHL and the female proband presented with secondary amenorrhea at 31 years of age. No neurological features were reported in this family. Whole exome sequencing showed the affected siblings were compound heterozygous for two variants in *LARS2*:c.899C>T p(.(Thr300Met), inherited maternally, and c.1912G>A p.(Glu638Lys) inherited paternally. Segregation of the variants with the phenotype was confirmed by Sanger sequencing. Neither of these variants have previously been associated with Perrault syndrome and were absent from an in-house

database of 3500 ethnically matched controls and ExAC (Solda et al. 2016). *LARS2*:c.899C>T p.(Thr300Met) lies in the editing domain of the protein and is predicted to interfere with editing (the removal of an incorrectly attached amino acid) or discrimination of amino acids. *LARS2* c.1912G>A p.(Glu638Lys) is situated in the catalytic domain of the protein and is predicted to interfere with the conformational change of the protein required for aminoacylation activity (Solda et al. 2016).

A single affected individual with Perrault syndrome due to variants in *LARS2* was reported in a Sri Lankan family. The affected female presented with primary amenorrhea and moderate SNHL which was not progressive and presented before the age of 3 years. The proband also had a cleft palate, which has not been previously associated with Perrault syndrome. It was not discussed if this cleft palate may be part of the Perrault syndrome phenotype or an unrelated phenotype. Using a next generation sequencing (NGS) panel of 35 genes including five Perrault syndrome genes (*HSD17B4, HARS2, LARS2, CLPP and C10orf2*) Lerat et al. (2016) identified the following biallelic variants in *LARS2*; c.1358G>A p.(Arg453Gln) and c.1886C>T p.(Thr629Met). *LARS2* c.1886C>T p.(Thr629Met) has been previously associated with Perrault syndrome in a family of Slovenian descent and was shown to have near wild type aminoacylation activity (Pierce et al. 2013). It is possible that the variant located *in trans* to p.(Thr629Met), *LARS2* c.1358G>A p.(Arg453Gln), in the proband reported by Lerat et al. (2016) is not as deleterious as the variant found the proband reported by Pierce et al. (2013) which was a frameshift variant producing a non-functioning protein. The possibly more deleterious frameshift variant could account for the difference in hearing loss between these affected individuals with the proband reported by Lerat et al. (2016) having moderate SNHL and the proband reported by Pierce et al. (2013) having severe hearing loss.

Two families were reported with Perrault syndrome and an unusual audiometric configuration of low frequency hearing loss. Affected members of both families were either homozygous or compound heterozygous for the variant *LARS2* c.1565C>A p.(Thr522Asn) (Demain et al. 2017b). *LARS2* c.1565C>A p.(Thr522Asn) has previously been seen as a homozygous change in a family with Perrault syndrome and low frequency SNHL (Pierce et al. 2013). The two reported families in Demain et al. (2017b) were both non-consanguineous, of Argentinian and white British descent and were referred to as P2

and P3 respectively in the report. Family P2 comprised the affected female proband, one affected male sibling, two unaffected male sibling and their unaffected parents. The proband presented with low frequency SNHL at eight years of age which was severe by the age of 21. She also presented with primary amenorrhea, small uterus and ovaries and hypergonadotropic hypogonadism. The affected male in this family showed mild low frequency SNHL diagnosed at age 26 with no additional clinical features. No neurological features were reported in this family. Whole exome sequencing performed on the proband showed that she was homozygous for the variant *LARS2* c.1565C>A p.(Thr522Asn) which was confirmed in the affected sibling by Sanger sequencing. Family P3 comprised the affected female proband, her affected male sibling and their unaffected parents. There were no unaffected siblings in this family. Both siblings presented with low frequency SNHL which was severe to profound. The proband also presented with oligomenorrhea, hypergonadotropic hypogonadism and a small uterus and ovaries. Both siblings have mild facial dysmorphism and the affected male in this family has hypospadias but no other urogenital phenotypes. Whole exome sequencing performed on the proband identified biallelic variants in *LARS2:* c.1565C>A p.(Thr522Asn), maternally inherited and c.351G>C p.(Met117Ile), paternally inherited. p.(Met117Ile) is a *LARS2* variant not previously associated with Perrault syndrome. Both variants were confirmed in the male sibling using Sanger sequencing (Demain et al. 2017b). The variant c.1565C>A p.(Thr522Asn) reduces the aminoacylation efficiency of *LARS2* by 9-fold relative to wild type *LARS2* (Riley et al. 2015). *LARS2* c.351G>C p.(Met117Ile), is predicted to interfere with the interaction between the catalytic and anticodon binding domains of mitochondrial leucyl-tRNA synthetase but to a lesser extent than p.(Thr522Asn) (Demain et al. 2017b).

It has been proposed that *LARS2* c.1565C>A p.(Thr522Asn) is a hotspot variant for Perrault syndrome and is linked to low frequency SNHL (Demain et al. 2017b;Pierce et al. 2013). Low frequency hearing loss has been evident in three families where the causative variant was either *LARS2* c.1565C>A p.(Thr522Asn) homozygous or *in trans* with an additional putative pathogenic variant (Pierce et al. 2013;Demain et al. 2017b). The mechanisms behind this unusual pattern of hearing loss are currently unknown. This is the first recessive variant to be linked to low frequency SNHL and Demain et al. (2017b)

suggest that it may be useful to screen males and pre-pubertal girls with recessive low frequency SNHL for the variant *LARS2* c.1565C>A p.(Thr522Asn).

Individual ID	Family 1, II-1	Family 1, II-2 Proband	Family 1, II-3	Family 2, Proband	II1	II3 Proband
Variant	c.1565C>A p.(Thr522Asn)			c.1077delT p.(Ile360PhefsTer15), c.1886C>T p.(Thr629Met)	c.899C>T p.(Thr300Met), c.1912G>A p.(Glu638Lys)	
Reference	(Pierce et al. 2013)				(Solda et al. 2016)	
Ethnicity	Palestinian			Slovenian	Italian	
Consanguinity	Y			N	N	
Sex	M	F	M	F	M	F
Karyotype	NR	46, XX	NR	46, XX	NR	46, XX
Age (yrs) at last assessment	17	17	13	30	40	31
Sensorineural hearing loss						
Age at diagnosis (yrs)	3-5	3-5	3-5	NR	Congenital	Congenital
Level of hearing loss	Severe to Profound	Right ear: Severe at lower frequencies, moderate at higher frequencies. Left ear: moderate at lower frequencies, mild at higher frequencies	Severe to moderate at low frequencies, moderate to mild at higher frequencies	Severe	Profound	Profound
Notes	LF	Unilateral LF	LF	None	None	None
Intervention	NR	No hearing aid used	NR	NR	Bilateral CI	Bilateral CI
Gonadal dysfunction						
pelvic ultrasound	N/A	Small uterus, ovaries not visualised	N/A	NR	N/A	Bicornate uterus, hypoplastic left ovary, right ovary not visualised
menarche	N/A	N	N/A	Y	N/A	Y
POI - Age if menarche achieved	N/A	Y	N/A	Y - 19	N/A	Y - 28
Follicle stimulating hormone	NR	76.9 IU/l	NR	101 IU/l	NR	118 IU/l
Luteinising hormone	NR	30.3 IU/l	NR	NR	NR	45.4 IU/l
estradiol	N/A	NR	N/A	NR	N/A	NR
Neurological features	N	N	N	N	N	N
Additional features	N	N	N	N	N	N

Table 1.2. The genotypes and phenotypes of individuals with Perrault syndrome due to variants in *LARS2*.

Continued next page.

Individual ID	P2:II-1 Proband	P2:II-2	P3:II-1 Proband	P3:II-2	Patient III-3
Variant	c.1565C>A p.(Thr522Asn)		c.351G>C p.(Met117Ile), c.1565C>A (p.Thr522Asn)		c.1358G>A p.(Arg453Gln), c.1886C>T p.(Thr629Met)
Reference	(Demain et al. 2017b)				(Lerat et al. 2016)
Ethnicity	Argentinian		White British		Sri Lankan
Consanguinity	N	N	N	N	N
Sex	F	M	F	M	F
Karyotype	46, XX	NR	46, XX	NR	NR
Age (yrs) at last assessment	27	26	25	26	NR
Sensorineural hearing loss					
age at diagnosis (yrs)	8	26	2.5	2.5	<3
degree of hearing loss	Moderate	Mild/Moderate	Severe/Profound	Severe/Profound	Moderate
Notes	LF	LF	LF	LF	Not progressive
Intervention	CI	NR	CI	NR	NR
Gonadal dysfunction					
pelvic ultrasound	Small uterus and ovaries	NA	Small uterus and ovaries	NA	NR
menarche	N	NA	Y	NA	N
POI - Age if menarche achieved	N/A	NA	Y	NA	NA
Follicle stimulating hormone	99.6 (2.3-29) IU/l	NR	74 (≤30) IU/l	3.1 (1-11) IU/l	NR
Luteinising hormone	48.0 (1.7 – 52) IU/l	NR	63 (≤30) IU/l	3.9 (1-11) IU/l	NR
estradiol	7.04 (10- 388) pg/ml	NA	91 (>180) pmol/l	NA	NR
Neurological features	N	N	N	N	N
Additional features	N	N	Mild facial dysmorphism, hemidystropy	Hypospadias, mild facial dysmorphism, normal testosterone 22.3 (9-25) IU/l	Cleft palate

Table 1.2. The genotypes and phenotypes of individuals with Perrault syndrome due to variants in *LARS2*.

Y, yes. N, no. M, male. F, female. NR, not recorded. NA, not applicable. CI, cochlear implant. LF, low frequency. If one variant is noted the individual is homozygous for this variant. All hearing loss is bilateral unless noted otherwise. For hormone levels the reference values, where available, are indicated in the brackets next to the patient levels.

There have been no neurological features reported in any of the individuals with Perrault syndrome due to variants in *HARS2* or *LARS2*. This may mean that neurological features are not associated with variants in *HARS2* or *LARS2*. Conversely, many of the affected individuals were young at the age of last examination and may develop neurological features over time. Follow up reports of these individuals may help to resolve some questions about genotype/phenotype correlations in Perrault syndrome due to variants in *HARS2* and *LARS2*.

Recently there has been a report of biallelic variants in *LARS2* associated with a more severe phenotype in an infant with hydrops, sideroblastic anemia, lactic acidosis and multisystem failure (Riley et al. 2016). The affected infant was compound heterozygous for the variants *LARS2* c.1289C>T p.(Ala430Val) and a variant previously associated with Perrault syndrome, *LARS2* c.1565C>A p.(Thr522Asn). The variant p.Ala430Val was found to reduce the aminoacylation efficiency of mitochondrial leucyl-tRNA synthetase by 18 fold. This in combination with the 9-fold reduction in aminocylation activity attributed to the variant p.Thr522Asn could account for the more severe phenotype in this infant (Riley et al. 2016). It has been previously proposed that hypomorphic variants in other aaRS genes may cause a milder phenotype such as Perrault syndrome (Pierce et al. 2013) and so it may be expected that there are more deleterious variants in *LARS2* which cause a more severe phenotype akin to some of those associated with variants in other mitochondrial aminoacyl synthetases. Although the identification of *LARS2* and *HARS2* as causative of Perrault syndrome makes additional mitochondrial aARS genes plausible targets for investigation, caution should be taken, as using a candidate approach in a syndrome as genetically heterogeneous as Perrault syndrome can be misleading.

1.3.4 *CLPP*

Biallelic variants in *CLPP* have been reported to cause Perrault syndrome in ten unrelated families to date. The *CLPP* gene encodes the protein caseinolytic mitochondrial matrix peptidase proteolytic subunit (CLPP). CLPP in conjunction with CLXP forms the macromolecular complex CLPXP. This complex, located in the mitochondria, is responsible for unfolding and degrading misfolded proteins. The CLXP subunit is responsible for unfolding the proteins tagged for degradation and feeding them into the active

proteolytic site of CLPP. It is also suggested that CLXP binding alters the conformation of the CLPP active site and increases its proteolytic activity, when not in complex with CLXP CLPP has a low level of proteolytic activity (Kang et al. 2005). Recently CLPXP has been found to have a role in the maturation of the mitochondrial ribosome likely by the removal of 12S RNA chaperone ERAL1 (Szczepanowska et al. 2016), variants in which are also associated with Perrault syndrome (Chatzispyrou et al. 2017).

In one study performed on 3 families with Perrault syndrome the causative variants were shown to be in the *CLPP* gene (Jenkinson et al. 2013). Three families were recruited for this study, PDF1, PKDF291 and DEM4395. There were three affected females in PDF1. They all displayed profound congenital SNHL and POI with raised gonadotropin levels. In addition the sisters also had a number of neurological symptoms and morphological features which have previously been associated with Perrault syndrome. These include: epilepsy, microcephaly, short stature, moderate intellectual disability, ataxia and lower limb spasticity (Jenkinson et al. 2013). In family PKDF291 there were four affected sisters, their hearing loss had been previously characterised and they had been screened for variants in the non-syndromic hearing loss associated gene *Gipc3*. All four affected siblings had moderate to severe SNHL but no other reported abnormalities (Rehman et al. 2011). On review, the sisters presented with primary amenorrhea and a hormone profile indicative of hypergonadotropic hypogonadism (Jenkinson et al. 2013). The family DEM4395 had one affected male and two affected females. All had profound SNHL but no hormone profiles were available for this family. A chromosomal region of interest was identified in all 3 families at 19p.13 via either linkage analysis or homozygosity mapping (Rehman et al. 2011;Jenkinson et al. 2013).

Whole exome sequencing was performed on one affected individual from each family. The only gene with novel variants for all three families was *CLPP,* which aligned with the linkage signal at 19p.13. Each family was homozygous for a different variant in *CLPP*. The affected individuals in PDF1 were homozygous for a missense variant *CLPP* c.433A>C p.(Thr145Pro). PKDF291 had a missense variant, *CLPP* c.440G>C p.(Cys147Ser). The family DEM4395 had a splice site variant, *CLPP* c.270+4A>G. All variants were absent in a panel of ethnically matched controls (Jenkinson et al. 2013).

Functional tests performed in COS-7 cells showed that the splice site variant, *CLPP* c.270+4A>G, caused cells to retain a low level of wild type transcripts. In comparison, a control variant (c.270+1G>A) retained no wild type transcripts. It was theorised that the variant weakened the splice site rather than eliminating its function. From the available models of CLPP it was proposed that the 2 missense variants may affect the docking of the CLPX protein to CLPP and therefore the formation and efficiency of the CLPXP complex. The variant *CLPP* c.433A>C in family PDF1 is expected to be the more deleterious variant possibly explaining the more severe phenotype and additional clinical presentations in this family. PDF1 also showed two additional homozygous variants in genes in the chromosomal region 19p.13 which may have contributed to the more severe phenotype. It was noted that the variants in *CLPP* led to severe SNHL in the three reported families and did not show the clinical heterogeneity associated with hearing loss in Perrault syndrome. This could be a phenotype of *CLPP* variants or it could be bias due to the most severe cases coming to the attention of physicians (Jenkinson et al. 2013).

CLPP was screened for variants in 20 other families where the genetic cause of Perrault syndrome was unknown, but no variants of significance were found (Jenkinson et al. 2013).

Recently a novel variant in *CLPP* was identified in a consanguineous Saudi Arabian family with a severe neurological phenotype. Perrault syndrome was subsequently diagnosed in this family due to the genetic data (Ahmed et al. 2015).

The proband in this family was a 12 year old male. He had displayed normal development until the age of 18 months where upon he entered a period of regression losing such acquired skills as walking and speech. After this period of regression he began to acquire skills again slowly. He was subsequently diagnosed with severe bilateral SNHL and had a cochlear implant fitted at 8 years of age, he is still unable to speak. At the time of publication he was able to stand with support and showed severe lower limb spastic diplegia. Brain MRI showed the loss of white matter volume and the thinning of the corpus callosum. All biochemical tests to detect metabolic disorders were normal and there was no evidence of visual impairment. There is also an affected female in this family. She was eight years old at the time of examination and had displayed the same

period of regression as her elder affected sibling. She also displayed severe bilateral SNHL, lower limb spastic diplegia and white matter loss (Ahmed et al. 2015).

A homozygous change missense in *CLPP*, c.685T>G p.(Tyr229Asp), was identified in this family through a combination of homozygosity mapping and whole exome sequencing. The variant was predicted *in silico* to be deleterious and segregated with the phenotype in the family. Of note was that the youngest child in the family was homozygous for the variant but had not reached the age at which his siblings had begun to display symptoms. It is possible that the child is affected and will experience the same period of regression as the two other affected siblings at approximately 18 months of age (Ahmed et al. 2015).

This is the first case of Perrault syndrome diagnosed from genetic data alone. A diagnosis of Perrault syndrome would not be achievable for this family at this point in time from the clinical features. The affected female sibling had not reached puberty and the presentation of POI is required for the clinical diagnosis of Perrault syndrome. In this case it was the severe neurological symptoms that prompted the whole exome sequencing that led to a diagnosis (Ahmed et al. 2015). Subsequently, multiple cases have been reported of males diagnosed with Perrault syndrome, due to variants in *CLPP*, based on the genetic data (Demain et al. 2017b;Theunissen et al. 2016). The genotypes and phenotypes of the individuals affected by Perrault syndrome due to variants in *CLPP* are presented in Table 1.3.

Perrault syndrome was diagnosed by genetic data in a male proband with neurological features reported by Demain et al. (2017b). The proband was the only affected member of this family and as such would have never been clinically diagnosed with Perrault syndrome. The proband presented with severe/profound SNHL, sensory motor peripheral neuropathy limited to the lower limbs and azoospermia. Azoospermia has not been previously reported in association with Perrault syndrome but infertility in both sexes is a phenotype of the *Clpp* knockout mouse (Gispert et al. 2013). A homozygous variant *CLPP* c.430T>C; p.(Cys144Arg) was identified in the proband which was predicted to interfere with the interaction of CLPP with CLPX (Demain et al. 2017b). Pathogenic variants, p.Thr145Pro and p.Cys147Ser, located in close proximity to this variant have also been predicted to affect the interaction of CLPP and CLPX (Jenkinson et al. 2013).

Three families with Perrault syndrome with a severe neurological phenotype due to variants in *CLPP* were identified through genetic and MRI data. Initially a homozygous frameshift variant in *CLPP*, c.21delA p.(Ala10Profs*117) was identified in a single family using whole exome sequencing. The two affected male siblings in this family, referred to as 1.1 and 1.2, presented with profound congenital SNHL, and a severe neurological phenotype (Table 1.3). The affected siblings in this family showed white matter anomalies on MRI especially affecting the deep and subcortical white matter. The variant in family 1, p.(Ala10Profs*117), was predicted to cause a premature stop codon resulting in nonsense mediated decay. CLPP mRNA expression in patient cells was approximately 50% of controls indicating the transcript was subject to nonsense mediated decay (Theunissen et al. 2016).

The white matter anomalies on the MRI scans from affected individuals from family 1 were used as a template to manually assess over 3000 unclassified leukoencephalopathy cases for similarities. Two additional families with similar MRI features found to have variants in *CLPP*. These non-consanguineous families were found to have a missense variant and a deletion spanning at least a partial area of *CLPP*. Family 2 was compound heterozygous for the variant *CLPP* c.484G>A p.(Gly162Ser) and a deletion spanning at least 2 exons and family 3 were compound heterozygous for the variant *CLPP* c.425C>T p.(Pro142Leu) and a deletion spanning at least exons 3-6 of *CLPP*. All of these affected individuals had a severe progressive neurological phenotype (detailed in Table 1.3), which included ataxia and epilepsy in the affected male from family 2 and psychomotor retardation, spastic diplegia and intellectual disability in both affected males in family 3. Both affected males from family 3 also had microcephaly (Theunissen et al. 2016).

The cases presented by Theunissen et al. (2016) as well as previous cases (Ahmed et al. 2015;Demain et al. 2017b) showed that it possible to diagnose Perrault syndrome in males and prepubescent females from genetic data. To date all of the affected individuals diagnosed by genetic data have presented with a severe neurological phenotype which is likely due to ascertainment bias with the individuals with the most severe phenotype receiving genetic investigation using whole exome sequencing.

A consanguineous family with two affected sisters with Perrault syndrome were found to have a homozygous variant in *CLPP*, c.439T>A p.(Cys147Ser) (Lerat et al. 2016). The sisters presented with progressive SNHL at ages 3 and 6 years respectively which was severe at the time of the report. The sisters also presented with secondary amenorrhea at ages 22 and 33 years. There were no neurological features reported in this family. The variants in CLPP were identified using a NGS panel containing 35 hearing loss genes including the five Perrault syndrome genes identified at the time of the report (Lerat et al. 2016). The variant in this family has been previously reported in another Perrault syndrome family as a change at the protein level with a different change at DNA level (Lerat et al. 2016;Jenkinson et al. 2013). The other affected family was also reported to have no neurological phenotype (Jenkinson et al. 2013).

A short report produced by Dursun et al. (2016) also described a family with Perrault syndrome due to variants in *CLPP* with no neurological phenotype. The family was non-consanguineous and comprised the female proband and her affected brother. There were no unaffected siblings in this family. Both affected individuals had SNHL the severity of which was not specified. The proband also presented with hypergonadotropic hypogonadism and absent ovaries. Neurological examination of both affected individuals was normal. The homozygous variant in *CLPP*; c.624C>G p.(Ile208Met), was detected in both patients using a combination of homozygosity mapping and candidate gene sequencing (Dursun et al. 2016).

Individual ID	PDF1, II-2	PDF1, II-4	PDF1, II-6	PKDF291, II-5	PKDF291, II-4	PKDF291, II-3	PKDF291, II-2
Variant	c.433A>C p.(Thr145Pro)			c.440G>C p.(Cys147Ser)			
Reference	(Jenkinson et al. 2013)						
Ethnicity	Pakistani			Pakistani			
Consanguinity	Y			Y			
Sex	F	F	F	F	F	F	F
Karyotype	NR			NR			
Age (yrs) at last assessment	22	21	15	25	23	20	15
Sensorineural hearing loss							
age at diagnosis (yrs)	Congenital			NR			
degree of hearing loss	Profound			Severe/Profound	Profound	Severe/Profound	Severe/Profound
Notes	N			Mixed hearing loss	SNHL	Mixed hearing loss	Mixed hearing loss
Intervention	NR			NR			
Gonadal dysfunction							
pelvic ultrasound	NR	NR	Streak ovaries	Rudimentary uterus and small ovaries			Small uterus and normal sized ovaries
menarche	Y	Y	N	N			
POI - Age if menarche achieved	Irratic menses at last assesment		NA	N/A			
Follicle stimulating hormone	41.5 (2–14 IU/l)	24.6 (2–14 IU/l)	45 (2–14 IU/l)	111 (2.8–11.1 IU/l)	104 (2.8–11.1 IU/l)	81 (2.8–11.1 IU/l)	101 (2.8–11.1 IU/l)
Luteinising hormone	64.6 (2–14 IU/l)	17.7 (2–14 IU/l)	104 (2–14 IU/l)	29.4 (0–11.6 IU/l)	49.8 (0–11.6 IU/l)	26 (0–11.6 IU/l)	31 (0–11.6 IU/l)
estradiol	777 (70–1,480 pmol/l)	281 (70–1,480 pmol/l)	89 (70–1,480 pmol/l)	<20 (NR–160 pg/ml)	<20 (NR–160 pg/ml)	<20 (NR–160 pg/ml)	<20 (NR–160 pg/ml)
Neurological features	Epilepsy, moderate learning difficulties, truncal and cerebellar ataxia with signs of lower-limb spasticity			N			
Additional features	Had two healthy sons, abnormally high signal intensity in the deep white matter and corticospinal tract, microcephaly, short stature	Microcephaly, short stature		N			

Table 1.3. The genotypes and phenotypes of individuals with Perrault syndrome due to variants in *CLPP*.

Continued next page.

Individual ID	DEM4395, IV-3	DEM4395, IV-4	DEM4395, IV-5	Ahmed, V-4	Ahmed, V-5	Ahmed, V-6	P8:II-1
Variant	c.270+4A>G			c.685T>G p.(Tyr229Asp)			c.430T>C; p.(Cys144Arg)
Reference	(Jenkinson et al. 2013)			(Ahmed et al. 2015)			(Demain et al. 2017b)
Ethnicity	Pakistani			Saudi Arabian			Arabic
Consanguinity	Y			Y			Y
Sex	M	F	F	M	F	M	M
Karyotype	NR			NR			46, XY
Age (yrs) at last assessment	25	28	22	12	8	8 months	32
Sensorineural hearing loss							
age at diagnosis (yrs)	Congenital			NR		NA	1.2
degree of hearing loss	Profound			Severe		None	Severe/Profound
Notes	None			None			None
Intervention	NR			CI	NR	NA	NR
Gonadal dysfunction							
pelvic ultrasound	NA	NR		NA			NA
menarche	NA	Y		NA			NA
POI - Age if menarche achieved	NA	NA		NA			NA
Follicle stimulating hormone	NR			NA			2.69 (1.50– 12.40) IU/L
Luteinising hormone	NR			NA			6.59 IU/L
estradiol	NR			NA			NA
Neurological features	N			Severe spastic diplegia affecting lower limbs, loss of white matter on MRI		N	Lower limb peripheral neuropathy,
Additional features	N	Reported to have normal menses at age of last assessment		Normal development until 18 months then a period of regression. Minor facial dysmorphism		Homozygous for the variant but no symptoms, younger than when his siblings first presented	Azoospermia, testosterone 2.24 (2.41–8.27) ng/mL

Table 1.3. The genotypes and phenotypes of individuals with Perrault syndrome due to variants in *CLPP*.

Continued next page.

Individual ID	Lerat XI-1	Lerat XI-2	Dursun III-1	Dursun III-2
Variant	c.439T>A p.(Cys147Ser)		c.624C>G p.(Ile208Met)	
Reference	(Lerat et al. 2016)		(Dursun et al. 2016)	
Ethnicity	Algerian		Turkish	
Consanguinity	Y		N	
Sex	F	F	M	F
Karyotype	NR		NR	46, XX
Age (yrs) at last assessment	NR		21	16
Sensorineural hearing loss				
age at diagnosis (yrs)	3	6	NR	
degree of hearing loss	Severe		NR	
Notes	Progressive		No information provided other than the affected individuals had SNHL	
Intervention	NR		NR	
Gonadal dysfunction				
pelvic ultrasound	NR		NA	Small uterus and ovaries
menarche	Y	Y	NA	Y
POI - Age if menarche achieved	22	33	NA	NR
Follicle stimulating hormone	NR	NR	NR	63.8 IU/L
Luteinising hormone	NR	NR	NR	20.7 IU/L
estradiol	NR	NR	NA	15 pg/mL
Neurological features	N		attention deficit disorder	N
Additional features	N		N	N

Table 1.3. The genotypes and phenotypes of individuals with Perrault syndrome due to variants in *CLPP*.

Continued next page.

Individual ID	Patient 1.1	Patient 1.2	Patient 2	Patient 3.1	Patient 3.2
Variant	c.21delA p.Ala10Profs*117		c.484G > A p.(Gly162Ser), deletion spanning at least 2 exons	c.425C > T p.(Pro142Leu), deletion spanning at least exons 3-6	
Reference	(Theunissen et al. 2016)				
Ethnicity	NR		NR	NR	
Consanguinity	Y		N	N	N
Sex	M	M	M	M	M
Karyotype	NR		NR	NR	
Age (yrs) at last assessment	20	22	20	25	21
Sensorineural hearing loss					
age at diagnosis (yrs)	1	16 months	1	4	3
degree of hearing loss	Profound	Profound	Profound	Profound	Profound
Notes	None		None	None	
Intervention	NR		NR	NR	
Gonadal dysfunction					
pelvic ultrasound	NA		NA	NA	
menarche	NA		NA	NA	
POI - Age if menarche achieved	NA		NA	NA	
Follicle stimulating hormone	NR		NR	NR	
Luteinising hormone	NR		NR	NR	
estradiol	NA		NA	NA	
Neurological features	Severe neurological phenotype including ataxia, epilepsy (1.1 only), autism and intellectual disability		Severe neurological phenotype including ataxia, epilepsy and sensorimotor neuropathy	Severe neurological phenotype psychomotor retardation, spastic diplegia, epilepsy (3.1 only) and intellectual disability	
Additional features	Neurological features are progressive and include episodes of regression, some facial dysmorphism		Neurological features are progressive and include episodes of regression	Neurological features are progressive and include episodes of regression, some facial dysmorphism, microcephaly and diabetes mellitus (3.1 only)	

Table 1.3. The genotypes and phenotypes of individuals with Perrault syndrome due to variants in *CLPP*.

Y, yes. N, no. M, male. F, female. NR, not recorded. NA, not applicable. CI, cochlear implant. If one variant is noted the individual is homozygous for this variant. All hearing loss is bilateral unless noted otherwise. For hormone levels the reference values, where available, are indicated in the brackets next to the patient levels.

There are a number of phenotypes which seem to be linked to variants in *CLPP* although small numbers of affected individuals and ascertainment bias make establishing genotype phenotype links difficult.

Many cases of Perrault syndrome due to variants in *CLPP* have reported a severe neurological phenotype. As noted above this may be ascertainment bias because individuals with severe phenotypes are more likely to be referred for genetic testing. A number of individuals with Perrault syndrome due to variants in *CLPP* have reported periods of neurological regression (Ahmed et al. 2015;Theunissen et al. 2016). Periods of neurological regression are seen in other syndromes associated with mitochondrial dysfunction such as Leigh syndrome (Thorburn and Rahman 2014) but to date have only been reported in individuals with Perrault syndrome due to variants in *CLPP*. Lower limb spasticity has been seen in a number of individuals with Perrault syndrome due to variants in *CLPP* (Ahmed et al. 2015;Demain et al. 2017b;Theunissen et al. 2016) and is not reported in other families with Perrault syndrome due to either variants in other known Perrault syndrome genes or of unknown genetic cause. It may be that lower limb spasticity and periods of regression are associated with Perrault syndrome due to some variants in *CLPP*.

It must be noted that not all individuals with Perrault syndrome due to variants in *CLPP* develop a neurological phenotype. Two families with the same homozygous variant at protein level, *CLPP* p.(Cys147Ser) reported no neurological phenotype (Jenkinson et al. 2013;Lerat et al. 2016) and it may be that this variant in not associated with a neurological phenotype.

All of the cases of Perrault syndrome due to variants in *CLPP* reported to date, where the hearing loss phenotype was recorded, have been associated with severe to profound SNHL. It is unclear at this time whether the inner ear is particularly sensitive to defects in *CLPP* or this is ascertainment bias with the most severe cases of hearing loss referred for genetic investigation (Jenkinson et al. 2013).

Mouse models have demonstrated that knockout of the *clpp* murine orthologue can result in features somewhat consistent with Perrault syndrome. Hearing loss, ovarian dysfunction and neuropathies were demonstrated. The development and function of the

testes was also affected (Gispert et al. 2013). Azoospermia was reported in one male with Perrault syndrome due to variants in *CLPP* (Demain et al. 2017b). In additional affected males the function of the testes was not assessed. It is still unclear whether azoospermia, as seen in the *clpp* knockout mouse model is a deviation from the human phenotype or an under reported clinical feature of Perrault syndrome due to variants in *CLPP* (Demain et al. 2017b).

Many of the variants in *CLPP* reported to be causative of Perrault syndrome to date are localised to a small region of CLPP, approximately residue 142 to 162 with a cluster around residues 144-147. This is a highly conserved region (Jenkinson et al. 2013) and some of the variants in this region are predicted to affect the interaction of CLPP with CLPX (Jenkinson et al. 2013;Demain et al. 2017b). Variants in the 142 to 162 region may also reduce the proteolytic activity of CLPP as the interaction of CLPX with CLPP induces a conformational change which improves the proteolytic activity of CLPP (Kang et al. 2005). This seems to be an important region of the CLPP protein and additional variants in this region may also be associated with Perrault syndrome.

Recently the role of CLPP in the mitochondrial matrix has been further elucidated. It has been reported that CLPXP is involved in mitochondrial ribosome biogenesis via the removal of ERAL1 from the immature mitochondrial ribosome (Szczepanowska et al. 2016). ERAL1 is a mitochondrial 12s RNA chaperone and its removal is required for ribosome maturation (Dennerlein et al. 2010). Variants in *ERAL1* are implicated in Perrault syndrome (Chatzispyrou et al. 2017) and so the work of Szczepanowska et al. (2016) molecularly links two Perrault syndrome genes. This work also highlights a possible pathogenic mechanism behind Perrault syndrome due to variants in *CLPP* which is more closely related to the rest of the Perrault syndrome genes, highlighting that Perrault syndrome seems to be associated with dysfunction of mitochondrial translation.

1.3.5 *C10orf2*

C10orf2 encodes the proteins Twinkle and Twinky. Twinkle is a mitochondrially located protein involved in mitochondrial DNA (mtDNA) unwinding. Twinkle has three domains, a helicase domain involved in the unwinding of DNA, a linker domain important for complex formation and a primase domain to which no specific function has yet been assigned.

Twinkle forms hexamer and heptamer complexes in the mitochondria. Twinky is the result of alternative splicing of *C10orf2* and is cytosolic and ubiquitous (Spelbrink et al. 2001). Variants in *C10orf2* are associated with two neuromuscular diseases characterised by deletions or depletion in mitochondrial DNA: mitochondrial DNA depletion syndrome 7 (MTDPS7) and progressive external ophthalmoplegia, autosomal dominant, 3 (PEOA3) (Spelbrink et al. 2001). MTDPS7 also known as infantile onset spinocerebellar ataxia (IOSCA) is an autosomal recessive condition characterised by ophthalmoplegia, hearing loss, ataxia, epilepsy, sensory neuropathy, hypergonadotropic hypogonadism in females and cerebellar atrophy (Nikali et al. 2005). PEOA3 is an autosomal dominant disorder characterised by ptosis, ophthalmoplegia and exercise intolerance. Additional clinical manifestations can include depression, neuropathy, ataxia and hearing loss (Fratter et al. 2010).

Variants in *C10orf2* were identified as the likely causative factor in two sets of sisters affected by Perrault syndrome with severe progressive neurological manifestations (Morino et al. 2014). Two families were recruited for the study conducted by Morino et al. (2014). Family 1 were non-consanguineous and of Japanese ancestry. This family comprised two affected sisters and an unaffected brother. The sisters were diagnosed with bilateral SNHL at 13 and eight years of age respectively. In their teens they presented with primary amenorrhea, hypergonadotropic hypogonadism and a lack of secondary sexual characteristics. The sisters also had high arched palate, pes cavus, mild external ophthalmoplegia, nystagmus, hyporeflexia and ataxia. A sensory axonal neuropathy was diagnosed. Both sisters had elevated lactate and pyruvate during exercise and the more severely affected older sister also had raised levels at rest. Family 2 were also non-consanguineous and were American with Greek and mixed European ancestry. There were two affected and two unaffected female siblings in this family. Both affected sisters were diagnosed with bilateral SNHL which at the time of publication was severe in the older sister and moderate in the younger. The older sister had been diagnosed with ataxia in her teens and with peripheral neuropathy in her twenties. She presented with nystagmus, distal atrophy of the hands and feet, hyporeflexia and type II myofibre atrophy. The younger sister also showed ataxia, peripheral neuropathy and hyporeflexia (Morino et al. 2014).

A number of affected and unaffected members in each family were exome sequenced. In each family the affected individuals were found to be compound heterozygote for variants in *C10orf2*. In family 1 both sisters were compound heterozygote for the maternally inherited variant, *C10orf2* c.1754A>G p.(Asn585Ser), and the paternally inherited variant, *C10orf2* c.1172G>A p.(Arg391His). The unaffected brother was heterozygous for *C10orf2* c.1172G>A p.(Arg391His). In family 2 both the affected sisters were compound heterozygote for the maternal variant *C10orf2* c.1321T>G p.(Trp441Gly) and the paternal variant *C10orf2* c.1519G>A p.(Val507Ile). The two unaffected sisters in this family were homozygous wild type for both variants (Morino et al. 2014).

All the variants in these families are located in the helicase domain of the Twinkle protein. A bacterial homologue was used to assess the possible impact of the variants on the structure and function of Twinkle. In the bacterial Twinkle the residues equivalent to p.Arg391 and p.Trp441 are proximal to the linker region and interact with each other. It is thought that the substitution of these residues will cause a shift in the conformation of Twinkle in regards to the linker region and affect heptamer/hexamer formation. The residue p.Trp441 is highly conserved in vertebrates. The bacterial equivalent of residue p.Val507 interacts with p.Ile514 and the linker of the neighbouring subunit in complex formation. The residues at these two positions are always two valines or valine and isoleucine. It is thought the combination of the two large isoleucine side chains will cause slight conformational shift altering interactions with the linker of the neighbouring subunit. The equivalent of p.Asn585 is located in the active site of the helicase domain and the substitution of this residue with a serine is thought to reduce the effectiveness of the active site (Morino et al. 2014).

Additional patients with Perrault syndrome due to variants in *C10orf2* have also been reported, all of these patients displayed neurological phenotypes (Table 1.4).

In a single Norwegian patient with Perrault syndrome causative variants in *C10orf2* were identified by whole exome sequencing (Demain et al. 2017b). The patient presented with severe/profound bilateral SNHL and primary amenorrhea. This proband displayed the severe neurological phenotype seen in other patients with variants in *C10orf2* including progressive ataxia, nystagmus, areflexia and a severe progressive peripheral neuropathy.

Severe atrophy of the cerebellum was seen on MRI. Whole exome sequencing performed on the proband identified compound heterozygous variants in *C10orf2*; c.968G>A, p.(Arg323Gln) and c.1196A>G p.(Asn399Ser). The residue Arg323 is situated in the linker region of Twinkle like the variants found in the families described by Morino et al. (2014). The residue Asn399 is situated in the helicase domain of Twinkle (Demain et al. 2017b).

A homozygous variant in *C10orf2* was identified in consanguineous Moroccan family with three affected individuals, two female and one male (Lerat et al. 2016). All affected individuals displayed severe pre-lingual SNHL and the two affected female patients had primary amenorrhea. Interestingly the affected male in this family was fertile and had 3 children. All affected individuals had sensorimotor neuropathy and ataxia and one affected female had arachnodactyly (Lerat et al. 2016). Affected individuals were homozygous for the variant *C10orf2* c.793C>T p.(Arg265Cys) which was identified using a next generation sequencing panel containing 35 hearing loss genes including the five Perrault syndrome genes identified at the time of publication (Lerat et al. 2016).

In a pair of sisters with Perrault syndrome due to variants in *C10orf2* in-depth examination showed atrophy of the vestibulocochlear nerve and auditory neuropathy was behind the hearing loss in these patients (Oldak et al. 2017). Both patients in this non-consanguineous Polish family presented with SNHL, which was significantly worse at high frequencies, and primary amenorrhea with streak ovaries. Both sisters displayed the neurological phenotype associated with Perrault syndrome due to variants in *C10orf2,* which was more severe in the elder sister, including ataxia, nystagmus and sensorimotor neuropathy. Whole exome sequencing identified compound heterozygous variants in *C10orf2* c.1196A>G p.(Asn399Ser) and c.1802G>A p.(Arg601Gln) (Oldak et al. 2017). *C10orf2* c.1196A>G p.(Asn399Ser), which has previously been reported in another patient with Perrault syndrome (Demain et al. 2017b) was predicted to disrupt hexamer/heptamer formation. c.1802G>A p.(Arg601Gln) was predicted to impair ATP binding required for the enzymatic function of Twinkle (Oldak et al. 2017). Detailed analysis of the auditory phenotype revealed atrophy of the vestibulocochlear nerve (Oldak et al. 2017) correlating with the results of Nishio et al. (2017) which showed other Perrault syndrome genes (*HSD17B4*, *HARS2*, *LARS2* and *CLPP*) were expressed at high levels in the auditory nerves. The authors proposed that the audiological data suggested

the defect behind the hearing loss in this family is situated in the synapse of the hair cells and auditory nerves (Oldak et al. 2017).

Individual ID	Family 1, II-1	Family 1, II-3	Family 2, II-2	Family 2, II-4	P4:II-1
Variant	c.1172G>A p.(Arg391His), c.1754A>G p.(Asn585Ser)		c.1321T>G p.(Trp441Gly), c.1519G>A p.(Val507Ile)		c.968G>A p.(Arg323Gln), c.1196A>G p.(Asn399Ser)
Reference	(Morino et al. 2014)				(Demain et al. 2017b)
Ethnicity	Japanese		American (Greek and mixed European)		Norwegian
Consanguinity	N		N		N
Sex	F	F	F	F	F
Karyotype	46, XX	46, XX	46, XX	46, XX	NR
Age (yrs) at last assessment	40	34	36	31	48
Sensorineural hearing loss					
age at diagnosis (yrs)	13	8	7	7	3
degree of hearing loss	NR	NR	Severe	Moderate	Severe/Profound
Notes	N		N		N
Intervention	NR	NR	NR	NR	Bilateral CI
Gonadal dysfunction					
pelvic ultrasound	Gonadal dysgenesis		Streak ovaries		Small uterus and ovaries
menarche	N		N		N
POI - Age if menarche achieved	NA		NA		NA
Follicle stimulating hormone	95 (3.5–12.5) IU/L	200 (3.5–12.5) IU/L	NR		NR
Luteinising hormone	31(2.4–12.6) IU/L	34 (2.4–12.6) IU/L	NR		NR
estradiol	10.5 (25–195) pg/mL	10.3 (25–195) pg/mL	NR		NR
Neurological features	Slowly progressive ataxia, sensory axonal neuropathy, mild opthalmoplegia, nystagmus		Ataxia, peripheral neuropathy, hyporeflexia, nystagmus, seizures (II-2 only), white matter changes		Severe progressive sensory motor neuropathy, atrophy of cerebellum, nystagmus
Additional features	high-arched palate, pes cavus		N		Scoliosis

Table 1.4. The genotypes and phenotypes of individuals with Perrault syndrome due to variants in *C10orf2*.

Continued next page.

Individual ID	XII-1	XII-2	XII-3	Oldak Proband	Oldak Sister
Variant	c.793C>T p.(Arg265Cys)			c.1196A>G p.(Asn399Ser), c.1802G>A p.(Arg601Gln)	
Reference	(Lerat et al. 2016)			(Oldak et al. 2017)	
Ethnicity	Moroccan			Polish	
Consanguinity	Y			N	
Sex	F	F	M	F	F
Karyotype	NR			46, XX	46, XX
Age (yrs) at last assessment	NR			27	19
Sensorineural hearing loss					
age at diagnosis (yrs)	>3			5	12
degree of hearing loss	Severe			Mild LF, Severe HF	NR
Notes	N			Worse at high frequencies	
Intervention	NR			Hearing aids (limited benefit)	NR
Gonadal dysfunction					
pelvic ultrasound	NR			Rudimentary uterus, streak ovaries	Ovarian dysgenesis
menarche	N			N	N
POI - Age if menarche achieved	NA			NA	NA
Follicle stimulating hormone	NR		NR	NR	
Luteinising hormone	NR		NR	NR	
estradiol	NR		NA	NR	
Neurological features	Ataxia, sensory-motor polyneuropathy			Ataxia, nystagmus, sensorimotor neuropathy, cerebellar atropy (proband only)	
Additional features	Arachnodactyly (XII-2 only), affected male fertile			High arched palate, Hashimoto's thyroiditis, partial atrophy of the vestibulocochlear nerve	

Table 1.4. The genotypes and phenotypes of individuals with Perrault syndrome due to variants in *C10orf2*.

Y, yes. N, no. M, male. F, female. NR, not recorded. NA, not applicable. CI, cochlear implant. LF, low frequency. HF, high frequency. If one variant is noted the individual is homozygous for this variant. All hearing loss is bilateral unless noted otherwise. For hormone levels the reference values, where available, are indicated in the brackets next to the patient levels.

To date all cases of Perrault syndrome due to variants in *C10orf2* have presented with a severe neurological phenotype. Neurological symptoms may be associated with Perrault syndrome due to variants in *C10orf2* or as suggested with *CLPP* this may be the result of ascertainment bias.

There is significant overlap between the symptoms of Perrault syndrome and MTDPS7. The proposed cases of Perrault syndrome noted above have many of the clinical presentations associated with MTDPS7 and no additional symptoms. The affected women reported by Morino et al. (2014) also showed elevated levels of lactate and pyruvate which has not been associated with Perrault syndrome. The symptoms make these severe cases of Perrault syndrome or mild cases of MTDPS7. Testing for mtDNA deletions and depletion, which would have confirmed or refuted a diagnosis of MTDPS7, was not performed on the muscle biopsies taken (Morino et al. 2014). It may be that given the symptoms and the molecular pathology that the diagnosis of Perrault syndrome will be revised in these cases.

1.3.6 *ERAL1*

A homozygous variant in *ERAL1* was identified in four individuals with Perrault syndrome in a genetically isolated population (Chatzispyrou et al. 2017). ERAL1 (Era-Like 1) is a chaperone of mitochondrial 12S rRNA and protects the rRNA from degradation during the biogenesis of the mitochondrial 28S small ribosomal subunit. Depletion of ERAL1 results in the degradation of 12S rRNA and halts the biogenesis of the mitochondrial 28S ribosomal subunit (Dennerlein et al. 2010). ERAL1 is removed from the mitochondrial ribosome by CLPXP a proteolytic complex containing CLPP, variants in which are also associated with Perrault syndrome (Szczepanowska et al. 2016;Jenkinson et al. 2013).

Using whole exome sequencing a homozygous variant, *ERAL1* c.707A > T p.(Asn236Ile), was identified in two unrelated individuals with Perrault syndrome from the same small village (Chatzispyrou et al. 2017). Patient 1 was 66 years of age and presented with hearing loss at 20 years of age and secondary amenorrhea at 27 years of age. Patient 2 was diagnosed with SNHL, with a greater loss at high frequencies, at 4 years of age. Primary amenorrhea with streak ovaries and a small uterus was noted at 18 years of age in patient 2. Ovarian biopsy showed no primordial follicles. The father of patient 2 was

also homozygous for the variant in *ERAL1* and presented with SNHL but had three children suggesting males with Perrault syndrome due to this *ERAL1* variant are fertile. This variant was not identified in any public database but was found to have a minor allele frequency of 4.6% in the village, which is a known genetic isolate, highlighting a possible founder variant. Subsequently an additional female with Perrault syndrome was identified with primary amenorrhea and congenital progressive SNHL who was also from the same village and was homozygous for the variant, *ERAL1* c.707A > T p.(Asn236Ile) (Chatzispyrou et al. 2017).

No neurological symptoms were reported in any of the four patients with Perrault syndrome due to *ERAL1*. Patient 1 was 66 years of age at the time of genetic diagnosis (Chatzispyrou et al. 2017). We would expect that any early onset neurological symptoms associated with Perrault syndrome would have been apparent at this age. It appears that neurological symptoms are not associated with the variant *ERAL1* c.707A > T p.(Asn236Ile). This contrasts with variants in *CLPP*, which as discussed above often are associated with neurological phenotypes. This may be due to slightly different pathological mechanisms, additional roles of CLPP in the mitochondrial matrix or ascertainment bias of *CLPP* cases toward neurological phenotypes. Other variants in *ERAL1* may be associated with Perrault syndrome, or additional phenotypes, which may include neurological features.

Using an alignment with a bacterial orthologue Chatzispyrou et al. (2017) predicted that the variant, *ERAL1* c.707A > T (p.Asn236Ile) may disrupt the protein conformational change and subsequently disrupt the interaction of ERAL1 with mitochondrial 12S rRNA. Detailed biochemical investigation was undertaken using fibroblasts from patient 1 and patient 2. Western blots showed that levels of ERAL1 were reduced in the patient cells. The levels of proteins of the 28S ribosomal subunit were reduced in patient cells, with levels of the 39S ribosomal subunit unaffected (Chatzispyrou et al. 2017). It has been previously shown in cells that depletion of ERAL1 causes the loss of the 28S ribosomal subunit and degradation of the 12S rRNA (Dennerlein et al. 2010). In line with the findings of Dennerlein et al. (2010) the ratio of 12S to 16S rRNA was reduced in the patient cells. The reduction of 12S rRNA was rescued by lentiviral expression of wildtype ERAL1 in patient fibroblasts (Chatzispyrou et al. 2017).

Mitochondrial translation was affected in patient cells with reduced levels of components of oxidative phosphorylation complexes encoded by mitochondrial DNA, with no reduction in those encoded by nuclear DNA, indicating a generalised defect of mitochondrial translation. The defect in mitochondrial translation led to a reduced rate of oxygen consumption in the patient cells (Chatzispyrou et al. 2017). Knockdown of *ERAL1* homologue E02H1.2 in *C. elegans* recapitulated the Perrault syndrome phenotype with the adult worms being infertile and showing a reduced rate of oxygen consumption (Chatzispyrou et al. 2017). *C. elegans* has previously been used a model for the fertility phenotype of Perrault syndrome with the knockdown of *HARS2* and *LARS2* homologues both resulting in infertility in adult *C. elegans* (Pierce et al. 2011;Pierce et al. 2013).

It has been theorised that disrupted mitochondrial proteostasis (Jenkinson et al. 2013), possibly leading to defects of the oxidative phosphorylation pathway (Mayr et al. 2015), is the pathology behind Perrault syndrome. The experimental data generated by Chatzispyrou et al. (2017) using fibroblasts from patients with defects in ERAL1 provides the first direct evidence linking defects in mitochondrial proteostasis and mitochondrial respiration with Perrault syndrome.

1.3.7 Screening genes

Some of the Perrault syndrome genes detailed above, and additional genes associated with either POI or SNHL, have been screened for causative variants in Perrault syndrome families. It is important to note than in all of these studies only the coding exonic regions were screened and not the introns and promoter regions.

In one study eight families with Perrault syndrome were screened for variants in *HSD17B4* and *HARS2* but no variants of significance were identified. (Jenkinson et al. 2012). *HSD17B4, HARS2* and *PSMC3IP*, a POI candidate gene, were screened in a single patient with Perrault syndrome and marfanoid proportions. No causative variants were identified (Kim et al. 2013). This patient was later screened by whole exome sequencing and no putative pathogenic variants were found in the three remaining Perrault syndrome genes known at the time of publication (*CLPP, LARS2* and *C10orf2*) or in 90 additional hearing loss genes (Demain et al. 2017b).

In four cases of Perrault syndrome across three families' five candidate genes were tested and excluded. The genes tested were: *GJB2,* variants which are responsible for the most common cause of genetic hearing loss; *FOXL2*, implicated in POI; and *POLG, FRDA* and *AOA1*, which are implicated in ataxia or ophthalmoplegia (Marlin et al. 2008).

Demain et al. (2017b) screened eight families with Perrault syndrome using whole exome sequencing. In five families causative variants were identified in known Perrault syndrome genes. In three families, including the individual with marfanoid body proportions noted above (Kim et al. 2013), there were no putative pathogenic variants identified in the five Perrault syndrome genes known at the time of the study (*HSD17B4, HARS2, LARS2, CLPP, C10orf2*). In the three families with genetically unresolved Perrault syndrome 90 hearing loss genes were also assessed with no putative pathogenic variants identified. In this report there were no obvious phenotypic differences identified between the resolved and genetically unresolved cases (Demain et al. 2017b).

Lerat et al. (2016) screened fourteen families with Perrault syndrome using a NGS panel containing the exonic regions for 35 hearing loss genes including the five Perrault syndrome genes known at the time of the publication (*HSD17B4, HARS2, LARS2, CLPP, C10orf2*). In four of the families causative biallelic variants were identified in known Perrault syndrome genes. In three families a single heterozygous variant was identified in a known Perrault syndrome gene. These cases are not considered genetically resolved. In one family two affected individuals (X-1 and X-2) were heterozygous for the variant *LARS2* c.1565C>A p.(Thr522Asn). The affected individuals in this family had low frequency hearing loss which has been previously associated with this variant in *LARS2*. In the additional two families a single rare heterozygous variant was identified in *LARS2* and *HSD17B4* respectively, the variants had not been previously associated with Perrault syndrome. It is not known in these three families whether there are additional undiscovered variants in *LARS2* or *HSD17B4* or that the causative variants are in a gene not currently associated with Perrault syndrome (Lerat et al. 2016). There were also seven Perrault syndrome families where no putative pathogenic variants were identified in any of the 35 genes comprising the panel, including the five Perrault syndrome genes. Again there were no phenotypic differences noted between the resolved and genetically unresolved cases (Lerat et al. 2016).

Whole exome sequencing and the NGS panel used in Lerat et al. (2016) only cover exonic regions. It is possible that in some genetically unresolved cases of Perrault syndrome screened by these methods there are additional variants in these genes which may be intronic, in a promotor region (Lerat et al. 2016) or large copy number variations which are difficult to identify using these methods. In these cases sequencing the full gene and cDNA may prove useful. Screening studies highlight the genetic heterogeneity of Perrault syndrome and also are a strong indicator there may be genes associated with Perrault syndrome which have not yet been identified (Demain et al. 2017b;Lerat et al. 2016).

1.4 Mitochondria and Perrault syndrome

Mitochondria are organelles which exist in varying numbers in every nucleated eukaryotic cell. The main function of mitochondria is to produce ATP from ADP using the oxidative phosphorylation (OXPHOS) process. During OXPHOS four complexes create a proton gradient across the mitochondrial inner membrane which the fifth complex harnesses to generate ATP from ADP. In addition to the OXPHOS process mitochondria have roles in pathways which include apoptosis, steroid metabolism, ion homeostasis and FeS cluster production (Reeve and Lightowlers 2012).

Mitochondria are thought to have originated from an event millions of years ago when a bacterium was engulfed by another cell with which it subsequently formed a symbiotic relationship. Mitochondria maintain a small circular genome of 16.5 kb, present in multiple copies per cell, and unique translation machinery (Reeve and Lightowlers 2012;Richman et al. 2014). Reflecting their bacterial origin mitochondrial DNA (mtDNA) is more similar to bacterial DNA than eukaryotic nuclear DNA. During the evolution of mitochondria most mitochondrial genes have been transferred to the nuclear genome and the majority of mitochondrial proteins are now encoded by nuclear DNA. MtDNA retains just 22 tRNAs, 2 ribosomal RNAs and 13 genes encoding components of the OXPHOS complexes (Reeve and Lightowlers 2012).

Mitochondrial transcription and translation are different from their nuclear counterparts in a number of aspects (Reeve and Lightowlers 2012). MtDNA is transcribed as long polycistronic transcripts in contrast to nuclear DNA which is transcribed as individual genes. These long mitochondrial transcripts contain multiple genes and other RNA species

with little non-coding RNA and no introns. These differences mean mitochondrial RNA is processed differently from nuclear RNA. Mitochondrial tRNAs are located between the genes and it is the processing of the tRNAs at the 5' and 3' ends which release the other RNA species from the polycistronic transcripts. This is known as the punctuation model of release (Ojala et al. 1981). Mitochondrial translation follows the same steps as nuclear translation; initiation, elongation, termination and recycling of the ribosome. The mitochondrial ribosome is considerably more protein rich than the nuclear ribosome with a protein to RNA ratio of approximately 70%. In contrast the nuclear ribosome is composed of approximately 35% protein to 65% RNA. There are also a number of codon differences between the mitochondrial and nuclear genome, for example UGA encodes tryptophan instead of a stop codon in vertebrate mitochondria (Reeve and Lightowlers 2012). This is not an exhaustive list but highlights some of the major differences in the nuclear and mitochondrial translation processes.

Mitochondrial dysfunction is associated with spectrum of disease with a wide phenotypic range. Variants in both mitochondrial DNA and nuclear genes encoding mitochondrial proteins have been linked to mitochondrial dysfunction (Chinnery 2014). Phenotypes may range from organ specific mild disorders such as Lebers hereditary optic neuropathy (Yu-Wai-Man et al. 2002) to severe early onset multisystemic conditions such as Leigh syndrome (Thorburn and Rahman 2014). Variants in both mitochondrial DNA and in nuclear genes encoding mitochondrial proteins have been linked to hearing loss. Variants in the mitochondrial DNA encoded gene *MT-TS1* have been linked to childhood onset SNHL (Pandya 2014). Variants in the nuclear encoded gene *BCS1L*, a mitochondrial ATPase, can cause Bjőrnstad syndrome, characterized by pili torti and sensorineural hearing loss (Hinson et al. 2007). Variants in three mitochondrial aminoacyl synthetase genes, *NARS2* as well as the previously mentioned *HARS2* and *LARS2*, have been linked to hearing loss (Simon et al. 2015;Pierce et al. 2011;Pierce et al. 2013). The pathogenic mechanisms behind hearing loss due to mitochondrial dysfunction are unclear.

Mitochondrial dysfunction has also been linked to infertility. Mitochondrial dysfunction associated with infertility is mainly associated with variants in nuclear genes and is often syndromic (Demain et al. 2017a). For example variants in *POLG* can cause Parkinsonism and premature menopause (Luoma et al. 2004). It appears fertility, especially the ovaries,

are sensitive to dysfunction in the mitochondrial translation pathway. As with mitochondrial linked hearing loss the pathogenic mechanisms behind this dysfunction are unclear (Demain et al. 2017a). Mitochondrial disorders often have unexplained tissue specificity. It has been suggested that different tissues have differing ways to supress the pro-apoptotic pathway induced by mitochondrial stress and thus supress the phenotype. The affected tissues may be more susceptible to the particular stress pathway induced by the variant (Raimundo et al. 2012)

Mitochondrial dysfunction has been shown to cause both hearing loss and infertility, with the ovaries appearing to be particularly affected by dysfunction of the mitochondrial translation pathway (Demain et al. 2017a). Five of the six Perrault genes function in the mitochondria. If we exclude the genes with an alternative diagnosis, *HSD17B4* and *C10orf2*, the remaining genes associated with Perrault syndrome function in the mitochondrial translation pathway. Variants in *ERAL1* have been directly linked to mitochondrial dysfunction through disruption of the mitoribosome (Chatzispyrou et al. 2017). It appears that disruption of mitochondrial translation may be the pathogenic mechanism behind a number of cases of Perrault syndrome. We might expect that novel Perrault syndrome genes would also function in the mitochondrial translation pathway (Demain et al. 2017b).

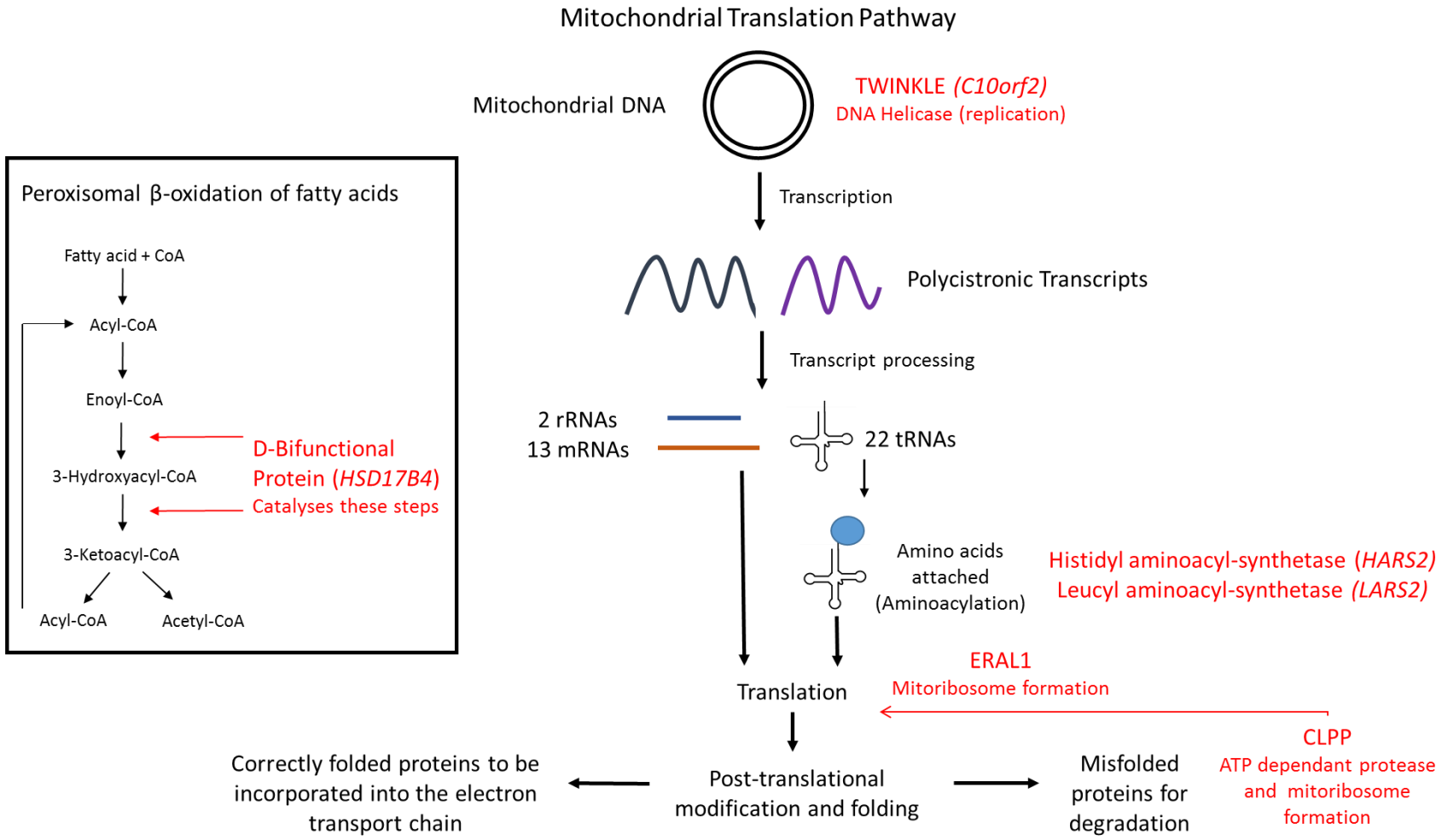

Figure 1.5. The function of Perrault syndrome Genes

Perrault syndrome genes are shown in red in the pathway in which they function.

1.5 Coincidental Perrault syndrome

There has been a report of an individual with Perrault syndrome due to digenetic inheritance, with variants in two separate genes causing hearing loss and POI respectively (Faridi et al. 2017). Bilateral severe to profound hearing loss was reported in multiple individuals in a large consanguineous family. Multiple females were reported to have hearing loss but only one female, the proband, was affected with hearing loss and POI. It was theorised that the genetic cause of hearing loss and POI in the proband was either a Perrault syndrome gene with partial penetrance for POI or that the hearing loss and POI seen in the proband were caused by variants in separate genes. Upon genetic investigation it was found that all the individuals with hearing loss including the proband with Perrault syndrome were homozygous for a known pathogenic variant, *CLDN14* c.254T>A p.(Val85Asp) (Faridi et al. 2017). *CLDN14* encodes a tight junction protein expressed in auditory hair cells and biallelic variants in *CLDN14* are known to cause SNHL (Wilcox et al. 2001). The proband was also found to be homozygous for a frameshift variant *SGO2* c.1453_1454delGA p.(Glu485Lysfs*5). There were no other individuals homozygous for *SGO2* c.1453_1454delGA p.(Glu485Lysfs*5) in the family although multiple members of the family were heterozygous for the variant (Faridi et al. 2017). In mice *SGO2* is involved in sister chromatid separation during meiosis and in knockout *SGO2* mice both sexes are infertile (Llano et al. 2008). This is the first reported case of *SGO2* in human disease (Faridi et al. 2017).

This project will not be focusing on cases of coincidental Perrault syndrome. The report from Faridi et al. (2017) highlights the importance of looking at common causes of hearing loss in Perrault syndrome patients who have no putative pathogenic variants in known Perrault syndrome genes. As both hearing loss and infertility are common there may be additional cases of coincidental Perrault syndrome and in small families it may be impossible to distinguish this from true Perrault syndrome without molecular diagnosis. As in the case presented by Faridi et al. (2017) the molecular mechanisms of coincidental Perrault syndrome may differ from monogenic Perrault syndrome and so prognosis and or treatment could differ. Therefore it is important to molecularly distinguish between Perrault syndrome and co-incidental Perrault syndrome.

1.6 The role of next generation sequencing in the discovery of novel and rare variants

Historically the task of detecting novel or rare variants was difficult. Linkage analysis requires the recruitment of large families with multiple affected individuals (Nsengimana and Bishop 2012) and homozygosity mapping is only possible in consanguineous families (Boycott et al. 2013). If families are non-consanguineous or small with few affected individuals, linkage analysis and homozygosity mapping are not viable methods to discover the cause of rare diseases. This has proved to be challenging in Perrault syndrome. The use of techniques such as Sanger sequencing necessitated a candidate gene or region hypothesis be formed, usually from data generated by the aforementioned techniques, or whole genome mapping be used. Whole genome mapping using Sanger sequencing was both prohibitively time-consuming and expensive so not a viable option in identifying these rare variants (Boycott et al. 2013). The advent of next generation sequencing changed the outlook for the discovery of novel and rare variants (Boycott et al. 2013) including those implicated in Perrault syndrome.

The rise of next generation sequencing (NGS), also referred to as massively parallel sequencing, has been exponential. When the human genome project was completed in 2003 it had taken 13 years and cost approximately 2.7 billion dollars (Voelkerding et al. 2009). In comparison modern next generation sequencers can generate a full human genome in under 3 days with a price fast approaching the $1000 genome target (Check Hayden 2014). All this means that it is possible to quickly and economically identify novel causative variants without having previously identified a region or candidate gene. In rare syndromes where families are small and few candidates are available for analysis this has meant gene identification has made rapid progress. It is expected the genetic causes of the approximately 3500 monogenic diseases remaining will be identified before 2020 (Boycott et al. 2013).

At this point in time the main limiting factor for whole genome sequencing has become the data analysis bottleneck. A vast amount of data is generated from whole genome next generation sequencing and requires massive computer processing power to reassemble the short sequence reads and filter out the irrelevant data (Bamshad et al. 2011). A

solution to this is to perform whole exome sequencing. The exome consists of 1-2 % of the entire genome but it is estimated that approximately 85% of the variants for Mendelian conditions lie within these coding regions. Using this approach the amount of relevant data generated is maximised and the analysis time minimised even compared to traditional linkage and homozygosity mapping (Bamshad et al. 2011). The coding regions of the human genome are also relatively well characterised and commercial kits are available for whole exome sequencing making this an easier option. There is a risk with exome sequencing that the variant of interest will not be situated in a coding region or it will lie in a region with poor coverage or sequence definition such as in a GC rich region. This risk is mitigated by the low likelihood of the variant being situated in a region not covered by whole exome sequencing versus the saving in time and cost in comparison to whole genome sequencing (Bamshad et al. 2011). All of the above factors make whole exome sequencing an excellent choice for identifying novel genes associated with Perrault syndrome.

Next generation sequencing is now being used for clinical diagnosis and targeted NGS panels such as OtoSCOPE are available for the molecular diagnosis of genetic hearing loss (Yan et al. 2013). It may be that if the genes for Perrault syndrome are included in these panels in the future we could detect the syndrome in sporadic males and pre-pubescent girls. While these panels are useful in a clinical setting, over two studies less than 50% of families with Perrault syndrome had causative variants in a known Perrault syndrome gene (Demain et al. 2017b;Lerat et al. 2016), making them of less use in a research setting. When NGS technology reaches a point where whole exome sequencing is routinely performed as a diagnostic test for genetic hearing loss then the characterisation of Perrault genes may also aid diagnosis.

1.7 Current challenges and controversies

There are currently a number of unanswered questions regarding Perrault syndrome. The lack of genotype phenotype links especially in the case of neurological features makes it difficult to provide a prognosis for some patients and makes using a phenotype to predict a genotype for genetic testing difficult. As more Perrault syndrome cases are reported upon the genotype phenotype links should become clearer.

The debate detailed previously over whether the two sisters with the variants in *HSD17B4* (Pierce et al. 2010) should be classified as DBP deficiency type IV raises a question, if there had been an affected male in that family would he have had gonadal failure or neurological symptoms, and if so would the diagnosis still have been Perrault syndrome? The newly defined DBP deficiency type IV has a large clinical overlap with Perrault syndrome and the lack of many of the classical biochemical markers of DBP deficiency in these patients (McMillan et al. 2012) has added another layer of difficulty to the diagnosis of Perrault syndrome. DBP is a known factor in the oestrogen and androgen pathway (de Launoit and Adamski 1999). The molecular basis of ovarian dysfunction in the two sisters may be different than in the other cases of genetically characterised Perrault syndrome, meaning the therapeutic opportunities may also be different. From the genes implicated in Perrault syndrome thus far five out of six are involved in mitochondrial function, *C10orf2* via mitochondrial DNA maintenance (Morino et al. 2014) and *HARS2, LARS2*, *CLPP* and *ERAL1* via mitochondrial translation (Pierce et al. 2011;Pierce et al. 2013;Jenkinson et al. 2013;Chatzispyrou et al. 2017). It has been suggested by Lieber et al. (2014) that *HSD17B4* might also be involved in mitochondrial function. The patient in their study was diagnosed as DBP deficient type IV but initially the clinical presentation had led to the speculation that there was mitochondrial involvement. This was supported by the discovery of a mild respiratory chain deficiency at muscle biopsy. It was noted that *HSD17B4* has been predicted *in silico* to be part of the mitochondrial proteome (Pagliarini et al. 2008) and Lieber et al. (2014) speculate that DBP may be dual localised to peroxisomes and mitochondria. This adds further difficulty in distinguishing between Perrault syndrome DBP deficient type IV, if there is in fact any difference. Perrault syndrome with neurological features has a significant phenotypic overlap with MTDSP7 (Morino et al. 2014) and the question of whether the reported cases with variants in *C10orf2* are Perrault syndrome or mild MTDSP7 is also applicable here.

A question that remains to be answered is whether males affected by Perrault syndrome have a fertility phenotype? Male fertility in Perrault syndrome is usually presumed to be normal although exceptions have been reported. A single male patient with Perrault syndrome due to variants in *CLPP* presented with azoospermia (Demain et al. 2017b) and in the knockout *Clpp* mouse both sexes are infertile (Gispert et al. 2013). Conversely

affected males in a family with Perrault syndrome due to variants in *HARS2* (Pierce et al. 2011) and a male with Perrault syndrome due to variants in *C10orf2* (Lerat et al. 2016) have had unaffected children. The uncertainty here is compounded by two factors; the under ascertainment of males with Perrault syndrome and the fact that male fertility is not routinely assessed in males with Perrault syndrome.

The diagnosis of Perrault syndrome based upon clinical data is difficult even with multiple affected members of the same family and without additional affected family members it is even more difficult. The ascertainment of individuals is heavily biased in favour of both post-pubertal females and individuals with neurological phenotypes. A way to answer the questions raised by the difficulty of clinical diagnosis may be to supplement it with genetic and molecular data. As Ahmed et al. (2015) demonstrated it is achievable to diagnose Perrault syndrome in prepubescent patients with a combination of the clinical and genetic data. This approach may also go some way to addressing some of the sex biased questions remaining around the syndrome such as male fertility. At present the genetic identification of Perrault syndrome in males and pre-pubescent females remains biased towards patients with neurological phenotypes. The increasing availability of next generation sequencing, through both panel testing and whole exome sequencing, in a diagnostic setting may improve ascertainment.

1.8 Project aims

Hypothesis: Variants in novel genes are associated with Perrault syndrome

Project Aims;

To undertake mapping and sequencing studies in families with Perrault syndrome for the identification of novel Perrault syndrome genes.

Screening has indicated that the cause of Perrault syndrome in a number of families may be in previously unidentified Perrault genes (Jenkinson et al. 2012;Kim et al. 2013;Demain et al. 2017b;Lerat et al. 2016).

The aim of this project is to use whole exome sequencing to uncover the genetic causes of Perrault syndrome in the Manchester cohort of affected patients. At least one affected member of each family will be screened using whole exome sequencing. Autozygosity

mapping will be used in consanguineous families to further filter the whole exome sequencing results. Sanger sequencing will be used to confirm the variants segregate with the affected individuals and are consistent with the mode of autosomal recessive inheritance.

The molecular evidence to date defines Perrault syndrome as a mitochondrial disorder. If the variants in *HSD17B4* and *C10orf2* are omitted due to differential diagnosis then it appears that Perrault syndrome is a disorder of mitochondrial translation. It is expected that any new genes discovered to be associated with Perrault syndrome will have a role in mitochondrial function and may be involved in mitochondrial translation.

To undertake functional characterisation of variants in novel disease causing genes.

While variants in known genes may provide insights into genotype phenotype correlations the main focus of this project is to identify novel Perrault syndrome genes. To provide some confirmation of pathogenicity functional work will be performed. The nature of the functional work and the direction the research will take will be defined by the variants and genes identified by exome sequencing. Promising candidate genes, especially those with a function within the mitochondrial translation pathway will be prioritised for study.

To further define the molecular cause of Perrault syndrome.

A promising strategy for genetically identifying Perrault syndrome may lie in elucidating the molecular pathway of this pathology. Elucidating the molecular basis of Perrault syndrome could assist in assessing the likelihood that any variants in previously unidentified genes are causative of the Perrault syndrome phenotype. By undertaking the variant identification strategy and functional characterisation detailed above we hope to generate data that can be used to aid in the molecular diagnosis of other patients, enable us to further understand the pathological mechanisms behind Perrault syndrome and may provide possible targets for therapeutics. It may also provide insight into some of the molecular mechanisms behind ovarian dysfunction and sensorineural hearing loss, which could identify possible therapeutic targets for these conditions.

Chapter 2. Materials and methods

This chapter details the general materials and methods used to produce the data in this thesis. Additional chapter specific details are available in each experimental chapter.

2.1. Ethical approval

All patients provided written informed consent in accordance with local regulations. Ethical approval for this study was granted by the National Health Service (NHS) Ethics Committee (16/WA/0017) and University of Manchester. The National Institutes of Health (NIH) Animal Use Committee approved protocol 1263-15 to Thomas B. Friedman for mice.

2.2. Patient samples

Patient samples were provided from the referring clinician as blood (for DNA extraction only), skin biopsies, primary fibroblast cultures or DNA.

2.2.1. Patient dermal fibroblasts

Patient Dermal Fibroblasts were provided as either primary fibroblast cultures or as skin biopsies. Primary fibroblast cultures were prepared and maintained in Eagle's minimal essential medium (MEM) (Sigma-Aldrich, St. Louis, MO, USA) supplemented with 10% (v/v) foetal calf serum, 1 × non-essential amino acids, 1 mm sodium pyruvate, 50 µg/ml uridine and 100 mg/L ampicillin, and stored in liquid nitrogen by the NHS Genomic Diagnostic Laboratory at the Manchester Centre for Genomic Medicine, an accredited medical laboratory.

2.2.2. Patient DNA storage

Patient DNA, either extracted as in section 2.3.1 or provided by the referring clinician was quantified using the NanoDrop 8000 (Thermo Fisher Scientific Inc, Waltham, MA, USA) and stored at -20°C in the NHS Genomic Diagnostic Laboratory Archive at the Manchester Centre for Genomic Medicine.

2.3. DNA extraction, precipitation and quantification

2.3.1. DNA extraction from patient blood samples.

DNA was extracted by the NHS Genomic Diagnostic Laboratory at the Manchester Centre for Genomic Medicine, an accredited medical laboratory. M-PVA Magnetic Bead

Technology processed using the chemagic MSM I instrument (both PerkinElmer, Waltham, MA, USA, extraction performed according to manufacturer protocol) was used to extract DNA from peripheral blood lymphocytes from affected individuals and relatives.

2.3.2. Plasmid DNA extraction.

Plasmid DNA was extracted using both the GenElute Plasmid Miniprep Kit (Sigma-Aldrich, St. Louis, MO, USA) and NucleoSpin Plasmid Miniprep Kit (Macherey-Nagel, Düren, Germany) according to manufacturer protocol. To produce large amounts of plasmid DNA for gene gun transfection or storage, a 50ml overnight culture of the transformed *E.coli* strain was prepared and plasmid DNA extracted using the GenElute Plasmid Midiprep Kit (Sigma-Aldrich, St. Louis, MO, USA) or NucleoSpin Plasmid Midiprep Kit (Macherey-Nagel, Düren, Germany) according to manufacturer protocol.

2.3.3. Genomic DNA extraction from yeast

1.5ml of yeast overnight culture was centrifuged (1000xg, 5mins). The supernatant was removed and the pellet resuspended in 500ml of water before repeating the previous centrifugation step. The supernatant was removed and lysis buffer (10mM Tris-Cl (pH 8), 1mM EDTA, 100mM NaCl, 1% sodium dodecyl sulfate (SDS) and 2% Triton-X 100) (200µl), acid washed glass beads (200-300µl) and PCA (Phenol:chloroform:isoamyl alcohol, Tris buffered) (200µl) were added. The solution was mixed by vortex and centrifuged (14,000xg, 5mins). The aqueous phase was transferred to a new tube and two volumes of 100% ethanol added. The solution was centrifuged (14,000xg, 5mins) and the supernatant discarded. The DNA pellet was washed with 95% ethanol and air dried. The dry pellet was re-suspended in 100µl of TE buffer (10mM Tris-Cl (pH8), 1mM EDTA).

2.3.4. DNA quantification

All DNA quantification was performed using NanoDrop spectrophotometer instruments. Models used were the NanoDrop 8000, NanoDrop 2000 and NanoDrop Lite (Thermo Fisher Scientific Inc, Waltham, MA, USA).

2.4. Autozygosity mapping

Genome wide single nucleotide polymorphism (SNP) and copy number variation (CNV) data was generated using the Genome-Wide Human SNP Array 6.0 (SNP 6.0 Array) (Affymetrix, Inc. Santa Clara, CA, USA) according to manufacturer protocol. Genotyping calls were made by the Affymetrix Genotyping console using the default parameters (Birdseed V2 algorithm, Confidence Threshold 0.1, Block Size 0). Autozygosity mapping was performed using the genotyping data and the AutoSNPa program (http://dna.leeds.ac.uk/autosnpa/) (Carr et al. 2006).

2.5. Whole exome sequencing

Whole Exome Sequencing in this project was performed using either the SOLiD (Thermo Fisher Scientific Inc, Waltham, MA, USA) or the HiSeq (Illumina, San Diego, CA, USA) instruments. The SOLiD and HiSeq use next generation sequencing technologies which function based on different principles.

SOLiD (Sequencing by Oligonucleotide Ligation and Detection) sequencing works on the principle of sequencing by oligonucleotide ligation. Prepared fragment libraries are attached to magnetic beads which are clonally populated using emulsion PCR. The beads are deposited onto a glass slide or flow chip. A primer anneals to an adaptor sequence which was attached to each fragment during library preparation. A set of four fluorescently labelled di-base probes compete for ligation to the sequencing primer. Specificity of the di-base probe is achieved by interrogating the 1st and 2nd base in each ligation reaction, the remaining bases in the probe are degenerate. The fluorescently label is cleaved from the probe leaving a 5 base pair nucleotide ligated to the primer. The ligation and interrogation of probes and cleavage of labels continues in cycles, the number of which depends on the read length to be achieved. Following a series of ligation cycles, the extension product is removed and the template is reset with a primer complementary to the n–1 position of the previous primer for a second round of ligation cycles. There are five primer resets and in this was all bases in a fragment are interrogated (Janitz 2011).

The Illumina HiSeq works on the principle of sequencing by synthesis. A library is prepared from fragmented DNA and specialised adapters ligated to the DNA fragments.

The DNA is loaded onto a flow cell and amplified into clonal clusters using bridge amplification. The distal end of a fragment "bridges" to a complementary oligo on the surface of the flow cell, and extends from the complementary oligo to form a double stranded bridge. Denaturation of the bridge produces two complementary sequences. Fluorescently labelled nucleotides are incorporated into the complementary sequence and recorded. The bridge amplification ensures the forward and reverse sequence for each clonal population are sequenced producing paired end reads (Illumina 2017).

2.5.1. Whole exome sequencing using the SOLiD system

The Agilent Technologies SureSelect Human All Exon V5 Panel was used for library preparation and sequencing previously detailed (Mitchell et al. 2012). Targeted enrichment and sequencing were performed using 3 µg of patient DNA. Enrichment was performed with the SureSelect Human All Exon 50 MB Kit (Agilent Technologies, Santa Clara, CA, USA) for the ABI SOLiD system following the manufacture protocol. qPCR (quantitative PCR) was performed and the sample was sequenced on a SOLiD 4 sequencer (Life Technologies, Carlsbad, CA, USA) following manufacturer protocols.

Sequence data was mapped with SOLiD Bioscope software (Life Technologies, Carlsbad, CA, USA) using hg19 as the reference sequence. Variants were called with a combination of Bioscope software suite, using diBayes tool with medium stringency, and Samtools. Data was filtered for single nucleotide polymorphisms (SNPs) with 5-fold or greater coverage. Variants were annotated using Ensembl v61 and Ensembl's defined consequence hierarchically system, with the highest impacting consequence for a variant in a gene being retained. Data was presented in an excel file format (Mitchell et al. 2012).

2.5.2. Whole exome sequencing using the HiSeq system

Whole exome sequencing using the HiSeq system (Illumina, San Diego, CA, USA) was performed as previously described (Smith et al. 2014). Whole exome targeted enrichment was performed using the SureSelect Human All Exon Kit (version 6; Agilent Technologies, Santa Clara, CA, USA) and the enriched library sequenced on the Illumina HiSeq 2500 system. Sequence data was mapped against the hg19 reference human genome using the Burrows-Wheeler aligner software (version 0.6.2; http://bio-bwa.sourceforge.net). The Genome Analysis Tool Kit software (version 2.4.7; https://www.broadinstitute.org/gatk)

was used for recalibration of base quality score and for indel realignment. The unified genotyper (https://www.broadinstitute.org/gatk) was used for variant calling. Variants were electronically annotated with information from the Exome Variant Server (ESP6500; National Heart, Lung, and Blood Institute Grand Opportunity Exome Sequencing Project, Seattle, WA; http://evs.gs.washington.edu/EVS), Single Nucleotide Polymorphism database (dbSNP137; http://www.ncbi.nlm.nih.gov/projects/SNP) and Exome Aggregation Consortium (ExAC Version 0.2, http://exac.broadinstitute.org/) (Smith et al. 2014). Data was presented in an excel file format.

2.5.3. Copy number variation detection using exome depth analysis

Copy number variation (CNV) detection was performed using Exome-Depth v1.1.6.13 (https://CRAN.R-project.org/package=ExomeDepth) algorithm (Plagnol et al. 2012) as previously described (Ellingford et al. 2017). Exome-Depth is an R package which detects deviations in sequencing read depth between queried samples and a set of pooled reference samples, for defined genomic windows. Exome-Depth was presented with 16 BAM files from individuals generated through identical enrichment, sequencing and computational procedures. All reference samples were individuals referred for genomic diagnostic testing who were not knowingly related to the tested individual. Copy number status was calculated for each of 281 exonic regions included within the enrichment region (the genomic region of *DAP3* plus one gene distal and one gene proximal from *DAP3*).

2.6. Software and online tools

Software and online tools not mentioned elsewhere in the materials and methods are noted here.

2.6.1. Audiograms

Patient audiograms were recreated from clinical audiograms using the Audgen online software. (http://audsim.com/audgen/).

2.6.2. *In Silico* prediction of pathogenicity

The tools for the *In silico* prediction of pathogenicity included both prediction software and large online variant databases. They are listed below:

Exome Variant Server (EVS) (NHLBI GO Exome Sequencing Project (ESP)), http://evs.gs.washington.edu/EVS/

dbSNP (Sherry et al. 2001) https://www.ncbi.nlm.nih.gov/projects/SNP/

ExAC (Exome Aggregation Consortium (ExAC)), http://exac.broadinstitute.org/

Gnomad (Lek et al. 2016) http://gnomad.broadinstitute.org/

Polyphen2 (Adzhubei et al. 2010), http://genetics.bwh.harvard.edu/pph2/

SIFT (Kumar et al. 2009), http://sift.jcvi.org/

Mutation Taster (Schwarz et al. 2014), http://www.mutationtaster.org/

2.6.3. Conservation mapping

Sequences were mapped using Clustal Omega (Sievers et al. 2011) http://www.ebi.ac.uk/Tools/msa/clustalo/.

2.6.4. Predictions of mitochondrial targeting sequences

Mitofates (Fukasawa et al. 2015) (http://mitf.cbrc.jp/MitoFates/cgi-bin/top.cgi) was used to predict if proteins contained a mitochondrial targeting sequence.

2.6.5. Prediction of functional domains

The following online software was used to predict possible functional domains of proteins.

SMART (Letunic et al. 2015) http://smart.embl-heidelberg.de/

NCBI conserved domains (Marchler-Bauer et al. 2015) https://www.ncbi.nlm.nih.gov/Structure/cdd/wrpsb.cgi

Interpro (Jones et al. 2014) https://www.ebi.ac.uk/interpro

2.7. Sanger sequencing

Sanger sequencing was performed to confirm variants in patients and confirm construct sequences. The confirmation of missense variants was performed in house. Plasmid

sequence confirmation was performed both in house and by Eurofins (Eurofins, GSC, LUX) as part of a service.

2.7.1. Designing primers for Sanger sequencing

Primers were designed used the Primer3 software (http://bioinfo.ut.ee/primer3-0.4.0/) using the default settings, unless stated otherwise. Primers for use with human DNA were checked for underlying sequence variants using SNPCheck software (https://secure.ngrl.org.uk/SNPCheck/snpcheck.htm). Primers were purchased from Sigma-Aldrich, (St. Louis, MO, USA) at a concentration of 100µM.

2.7.2. Polymerase Chain Reaction (PCR) for Sanger sequencing

For the confirmation of variants PCR reactions (10µl GoTaq Green Mastermix (Promega, Madison, WI, USA), 10ng of DNA, 1µl Forward Primer at 5µM, 1µl Reverse Primer at 5µM, H_2O to 20µl) were run on the following PCR program.

Stage	Temp °C	Time
1	95	3 min
2 (35 cycles)	95	30s
	56-60*	30s
	72	30s
3	72	5 min
	4	hold

Table 2.1. Thermal cycler program for PCR

*The annealing temperatures used are stated with the appropriate primer in the appendix.

2.7.3. Agarose gel glectrophoresis

PCR product was confirmed by running 5µl of PCR product with a 100bp ladder on a 1.5% agarose gel (1.5g of agarose in 100ml of TBE) stained with SafeView (5µl added to the cooled agarose. NBS Biologicals, Huntingdon, UK). Samples were run in an electrophoresis tank containing Tris/Borate/EDTA (TBE) buffer at 120V for 30 minutes and visualised using U.V. transillumination.

2.7.4. Purification of PCR products

PCR samples were purified using either the QIAquick PCR purification kit (Qiagen, Hilden, Germany) following the manufacturer protocol and eluting in 50µl of elution buffer or using Agencourt AMPure XP paramagnetic beads (Beckman Coulter, Brea, CA, USA). AMPure beads were added to the PCR products in a 1:1 ratio. Samples were processed using a Biomek NX robotics instrument (Beckman Coulter, Brea, CA, USA) following manufacturer protocol and eluted in 100µl of dH2O.

2.7.5. Cycle sequencing

Plasmid DNA was not subject to the initial PCR stage prior to cycle sequencing.

Sequencing reactions (5.275µl Water, 1µl PCR product, 0.25µl Big Dye mastermix, 1.875µl 5X sequencing buffer, 1.6µl Primer at 5µM) were prepared using the BigDye™ Terminator v3.1 Cycle Sequencing Kit (Thermo Fisher Scientific Inc, Waltham, MA, USA) and run on the following thermal cycler program.

Stage	Temp °C	Time
1	98	1 min
2 (30 cycles)	98	10s
	55	10s
	60	4 min
3	4	hold

Table 2.2. Thermal cycler program for cycle sequencing

After cycle sequencing the reactions were purified using either CleanSEQ beads or ethanol precipitation.

2.7.6. CleanSEQ purification of sequencing reactions

After cycle sequencing 5µl of Agencourt CleanSEQ paramagnetic bead solution (Beckman Coulter, Brea, CA, USA) were added to the sequencing reaction (1:2 ratio) and the samples were processed using a Biomek NX robotics (Beckman Coulter, Brea, CA, USA) instrument according to manufacturer protocol. Samples in 10µl of HiDi formamide (Thermo Fisher Scientific Inc, Waltham, MA, USA) were heated at 95°C for 3-5 minutes

before being sequenced using the 3730 DNA analyser (Thermo Fisher Scientific Inc, Waltham, MA, USA).

2.7.7. Ethanol precipitation of sequencing reactions

After cycle sequencing 28µl of precipitation solution was added per well (100% EtOH and 125mM EDTA, pH8). Plates were sealed, vortexed and incubated for 15 min at room temperature. The DNA was precipitated by centrifugation (30 min, 2200xg, 4°C). The plate seal was removed, the plate inverted and the liquid removed by centrifugation (30 sec, 100xg, room temperature). To wash the DNA 75µl of 70% ethanol was added per well. Plates were sealed and vortexed. The DNA was precipitated by centrifugation (15 min, 2200xg, 4°C). The plate seal was removed, the plate inverted and the liquid removed by centrifugation (30 sec, 100xg, room temperature). The DNA was air dried for 10 minutes. 10µl of HiDi formamide (Thermo Fisher Scientific Inc, Waltham, MA, USA) was added to each well. The plate was sealed and incubated for 3 minutes at 90°C. Plates were submitted to NIDCD sequencing core for sequence analysis using the 3730 DNA analyser (Thermo Fisher Scientific Inc, Waltham, MA, USA).

2.7.8. Analysis of Sanger Sequencing

Sequencing traces were analysed using either the Seq Scanner 2 software (Applied Biosystems, Foster City, CA, USA) or Lasergene SeqMan Pro software (DNASTAR, Madison, WI, USA).

2.8. Assessment of proteins from patient dermal fibroblasts

2.8.1. Western blots for mitochondrial RNase P

Western blot analyses for mitochondrial RNase P subunits were performed as previously described (Deutschmann et al. 2014). Cell extracts were prepared from patient and control dermal fibroblasts using lysis buffer (50 mM Tris–HCl (pH 7.4), 154 mM NaCl, 1 mM EDTA, 0.5% Triton X-100, 0.05% SDS). Protein concentration was determined using Bradford Assay (Bio-Rad, Hercules, CA, USA). 30 µg of protein was separated by sodium dodecyl sulphate—polyacrylamide gel electrophoresis (SDS-PAGE) on a 10% SDS-polyacrylamide gel and transferred to a polyvinylidene difluoride membrane (GE Healthcare, Little Chalfont, UK). Membrane blots were blocked with tris phosphate-

buffered saline containing 0.1% Tween-20 and 5% skim milk powder (Fluka, Sigma-Aldrich, St. Louis, MO, USA) for 1 hour at room temperature. Membranes were incubated with the following antibodies; HSD10 anti-ERAB [5F3] (SDR5C1, 1:500, Abcam, Cambridge, UK), anti-RG9MTD1 (TRMT10C,1:250, Sigma-Aldrich, St. Louis, MO, USA) and anti-MRPP3 (PRORP, 1:2000, Abcam, Cambridge, UK). Alpha Tubulin (1:8000, Abcam, Cambridge, UK) was used as a loading control. Proteins were detected with horseradish peroxidase conjugated secondary antibodies (Dako, Agilent Technologies, Santa Clara, CA, USA). The blots were developed using the ECL Western Blotting Analysis Detection system (GE Healthcare, Little Chalfont, UK) (Deutschmann et al. 2014). Antibody details are available in Deutschmann et al. (2014)

2.8.2. Western blots for components of the mitochondria oxidative phosphorylation pathway

Cultured fibroblasts were harvested and lysed in 50 mm Tris-HCl pH 7.5, 130 mmNaCl, 2 mm $MgCl_2$, 1 mm phenylmethanesulfonyl fluoride (PMSF), 1% Nonidet P-40 (v/v) and 1 × EDTA free protease inhibitor cocktail (Pierce Biotechnology, Waltham, MA, USA). Protein lysates (40 µg) were incubated with sample dissociation buffer and separated according to size on 12% gels by SDS-PAGE and immobilized by electrophoretic transfer on to PVDF membrane (Immobilon-P, Millipore Corporation, Billerica, USA). Proteins of interest were bound by overnight incubation at 4°C with primary antibodies followed by HRP-conjugated secondary antibodies (Dako Cytomation, Agilent Technologies, Santa Clara, CA, USA). Chemiluminescence ECL Prime Kit (Amersham, GE Healthcare, Little Chalfont, UK) and ChemiDocMP Imaging System (Bio-Rad, Hercules, CA, USA) were used for signal detection and Image lab 4.0.1 (Bio-Rad, Hercules, CA, USA) software for analysis. Antibody details are available in the relevant experimental chapter.

2.9. Assessment of RNA from patient dermal fibroblasts

Northern blot analysis was performed as previously described (Deutschmann et al. 2014). Northern blot analysis was performed using the NorthernMax kit (Ambion, Thermo Fisher Scientific Inc, Waltham, MA, USA) according to manufacturer protocol. 2–5 µg of total RNA was separated on a 1% denaturing agarose gel. After electrophoresis, RNA was transferred to nylon membrane (Hybond-N+, GE Healthcare, Little Chalfont, UK) by

capillary transfer, UV cross-linked and hybridised with biotinylated probes (10 pmol/l in Ultrahyb-Oligo hybidization buffer, Ambion, Thermo Fisher Scientific Inc, Waltham, MA, USA). Signals were detected using the BrightStar BioDetect kit (Ambion, Thermo Fisher Scientific Inc, Waltham, MA, USA) according to the manufacturer protocol. Strand-specific 5'biotinylated probes for the mitochondrial tRNAs, rRNAs and mRNAs were purchased from Microsynth AG (Balgach, Switzerland). A biotinylated RNA size marker (BrightStar RNA Millenium Marker, Ambion, Thermo Fisher Scientific Inc, Waltham, MA, USA) was used to determine the size of RNA species. Probe sequences are available in (Deutschmann et al. 2014)

2.10. *E.coli* methods

2.10.1. Strains

The following *E.coli* strains were used; XL-1 blue (XL-10 Gold, Agilent Technologies, Santa Clara, CA, USA), BW313, Rosetta (DE3) (Novagen, Merck, Kenilworth, NJ, USA) and TOP10 (Invitrogen, Carlsbad, CA, USA).

2.10.2. Bacterial culture

Unless otherwise stated *E.coli* strains were grown in standard Luria-Bertani (LB) media (10 g/L Tryptone, 5 g/L Yeast Extract, 5 g/L NaCl (Sigma-Aldrich, St. Louis, MO, USA)) or on LB plates (LB media and 1.5% w/v agar) containing the appropriate antibiotic at the concentration recommended for plasmid selection (Table 2.3). For blue/white colour screening XL-1 (XL10-gold, Agilent Technologies, Santa Clara, CA, USA) cells were grown on LB-antibiotic plates coated with 100µl of 40µM IPTG and 100µl of 2% XGAL. Strains were stored in media with 50% glycerol (v/v) at -80°C.

Antibiotic	**Concentration**
Kanamycin	50 µg/mL
Ampicillin	100 µg/mL
Carbenicillin	100 µg/mL
Chloramphenicol	25 µg/mL

Table 2.3. Antibiotic concentrations used for plasmid selection.

2.10.3. Bacterial transformations

Bacterial transformations were performed as described unless stated otherwise. Cells were thawed on ice and a 25µl aliquot removed and kept on ice. 1µl of β-mercaptoethanol was added and the cells were incubated on ice for 10 minutes (XL-1 blue only). 25-50ng of the construct was added to the cells and incubated on ice for 30 minutes. Cells were heat shocked at 42°C for 30 seconds and incubated on ice for 2 minutes. 100µl of LB media was added and the cells incubated at 37°C for 30 minutes to 1 hour. The transformed cells were plated onto the appropriate LB-antibiotic plates.

2.11. Preparation of expression plasmids

The following plasmids were prepared using T4 ligation; pBlueScript II SK (+) pre- tRNA transcript histidine-serine(AGY)-leucine(CUN) and pSF-STE5-MouseNop14.

Templates for cloning into plasmid vectors were subject to PCR amplification. The PCR reaction was as follows; 72µl H_2O, 20µl Phusion HF Buffer (New England Biolabs, Ipswich, MA, USA) 4µl 5mM DNTPs, 0.5µl of forward primer at 100µM, 0.5µl of reverse primer at 100µM, 2µl of template DNA and 1µl of Phusion high fidelity DNA polymerase (New England Biolabs, Ipswich, MA, USA). The PCR reaction was run on the thermal cycler program in table 2.4.

Stage	Temp °C	Time
1	98	5 min
2 (30 cycles)	98	10s
	55	30s
	72	1 min
3	4	hold

Table 2.4. Thermal cycler program for PCR with Phusion polymerase

The PCR products were assessed using agarose gel electrophoresis as detailed in section 2.7.3. A 1kb ladder (New England Biolabs, Ipswich, MA, USA) was used for the assessment of larger transcripts. PCR products were purified using the QiaQuick PCR purification kit (Qiagen, Hilden, Germany) according to manufacturer instructions and eluted in 50µl of elution buffer.

Restriction digest of PCR products was performed using the following reaction; 45µl PCR product, 8µl H_2O, 6µl of CutSmart buffer (New England Biolabs, Ipswich, MA, USA) and 0.5µl of each restriction enzyme (specified in the appropriate experimental chapter). The restriction digest was incubated for 1.5 hours at 37°C and the digested product purified using the QiaQuick PCR purification kit (Qiagen, Hilden, Germany) according to manufacturer protocol and eluted in 30µl of elution buffer. The vectors were digested using the same restriction enzymes as the insert in the following reaction; 2µg plasmid, 2µl of CutSmart buffer (New England Biolabs, Ipswich, MA, USA) 0.5µl of each restriction enzyme and H_2O to 20µl. The restriction digest reactions were incubated at 37°C for 1.5 hours. The linearized plasmids were dephosphorylated to prevent re-ligation. 2µl of Antarctic phosphatase buffer and 1µl of Antarctic phosphatase (both New England Biolabs, Ipswich, MA, USA) were added to the restriction reaction which was then incubated at 37°C for 1 hour. The reaction was purified using the QiaQuick PCR purification kit (Qiagen, Hilden, Germany) according to manufacturer protocol and eluted in 50µl of elution buffer. The ligation reaction is as follows; 2µl dephosphorylated linearized vector, 15µl PCR product, 2µl of T4 DNA ligase buffer and 1µl of T4 DNA ligase enzyme (both New England Biolabs, Ipswich, MA, USA). The ligation reactions were incubated at room temperature for 1-2 hours and then transformed directly into the appropriate *E.coli* strain.

2.11.1. Primers for the preparation of pSF-STE5-MouseNop14

MoNOP14-F(NcoI) 5’ GCGCGCCCATGGGGAAAGCCAAGCGGAC 3’

MoNOP14-B(XbaI) 5’ GGGGGTCTAGATTATTTTTTGAACTTTTTCCTC 3’

Reference sequence BC043043.

2.11.2. Primers for the mitochondrial pre- tRNA Transcript histidine-serine(AGY)-leucine(CUN)

Forward Primer – 5’ GGGTACCTCCTCCTATCCCTCAACCCCGACATC 3’

Reverse Primer – 5’ CGGGATCCGTTAACGAGGGTGGTAAGGATGGGGGGAATTAGG 3’

The reference sequence is Genbank: NC_012920.

2.12. Preparation of plasmids containing EGFP tagged constructs

Plasmids for the expression of EGFP tagged Nop14 and Dap3 were prepared as below using the In-Fusion method of homologous recombination (Clontech, Mountain View, CA, USA).

2.12.1. Digest of the vector for EGFP-tagged contsructs.

A C-terminal EGFP vector, pEGFP-N1 (Clontech, Mountain View, CA, USA. Discontinued), was linearized using BglII and PstI fast digest restriction enzymes (both Thermo Fisher Scientific Inc, Waltham, MA, USA). The digest reaction is as follows; 10µg of vector, 5µl each of BglII and PstI, 10µl of 10x Fast Digest buffer (Thermo Fisher Scientific Inc, Waltham, MA, USA) and H_2O to a volume of 100µl. The fast digest reaction was incubated for 15min at 37°C and stored at 4°C.

2.12.2. In-Fusion primer design

In-Fusion primers were designed using primer3 with 15-20bp complementary to the recipient vector, including restriction sites used to linearize the vector, added manually to the sequence.

2.12.3 In-Fusion primers

DAP3_In-Fusion_1: TACCGGACTCAGATCTATGCTGACAGGAATAACAA

DAP3_In-Fusion_2: CGCGGTACCGTCGACTGCAGCAGCGAGGCACAGAGC

Underlined = Dap3, red = restriction sites

NOP14_In-Fusion_1: TACCGGACTCAGATCTATGGGGAAAGCCAAG

NOP14_In-Fusion_2: CGCGGTACCGTCGACTGCAGTTTTTTGAACTTTTTCCTCT

Underlined = Nop14, red = restriction sites

2.12.4 PCR for In-Fusion

The open reading frame (ORF) cDNA sequences minus the stop codons for Dap3 (BC019566) and Nop14 (BC043043) were amplified by PCR. A 50µl PCR reaction was prepared (1mM MgCl2, 0.8 mM dNTPs, 1.25U PrimeSTAR Polymerase (TaKaRa, Shiga,

Japan), 200nM forward primer, 200nM reverse primer and 10ng DNA template) and run on the following thermal cycler program.

Stage	Temp °C	Time
1	94	30 sec
2 (30 cycles)	98	10s
	68	5s
	72	1.8 or 2.5 min
3	72	4 min
	25	hold

Table 2.5. Thermal cycler program for PCR for In-Fusion reaction

The PCR products were assessed by running them on a 1.2% Egel (Invitrogen, Carlsbad, CA, USA) at 120v for 30 minutes using a 1kb ladder (Thermo Fisher Scientific Inc, Waltham, MA, USA).

The PCR products and digested EGFP vector were gel purified. The samples were run on a 2% agarose gel with TAE (150ml of TAE (Tris base, acetic acid and EDTA.) and 3g of agarose) at 110v for 2 hours alongside a 1kb ladder (Thermo Fisher Scientific Inc, Waltham, MA, USA). After electrophoresis the gel was stained for 30 minutes with SybrSafe stain (Thermo Fisher Scientific Inc, Waltham, MA, USA). The bands corresponding to the purified products were excised with a razor blade and the DNA was extracted using a Nucleospin Gel extraction kit (Macherey-Nagel, Düren, Germany) according to manufacturer instructions.

2.12.5. In-Fusion reactions

The amount of each PCR product and the linearized vector to input into the In-Fusion reaction was calculated using the In-Fusion calculator (http://bioinfo.clontech.com/In-Fusion/molarRatio.do) with an insert to vector ratio of 2.

The In-Fusion cloning procedure was performed according to manufacturer protocols. Briefly, 10µl of the insert and vector mix was added to an In-Fusion HD Eco Dry Pellet (Clontech, Mountain View, CA, USA) and mixed by pipetting. The reaction was incubated for 15 minutes at 37°C, followed by 15 minutes at 50°C and then placed on ice. The In-

Fusion reaction was immediately diluted 1 in 5 with H_2O and 5µl transformed into TOP10 cells (Invitrogen, Carlsbad, CA, USA). The cells were plated and incubated overnight on LB-Kanamycin plates. Colonies from the plates were grown overnight in LB-Kanamycin media and the Plasmid DNA extracted using NucleoSpin® Plasmid Miniprep Kit (Macherey-Nagel, Düren, Germany). The inserts were confirmed using Sanger sequencing (in house).

2.13. Plasmids prepared by Gibson assembly

The plasmid, p426GPD-DAP3, was prepared using the Gibson assembly technique (Gibson et al. 2009); The Gibson assembly technique uses a one-step isothermal reaction to join oligonucleotides with overlapping ends.

An assembly master mixture was prepared by combining 320 µl 5 × isothermal reaction buffer (0.5M Tris-HCl pH 7.5, 0.05M MgCl2, 1mM of each dNTP, 0.05M DTT, 25% PEG-8000 (w/v) and 5 mM NAD), 0.64 µl of 10 U µl−1 T5 exonuclease (New England Biolabs, Ipswich, MA, USA) 20 µl of 2 U µl−1 Phusion DNA polymerase (Thermo Fisher Scientific Inc, Waltham, MA, USA), 160 µl of 40 U µl−1 Taq DNA ligase (New England Biolabs, Ipswich, MA, USA) and water up to a final volume of 1.2 ml. 5µl of the vector and insert (amplified, digested and dephosphorylated as in section 2.10) to be assembled were added to 15µl of the master mixture in equimolar amounts. 10- 100 ng of each DNA fragment was added. Reactions were incubated at 50°C for 1 hour (Gibson et al. 2009).

The plasmid p426GPD-DAP3C395Y was prepared from p426GPD-DAP3 as detailed in (Kunkel et al. 1987) and section 2.13.3 using the oligonucleotide detailed below.

2.13.1. Primers for preparation of p426GPD-DAP3

GDP_hDAP3.for 5’ CTGCAGGAATTCGATATCAATGATGCTGAAAGGAATAACAAGGCT3’

GDP_hDAP3.rev 5’GGTCGACGGTATCGATATTAGAGGTAGGCACAGTGCCG3’

2.13.2. Oligonucleotide for the preparation of p426GPD-DAP3C395Y

DAP3-Cys395Tyr-rev 5’GGTCGACGGTATCGATATTAGAGGTAGGCATAGCGCCG3’

The base that differs from the wild type sequence is highlighted.

2.14. tRNA processing assays

tRNA processing assays were performed on radiolabelled precursor tRNA templates as detailed in Holzmann et al. (2008) using mitochondrial RNase P complexes containing both wild type (wt) and variant PRORP (p.Ala485Val).

2.14.1. Templates for recombinant expression of TRMT10C, SDR5C1, PRORP (Wt and p.Ala485Val)

Templates for recombinant expression of TRMT10C, SDR5C1 and PRORP were gifted by Walter Rossmanith and are as previously described (Holzmann et al. 2008). All templates were inserted into the vector pET28-b(+) (Novagen, Merck, Kenilworth, NJ, USA). pET28-b(+)TRMT10C comprised an N-terminal 6×His-tag, a thrombin cleavage site, and amino acids 40-403 of the protein. pET28-b(+)SDR5C1 comprised N-terminal 6×His-tag and the full coding sequence of SDR5C1. pET28-b(+)PRORP was preceded by Met-Gly and contained the coding sequence of PRORP from amino acid 46 onwards which extended into a tandem myc- and 6×His-tag at the C-terminus (Holzmann et al. 2008). The plasmid pET28-b(+)PRORP (Holzmann et al. 2008) was mutagenized as previously described (Kunkel et al. 1987) with the synthetic oligonucleotide PRORP_p.Ala485Val (sequence below)

2.14.2. Oligonucleotide sequence PRORP_p.Ala485Val

PRORP_Ala485Val - 5'GGAGTGCAGTGTGACATACAGAAGGAATGG3'

The base altered from the wild type sequence is highlighted (Genbank: NM_014672.3).

2.14.3. Mutagenesis of pET28-b(+)PRORP

90ng of pET28-b(+)PRORP was transformed into *E.coli* strain BW313 to produce single stranded DNA for mutagenesis. The transformed cells were incubated overnight at 37°C on LB- kanamycin plates. Transformed BW313 colonies were inoculated into 1ml of LB-kanamycin media with 2µl of 1mg/ml uridine and incubated at 37°C for 2 hours with shaking. 1µl of VCSM13 helper phage (Agilent Technologies, Santa Clara, CA, USA) was added and the culture was incubated at 37°C for 2 hours with shaking. The concentration of kanamycin in the culture was brought to 70µg/ml. The culture was incubated at 37°C overnight with shaking.

Overnight single stranded DNA was extruded into the culture media by the helper phage. The culture was centrifuged (5 minutes at 14,000xg) and 800µl of the supernatant removed and transferred to a new tube. 200µl of 20% PEG/2.5mM NaCl was added to the supernatant and the solution well mixed and incubated on ice for 30 minutes. The solution was centrifuged for 5 minutes at 14,000xg. The supernatant was removed and discarded and the DNA pellet resuspended in 120µl of 0.3M sodium acetate (pH 5.3)/1mM EDTA. 120µl of PCA (tris-buffered) was added, the sample was vortexed and briefly centrifuged. The aqueous phase was transferred to a new tube and 475µl of ethanol added. The solution was vortexed and incubated at -20 °C for 1 hour. The solution was centrifuged for 5 minutes at 14,000xg and the supernatant discarded. The DNA pellet was washed in 70% ethanol and resuspended in 20µl of TE buffer.

The oligonucleotide PRORP_Ala485Val underwent 5'-phosphorylation. The phosphorylation solution (4µl oligo at 10ng/µl, 2µl 10X reaction buffer (New England Biolabs, Ipswich, MA, USA) 13µl H_2O, 1µl T4 polynucleotide kinase (New England Biolabs, Ipswich, MA, USA)) was incubated at 37°C for 30 minutes then at 70°C for 20 minutes. The oligo was hybridized to the single stranded DNA by adding 3µl of DNA and 1.3µl of 20X SSC buffer (3 M sodium chloride and 300 mM trisodium citrate adjusted to pH 7.0 with HCl) to the oligo solution, incubating at 70°C for 5 minutes and allowing to cool to room temperature. For the extension of the oligo an extension cocktail was prepared containing 20µl of hybridised oligo and DNA, 10µl of 10X T4 extension cocktail, 68µl of H_2O, 1µl of T4 DNA polymerase (New England Biolabs, Ipswich, MA, USA) and 0.5µl of T4 DNA ligase (New England Biolabs, Ipswich, MA, USA). The 10X T4 extension cocktail comprises 200mM HEPES pH7.8, 20mM DTT, 100mM $MgCl_2$, 5mM of each dNTP and 10mM ATP. The complete extension cocktail was incubated on ice for 5 minutes, at room temperature for 5 minutes and for 1.5 hours at room temperature before storage on ice. 2µl of the cocktail containing the mutagenized plasmids was transformed into 100µl of XL1-blue cells. Transformed cells were plated onto LB-Kanamycin plates and incubated overnight at 37°C. Colonies that were indicated transfected by the blue white colour screening were inoculated into 50 ml of LB-kanamycin media and incubated overnight at 37°C with shaking. Plasmid DNA was extracted using the GenElute™ HP Plasmid Midiprep Kit (Sigma-Aldrich, St. Louis, MO, USA) according to manufacturer instructions. The

variant was confirmed in the plasmid by Sanger sequencing (Eurofins, T7 Terminator primer, 5' CTA GTT ATT GCT CAG CGG T 3').

2.14.4. Recombinant expression and purification of TRMT10C, SDR5C1 and PRORP (wt and p.Ala485Val)

Expression of recombinant templates was induced in *E.coli* Rosetta2 DE3 (Novagen, Merck, Kenilworth, NJ, USA) using Overnight Express medium (Novagen, Merck, Kenilworth, NJ, USA). The plasmids pET28-b(+)TRMT10C, pET28-b(+)SDR5C1, pET28-b(+)PRORP and pET28-b(+)PRORPAla485Val were transformed into the *E.coli* Rosetta2 DE3 strain (Novagen, Merck, Kenilworth, NJ, USA) according to manufacturer protocol. The transformed cells were plated onto LB-Kanamycin plates and incubated overnight at 37°C. Colonies containing the plasmids were inoculated into 30ml of overnight express media with kanamycin and chloramphenicol and incubated for 6 hours. The cultures were transferred into 500ml of overnight express media with kanamycin and chloramphenicol and incubated for 24 hours at 37°C (pET28-b(+)SDR5C1 and pET28-b(+)PRORP) or 19°C for 40 hours (pET28-b(+)TRMT10C and pET28-b(+)PRORPAla485Val). The cultures were centrifuged at 12,000xg for three minutes to pellet the cells and the supernatant discarded. The Affinity chromatography of the His-tagged proteins was performed as previously described (Holzmann et al. 2008) at 4°C. Cell pellets were resuspended in 15ml of lysis/wash buffer (20mM Tris-Cl pH7.4, 150mM NaCl, 0.1M DTT, 0.02% Tween 20, 20mM imidazole, 15% glycerol) and sonicated. The lysate was cleared by centrifugation and applied to a column with a 1ml bed volume of His-select column matrix slurry (Sigma-Aldrich, St. Louis, MO, USA). After the lysate flowed through the column was washed with 10 ml of lysis/wash buffer. The protein was eluted with 10 ml of elution buffer (20mM Tris-Cl pH7.4, 150mM NaCl, 0.1mM DTT, 0.02% Tween 20, 250mM imidazole, 15% glycerol) and collected in 1ml fractions. Protein purity was assessed by SDS-PAGE. Purified proteins were dialysed overnight at 4°C in 20 mM Tris-Cl pH 7.4, 100 mM NaCl, 15% glycerol, and dialysed proteins were assessed using SDS-PAGE and quantified using the NanoDrop Lite spectrophotometer (Thermo Fisher Scientific Inc, Waltham, MA, USA). Aliquots of purified protein were flash frozen and stored at -80°C.

2.14.5. SDS-PAGE

All protein aliquots were run on 12% SDS-polyacrylamide gels (3.35ml H_2O, 2.5ml 1.5M Tris-HCl pH 6.8, 100µl 10% SDS, 4ml acrylamide gel (Protogel, National Diagnostics, Atlanta, GA, USA), 50µl 10% ammonium persulphate, 5µl TEMED (Sigma-Aldrich, St. Louis, MO, USA)) with a 4% stacking gel (6.1ml H_2O, 2.5ml 0.5M Tris-HCl pH 6.8, 100µl 10% SDS, 1.33ml acrylamide gel (Protogel, National Diagnostics, Atlanta, GA, USA), 50µl 10% ammonium persulphate, 5µl TEMED (Sigma-Aldrich, St. Louis, MO, USA)). Protein aliquots were mixed 1:1 with 2X SDS loading buffer (100 mM Tris-Cl (pH 6.8) 4% SDS 0.2% bromophenol blue, 20% glycerol 200 mM mM β-mercaptoethanol). The samples and an aliquot of precision plus protein standard all blue (Bio-Rad, Hercules, CA, USA) were heated for 10 minutes at 90°C and run on the polyacrylamide gel for 40 minutes at 200V. Gels were stained with Instant blue stain (Expedeon, Harston, UK) for at least 15 minutes with agitation.

2.14.6. Calculation of protein concentration

To achieve the correct protein stoichiometry for the tRNA protein assays the concentration of the proteins were calculated from the spectrophotometer absorbance readings. Protein concentration by absorbance was calculated using Beers law.

Beers law $A = \xi * b * c$

A = absorbance at 280nm

ξ = the extinction coefficient (absorbance prediction given amino acid content)

b = the path length in cm

c= the analyte concentration (in molarity)

Only tryptophan, tyrosine and cysteine absorb at 280 nm. The extinction coefficient was calculated using the formula below taking into account the modification in the recombinant proteins.

ξ = (number of tryptophan residues x 5500) + (number of tyrosine residues x 490) + (number of cysteine residues x 125)

The ξ values were confirmed using an online protein extinction coefficient calculator (http://www.biomol.net/en/tools/proteinextinction.htm). The concentrations as determined by NanoDrop (Thermo Fisher Scientific Inc, Waltham, MA, USA) are normalised to a pathway length of 1cm. So the pathway length used was 1cm. The equation below was used to calculate protein concentration in M

Concentration (M) = Absorbance at 280 nm / (extinction coefficient x pathway length (cm))

2.14.7. Thermal stability testing of wild type PRORP and PRORP p.Ala485Val

The thermal stability of wild type Δ94-PRORP and Δ94-PRORP p. Ala485Val were assessed using differential scanning fluorimetry in a standard buffer (150 mM NaCl, 10 mM HEPES pH 7.5) and a buffer predicted to produce the most stable PRORP protein (50 mM MES pH 6.5, 5% glycerol, 100mM NaCl, 100mM $(NH_4)2SO_4$).

2.14.8. Precursor tRNA (pre-tRNA) templates

The templates for pre-tRNA^{Tyr} and pre-tRNA^{Ile} were as described in (Holzmann et al. 2008) and were gifted by Walter Rossmanith. phY1, the template for mitochondrial pre-tRNA^{Tyr} contains nucleotides 5792 to 5931 of the human mitochondrial genome (Anderson et al. 1981) cloned into the BamHI and EcoRI sites of pGEM-1 (Promega, Madison, WI, USA). phI2, the template for mitochondrial pre-tRNA^{Ile} contains nucleotides 4235 to 4350 of the human mitochondrial genome (Anderson et al. 1981) cloned into the XbaI and EcoRI sites of pGEM-1 (Promega, Madison, WI, USA) (Holzmann et al. 2008). The template for the pre-tRNA$^{His\text{-}Ser(AGY)\text{-}Leu(CUN)}$ transcript contains nucleotides 12092 to 12412 of the human mitochondrial genome (Genbank: NC_012920) cloned into the KpnI and BamHI sites of pBluescript II SK (+) plasmid (Stratagene, San Diego, CA, USA,) in the T7 orientation.

Run off *in vitro* transcription to produce body labelled pre-tRNA substrate was performed as previously described (O'Keefe et al. 1996). Plasmids were linearized as in section 2.10, precipitated and rehydrated in 10µl of TE buffer. A transcription reaction was prepared as follows; 2µl of 5X T7 transcription buffer (Promega, Madison, WI, USA), 1µl 100mM DTT, 2µl nucleotides (all 2.4mM except UTP (125µM)), 2µl α ^{2}P UTP (800Ci/mM), 0.5µl RNasin and 1µl T7 polymerase (Promega, Madison, WI, USA). The reaction was incubated at 37°C

for 1 hour. After incubation 2µl of 0.5M EDTA, 100µl H_2O and 100µl pf phenol, buffered to pH5.3 were added. The sample was vortexed, briefly centrifuged and 100 µl of the aqueous phase removed. 20µl of 5M ammonium acetate, 2µl of glycogen and 300µl of ethanol was added to the aqueous phase. The solution was vortexed and incubated at -20 °C for 1 hour. The solution was centrifuged for 5 minutes at 14,000xg and the supernatant discarded. The RNA pellet was resuspended in 6µl formamide loading buffer (95% formamide, Bromophenol blue 0.025% (w/v), Xylene cyanol FF 0.025% (w/v), EDTA pH8.0 5mM) and heated to 90°C for 5 minutes. The RNA was loaded onto a 6% acrylamide/8M urea gel (12ml UreaGel6 (Protogel, National Diagnostics, Atlanta, GA, USA), 3ml Urea-Gel buffer (Protogel, National Diagnostics, Atlanta, GA, USA), 30µl TEMED, 30µl APS) and run for 40 minutes at 22 watts. The gel was exposed to film and the bands corresponding to the radiolabelled RNA excised. The RNA was eluted for 2 hours in passive elution solution (898µl H2O, 100µl 3M sodium acetate and 2µl 0.5M EDTA). The RNA was precipitated from the passive elution solution by removing 2 aliquots of 400µl of passive elution solution and adding 1ml of ethanol and 2µl of glycogen to each. The samples were centrifuged at 14,00xg for 5 minutes, washed with 95% ethanol and rehydrated in 50µl of H_2O. The radioactivity of each transcript was quantified using a liquid scintillation counter.

Phy1 linearization with BamHI and in vitro transcription with T7 RNA polymerase resulted in a precursor-tRNA (pre-tRNA) containing a 55-nucleotide leader sequence and 39 nucleotides of 3'-trailer sequence. PhI2 linearization with XbaI and in vitro transcription with T7 RNA polymerase result in a pre-tRNA containing a 42-nucleotide leader sequence and 24 nucleotides of 3'-trailer sequence (Holzmann et al. 2008). pHis-Ser(AGY)-Leu(CUN) linearized with HpaI and In vitro transcription with T7 polymerase resulted in a pre-tRNA transcript with a 20 nucleotide 5' leader sequence and a 72 nucleotide 3' trailer sequence.

2.14.9. t-RNA processing assays

tRNA processing assays were performed as detailed in (Holzmann et al. 2008). Two reactions were prepared per assay, one containing wild type PRORP and one containing PRORP p.Ala485Val. TRMT10C, SDR5C1 and PRORP (Wt or p.Ala485Val) were mixed in a 2:4:1 molar ratio in 10 µl and incubated in 20 mM Tris-HCl (pH 7.4), 100 mM NaCl at room

temperature for 30 min. The final concentration in activity assays was 50/100/25 nM of TRMT10C, SDR5C1 and PRORP respectively. The pre-tRNA substrate was prepared on ice in the following reaction; 4 µl 5X reaction buffer (150mM Tris-HCl pH8, 200mM NaCl, 22.5mM MgCl2, 10mM DTT, 100µg/ml bovine serum albumin (BSA)), 6 µl mtRNA substrate diluted with H_2O to 300,000 dpm total and 0.5µl RNasin (20 units, New England Biolabs, Ipswich, MA, USA). Proteins were added to the pre-tRNA substrate on ice. 4µl of reaction was removed and added to 2µl stop mix (100mM EDTA, 100mM Tris-HCl pH8) on ice and labelled time point 0. The tRNA processing reaction was incubated at 21°C and 4µl of reaction was removed and added to 2µl stop mix on ice at each of the prescribed time points. After the reactions had finished the stopped reactions were incubated at 37°C for 15 minutes. After incubation 200µl of splicing diluent (300 mM NaOAc pH 5.3, 1 mM EDTA, 0.1% SDS, 25 µg/ml *E. coli* tRNA) and 200µl of PCA (citrate buffered) were added to the reactions. The sample was vortexed, briefly centrifuged and 190 µl of the aqueous phase removed. 475µl of ethanol was added to the aqueous phase. The solution was vortexed and incubated at -20 °C for 1 hour. The solution was centrifuged for 5 minutes at 14,000xg and the supernatant discarded. The DNA pellet was resuspended in 3.5µl formamide loading buffer and heated to 90°C for 5 minutes. The DNA was loaded onto a 6% acrylamide/8M urea gel (24ml UreaGel6 (Protogel, National Diagnostics, Atlanta, GA, USA), 6ml Urea-Gel buffer (Protogel, National Diagnostics, Atlanta, GA, USA), 60µl TEMED, 60µl APS) and run for 1 hour 45 minutes at 32 watts. The gel was fixed in 10% methanol/10% acetic acid and dried onto filter paper.

2.14.10. Phosphorimaging and subsequent analysis

The pre-tRNA tyrosine and isoleucine assays were imaged using the Molecular Imager FX (Bio-Rad, Hercules, CA, USA) and analysis of the image performed in the Quantity One software (Bio-Rad, Hercules, CA, USA). The pre-tRNA three tRNA transcript assays were imaged using a FLA5000 Phosphorimager (Fujifilm, Tokyo, Japan) and analysed using the AIDA software (Raytest, Straubenhardt, Germany). The dried gels were exposed to phosphorimager screens overnight. The gels were also exposed to x-ray films for 24-48 hours to visualise the bands.

2.14.11. Statistical analysis

The Wilcoxon paired test (N=<20) was used with a significance value of 0.05 to test for differences between the wild type and p.Ala485Val pairs for each pre-tRNA substrate.

To test for differences in the percentage reduction in the tRNA output of the p.Ala485Val variant between substrates the data was determined to be normally distributed using the Shapiro-Wilk test. One-way ANOVA with a significance value of 0.05 was used to test for differences.

2.15. Rescue experiments

2.15.1. Culture and transfection

The coding sequence of wild type *KIAA0391* was cloned in an expression vector as described previously (Deutschmann et al. 2014). The coding sequence was verified by Sanger sequencing. Patient dermal fibroblasts (2.0 x 10^5) were seeded in 25 cm^2 flasks and cultivated in 4 ml MEM (minimal essential media) overnight. The next day cells were transfected using 3µg plasmid DNA (PRORP-vector and empty vector) and 7.5 µl Turbofect transfection reagent (Thermo Fisher Scientific Inc, Waltham, MA, USA) and cultured for additional 48 hours. The cells were harvested and precursor tRNAs were quantified by real-time PCR as described previously (Deutschmann et al. 2014).

2.15.2. RNA extraction and reverse transcription

Total RNA from the confluent cell monolayers were isolated using the RNeasy Kit (Qiagen, Hilden, Germany) according to the manufacturer protocol. RNA concentration was determined by NanoDrop spectrophotometer (Thermo Fisher Scientific Inc, Waltham, MA, USA) and RNA integrity was confirmed by gel electrophoresis. 2 µg of total RNA was treated with Turbo™ DNase (Ambion, Thermo Fisher Scientific Inc, Waltham, MA, USA) for 60 min at 37°C. DNase was inactivated by addition of 15 mM EDTA and incubation at 75°C for 10 min. First-strand cDNA synthesis was carried out using the Maxima H minus first-strand cDNA synthesis kit (Fermentas, Waltham, MA, USA). 1 µg of DNase-treated total RNA and 2 µl of a primer mix in a total volume of 15 µl were incubated at 70°C for 10 min and chilled on ice. After adding of 4 µl of first-strand buffer and 1 µl Revert-Aid reverse transcriptase, the reaction was incubated at 60°C for 1 h and finally, for 5 min at 85°C.

The cDNA was diluted 1:4 for use in real-time PCR. The primer mix used in first-strand synthesis contained reverse primers specific tRNAs and Ubiquitin B (*UBB*, reference gene). An adaptor sequence was fused to each gene-specific primer which served as a reverse primer in real-time PCR analysis. Primers are available in (Deutschmann et al. 2014)

2.15.3. Strand-specific qRT-PCR

Real-time PCR analysis was performed on ABI PRISM 7000 Sequence Detection System using the Maxima SYBR Green qPCR Master Mix (Fermentas, Waltham, MA, USA). Primers available in Deutschmann et al. (2014). The qPCR reaction contained 12.5 µl SYBR Green qPCR master mix, 350 nM of forward and adaptor primers, and 2 µl of 1:4 diluted template cDNA in a total volume of 25 µl. PCR was performed using following conditions: 10 min at 95°C followed by 40 cycles of 15 s at 95°C and 1 min at 60°C. A dissociation protocol (65–95°C) was added after the PCR. Each assay included a non-template control, and a control for DNase digestion. Raw data was analysed in ABI Sequence Detection System software v.1.2.3 and exported to Excel for final analysis. Ct values were normalized against *UBB* and relative expression levels were calculated according to the 2ΔΔCt method (Deutschmann et al. 2014).

2.16. Yeast

2.16.1. Strains

The strains used were *Saccharomyces cerevisiae* BY4743, YPH500 and YPH501 strains. Genotypes and genetic modifications are detailed in the relevant experimental chapter.

2.16.2. Culture

Yeast cells were grown in standard YPD media (yeast extract peptone dextrose; 1% yeast extract, 2% bacto peptane, 2% glucose) or on YPD agar plates (YPD media and 2% agar) unless otherwise indicated. Strains YPH501_NOP14Δ Mouse Nop14, RSM23Δ_ Vector, RSM23Δ_ DAP3 and RSM23Δ_ DAP3C395Y were grown on Synthetic defined (SD)-URA plates (0.7% yeast nitrogen base without amino acids, 0.075% amino acids-URA, 2% glucose and 2% agar) for plasmid selection. YP-Ethanol (3%), YP-Acetate (2%) and YP-Glycerol (3%) plates were used as a non-fermentable carbon source. YP media is YPD

without dextrose (1% bacto-yeast extract 2% bacto-peptone). Yeast was always grown at 30°C unless stated otherwise.

2.16.3. Gene knockout

Gene knockout in yeast involved removing the entire open reading frame of the gene and replacing it with a selectable marker using homologous recombination. The deletion module containing the selectable marker, kanMX4, was amplified by PCR from a plasmid template. The primers contained sequence complementary to the deletion module at the 3' end and sequence complementary to the sequencing flanking the appropriate yeast gene at the 5' end for homologous recombination. The PCR product was assessed my agarose gel electrophoresis as in section 2.7.3 and purified using the QIAquick PCR Purification Kit (Qiagen, Hilden, Germany) according to manufacturer instruction. 35-50 µl of the deletion module was transformed into yeast using the High efficiency transformation protocol. The transformed cells were plated onto YPD and incubated overnight at 30°C. Colonies were transferred to selective medium and incubated for 2-3 days at 30°C. Gene knockout was confirmed using PCR and agarose gel electrophoresis.

2.16.4. Transformation

Plasmids were transformed into yeast using the one-step transformation method (Chen et al. 1992) or the high efficiency yeast transformation method (Gietz and Schiestl 2007).

For the one one-step transformation method (Chen et al. 1992) 1ml of overnight yeast culture was centrifuged (5000rpm, 2 mins) and the supernatant discarded. The cells were resuspended in H_2O and centrifuged (5000rpm, 2 mins). The supernatant was discarded and the cells resuspended in transformation mix (100µl of buffer (0.2M lithium acetate, 40% PEG, 0.1M DTT, at pH 5.0), 5µl salmon sperm (boiled then placed on ice) and 5µl of DNA (1µg/µl). The cells were heat shocked at 42°C for 30 minutes. The cells were centrifuged (5000rpm, 30 sec), the supernatant discarded and the cells resuspended in H_2O. The cells were plated onto the appropriate media and incubated at 30°C.

For the high efficiency yeast transformation method (Gietz and Schiestl 2007) an overnight culture of cells was diluted in 25ml of YPD to give an A_{600} of 0.5 units. The culture was incubated at 30°C with shaking until the A_{600} was 2 units. The cells were

centrifuged (3000rpm, 5mins) and the supernatant discarded. The cells were resuspended in H_2O and centrifuged (3000rpm, 5 mins). The supernatant was discarded and the cells resuspended in 700µl of 0.1 M lithium acetate and transferred to a microcentrifuge tube. The cells were centrifuged (14000rpm, 30 secs) and the supernatant discarded. The cells were resuspended in 200µl of 0.1 M lithium acetate and 50µl of cells were added to the transformation mix (36µl 1M lithium acetate, 240µl of 50% PEG 3500, 50µl salmon sperm (boiled then placed on ice) 1µg of DNA and H_2O to 360µl). The mix was vortexed and incubated at 30°C for 30 minutes. The cells were heat shocked at 42°C for 30 minutes. The cells were centrifuged (7000rpm, 15 secs), the supernatant removed and the cells resuspended in 1ml of YPD media. The cells were incubated for 1-3 hours at 30°C then centrifuged (7000rpm, 15 secs), the supernatant removed. The cell were resuspended in H_2O and plated on the appropriate media.

2.16.5. Yeast growth assay

Transformed cells (RSM23Δ_ DAP3 and RSM23Δ_ DAP3C395Y) were cultured in SD-URA liquid media for 2 days at 30°C before loading into a 96 well plate containing glucose media (SD-URA) and galactose media (SD- URA with galactose in place of glucose) Using an infinite F200 Pro machine the plate was incubated at 30°C for a total of 580 kinetic cycles over 48 hours and the cell growth measured. Each transformation had 8 replicates, including a negative control.

2.16.6. Sporulation

Yeast colonies were inoculated into sporulation media (1% potassium acetate, 0.005% zinc acetate, ura, his and leu supplement) and incubated with agitation for 5 days at room temperature and 3 days at 30°C before tetrad dissection.

2.17. Dermal fibroblast cell culture

2.17.1. Dermal fibroblast culture

Fibroblasts were cultured in Eagle's minimal essential medium (Sigma-Aldrich, St. Louis, MO, USA) supplemented with 10% (v/v) foetal bovine serum (FBS), 1 × non-essential amino acids, 1 mm sodium pyruvate and 50 µg/ml uridine, at 37 °C and 5% CO2.

2.17.2. Dermal fibroblast culture – stress conditions

The cells were cultured under the conditions above prior to seeding. Cells were seeded at 4,000 cells per well in a TPP 96 well plate with modified glucose media (Dulbecco's Modified Eagle's Medium (no glucose) (Thermo Fisher Scientific Inc, Waltham, MA, USA), 10% Dialysed FBS, 4.5 mg/ml glucose, 1mM pyruvate, 1X Penicillin/Streptomycin, 50mg/ml uridine). After 24 hours, the media was removed from all wells. Modified glucose media was added to half the wells of each cell line, and galactose media Galactose Media(Dulbecco's Modified Eagle's Medium (no glucose), 10% Dialysed FBS, 0.9 mg/ml galactose, 1mM pyruvate, 1X Penicillin/Streptomycin, 50mg/ml uridine) added to the other half. The plate was imaged, and confluence measured, every 2 hours for a period of 5 days using an Incucyte live cell imager.

2.18. HeLa cell methods

2.18.1 HeLa cell culture

HeLa cells were cultured in Dulbecco's Modified Eagle Medium (DMEM, Gibco, Thermo Fisher Scientific Inc, Waltham, MA, USA) with 10% FBS and 2mM Glutamax at 37°C in 10% CO_2. Cells were split upon 80-90% confluency as detailed below.

The culture media was removed. 5ml of phosphate buffered saline (PBS, Gibco, Thermo Fisher Scientific Inc, Waltham, MA, USA) was added and gently mixed. The PBS was aspirated and 1ml of TrypLE (Gibco, Thermo Fisher Scientific Inc, Waltham, MA, USA) added to the cells. The cells were incubated for 2-3 minutes at 37C. When removed from the incubator the dish was gently tapped to dislodge the cells and 3ml of DMEM media added to inactivate the TrypLE. The cells were mixed and the counted using a bright field automated cell counter and the appropriate amount of cells added to a fresh dish containing 9ml of pre-heated media.

2.18.2. HeLa cell transfection

HeLa cells were transfected with the plasmids Nop14-EGFP, Nop14-TurboGFP and Dap3-EGFP using Lipofectamine 3000 (Thermo Fisher Scientific Inc, Waltham, MA, USA) according to the manufacturers protocol. 1.6-1.75 ug of plasmid DNA was used per 2.5ul

of lipofetamine 3000 reagent. Briefly $10x^4$ cells were seeded into each well of a six well, when attached the cells were transfected using lipofectamine 3000 as below.

DNA master mixes were prepared for each plasmid (1.6µg DNA, 5µl P3000, 125µl Optimem media (Gibco, Thermo Fisher Scientific Inc, Waltham, MA, USA)). 125µl of the lipofectamine master mix (125µl Optimem and 2.5µl Lipofectamine 3000 per reaction) was added to each DNA master mix and gently mixed. Transfection master mixes were incubated at room temperature for 15 minutes. All but 500µl to 1ml of the media was removed from the cells to be transfected. 1-1.5ml of fresh warm media was added to the transfection master mix and which was then added to the cells and gently mixed. The transfected cells were incubated overnight at 37°C with 10% CO_2.

2.18.3. Preparation of fibronectin plates

Fibronectin (Sigma-Aldrich, St. Louis, MO, USA) was diluted 1 in 100 with PBS. 400µl of diluted fibronectin was added to the well in the centre of the glass bottomed plates (MatTek, Ashland, MA, USA). As much liquid as possible was removed without breaking the surface tension. The plates were incubated for 1 hour at 37°C or at 4°C overnight. The wells were washed 3 times with 1X PBS and DMEM (supplemented as noted previously) was added. The plates were stored at 37°C with 10% CO_2.

2.18.4. HeLa cell immunocytochemistry

For imaging cells using the confocal microscope HeLa cells were seeded onto glass bottom plates prepared with fibronectin. The cells were split as described above and approximately 200ul of cells were added to each fibronectin plate. The cells were incubated 37°C with 10% CO_2 for approximately 4 hours (3-5) until optimum cell density and attachment was achieved. The cells were then fixed in the following solution for 15 minutes at room temperature; 4% paraformaldehyde, 2% sucrose in PBS. After fixation the cells were washed 3 times in PBS and stored at 4°C until staining. Cells were permeabilised and blocked in 0.2% Triton X and 10% normal goat serum in PBS for 1 hour at room temperature with mild agitation. After permeabilisation/blocking the samples were washed 3 times with PBS. Cells were incubated with the primary antibodies in blocking solution (blocking solution - 2% normal goat serum in PBS) for 1-2 hours at room temperature with gentle agitation. Primary antibody details and concentrations are listed

in the appropriate experimental chapter. Samples were washed 3 times with PBS. The samples were incubated in secondary antibody solution (Phalloidin Alexa 647 (1 in 50), Hoechst (2.5µg/ml) and secondary antibody (1 in 250) in blocking solution) for 2 hours at room temperature with gentle agitation. After incubation the cells were washed 3 times in PBS and stored at 4°C in PBS to be imaged within 24 hours. The cells were imaged using a LSM780 confocal microscope (Zeiss Inc, Oberkochen, Germany) equipped with 63X, 1.4 N.A. objective. Images were viewed and exported using the Zen 2.3 SP1 software (Zeiss Inc, Oberkochen, Germany).

2.19. Immunohistochemistry in the mouse organ of Corti

2.19.1. Mouse strains

The NIH Animal Use Committee approved protocol 1263-15 to T.B.F. for mice. All the mice used were C57/BJ6 mice aged postnatal day 1 (P1) to P30.

2.19.2. Dissection of the organ of Corti

The mice were euthanized. Mice aged P10 or younger were euthanized by decapitation. Mice aged P11 or older were euthanized by CO_2 which was confirmed by decapitation. The cochlear capsule was removed in Leibowitz cell culture medium (Invitrogen, Carlsbad, CA, USA) and fixed with 4% paraformaldehyde in PBS for 2 hours. The samples were transferred to PBS and micro-dissected. The cochlear capsule was removed. The stria vascularis and Reissner membrane were removed and the tectorial membrane lifted away from the organ of Corti. A needle was used to dissociate the organ of Corti from the modiolus.

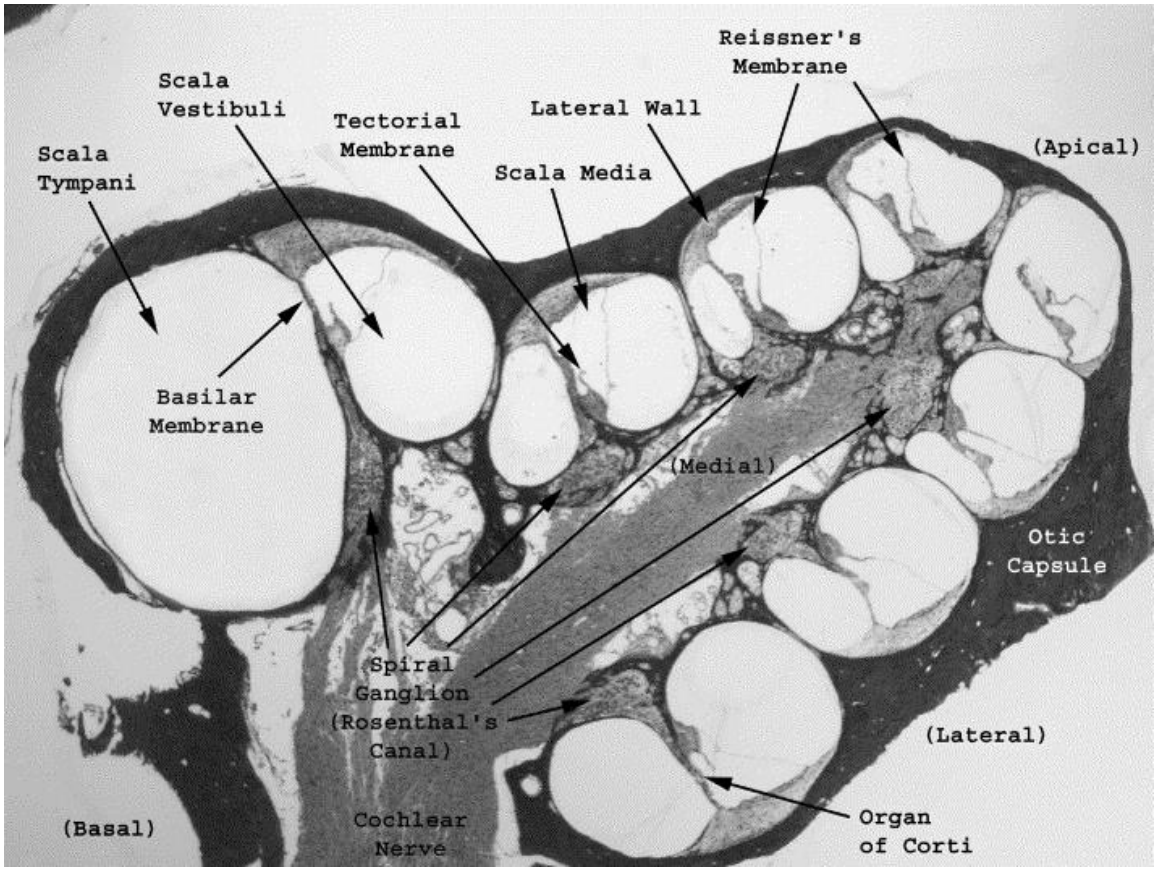

Figure 2.1. A low magnification light micrograph of a plastic cross-section of the guinea pig cochlea.

The general organisation of the cochlea is shown. The stria vascularis is attached to the lateral wall and the modiolus is the bone surrounding the cochlear nerve in the medial section. Image taken from Raphael and Altschuler (2003)

2.19.3. Immunohistochemistry

The organ of Corti was permeabilised with 1% Triton X-100 in PBS for 30 min followed by three 10 min washes with PBS. Nonspecific binding sites were blocked with 5% normal goat serum and 2% BSA in PBS for 1 hour at room temperature. Samples were incubated for 2 hours with the primary antibodies (detailed in the relevant experimental chapters) followed by three 10 min washes with PBS. Samples were incubated with secondary antibodies and cytoskeletal markers (see experimental chapters) for 30 min followed three 10 min washes with PBS and were mounted with ProLongGold Antifade staining reagent with DAPI (Molecular Probes, Invitrogen, Carlsbad, CA, USA). Slides were examined using LSM780 confocal microscope (Zeiss Inc, Oberkochen, Germany Inc,

Oberkochen, Germany) equipped with 63X, 1.4 N.A. objective. Images were viewed and exported using the Zen 2.3 SP1 software (Zeiss Inc, Oberkochen, Germany).

2.20 Gene gun explant transfections

The gene gun technique is used to transfect difficult to transfect tissues. The organ of Corti is difficult to transfect as the cuticular plate on which the auditory hair cells sit is dense (Belyantseva 2016). We used the gene gun method of transfection, which propels gold particles coated with plasmid DNA into the tissue past the cuticular plate. Gene gun explant transfections were performed as detailed in Belyantseva (2016).

2.20.1 Explant dish preparation

For the culture of tissue explants a collagen surface needs to be created for the explants to attach to the dish. Rat tail collagen for cell culture (Thermo Fisher Scientific Inc, Waltham, MA, USA) was diluted 1:1 with cell culture water (Gibco, Thermo Fisher Scientific Inc, Waltham, MA, USA). 7µl of the diluted collagen solution was added into the well of the culture dish (MatTek, Ashland, MA, USA). The solution was spread to cover the full surface of the well. The small dishes were placed inside a large petri dish. Filter paper was attached to the lid of the large petri dish. The filter paper was soaked with ammonium hydroxide and the excess removed. The lids were removed from the collagen coated dishes and the lid of the large dish returned. The collagen dishes were exposed to the ammonium hydroxide for 15-20 minutes to polymerise the collagen. After ammonium hydroxide exposure the collagen dishes were washed three times with cell culture water and stored with DMEM at 37°C with 5% CO_2 until use.

2.20.2. Preparation of explants

Organ of Corti explants were prepared under sterile conditions from P1 C57/BJ6 mice. Mice were euthanised and the organ of Corti was dissected as in section 2.17.2 in Leibovitz's L-15 Media (Gibco, Thermo Fisher Scientific Inc, Waltham, MA, USA) in a 60-mm sterile cell culture dish. The organ of Corti was transferred into the pre-prepared collagen dish containing 2 mL of DMEM supplemented with 7 % (v/v) Foetal Bovine Serum. The organ of Corti was submerged and gently pushed against the collagen substrate to facilitate attachment. The media was removed from the dish and replaced

with just enough to touch the explants without disturbing them. The explants were placed at 37°C with 5 % CO_2 and left undisturbed for one to three days.

2.20.3. Preparation of gene gun gullets

25 mg of gold microcarrier (Bio-Rad, Hercules, CA, USA) was weighed into a 1.5 mL centrifuge tube. 100µL of 0.05 M spermidine was added. The solution was vortexed for 10-15 seconds. The tube was sonicated for 30 seconds in a water bath sonicator. 50 µg of plasmid DNA (50 µL at1 µg/µL) was added and the solution was vortexed briefly to ensure even distribution of DNA in gold. 100 µl of 1 M $CaCl_2$ was added one drop at a time to DNA/gold solution which was vortexed after each drop. The DNA/Gold solution was incubated at room temperature for 10 minutes.

Approximately 76 cm of Tefzel tubing was cut and trimmed at both ends using the Bio-Rad Tubing cutter (Bio-Rad, Hercules, CA, USA). The tubing was inserted into the Tubing Prep Station (Bio-Rad, Hercules, CA, USA), leaving a 10 cm of the tube exposed. The nitrogen gas was turned on to 0.3-0.4L/min and the tubing flushed with nitrogen for 10-15 minutes.

20mg/ml of polyvinylpyrrolidone (PVP) was diluted to 50µg/ml (10µl of PVP to 4 mL of 100% ethanol in 15 mL conical tube). The gold particles were pelleted by centrifugation for 2 mins at 1000xg. Supernatant was aspirated leaving ~ 20µl in the tube in which the gold was resuspended through gentle tapping. The gold particles were washed 3 times in 1ml of 100% ethanol centrifuging at 1000xg for 2 minutes to pellet the gold particles before aspirating the supernatant. After the third ethanol wash most of the ethanol was removed and the gold particles resuspended in 200µl of 50µg/ml PVP and mixed by pipetting. The gold solution was transferred to a 15ml tube and the original tube washed out twice with 200µl of 50µg/ml PVP which was subsequently transferred into the 15ml tube containing the gold solution. The final volume of the gold solution was brought to 3ml with 50µg/ml PVP and vortexed. The gold solution was inverted continually to prevent clumping.

A syringe was attached to the exposed end of the Tefzel tubing. The Tefzel tubing was removed from the tubing station and the end not attached to the syringe was inserted

into the gold suspension. The gold suspension was steadily drawn into the tubing using the attached syringe drawing in the entire volume and leaving 2-3cm of tubing empty at the end where the solution was drawn in. The solution was inserted back into the tubing station and left undisturbed for 3 minutes. After the 3 minute incubation the supernatant was slowly removed using the syringe and the tubing rotated for 20-30 seconds. The nitrogen was slowly turned to 0.35-0.4 L/min while the tube rotated for 5 minutes. After 5 minutes the rotation and nitrogen were turned off and the coated tubing removed from the prep station. The tubing which was evenly coated in gold was cut into 1.3 cm sections using the tubing cutter and stored at 4°C in vials with DRICAP Capsule Dehydrators (Ted Pella, Redding, CA, USA). These gene gun cartridges contain approximately 1µg of plasmid DNA per cartridge.

2.20.4. Gene gun transfection of organ of Corti

Gene gun transfection was performed under sterile conditions and special care was taken to ensure the plastic barrel ring and diffusion screen, which are disposable components of the gene gun were sterile. The relevant plasmid bullets were loaded into the gene gun cartridge, leaving the first slot empty, and the gene gun (Bio-Rad, Hercules, CA, USA) assembled. The gene gun was connected to a helium tank and the pressure set to 110psi. The gene gun was fired using the blank slot one to ensure pressure was stable at 110psi. The slot was switched to one containing a cartridge and a diffusion screen inserted. A previously prepared explant was removed from the incubator and the culture medium removed and discarded. The plastic barrel ring was placed at the bottom of the culture dish with the tissue in the centre and the gene gun discharged. 2 mL of DMEM supplemented with 7 % (v/v) FBS was added to the culture which was returned to the incubator. The process was repeated for additional tissue explants. After an additional 8 hours to 4 days in culture, samples were fixed in 4% paraformaldehyde and stained using the same method as the tissue samples above.

Chapter 3: Expanding the genotypic spectrum of Perrault syndrome

CLINICAL GENETICS An International Journal of Genetics, Molecular and Personalized Medicine

Clin Genet 2017: 91: 302–312
Printed in Singapore. All rights reserved

CLINICAL GENETICS
doi: 10.1111/cge.12776

Original Article

Expanding the genotypic spectrum of Perrault syndrome

Demain L.A.M., Urquhart J.E., O'Sullivan J., Williams S.G., Bhaskar S.S., Jenkinson E.M., Lourenco C.M., Heiberg A., Pearce S.H., Shalev S.A., Yue W.W., Mackinnon S., Munro K.J., Newbury-Ecob R., Becker K., Kim M.J., O' Keefe R.T., Newman W.G. Expanding the genotypic spectrum of Perrault syndrome.
Clin Genet 2017: 91: 302–312. © John Wiley & Sons A/S. Published by John Wiley & Sons Ltd, 2016

Perrault syndrome is a rare autosomal recessive disorder characterized by sensorineural hearing loss (SNHL) in both sexes and primary ovarian insufficiency in 46, XX karyotype females. Biallelic variants in five genes are reported to be causative: *HSD17B4*, *HARS2*, *LARS2*, *CLPP* and *C10orf2*. Here we present eight families affected by Perrault syndrome. In five families we identified novel or previously reported variants in *HSD17B4*, *LARS2*, *CLPP* and *C10orf2*. The proband from each family was whole exome sequenced and variants confirmed by Sanger sequencing. A female was compound heterozygous for a known, p.(Gly16Ser) and novel, p.(Val82Phe) variant in D-bifunctional protein (*HSD17B4*). A family was homozygous for mitochondrial leucyl aminocyl tRNA synthetase (mtLeuRS) (*LARS2*) p.(Thr522Asn), previously associated with Perrault syndrome. A further family was compound heterozygous for mtLeuRS, p.(Thr522Asn) and a novel variant, p.(Met117Ile). Affected individuals with *LARS2* variants had low frequency SNHL, a feature previously described in Perrault syndrome. A female with significant neurological disability was compound heterozygous for p.(Arg323Gln) and p.(Asn399Ser) variants in Twinkle (*C10orf2*). A male was homozygous for a novel variant in CLPP, p.(Cys144Arg). In three families there were no putative pathogenic variants in these genes confirming additional disease-causing genes remain unidentified. We have expanded the spectrum of disease-causing variants associated with Perrault syndrome.

Conflict of interest

The authors declare no conflicts of interest. The study sponsor had no role in any aspect of the report.

L.A.M. Demain[a], J.E. Urquhart[a], J. O'Sullivan[a], S.G. Williams[a], S.S. Bhaskar[a], E.M. Jenkinson[a], C.M. Lourenco[b], A. Heiberg[c], S.H. Pearce[d], S.A. Shalev[e,f], W.W. Yue[g], S. Mackinnon[g], K.J. Munro[h,i], R. Newbury-Ecob[j], K. Becker[k], M.J. Kim[l], R.T. O' Keefe[m] and W.G. Newman[a,i]

[a]Manchester Centre for Genomic Medicine, Institute of Human Development, University of Manchester, Manchester, UK, [b]Clinics Hospital of Ribeirao Preto, University of São Paulo, São Paulo, Brazil, [c]Department of Medical Genetics, Oslo University Hospital, Oslo, Norway, [d]Institute of Genetic Medicine, Newcastle University, Newcastle upon Tyne, UK; and Endocrine Department, Newcastle upon Tyne Hospitals, Newcastle upon Tyne, UK, [e]The Institute for Genetics, Ha'Emek Medical Centre, Afula, Israel, [f]Rapapport faculty of Medicine, Technion Haifa, Haifa, Israel, [g]Structural Genomics Consortium, Nuffield Department of Clinical Medicine, University of Oxford, Oxford, UK, [h]School of Psychological Sciences, University of Manchester, Manchester, UK, [i]Central Manchester University Hospitals NHS Foundation Trust, Manchester Academic Health Science Centre, Manchester, UK, [j]Clinical Genetics, St Michaels Hospital, Bristol Genetics Laboratory Pathology Sciences, Southmead Hospital Bristol, Bristol, UK, [k]Medical Genetics Center, Munich, Germany, [l]Department of Obstetrics and Gynecology, The Catholic University of Korea, Seoul, Korea, and [m]Faculty of Life Sciences, University of Manchester, Manchester, UK

Key words: low frequency hearing loss – Perrault syndrome – primary ovarian insufficiency – sensorineural hearing loss

Corresponding author: William G. Newman, Manchester Centre for Genomic Medicine, University of

Manchester, 6th Floor, St Mary's Hospital, Oxford Road, Manchester, M13 9WL, UK.
Tel.: +44 161 276 6276;
fax: +44 161 276 6145;
e-mail:
william.newman@manchester.ac.uk

Received 21 December 2015, revised and accepted for publication 7 March 2016

Perrault syndrome (MIM 233400) (1) is a rare autosomal recessive disorder (2). Approximately 40 families worldwide have been reported (3). The syndrome is characterized by sensorineural hearing loss (SNHL) in both sexes and primary ovarian insufficiency (POI) in 46, XX karyotype females (2). Additional features have been noted in some individuals with Perrault syndrome, the most common of which are neurological, including ataxia, neuropathies and intellectual disability (4). Marfanoid habitus without the other features of Marfan syndrome have also been noted in some individuals (5, 6). Perrault syndrome is clinically and genetically heterogeneous with disease-causing variants identified in five genes; *HSD17B4* (MIM 233400) (7), *HARS2* (MIM 614926) (8), *LARS2* (MIM 615300) (9), *CLPP* (MIM 614129) (10) and *C10orf2* (MIM 616138) (11). Variants in the *HSD17B4* gene are associated with both D-bifunctional protein (DBP) deficiency (MIM 261515) (1), a peroxisomal disorder (12) and Perrault syndrome (7). The other four genes associated with Perrault syndrome encode mitochondrial proteins (8–11) and indicate that dysregulation of mitochondrial homeostasis through altered mitochondrial protein synthesis and degradation can lead to this specific phenotype.

In the majority of reported individuals with Perrault syndrome the genetic basis has not been determined (13). Here we describe novel and previously reported variants in *HSD17B4*, *LARS2*, *C10orf2* and *CLPP* in five families. In three families we did not identify pathogenic variants in the known Perrault syndrome genes.

Materials and methods

All patients provided written informed consent in accordance with local regulations. Ethical approval for this study was granted by the National Health Service Ethics Committee (05/Q1404/49) and the University of Manchester. DNA was extracted by standard methods from blood or saliva samples from affected individuals and their relatives where available. Autozygosity mapping was performed on the proband from family P8 using the Genome-wide SNP6.0 arrays (Affymetrix, High Wycombe, UK), as previously described (14). Whole exome sequencing was performed on the proband from each family. The SureSelect Human All Exon V5 Panel (Agilent, Stockport, UK) was used for library preparation and sequencing was performed on the HiSeq 2500 (Illumina, Cambridge, UK) as previously described (15). The exome data for the probands of the families P1–P7 were filtered for any possible causative variants in the five genes associated with Perrault syndrome. For the proband from family P8 the exome data were filtered to only include variants in regions of homozygosity >2 Mb as identified from the array data. Heterozygous variants were removed, as were variants previously seen in-house as homozygous, and variants present on ExAC (16) (http://exac.broadinstitute.org), EVS (17) (http://evs.gs.washington.edu/EVS/) or dbSNP (18) (http://www.ncbi.nlm.nih.gov/SNP/) with a frequency greater than 1%. The remaining variants were assessed by gene function, any known pathogenicity and by the predicted functional effect from SIFT (19) (http://sift.jcvi.org/), POLYPHEN 2 (20) (http://genetics.bwh.harvard.edu/pph2/) and MUTATION TASTER (21) (http://www.mutationtaster.org/).

Sequence variants were confirmed in the probands and available family members via Sanger sequencing using ABI big Dye v3.1 sequencing technology (Thermo Fisher Scientific Inc.). Primer sequences are available on request. Segregation with autosomal recessive inheritance was confirmed in families P1, P3 and P4. Parental samples were not available for family P2 or P8. Samples were not available from unaffected siblings in families P1, P2 and P8.

Variants have been submitted to the following LOVD databases: *HSD17B4* (http://databases.lovd.nl/shared/genes/HSD17B4), *LARS2* (http://databases.lovd.nl/shared/genes/LARS2), *C10orf2* (http://databases.lovd.nl/shared/genes/C10orf2) and *CLPP* (http://databases.lovd.nl/shared/genes/CLPP). Variant information and allele frequencies are provided in Table 1.

Results

Clinical reports

The clinical details of all affected individuals are presented in Table 2 and the family pedigrees for P1–P4 and P8 in Fig. 1.

Family P1 are non-consanguineous and of Brazilian descent. The family consists of the female proband, her unaffected brother and their unaffected parents. The proband presented with bilateral progressive, severe-to-profound SNHL (Fig. 2), POI and progressive cerebellar ataxia. She wears bilateral hearing aids. Her hormone profile is consistent with hypergonadotropic hypogonadism (Table 2). Thyroid stimulating hormone (TSH) levels are normal. The uterus and both ovaries

Table 1. Variants identified in five Perrault syndrome families[a]

Gene	*HSD17B4*	*HSD17B4*	*LARS2*	*LARS2*	*C10orf2*	*C10orf2*	*CLPP*
Variant	c.46G>A p.(Gly16Ser)	c.244G>T p.(Val82Phe)	c.351G>C p.(Met117Ile)	c.1565C>A p.(Thr522Asn)	c.968G>A (Arg323Gln)	c.1196A>G p.(Asn399Ser)	c.430T>C p.(Cys144Arg)
Ref Seq transcript	NM_000414	NM_000414	NM_015340	NM_015340	NM_021830	NM_021830	NM_006012
Novel or known variant	Known (12)	Novel	Novel	Known (9)	Known (16)	Known (43)	Novel
ExAC (16)	27 of 121,004 alleles, no homozygotes	Not present	Not present	31 of 121,404 alleles, no homozygotes	1 of 121,316 alleles	Not present	Not present
EVS minor allele frequency (17)	A = 0.0231	Not present	Not present	Not present	Not present	Not present	Not present
dbSNP (18)	rs137853096	Not present	Not present	rs199589947	Not present	Not present	Not present
POLYPHEN 2 (human div score) (20)	Probably damaging (0.999)	Possibly damaging (0.884)	Probably damaging (0.997)	Probably damaging (1.00)	Probably damaging (1.00)	Probably damaging (0.993)	Possibly damaging (0.920)
SIFT (19)	Deleterious (0)	Deleterious (0)	Deleterious (0)	Deleterious (0)	Tolerated (0.2)	Tolerated (0.09)	Deleterious (0.03)
MUTATION TASTER (probability of prediction) (21)	Disease causing (0.9999)	Polymorphism (0.9970)	Disease causing (0.9999)	Disease causing (0.9999)	Disease causing (0.9998)	Disease causing (0.9984)	Disease causing (0.9999)
Additional information	Associated with DBP deficiency (23); 3D structure available	A different variant (p.Val82Ile) is seen at this residue in ExAC and EVS; 3D structure available	Structure of homologue available	Associated with Perrault syndrome (9); structure of homologue available	None	Seen in COSMIC (44) – COSM1745577	3D structure available

DBP, D-bifunctional protein.

[a]Minor allele frequencies are included where applicable.

Table 2. Clinical details for the affected members of families P1–P8[a]

Individual ID	P1:II-1	P2:II-1	P2:II-2	P3:II-1 (22)	P3:II-2 (22)	P4:II-1	P5:II-1	P5:II-2	P6:II-1 (5)	P7:II-1	P8:II-1
Ethnicity	Brazilian	Argentinian	Argentinian	White British	White British	Norwegian	White British	White British	Korean	Kurdish Turkish	Arabic
Sex	F	F	M	F	M	F	F	F	F	F	M
Karyotype	NR	46, XX	NR	46, XX	NR	NR	46, XX	46, XX	46, XX	46, XX	46, XY
Age (yrs) at last assessment	43	27	26	25	26	48	17	14	15	19	24
Age (years) at molecular diagnosis	43	30	27	25	26	48	NA	NA	NA	NA	32
Sensorineural hearing loss											
Age (years) at hearing loss diagnosis	NR	8	26	2.5	2.5	3	Childhood	Childhood	4	Prelingual	1.2
Degree of hearing loss	Severe/ profound	Moderate	Mild/ moderate	Severe/ profound	Severe/ profound	Severe/ profound	Moderate	Moderate	Profound, unilateral	Profound	Severe/ profound
Gonadal dysfunction											
Pelvic ultrasound	Small uterus and ovaries	Small uterus and ovaries	NA	Small uterus and ovaries	NA	Small uterus and ovaries	Ovarian dysgenesis	Ovarian dysgenesis	Hypoplasic uterus and ovaries	Absent uterus, ovarian dysgenesis	NA
Menarche	NR	N	NA	Y	NA	N	N	N	N	N	NA
POI	Y	Y	NA	Y	NA	Y	Y	Y	Y	Y	NA
FSH	72 (0.9–15) IU/l	99.6 (2.3–29) IU/l	NR	74 (≤30) IU/l	3.1 (1–11) IU/l	NR	86.1 IU/l	81.2 IU/l	108.76 (0.3–9.0) IU/l	NR	2.69 (1.50–12.40) IU/L
LH	59 (1.3–13) IU/l	48.0 (1.7–52) IU/l	NR	63 (≤30) IU/l	3.9 (1–11) IU/l	NR	27.5 IU/l	24.5 IU/l	21.8 (0.1–10.6) IU/l	NR	6.59 IU/L
Estradiol	12.6 pg/ml	7.04 (10–388) pg/ml	NA	91 (>180) pmol/l	NA	NR	<1	<44 pmol/l	12.01 (20–50) pg/ml	NR	NA
Azoospermia	NA	NA	NR	NA	NR	NA	NA	NA	NA	NA	Y
Neurological features											
Ataxia	Y	N	N	N	N	Y	N	N	N	N	N
Other	N	N	N	N	N	Severe progressive sensory motor neuropathy, atrophy of cerebellum, nystagmus	N	N	N	N	Lower limb peripheral neuropathy,
Additional features											
Very long chain fatty acids normal		N	N	Mild facial dysmorphia, hemidystropy	Hypospadias, mild facial dysmorphia, normal testosterone 22.3 (9–25)	Scoliosis	TPO antibodies	Hypothyroidism, TPO antibodies	Marfanoid proportions, cataracts	Marfanoid proportions	Testosterone 2.24 (2.41–8.27) ng/mL

F, female; FSH, follicle stimulating hormone; LH, luteinising hormone; M, male; NA, not applicable; NR, not recorded; POI, primary ovarian insufficiency; TPO, thyroid peroxidase.

[a]Where available the reference values for the hormone profiles are provided in brackets next to the patient measurements. Family P3 was previously presented in Jenkinson et al. (22) as family P8. The proband from P6 was previously presented by Kim et al. (5).

N = absent, Y = present

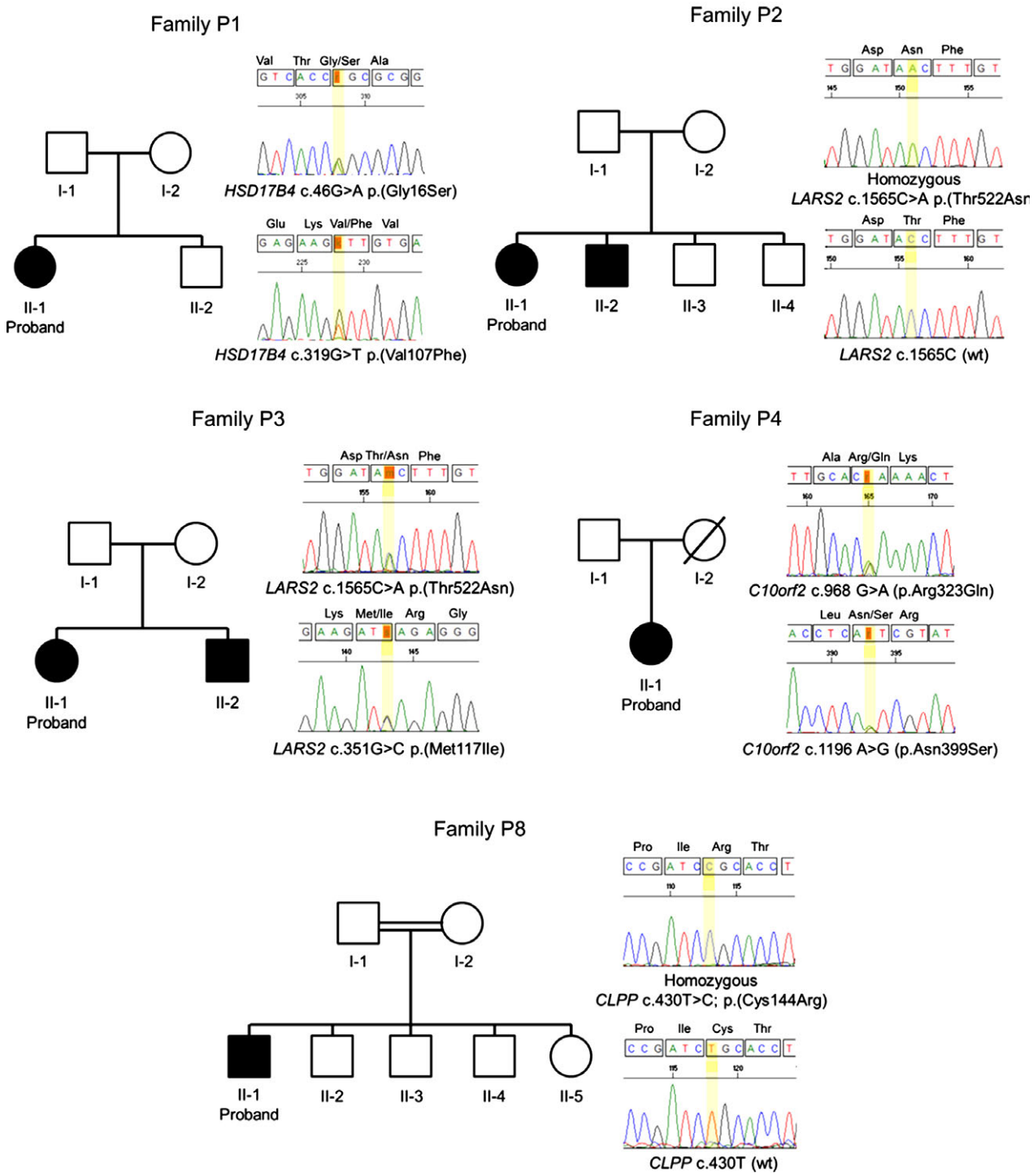

Fig. 1. Pedigrees and Sanger sequencing traces for families P1–P4 and P8. Filled icons indicate affected individuals.

appear small but structurally normal on ultrasound. The proband also has a mild intellectual disability. Very long chain fatty acid (VLCFA) analysis was normal.

Family P2 are non-consanguineous and of Argentinian descent. The family consists of the female proband, one affected male sibling, two unaffected male siblings and their unaffected parents. The proband was diagnosed with bilateral moderate SNHL at 8 years, which was progressive to severe SNHL by age 21 and she has now been fitted with a cochlear implant. The affected male sibling was diagnosed with SNHL at the age of 26 years and has no additional clinical features. The audiograms for both affected siblings show an uncommon pattern of low frequency loss (Fig. 2). The proband was diagnosed with primary amenorrhea at 15 years of age with a 46, XX karyotype. The uterus and both

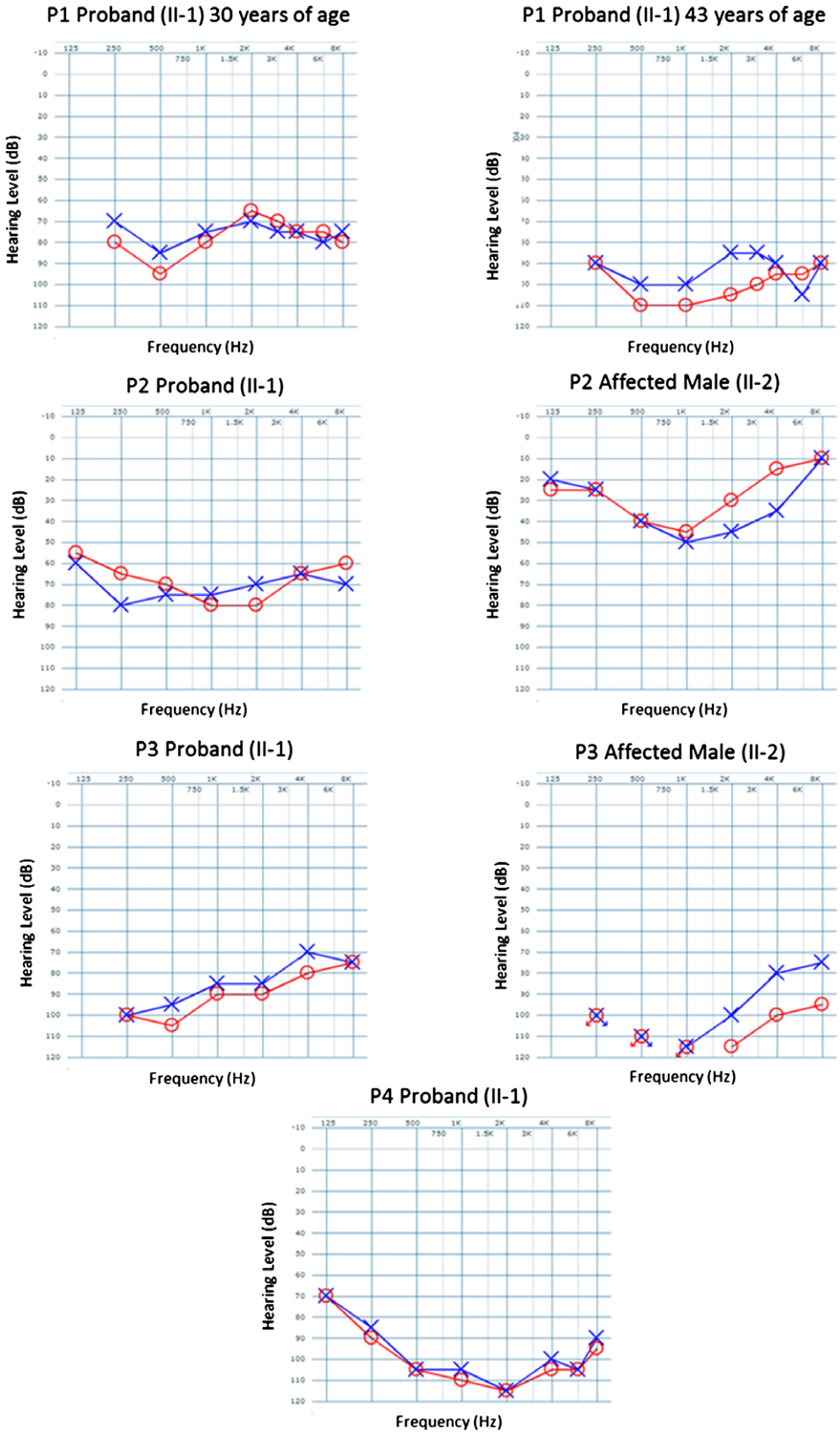

Fig. 2. Audiograms from affected members of families P1, P2, P3 and P4. Audiograms were not available for the proband from family P8. The hearing level of the left ear is represented by the crosses and the right ear by circles. The arrows indicate no response to stimuli. Audiograms were created using the AUDGEN online tool (version 0.71) (http://audsim.com/audgen/).

ovaries are visible and structurally normal on ultrasound but small. Measurement of hormone levels confirmed a diagnosis of hypergonadotropic hypogonadism in the proband (Table 2) and she is currently receiving estrogen replacement therapy. Hormone levels were not assessed in the affected male sibling. No neurological features have been noted in this family and all members have normal levels of intelligence.

Family P3 are a non-consanguineous family of British descent, consisting of the female proband, one affected male sibling and their unaffected parents. Both siblings have bilateral severe-to-profound SNHL which presents as an uncommon audiometric configuration of low frequency hearing loss resulting in an up-sloping audiogram (Fig. 2). The proband has been fitted with a cochlear implant. At puberty the proband presented with oligomenorrhea with a hormone profile indicative of hypergonadotropic hypogonadism and a 46, XX karyotype (Table 2.). On ultrasound the uterus and ovaries appear small but structurally normal. The affected male in this family has presented with hypospadias but displays no other urogenital features and hormone levels were normal (Table 2.). Both siblings have mild facial dysmorphic features, including low-set ears and a hypoplastic midface. The proband also has slight hemi-dystrophy with a smaller left hand, arm and foot. Peripheral nerve conduction tests performed on the proband aged 10 years were normal and no other neurological features have been observed in this family. All family members have normal levels of intelligence. This family has previously been screened for variants in *HSD17B4* and *HARS2* with no putative pathogenic variants identified (22).

Family P4 is a non-consanguineous family of Norwegian descent. The family consists of the female proband and her unaffected parents, the mother in this family is deceased. The proband had normal early development, but ataxia and bilateral SNHL became apparent before the age of 3 years, both were progressive (Fig. 2). At age 48 years the affected woman requires a wheelchair and has had bilateral cochlear implants fitted. The proband was also diagnosed with primary amenorrhea and a small uterus and ovaries on ultrasound. Hormone profiles are indicative of hypergonadotropic hypogonadism (values not available). She has a number of neurological signs including areflexia, oculomotor paresis, nystagmus and a severe progressive peripheral neuropathy, which is more pronounced distally. An magnetic resonance imaging (MRI) of the brain at 35 years showed severe atrophy of the cerebellum and atrophy of the cervical medulla. The assessment of intelligence is difficult but is considered to be normal or slightly below average.

Family P5 is a non-consanguineous family of British descent consisting of two affected female siblings and their unaffected parents. Both sisters have moderate progressive bilateral SNHL with childhood onset (Fig. S1, Supporting information). Both sisters have also presented with primary amenorrhea, ovarian dysgenesis and hormone profiles consistent with hypergonadotropic hypogonadism. No neurological presentations were noted in the sisters and both have normal levels of intelligence.

Family P6 is comprised of a female proband from a previously reported non-consanguineous Korean family (Fig. S1) (5).The proband is the only child of unaffected parents. Profound SNHL was diagnosed in the left ear at 4 years of age. The right ear showed a mild loss at higher frequencies at 15 years of age. Primary amenorrhea with a lack of secondary sexual characteristics was noted at 15 years of age with a 46, XX karyotype and hormone profiles of hypergonadotropic hypogonadism (Table 2). She developed cataracts at 11 years and marfanoid proportions were noted No neurological phenotypes were noted in this individual and intelligence levels were normal (5). Prior to whole exome sequencing, *HSD17B4*, *HARS2* and *PSMC3IP* were screened with no causative variants found. A microarray identified a heterozygous maternally inherited 0.32 Mb microdeletion at 16p12.2 (5). Exome sequencing identified no potential pathogenic variants on the paternal allele encompassing the microdeletion.

An affected female from a family of Kurdish Turkish descent (P7) was ascertained. The proband has six unaffected siblings and unaffected parents. The parents of the proband are third cousins. The proband has bilateral profound SNHL with prelingual onset and has bilateral cochlear implants (audiograms not available). She presented with primary amenorrhea at 19 years of age. Breast development was absent and ovarian dysgenesis was determined. Her karyotype is 46, XX. The uterus was absent, a feature which has not previously been noted in individuals with Perrault syndrome. She also has marfanoid proportions. No neurological phenotype was noted and her intelligence is normal. Prior to whole exome sequencing four genes for Perrault syndrome had been screened; *HSD17B4*, *HARS2*, *LARS2* and *CLPP* and no causative variants were identified.

Families P1–P7 were ascertained after being clinically diagnosed with Perrault syndrome, subsequent molecular investigations were undertaken. Family P8 are unusual in this study as they were investigated on the basis of a phenotype of SNHL and peripheral neuropathy. The clinical diagnosis of Perrault syndrome was achieved on the basis of the molecular data.

Family P8 is a consanguineous family of Arabic descent consisting of the male proband, four unaffected siblings and their unaffected parents. As the proband from this family is an adult male with no affected siblings he was not initially identified as having Perrault syndrome. Bilateral SNHL was identified at 14 months of age and is currently severe-to-profound (audiograms are not available), speech is near normal. The father of the proband has cerebellar ataxia, the cause of which is undetermined despite extensive investigation. Foot drop with sudden onset was noted in the proband at 24 years of age. Examination in adulthood noted no dysmorphic features, no cerebellar signs and no neurological symptoms other than the foot drop. The upper limbs were found to be normal. The proband is also azoospermic. Neurophysiology revealed a sensory-motor demyelinative axonal peripheral neuropathy of the lower limbs. Spinal CT

(computerized tomography) and lumbar MRI were normal. High levels of protein in the cerebrospinal fluid were reported which did not alter with steroid treatment. Sequencing of the connexin 26 gene *GJB2* was performed but no putative pathogenic variants were found. Chromosome testing showed a 46, XY karyotype and genetic testing excluded Charcot–Marie–Tooth disease.

Variants and structural predictions

Family P1

The proband was compound heterozygous for the variants *HSD17B4*, c.46G>A, p.(Gly16Ser) on the maternal allele and c.244G>T, p.(Val82Phe) on the paternal allele. p.(Gly16Ser) is the most common variant associated with DBP deficiency and is functionally deleterious (23). p.(Val82Phe) is a novel variant. *HSD17B4* encodes the DBP and catalyzes two steps of the β-oxidation of fatty acids via the function of separate dehydrogenase and hydratase domains (24). Both variants are located in the dehydrogenase domain of the enzyme (Fig. S2a)(23). Gly16 is an almost invariant residue located within the binding site for the essential cofactor NAD+. The substitution for serine at this position is likely to reduce NAD+ binding, by altering the shape of the binding site and causing steric clash (23). In contrast, Val82 is not in direct contact with NAD+, but located in an alpha helix immediately following a NAD binding site loop. The substitution of valine for the slightly bulkier phenylalanine residue may cause a small rearrangement that interferes with NAD binding, but to a lesser extent than predicted for the Gly16Ser variant.

Family P2

Affected members of family P2 were homozygous for the variant *LARS2* c.1565C>A p.(Thr522Asn). This variant has been previously associated with Perrault syndrome in a consanguineous family of Palestinian descent (9). *LARS2* p.(Thr522Asn) is located in the catalytic domain of the protein at a conserved residue (9).

Family P3

The proband and her affected brother were compound heterozygous for the variants in *LARS2*: c.1565C>A p.(Thr522Asn) (9), on the maternally inherited allele and c.351G>C p.(Met117Ile), on the paternally inherited allele. p.(Met117Ile) is a novel *LARS2* variant.

LARS2 encodes mitochondrial leucyl aminocyl tRNA synthetase (mtLeuRS) which is responsible for the addition of leucine to the appropriate tRNA molecule during mitochondrial translation (25).The human structure of mtLeuRS has not been elucidated. The closest structural ortholog is leucyl tRNA-transferase from *Thermus thermophilus*, LeuRSTT (35% identity). Both human residues Met117 and Thr522 are conserved in LeuRSTT *thermophilus* (Met68 and Thr500, respectively) (Fig. S2b). Met68 is an evolutionarily variable residue in the catalytic Rossmann domain, and its side-chain interfaces with the nearby anticodon binding domain. The Met-to-Ile substitution introduces a shorter but more branched side chain at the domain–domain interface. In contrast, Thr500 is a highly conserved residue within the LeuRSTT *thermophilus* catalytic domain. Thr500 contacts several invariant residues at the nearby leucine-binding pocket (Tyr43, Asp80 and Phe501) for the ATP-dependent synthetase reaction. The Thr-to-Asn substitution introduces a residue of similar size, but replaces the hydroxyl group with an amine group. While the change is subtle, the strictly invariant nature of nearby residues in the ligand binding pocket implicates less tolerance for the Thr522Asn change, compared with Met117Ile. Recently, it was shown that the change Thr522Asn results in a ninefold reduction in the catalytic activity of mtLeuRS (26).

Family P4

The proband was compound heterozygous for variants: *C10orf2* c.968G>A, p.(Arg323Gln) and c.1196A>G p.(Asn399Ser) on the paternally inherited allele. A sample from the mother was not available for analysis. *C10orf2* encodes Twinkle, a mitochondrial hexameric helicase which is part of the DNA replisome. It comprises the C-terminal domain homologous to the T7 phage gp4 helicase domain (24% sequence identity), and the N-terminal domain of unknown fold or function. Most known disease-causing mutations, including p.(Arg323Gln) and p.(Asn399Ser), map to the C-terminal domain or the inter-domain linker, neither of which has available structural information. Arg323 lies in the inter-domain linker, while Asn399 is a highly conserved residue located in the helicase domain (27). Asn399 is positioned near the interface between any two subunits of the hexamer, but it is not involved in hexamer formation, nucleotide binding or the DNA unwinding action.

Family P8

The proband was homozygous for the variant *CLPP* c.430T>C; p.(Cys144Arg). Samples from additional family members were not available for analysis. CLPP is a protease subunit of the ClpXP complex, composed of one hexameric CLPX ring sitting on top of two heptamer CLPP rings. ClpXP is responsible for unfolding and degrading misfolded proteins in the mitochondrial matrix (28). The structure of human CLPP has been elucidated. Cys144 is a conserved residue on the surface of a CLPP subunit, and of the heptamic ring (Fig. S2c). While the Cys144 amino acid position tolerates similar uncharged amino acids, mutation of Cys144Arg introduces a bulkier, positively charged residue within a sterically packed environment of bulky residues (Trp90, Tyr62, and His112). The conservation and location of Cys144 suggests a role in interaction with ClpX, which the variant may interfere with. p.(Cys144Arg) lies adjacent to the variants c.433A>C, p.(Thr145Pro) and c.440G>C, p.(Cys147Ser) previously identified in families with Perrault syndrome (10).

Putative pathogenic variants in the five genes previously associated with Perrault syndrome were not

identified in families P5, P6 or P7. The exome data from these three families was examined for variants in 96 genes, including Perrault syndrome genes, and those associated with both syndromic and non-syndromic hearing loss (Table S1). No putative pathogenic variants were identified (Table S2). Therefore these individuals will form part of an additional gene discovery cohort.

Discussion

We report the identification of very rare or novel variants in genes previously associated with Perrault syndrome, in five families. The lack of variants in the known genes in the three other families is consistent with the known genetic heterogeneity in Perrault syndrome (13, 22) and supports the contention that further disease-causing genes remain to be discovered. There were no obvious clinical features differentiating the individuals in whom disease-causing variants were identified compared with those in whom the molecular basis remains unresolved.

There is a large clinical overlap between DBP deficiency and Perrault syndrome (29). DBP deficiency types I–III are severely life limiting with affected individuals rarely surviving beyond 2 years of age. The clinical presentations include: hypotonia, seizures, hearing and vision loss, myelination defects and failure to achieve developmental milestones (30). DBP deficiency type IV has been defined as DBP deficiency due to compound heterozygous variants affecting two different domains of DBP, but associated with a relatively milder clinical and biochemical phenotype (29). The clinical features include moderate-to-severe bilateral SNHL, ataxia, pes cavus, sensory motor neuropathy, retinal atrophy, intellectual disability and fertility problems in males and females. To date, all individuals with DBP deficiency type IV have been diagnosed in adolescence or adulthood (29, 31, 32). The affected sisters with Perrault syndrome due to *HSD17B4* variants (7) from the original report share clinical features with DBP deficiency (29). VLCFA levels were not reported in the sisters (7). However, they were normal in the affected individual in our report, consistent with reports of normal, or only slightly increased, levels in DBP deficiency type IV (29). The proband would not meet the new definition of DBP deficiency type IV as both the variants are located in the dehydrogenase domain of the protein. The combination of the variant known to be highly deleterious, p.(Gly16Ser) (23), and the variant predicted to be hypomorphic, p.(Val82Phe), may have reduced the activity of DBP below a threshold level to produce a phenotype, although one less severe than that of individuals affected by DBP deficiency.

Both families in this study with Perrault syndrome due to *LARS2* variants were homozygous or compound heterozygous for the previously reported *LARS2* variant, c.1565C>A p.(Thr522Asn) (9). The low prevalence of this allele (allele frequency, ExAC – 0.0003) in the general population and its presence in three families with Perrault syndrome suggests that it may be a hotspot variant for Perrault syndrome. The uncommon pattern of low frequency hearing loss with some preservation at higher frequencies is now reported in three families with *LARS2* variants (9). Two other families with Perrault syndrome due to different *LARS2* variants (9, 33) did not have this audiological pattern of hearing loss suggesting that the p.(Thr522Asn) substitution may be associated with this specific phenotype. Autosomal dominant non-syndromic low frequency SNHL can also be caused by heterozygous variants in *WFS1* and *DIAPH1* (34). Recently, variants in *LARS2* were identified in an infant with hydrops, lactic acidosis, sideroblastic anemia, and multisystem failure. The affected infant was compound heterozygote for the variants *LARS2* c.1289C>T p.(Ala430Val) and p.(Thr522Asn) (26). This represents a significantly more severe phenotype than seen in individuals with Perrault syndrome due to *LARS2* variants. The two families included in this report with the variant p.(Thr522Asn) did not display any of the phenotypic features associated with this more severe case (26). The variant p.(Ala430Val) is reported to cause an 18-fold loss of aminoacylation catalytic efficiency in comparison to a 9-fold catalytic efficiency loss associated with the p.(Thr522Asn) variant which may account for the more severe phenotype (26). The different phenotypes are consistent with those seen for other mitochondrial aminoacyl-synthetase gene disorders, including variants in *NARS2* which may cause non-syndromic hearing loss or Leigh syndrome (35) and variants in *AARS2* which may cause infantile mitochondrial cardiomyopathy (36) or leukoencephalopathy with POI (37).

Variants in *C10orf2* have been associated with two neuromuscular diseases characterized by deletions or depletion in mtDNA: mitochondrial DNA depletion syndrome 7 (MTDPS7) and progressive external ophthalmoplegia 3 (PEOA3) (27). MTDPS7 is an autosomal recessive condition characterized by ophthalmoplegia, SNHL, ataxia, epilepsy, sensory neuropathy, hypergonadotropic hypogonadism in females and cerebellar atrophy (38), whereas PEOA3 is an autosomal dominant disorder characterized by ptosis, ophthalmoplegia and exercise intolerance, and in some affected individuals neuropathy, ataxia and hearing loss (39). In the two reported families with Perrault syndrome due to variants in *C10orf2* and in our affected individual (P4) there was significant clinical overlap with MTDPS7, including nystagmus, ataxia and neuropathies (11).

CLPP encodes the caseinolytic mitochondrial matrix peptidase proteolytic subunit, forming a complex responsible for unfolding and degrading misfolded mitochondrial proteins (28). Two of the four previously identified families with Perrault syndrome due to variants in *CLPP* have had neurological features, including epilepsy, moderate intellectual disability, ataxia, lower limb spasticity and white matter loss (10, 40). The affected male reported here also has a lower limb peripheral neuropathy. In sporadic males and pre-pubescent females the absence of POI means a definitive diagnosis of Perrault syndrome cannot be made from clinical features alone, demonstrated here by the proband in family P8. As described here and in Ahmed et al. (40) it is possible to identify sporadic male cases of Perrault syndrome from genomic data. In both cases the

presence of neurological features was required to distinguish what was subsequently identified as Perrault syndrome from non-syndromic hearing loss. The presentation of neurological symptoms has resulted in the proposal that Perrault syndrome be split into two classifications, type I and type II. Type I represents the classical Perrault syndrome with no additional neurological features. Type II encompasses patients with the additional features (41). We considered that the neurological symptoms may be due to an unrelated recessive disorder. However due to co-segregation of features and the previously reported neurological symptoms in both consanguineous and non-consanguineous Perrault syndrome families (11, 22, 41) we considered that the most likely explanation was that these features are part of the syndrome in some cases. The neurological features distinguish these cases from non-syndromic hearing loss, but there is a large clinical heterogeneity in the Perrault syndrome case studies reported in literature, both between and within families. To date, there is no clear genotype–phenotype correlation (13) and as such we cannot recommend any phenotype directed screening in Perrault syndrome genes in cases of SNHL and neurological features in males and pre-pubescent females. However, whole exome sequencing is clearly a powerful diagnostic tool in these cases.

Azoospermia has not been previously associated with Perrault syndrome and two males with Perrault syndrome due to *HARS2* variants have had unaffected children (8). Males with variants in *HSD17B4* classed as having DBP deficiency type IV have been reported to have azoospermia or hypogonadism (31, 32). In the two males with variants in *CLPP* reported previously, one is 12 years of age and did not have gonadal function assessed (40) and in the other hormone profiles were not available (10). Of note, *Clpp* knock out mice have hearing loss, ovarian dysfunction, ataxia and testicular dysfunction, with both male and female knockout mice being completely sterile (42). Due to the partial sex-limited phenotype, the ascertainment bias in Perrault syndrome means that there are few affected males reported and it may be that azoospermia is an under-recognized feature.

The proband from family P6 has a pattern of hearing loss unusual in Perrault syndrome, with mild loss in the right ear and profound loss in the left ear. Perrault syndrome patients usually present with a significant bilateral hearing loss. Unilateral hearing loss has been previously reported in a Perrault syndrome patient with variants in *LARS2* (9). The proband from the reported *LARS2* family (family 1) had mild hearing loss in both ears at age 8 years. At 17 years she had a moderate-to-severe hearing loss in the right ear and an unchanged mild loss in the left ear. It is possible that both reported cases of unilateral hearing loss may be caused by insult to the inner ear and that the pathology of mitochondrial dysfunction makes Perrault syndrome patients sensitive to these insults.

In summary, we have expanded the spectrum of disease-causing variants associated with Perrault syndrome; provide additional evidence that variants in *LARS2* are associated with low frequency SNHL and demonstrate the further genetic heterogeneity of the disorder as pathogenic variants in known genes were not identified in three affected families.

Supporting Information

Additional supporting information may be found in the online version of this article at the publisher's web-site.

Acknowledgements

We thank the families for their participation in this study and Prof Maria Bitner-Glindzicz for providing the list of hearing loss genes. The work was funded by Action on Hearing Loss.

References

1. Online Mendelian Inheritance in Man OMIM®. Retrieved August 7, 2015, from: http://omim.org/.
2. Pallister PD, Opitz JM, Lowry RB. The Perrault syndrome: autosomal recessive ovarian dysgenesis with facultative, non-sex-limited sensorineural deafness. Am J Med Genet 1979: 4 (3): 239–246.
3. Geethalakshmi S, Geethalakshmi V, Narendrakumar V. Perrault syndrome – a rare case report. J Clin Diagn Res 2015: 9 (3): OD01–OD02.
4. Gottschalk ME, Coker SB, Fox LA. Neurologic anomalies of Perrault syndrome. Am J Med Genet 1996: 65 (4): 274–276.
5. Kim MJ, Kim SJ, Kim J, Chae H, Kim M, Kim Y. Genotype and phenotype heterogeneity in Perrault syndrome. J Pediatr Adolesc Gynecol 2013: 26 (1): e25–e27.
6. Ameen KHN, Pinninti R. A rare cause for primary amenorrhea: sporadic Perrault syndrome. Indian J Endocrinol Metab 2012: 16 (5): 843–845.
7. Pierce SB et al. Mutations in the DBP-deficiency protein HSD17B4 cause ovarian dysgenesis, hearing loss, and ataxia of Perrault syndrome. Am J Hum Genet 2010: 87 (2): 282–288.
8. Pierce SB et al. Mutations in mitochondrial histidyl tRNA synthetase HARS2 cause ovarian dysgenesis and sensorineural hearing loss of Perrault syndrome. Proc Natl Acad Sci U S A 2011: 108 (16): 6543–6548.
9. Pierce SB et al. Mutations in LARS2, encoding mitochondrial leucyl-tRNA synthetase, lead to premature ovarian failure and hearing loss in Perrault syndrome. Am J Hum Genet 2013: 92 (4): 614–620.
10. Jenkinson EM et al. Perrault syndrome is caused by recessive mutations in CLPP, encoding a mitochondrial ATP-dependent chambered protease. Am J Hum Genet 2013: 92 (4): 605–613.
11. Morino BH et al. Mutations in Twinkle primase-helicase cause Perrault syndrome with neurologic features. Neurology 2014: 83 (22): 2054–2061.
12. van Grunsven E et al. Peroxisomal D- hydroxyacyl- CoA dehydrogenase deficiency: resolution of the enzyme defect and its molecular basis in bifunctional protein deficiency. Proc Natl Acad Sci U S A 1998: 95 (5): 2128–2133.
13. Newman WG, Friedman TB, and Conway GS. Perrault syndrome. GeneReviews® [Internet]. 2014. Retrieved November 17, 2014, from http://www.ncbi.nlm.nih.gov/books/NBK242617/.
14. Daly SB et al. Mutations in HPSE2 cause urofacial syndrome. Am J Hum Genet 2010: 86 (6): 963–969.
15. Smith MJ et al. Germline mutations in SUFU cause Gorlin syndrome-associated childhood medulloblastoma and redefine the risk associated with PTCH1 mutations. J Clin Oncol 2014: 32 (36): 4155.
16. Exome Aggregation Consortium (ExAC). Exome Aggregation Consortium (ExAC). Retrieved August 7, 2015, from http://exac.broadinstitute.org.
17. NHLBI GO Exome Sequencing Project (ESP). Exome Variant Server. Exome Variant Server. Retrieved September 7, 2015, from http://evs.gs.washington.edu/EVS/.
18. Sherry S et al. dbSNP: the NCBI database of genetic variation. Nucleic Acids Res 2001: 29 (1): 308–311.
19. Prateek K, Steven H, Pauline CN. Predicting the effects of coding non-synonymous variants on protein function using the SIFT algorithm. Nat Protoc 2009: 4 (8): 1073.
20. Ivan AA et al. A method and server for predicting damaging missense mutations. Nat Methods 2010: 7 (4): 248.

21. Jana Marie S et al. MutationTaster2: mutation prediction for the deep-sequencing age. Nat Methods 2014: 11 (4): 361.
22. Jenkinson EM et al. Perrault syndrome: further evidence for genetic heterogeneity. J Neurol 2012: 259 (5): 974–976.
23. Ferdinandusse S et al. Mutational spectrum of D-bifunctional protein deficiency and structure-based genotype-phenotype analysis. Am J Hum Genet 2006: 78 (1): 112–124.
24. de Launoit Y, Adamski J. Unique multifunctional HSD17B4 gene product: 17 beta-hydroxysteroid dehydrogenase 4 and D-3-hydroxyacyl-coenzyme A dehydrogenase hydratase involved in Zellweger syndrome. J Mol Endocrinol 1999: 22 (3): 227–240.
25. Konovalova S, Tyynismaa H. Mitochondrial aminoacyl- tRNA synthetases in human disease. Mol Genet Metab 2013: 108 (4): 206–211.
26. Riley LG et al. LARS2 variants associated with hydrops, lactic acidosis, sideroblastic anemia, and multisystem failure. JIMD Rep 2015: 24: 1–9.
27. Spelbrink JN et al. Human mitochondrial DNA deletions associated with mutations in the gene encoding Twinkle, a phage T7 gene 4-like protein localized in mitochondria. Nat Genet 2001: 28 (3): 223–231.
28. Kang SG et al. Human mitochondrial ClpP is a stable heptamer that assembles into a tetradecamer in the presence of ClpX. J Biol Chem 2005: 280 (42): 35424–35432.
29. McMillan HJ et al. Specific combination of compound heterozygous mutations in 17β-hydroxysteroid dehydrogenase type 4 (HSD17B4) defines a new subtype of D-bifunctional protein deficiency. Orphanet J Rare Dis 2012: 7: 90.
30. Ferdinandusse S et al. Clinical and biochemical spectrum of D-bifunctional protein deficiency. Ann Neurol 2006: 59 (1): 92–104.
31. Lines MA et al. Peroxisomal D-bifunctional protein deficiency: three adults diagnosed by whole-exome sequencing. Neurology 2014: 82 (11): 963–968.
32. Lieber DS et al. Next generation sequencing with copy number variant detection expands the phenotypic spectrum of HSD17B4- deficiency. BMC Med Genet 2014: 15: 30.
33. Solda G et al. First independent replication of the involvement of LARS2 in Perrault syndrome by whole-exome sequencing of an Italian family. J Hum Genet. 2015 Dec 10. doi: 10.1038/jhg.2015.149. [Epub ahead of print]
34. Bespalova I et al. Mutations in the Wolfram syndrome 1 gene (WFS1) are a common cause of low frequency sensorineural hearing loss. Hum Mol Genet 2001: 10 (22): 2501–2508.
35. Simon M et al. Mutations of human NARS2, encoding the mitochondrial asparaginyl-tRNA synthetase, cause nonsyndromic deafness and Leigh syndrome (NARS2 mutations cause nonsyndromic deafness and Leigh syndrome). PLoS Genet 2015: 11 (3): e1005097.
36. Götz A et al. Exome sequencing identifies mitochondrial alanyl-tRNA synthetase mutations in infantile mitochondrial cardiomyopathy. Am J Hum Genet 2011: 88 (5): 635–642.
37. Dallabona C et al. Novel (ovario) leukodystrophy related to AARS2 mutations. Neurology 2014: 82 (23): 2063–2071.
38. Nikali K et al. Infantile onset spinocerebellar ataxia is caused by recessive mutations in mitochondrial proteins Twinkle and Twinky. Hum Mol Genet 2005: 14 (20): 2981–2990.
39. Fratter CM et al. The clinical, histochemical, and molecular spectrum of PEO1 (Twinkle)-linked adPEO. Neurology 2010: 74 (20): 1619–1626.
40. Ahmed S et al. Exome analysis identified a novel missense mutation in the CLPP gene in a consanguineous Saudi family expanding the clinical spectrum of Perrault Syndrome type-3. J Neurol Sci 2015: 353 (1–2): 149–154.
41. Fiumara A et al. Perrault syndrome: evidence for progressive nervous system involvement. Am J Med Genet A 2004: 128A (3): 246–249.
42. Gispert S et al. Loss of mitochondrial peptidase Clpp leads to infertility, hearing loss plus growth retardation via accumulation of CLPX, mtDNA and inflammatory factors. Hum Mol Genet 2013: 22 (24): 4871–4887.
43. Guangwu G et al. Whole-genome and whole-exome sequencing of bladder cancer identifies frequent alterations in genes involved in sister chromatid cohesion and segregation. Nat Genet 2013: 45 (12): 1459.
44. Forbes SA et al. COSMIC: exploring the worlds knowledge of somatic mutations in human cancer. Nucleic Acids Res 2015: 43 (Database issue): D805.

Chapter 4: Marfanoid Habitus is a Non-specific Feature of Perrault Syndrome

Marfanoid habitus is a nonspecific feature of Perrault syndrome

Maria Zerkaoui[a,c,*], Leigh A.M. Demain[d,e,*], Imane Cherkaoui Jaouad[c], Ilham Ratbi[a], Karima Amjoud[b], Jill E. Urquhart[d,e], James O'Sullivan[d,e], William G. Newman[d,e] and Abdelaziz Sefiani[a,c]

The objective of this study was to report the clinical and biological characteristics of two Perrault syndrome cases in a Moroccan family with homozygous variant c.1565C > A in the *LARS2* gene and to establish genotype–phenotype correlation of patients with the same mutation by review of the literature. Whole-exome sequencing was performed. Data analysis was carried out and confirmed by Sanger sequencing and segregation. The affected siblings were diagnosed as having Perrault syndrome with sensorineural hearing loss at low frequencies; the female proband had primary amenorrhea and ovarian dysgenesis. Both affected individuals had a marfanoid habitus and no neurological features. Both patients carried the homozygous variant c.1565C > A; p.Thr522Asn in exon 13 of the *LARS2* gene. This variant has already been reported as a homozygous variant in three other Perrault syndrome families. Both affected siblings of a Moroccan consanguineous family with *LARS2* variants had low-frequency sensorineural hearing loss, marfanoid habitus, and primary ovarian insufficiency in the affected girl. According to the literature, this variant, c.1565C > A; p.Thr522Asn, can be correlated with low-frequency hearing loss. However, marfanoid habitus was been considered a nonspecific feature in Perrault syndrome, but we believe that it may be more specific than considered previously. This diagnosis allowed us to provide appropriate management to the patients and to provide more accurate genetic counseling to this family. *Clin Dysmorphol* 26:200–204

Clinical Dysmorphology 2017, **26**:200–204

Keywords: hearing loss, *LARS2*, Perrault syndrome, primary ovarian insufficiency

[a]Center for Human Genomics, Faculty of Medicine and Pharmacy, [b]Department of Endocrinology, Diabetology and Nutrition, Avicenna Hospital, Mohammed V University, [c]Department of Medical Genetics, National Institute of Health, Rabat, Morocco, [d]Division of Evolution and Genomic Sciences, Faculty of Biology, Medicine and Health, School of Biological Sciences, University of Manchester and [e]Manchester Centre for Genomic Medicine, Central Manchester University Hospitals NHS Foundation Trust, Manchester, UK

Correspondence to Maria Zerkaoui, MD, Department of Medical Genetics, National Institute of Hygiene, BP 769 Agdal, 10090 Rabat, Morocco
Tel: + 212 661 442 936; fax: + 212 537 772 067;
e-mail: maria.zerkaoui@gmail.com

*Maria Zerkaoui and Leigh A.M. Demain contributed equally to the writing of this article.

Received 12 June 2017 **Accepted** 18 July 2017

Introduction

Perrault syndrome (MIM #233400), the association of primary ovarian insufficiency and bilateral sensorineural hearing loss (SNHL), is an autosomal recessive disorder first described in 1951 by Perrault *et al.* (1951). It is a rare disorder affecting both females and males. However, only females have gonadal dysgenesis or primary ovarian insufficiency in the context of a normal female karyotype (46,XX) (Newman *et al.*, 1993–2017). Azoospermia has been reported in one male with Perrault syndrome (Demain *et al.*, 2016). Male fertility is not assessed routinely in families with Perrault syndrome; thus, the male fertility phenotype, if there is one, remains unclear. The SNHL, present in both sexes, is bilateral and ranges in severity from progressive moderate with early-childhood onset to congenital profound. Neurological features described in some affected individuals include developmental delay or intellectual disability, cerebellar ataxia, and motor and sensory peripheral neuropathy. SNHL is the first clinical manifestation, although a formal diagnosis of Perrault syndrome may not be made until a failure of puberty (primary amenorrhea) or secondary amenorrhea is noted in affected young women (Newman *et al.*, 1993–2017); SNHL is usually identified in a sibling of a known affected individual or increasingly through genetic testing of an individual with childhood hearing loss (Ahmed *et al.*, 2015; Demain *et al.*, 2016).

Biallelic pathogenic variants in five different genes have been identified in Perrault syndrome to date: *HSD17B4* (MIM #233400) (Pierce *et al.*, 2010), *HARS2* (MIM #614926) (Pierce *et al.*, 2011), *CLPP* (MIM #614129) (Jenkinson *et al.*, 2013), *LARS2* (MIM #615300) (Pierce *et al.*, 2013), and *C10orf2* (MIM #616138) (Morino *et al.*, 2014).

Here, we report on a Moroccan family with Perrault syndrome and marfanoid habitus because of a previously reported homozygous c.1565C > A p.(Thr522Asn) variant (Pierce *et al.*, 2013; Demain *et al.*, 2016) in *LARS2*.

0962-8827 Copyright © 2017 Wolters Kluwer Health, Inc. All rights reserved. DOI: 10.1097/MCD.0000000000000198

Patients and methods

Case report

The proband was a 23-year-old woman who presented to the Genetics Department in Rabat with primary amenorrhea and hearing loss. She was the eldest child of five siblings. The parents were first cousins and both are healthy (Fig. 1a). Because of speech delay, an audiogram was performed at 6 years of age. She was diagnosed with bilateral moderate to severe SNHL that presented as an uncommon audiometric configuration of low-frequency hearing loss. On examination at 23 years, she had a long face, thin fingers, and a high-arched palate. She had marfanoid body proportions, measuring 170 cm in height with a 180 cm arm span (ratio: 1.06, normal < 1.05) and a weight of 60 kg. The upper-to-lower body segment ratio was reduced at 0.81 (normal ratio: 0.89–0.95). Physical examination indicated that axillary hair was present, pubic hair was at stage 4, and breast development was bilaterally at Tanner stage 2. Neurological and systemic examinations were normal. Hormone studies were consistent with hypergonadotropic hypogonadism, with elevated levels of follicle stimulating hormone (51 mIU/ml, normal range: 1.24–7.8 mIU/ml), and luteinizing hormone (16.29 mIU/ml, normal range: 1.42–15.4 mIU/ml). Her karyotype was 46,XX. Pelvic ultrasonography indicated a hypoplasic uterus and her ovaries could not be visualized.

Audiometric evidence was consistent with a unifying diagnosis of Perrault syndrome. She has now been fitted with a hearing aid that has improved her hearing, and is currently receiving estrogen-replacement therapy that led to the appearance of secondary sexual characteristics and a normal menstruation cycle.

The 16-year-old brother of the proband was diagnosed with bilateral moderate to severe SNHL and fitted with a hearing aid. He also had a long face and a high-arched palate. He had progressed to Tanner stage 5 of puberty, with a height and weight of 175 cm and 75 kg, respectively. His neurological examination was normal. The three additional female siblings were unaffected.

Blood samples from all the seven members of the family were collected after written informed consent was obtained in accordance with the Declaration of Helsinki protocols and approval of the local institutional review boards (NRES 16/WA/0017). DNA was isolated using standard techniques (Miller *et al.*, 1988).

Fig. 1

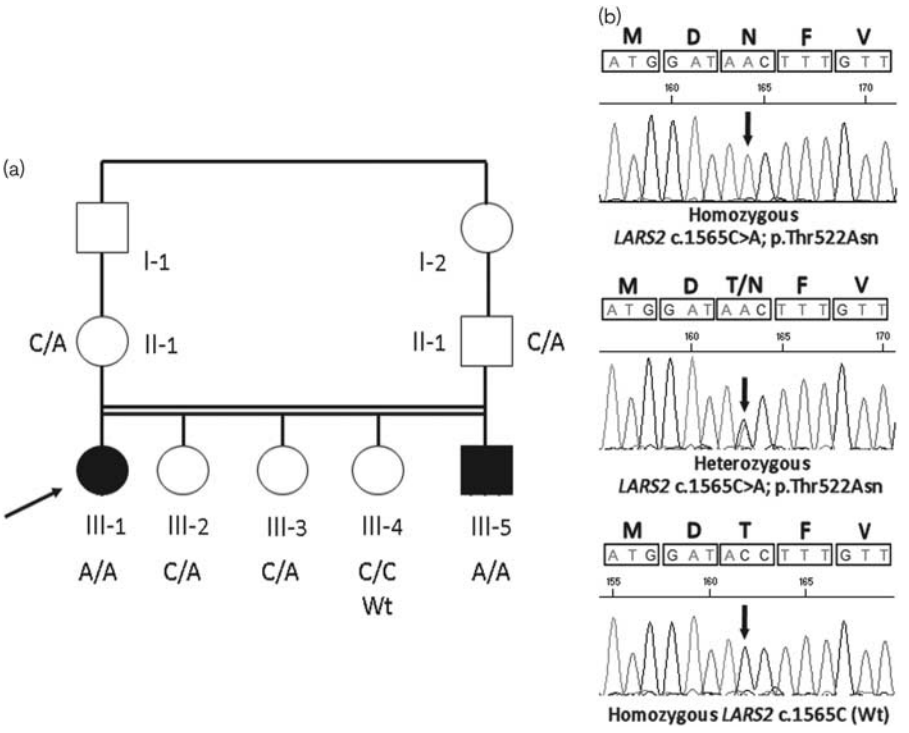

(a) Pedigree of the reported family. The proband is indicated by an arrow. (b) Electropherograms of the *LARS2* variants in the affected family. Two patients (III-1 and III-5) are homozygous for the variant c.1565C > A (p.Thr522Asn), and both parents (II-1 and II-2) and two sisters (III-2 and III-3) are heterozygotes for the variant. One healthy sister (III-4) is homozygous wild type at this locus. The variant base is indicated by an arrow.

Whole-exome sequencing

Whole-exome sequencing was performed on the proband. The SureSelect Human All Exon V5 Panel (Agilent, Santa Clara, California, USA) was used for library preparation and sequencing was performed on the HiSeq 2500 (Illumina, San Diego, California, USA) as described previously (Smith *et al.*, 2014). The exome data were filtered for possible causative variants in the five genes associated with Perrault syndrome.

Sanger sequencing confirmation and segregation

The sequence variants were confirmed in the proband and available family members by Sanger sequencing using ABI big Dye v3.1 sequencing technology (Thermo Fisher Scientific Inc., Waltham, Massachusetts, USA) (Fig. 1b). Primer sequences are available on request.

Results

Whole-exome sequencing data analysis

A homozygous known pathogenic variant in *LARS2*, c.1565C > A p.(Thr522Asn) (NM_015340) (Pierce *et al.*, 2013; Demain *et al.*, 2016; www.ncbi.nlm.nih.gov/nuccore/NM_015340.3), was identified in the proband. No additional coding variants were identified in *LARS2* or in any other Perrault syndrome genes.

Sanger sequencing confirmation and segregation

The variant segregated with the phenotype in that the affected brother was also homozygous for the variant, two unaffected sisters were heterozygous, and an unaffected sister was homozygous wild type.

Discussion

To date, eight variants have been identified in *LARS2* in 11 individuals with Perrault syndrome (Table 1). Here, we present, for the first time, a Moroccan family carrying a previously reported homozygous c.1565C > A; p.Thr522Asn variant in *LARS2* (Pierce *et al.*, 2013). The variant in this family has been reported as a homozygous variant in two families and as a compound heterozygous variant in one family (Table 1) (Pierce *et al.*, 2013; Demain *et al.*, 2016). Previously reported Moroccan families with Perrault syndrome had variants identified in *HARS2* or *C10orf2* (Lerat *et al.*, 2016).

LARS2 encodes a 903 amino-acid protein, mitochondrial leucyl-tRNA synthetase (mtLeuRS) (Bullard *et al.*, 2000). Aminoacyl-tRNA synthetases attach specific amino acids to the 3′ ends of their cognate tRNAs. Aminoacyl-tRNA-synthetase activity is required in the cytoplasm and mitochondria for the translation of nuclear and mitochondrial encoded genes, respectively. All except two aaRS, glycyl-tRNA synthetase and lysyl-tRNA synthetase, are encoded by separate genes for nuclear and mitochondrial functions (Diodato *et al.*, 2014). The human structure of mtLeuRS has not been elucidated. The variant residue, LeuRS (of *Escherichia coli*) p.Thr492 (analogous to human mtLeuRS p.Thr522), is located in the catalytic site and is in contact with several residues in the leucine-binding pocket (Pierce *et al.*, 2013). It has been suggested that substitution at this position might shift the position of the tRNA in the binding pocket, subsequently reducing aminoacylation efficiency (Pierce *et al.*, 2013). Recently, this variant has been shown to reduce the aminoacylation efficiency of human mtLeuRS nine-fold, although the mechanism of impairment is unknown (Riley *et al.*, 2015).

All individuals to date with Perrault syndrome because of the variant Thr522Asn, whether homozygous or compound heterozygous, have presented with SNHL, which is worse at low frequencies and can be progressive. The variability in the severity of hearing loss between families may be attributed to different genetic backgrounds. The low-frequency hearing loss appears to be a specific phenotype–genotype correlation linked to the variant Thr522Asn (Demain *et al.*, 2016). Our report supports the assertion by Demain *et al.* (2016) when they suggested that the variant *LARS2* c.1565C > A (p.Thr522Asn) may be a hotspot and may be correlated to this unusual audiological pattern.

The ovarian dysfunction is variable in severity in Perrault syndrome and there seems to be no obvious genotype–phenotype correlations associated with any of the Perrault syndrome genes to date.

Although no individuals with Perrault syndrome because of variants in *LARS2* have been reported to have neurological symptoms, all the patients were relatively young at genetic diagnosis. It is unclear whether neurological symptoms may develop later in life as part of a progressive aspect of the disease. Variants in *LARS2* can be associated with a more severe phenotype. Compound heterozygous variants in *LARS2*, including p.Thr522Asn, were implicated in a severe multisystem phenotype in a baby. The variant in *trans* had a greater effect on catalytic activity than that shown for p.Thr522Asn (Riley *et al.*, 2016).

Marfanoid habitus has been noted previously in some individuals with Perrault syndrome, but this is the first genetically resolved case. Two previously reported unrelated individuals with Perrault syndrome and marfanoid habitus have undergone genetic testing, but no causative variants were identified (Kim *et al.*, 2013; Demain *et al.*, 2016). In most cases of Perrault syndrome with marfanoid habitus, no genetic testing has been performed (Jacob *et al.*, 2007; Ameen and Pinninti, 2012; Geethalakshmi *et al.*, 2015). Arachnodactyly has been reported in one individual with Perrault syndrome because of variants in *C10orf2* and it has also been reported in a genetically unresolved case of Perrault syndrome (Lerat *et al.*, 2016). High-arched palate has also been reported as a clinical feature in a number of cases of Perrault syndrome (Nishi *et al.*, 1988), which, alongside

Table 1 **Genotypes and phenotypes of individuals with Perrault syndrome because of variants in *LARS2***

Individual ID	Family 1, II-1	Family 1, II-2	Family 1, II-3	Family 2, proband	II1	II3 proband	P2:II-1 proband	P2:II-2	P3:II-1 proband	P3:II-2	Patient III-3	III-1 proband	III-5
Variants	c.1565C > A (p.Thr522Asn)	c.1565C > A (p.Thr522Asn)	c.1565C > A (p.Thr522Asn)	c.1077delT (p.Ile360PhefsTer15) c.1886C > T (p.Thr629Met)	c.899C > T (p.Thr300Met) c.1912G > A (p.Glu638Lys)	c.899C > T (p.Thr300Met) c.1912G > A (p.Glu638Lys)	c.1565C > A (p.Thr522Asn)	c.1565C > A (p. Thr522Asn)	c.351G > C p. (Met117Ile) c.1565C > A (p.Thr522Asn)	c.351G > C p. (Met117Ile) c.1565C > A (p.Thr522Asn)	c.1358G > A (p. Arg453Gln) c.1886C > T (p. Thr629Met)	c.1565C > A (p. Thr522Asn)	c.1565C > A (p.Thr522Asn)
References	Pierce *et al.* (2013)	Pierce *et al.* (2013)	Pierce *et al.* (2013)	Pierce *et al.* (2013)	Solda *et al.* (2016)	Solda *et al.* (2016)	Demain *et al.* (2016)	Demain *et al.* (2016)	Demain *et al.* (2016)	Demain *et al.* (2016)	Lerat *et al.* (2016)	This study	This study
Ethnicity	Palestinian	Palestinian	Palestinian	Slovenian	Italian	Italian	Argentinian	Argentinian	White British	White British	Sri Lankan	Moroccan	Moroccan
Consanguinity	Yes	Yes	Yes	No	No	No	No	No	No	No	No	Yes	Yes
Sex	Male	Female	Male	Female	Male	Female	Female	Male	Female	Male	Female	Female	Male
Karyotype	NR	46,XX	NR	46, XX	NR	46,XX	46,XX	NR	46,XX	NR	NR	46,XX	NR
Age at last assessment (years)	17	17	13	30	40	31	27	26	25	26	NR	23	16
Sensorineural hearing loss													
Age at diagnosis (years)	3–5	3–5	3–5	NR	Congenital	–	8	26	2.5	2.5	< 3	23	16
Degree of hearing loss	Severe to profound	Right ear: severe at lower frequencies, moderate at higher frequencies. Left ear: Moderate at lower frequencies, mild at higher frequencies.	Severe to moderate at low frequencies, moderate to mild at higher frequencies	Severe	Profound	Profound	Moderate	Mild/moderate	Severe/ profound	Severe/ profound	Moderate	Moderate/ profound	Moderate/ profound
Notes	Bilateral LF SNHL	LF SNHL	Bilateral LF SNHL	None	Progressive bilateral SNHL	Progressive bilateral SNHL	LF	LF	LF	LF	Not progressive	Progressive	Progressive
Intervention	NR	No hearing aid used	NR	NR	Bilateral CI	Bilateral CI	CI	NR	CI	NR	NR	Hearing aid	Hearing aid
Gonadal dysfunction													
Pelvic ultrasound	NA	Small uterus, ovaries not visualized	NA	NR	NA	Bicornate uterus, hypoplastic left ovary, right ovary not visualized	Small uterus and ovaries	NA	Small uterus and ovaries	NA	NR	Small uterus, ovaries not visualized	NA
Menarche	NA	No	NA	Yes	NA	Yes	No	NA	Yes	NA	No	NR	NA
POI– age if menarche achieved	NA	Yes	NA	Yes – 19	NA	Yes – 28	NA	NA	Yes	NA	NA	NA	NA
Follicle stimulating hormone (IU/l)	NR	76.9	NR	101	NR	118	99.6 (2.3–29)	NR	74 (≤ 30)	3.1 (1–11)	NR	51	NR
Luteinising hormone (IU/l)	NR	30.3	NR	NR	NR	45.4	48.0 (1.7–52)	NR	63 (≤ 30)	3.9 (1–11)	NR	16.29	NR
Estradiol	NA	NR	NA	NR	NA	NR	7.04 (10–388) pg/ml	NA	91 (>180) pmol/l	NA	NR	NR	NA
Neurological features	No	No	No	No	No	No	No	No	No	No	No	No	No
Additional features	No	No	No	No	No	No	No	No	Mild facial dysmorphia, hemidystropy	Hypospadias, mild facial dysmorphia, normal testosterone 22.3 (9–25)	Cleft palate	Marfanoid habitus	Marfanoid habitus

CI, cochlear implant; LF, low frequency; NA, not applicable; NR, not recorded; POI, primary ovarian insufficiency; SNHL, sensorineural hearing loss.

arachnodactyly, may represent a more subtle form of the marfanoid habitus phenotype. However, the evidence to date indicates that although marfanoid habitus is definitely a clinical feature associated with Perrault syndrome, it is not associated with any specific disease-causing gene or variant.

It is difficult to confidently assert genotype–phenotype correlations in Perrault syndrome because of the low numbers of characterized and reported individuals and the high level of phenotypic and genotypic heterogeneity. Several studies have suggested factors that could modulate mitochondrial translation or replication to explain the phenotypic heterogeneity (Jenkinson *et al.*, 2012; Pierce *et al.*, 2013; Lerat *et al.*, 2016).

Perrault syndrome cases have been reported in countries worldwide. However, it is underestimated because males without an affected sister will likely be diagnosed with nonsyndromic deafness. Further, the prevalence of this condition is likely to be higher in countries with high levels of consanguinity, including Morocco (15.25%) (Jaouad *et al.*, 2009).

Conclusion

Perrault syndrome is an under-ascertained, genetically complex condition with further disease-associated genes still to be elucidated. The clinical spectrum of the disease remains incomplete; as new cases of Perrault syndrome are reported, new phenotypic features become apparent. Consequently, phenotype–genotype correlations remain difficult to establish and more patients are required to better define these relationships. Here, we have described the clinical and genetic data of a consanguineous Moroccan family with Perrault Syndrome carrying the previously reported mutation c.1565C > A; p.Thr522Asn. This diagnosis allowed us to provide appropriate management to the patients and to provide more accurate genetic counseling to this family.

Acknowledgements

The authors thank the family for its participation in this study. L.A.M.D. is funded by Action on Hearing Loss. The work is also supported by Action Medical Research (GN2484).

Conflicts of interest

There are no conflicts of interest.

References

Ahmed S, Jelani M, Alrayes N, Mohamoud HSA, Almramhi MM, Anshasi W, *et al.* (2015). Exome analysis identified a novel missense mutation in the CLPP gene in a consanguineous Saudi family expanding the clinical spectrum of Perrault syndrome type-3. *J Neurol Sci* **353**:149–154.

Ameen KHN, Pinninti R (2012). A rare cause for primary amenorrhea: sporadic perrault syndrome. *Indian J Endocrinol Metab* **16**:843–845.

ANNOVAR. Available at: *http://www.openbioinformatics.org/annovar/*.

Bullard JM, Cai YC, Spremulli LL (2000). Expression and characterization of the human mitochondrial leucyl-tRNA synthetase. *Biochim Biophys Acta* **1490**:245–258.

dbSNP. Available at: *http://www.ncbi.nlm.nih.gov/SNP/*.

Demain LA, Urquhart JE, O'Sullivan J, Williams SG, Bhaskar SS, Jenkinson EM, *et al.* (2017). Expanding the genotypic spectrum of Perrault syndrome. *Clin Genet* **91**:302–312.

Diodato D, Ghezzi D, Tiranti V (2014). The mitochondrial aminoacyl tRNA synthetases: genes and syndromes. *Int J Cell Biol* **2014**:787956.

Geethalakshmi S, Geethalakshmi V, Narendrakumar V (2015). Perrault syndrome–a rare case report. *J Clin Diagn Res* **9**:OD01–OD02.

1000 Genomes Project. Available at: *http://www.1000genomes.org*.

Jacob JJ, Paul TV, Mathews SS, Thomas N (2007). Perrault syndrome with marfanoid habitus in two siblings. *J Pediatr Adolesc Gynecol* **20**:305–308.

Jaouad IC, Elalaoui SC, Sbiti A, Elkerh F, Belmahi L, Sefiani A (2009). Consanguineous marriages in Morocco and the consequence for the incidence of autosomal recessive disorders. *J Biosoc Sci* **41**:575–581.

Jenkinson EM, Clayton-Smith J, Mehta S, Bennett C, Reardon W, Green A, *et al.* (2012). Perrault syndrome: further evidence for genetic heterogeneity. *J Neurol* **259**:974–976.

Jenkinson EM, Rehman AU, Walsh T, Clayton-Smith J, Lee K, Morell RJ, *et al.* (2013). Perrault syndrome is caused by recessive mutations in CLPP, encoding a mitochondrial ATP-dependent chambered protease. *Am J Hum Genet* **92**:605–613.

Kim MJ, Kim SJ, Kim J, Chae H, Kim M, Kim Y (2013). Genotype and phenotype heterogeneity in perrault syndrome. *J Pediatr Adolesc Gynecol* **26**:e25–e27.

Lerat J, Jonard L, Loundon N, Christin-Maitre S, Lacombe D, Goizet C, *et al.* (2016). An application of NGS for molecular investigations in Perrault syndrome: study of 14 families and review of the literature. *Hum Mutat* **37**:1354–1362.

Miller SA, Dykes DD, Polesky HF (1988). A simple salting out procedure for extracting DNA from human nucleated cells. *Nucleic Acids Res* **16**:1215.

Morino H, Pierce SB, Matsuda Y, Walsh T, Ohsawa R, Newby M, *et al.* (2014). Mutations in Twinkle primase-helicase cause Perrault syndrome with neurologic features. *Neurology* **83**:2054–2061.

NCBI Map Viewer. Available at: *http://www.ncbi.nlm.nih.gov/mapview/*.

Newman WG, Friedman TB, Conway GS (1993–2017). Perrault syndrome. In: Pagon RA, Adam MP, Ardinger HH,Wallace SE, Amemiya A, Bean LJH, *et al.* editors. *GeneReviews(R)*. Seattle, WA: University of Washington. Available at: *https://www.ncbi.nlm.nih.gov/books/NBK242617/*.

NHLBI GO Exome Sequencing Project. NHLBI ESP6500 databases. Available at: *http://evs.gs.washington.edu/EVS/*.

Nishi Y, Hamamoto K, Kajiyama M, Kawamura I (1988). The Perrault syndrome: clinical report and review. *Am J Med Genet* **31**:623–629.

Perrault M, Klotz B, Housset E (1951). Two cases of Turner syndrome with deafmutism in two sisters. *Bull Mem Soc Med Hop Paris* **67**:79–84.

Pierce SB, Walsh T, Chisholm KM, Lee MK, Thornton AM, Fiumara A, *et al.* (2010). Mutations in the DBP-deficiency protein HSD17B4 cause ovarian dysgenesis, hearing loss, and ataxia of Perrault syndrome. *Am J Hum Genet* **87**:282–288.

Pierce SB, Chisholm KM, Lynch ED, Lee MK, Walsh T, Opitz JM, *et al.* (2011). Mutations in mitochondrial histidyl tRNA synthetase HARS2 cause ovarian dysgenesis and sensorineural hearing loss of Perrault syndrome. *Proc Natl Acad Sci USA* **108**:6543–6548.

Pierce SB, Gersak K, Michaelson-Cohen R, Walsh T, Lee MK, Malach D, *et al.* (2013). Mutations in LARS2, encoding mitochondrial leucyl-tRNA synthetase, lead to premature ovarian failure and hearing loss in Perrault syndrome. *Am J Hum Genet* **92**:614–620.

Riley LG, Rudinger-Thirion J, Schmitz-Abe K, Thorburn DR, Davis RL, Teo J, *et al.* (2015). LARS2 variants associated with hydrops, lactic acidosis, sideroblastic anemia, and multisystem failure. *JIMD Rep* **24**:1–9.

Riley LG, Rudinger-Thirion J, Schmitz-Abe K, Thorburn DR, Davis RL, Teo J, *et al.* (2016). LARS2 variants associated with hydrops, lactic acidosis, sideroblastic anemia, and multisystem failure. *JIMD Rep* **28**:49–57.

Smith MJ, Beetz C, Williams SG, Bhaskar SS, O'Sullivan J, Anderson B, *et al.* (2014). Germline mutations in SUFU cause Gorlin syndrome-associated childhood medulloblastoma and redefine the risk associated with PTCH1 mutations. *J Clin Oncol* **32**:4155–4161.

Solda G, Caccia S, Robusto M, Chiereghin C, Castorina P, Ambrosetti U, Duga S, Asselta R (2016). First independent replication of the involvement of LARS2 in Perrault syndrome by whole-exome sequencing of an Italian family. *Journal of human genetics* **61**:295–300.

VariantDB. Available at: *http://www.biomina.be\app\variantdb*.

Chapter 5: A homozygous variant in mitochondrial RNase P subunit PRORP is associated with Perrault syndrome characterized by hearing loss and primary ovarian insufficiency

A homozygous variant in mitochondrial RNase P subunit PRORP is associated with Perrault syndrome characterized by hearing loss and primary ovarian insufficiency

Irit Hochberg,[1,¶] Leigh A. M. Demain,[2,3,¶] Jill E. Urquhart, [2,3] Albert Amberger,[4] Andrea J. Deutschmann,[4] Sandra Demetz,[4] Kyle Thompson,[5] James O'Sullivan, [2,3] Inna A. Belyantseva,[6] Melanie Barzik, [6] Simon G. Williams,[2,3] Sanjeev S. Bhaskar,[2,3] Emma M. Jenkinson,[2] Nada AlSheqaih,[2] Zeev Blumenfeld [7] Sergey Yalonetsky,[8] Stephanie Oerum,[9] Walter Rossmanith,[10] Wyatt W. Yue,[9] Johannes Zschocke,[4] Robert W. Taylor,[5] Thomas B. Friedman,[6] Kevin J. Munro,[11,12] Raymond T. O'Keefe,[13,*] William G. Newman[2,3,*]

[1] Institute of Endocrinology, Diabetes and Metabolism, Rambam Health Care Campus, Haifa, Israel
[2] Division of Evolution and Genomic Sciences, Faculty of Biology, Medicine and Health, School of Biological Sciences, University of Manchester, Manchester, UK
[3] Manchester Centre for Genomic Medicine, Central Manchester University Hospitals NHS Foundation Trust, Manchester, UK
[4] Division of Human Genetics, Innsbruck Medical University, Innsbruck 6020, Austria
[5] Wellcome Centre for Mitochondrial Research, Institute of Neuroscience, Newcastle University, Medical School, Newcastle upon Tyne, UK
[6] Laboratory of Molecular Genetics, National Institute on Deafness and Other Communication Disorders, National Institutes of Health, Bethesda, MD, USA
[7] Department of Obstetrics and Gynecology, Reproductive Endocrinology, Rambam Health Care Campus, The Rappaport Faculty of Medicine, Technion - Israel Institute of Technology, Haifa, Israel
[8] Department of Pediatric Cardiology, Rambam Health Care Campus, Haifa, Israel
[9] Structural Genomics Consortium, Nuffield Department of Medicine, University of Oxford, Oxford, UK
[10] Center for Anatomy and Cell Biology, Medical University of Vienna, 1090 Vienna, Austria
[11] School of Health Sciences, University of Manchester, Manchester, UK
[12] Central Manchester University Hospitals NHS Foundation Trust, Manchester Academic Health Science Centre, Manchester, UK
[13] Division of Cellular & Molecular Function, Faculty of Biology, Medicine and Health, University of Manchester, Manchester, UK

¶ Co-first author
* Co-senior author

5.1. Abstract

Perrault syndrome is a rare autosomal recessive condition characterised by sensorineural hearing loss in both sexes and primary ovarian insufficiency in 46 XX, females. It is genetically heterogeneous with biallelic variants in six genes identified to date (*HSD17B4, HARS2, LARS2, CLPP*, *C10orf2* and *ERAL1*). Most genes possessing variants associated with Perrault syndrome are involved in mitochondrial translation. We describe a consanguineous family with three affected individuals homozygous for a novel missense variant c.1454C>T; p.(Ala485Val) in *KIAA0391,* encoding proteinaceous RNase P (PRORP), the metallonuclease subunit of the mitochondrial RNase P complex, responsible for the 5'-end processing of mitochondrial precursor tRNAs. In RNase P activity assays, RNase P complexes containing the PRORP disease variant produced ~35-45% less 5'-processed tRNA than wild type PRORP. Consistently, the accumulation of unprocessed polycistronic mitochondrial transcripts was observed in patient dermal fibroblasts, leading to an observable loss of steady-state levels of mitochondrial oxidative phosphorylation components. Expression of wild type *KIAA0391* in patient fibroblasts rescued tRNA processing. Immunohistochemistry analyses of the auditory sensory epithelium from postnatal and adult mouse inner ear showed a high level of PRORP in the efferent synapses and nerve fibres of hair cells, indicating a possible mechanism for the sensorineural hearing loss observed in affected individuals. We have identified a variant in an additional gene associated with Perrault syndrome. With the identification of this disease-causing variant in *KIAA0391*, reduced function of each of the three subunits of mitochondrial RNase P have now been associated with distinct clinical presentations.

5.2. Author Summary

Perrault syndrome is a rare genetic condition which results in hearing loss in both sexes and ovarian dysfunction in females. Perrault syndrome may also cause neurological symptoms in some patients. Here, we present the features and genetic basis of the condition in three sisters affected by Perrault syndrome. The sisters did not have pathogenic variants in any of the genes previously associated with Perrault syndrome. We identified a change in the gene *KIAA0391,* encoding PRORP, a subunit of the mitochondrial RNase P complex. Mitochondrial RNase P is a key enzyme in RNA processing in mitochondria. Impaired RNA processing reduces protein production in mitochondria, which we observed in patient cells along with high levels of unprocessed RNA. When we expressed wild type PRORP in patient cells, the RNA processing improved. We also investigated PRORP localisation in the mouse inner ear and found high levels in the synapses and nerve fibers that transmit sound. It may be that disruption of RNA processing in the mitochondria of these cells causes hearing loss in this family.

5.3. Introduction

Perrault syndrome (MIM 233400) is a rare autosomal recessive condition characterised by bilateral sensorineural hearing loss (SNHL) affecting both sexes and primary ovarian insufficiency (POI) in 46, XX karyotype females (Pallister and Opitz 1979). Additional clinical features may be present in some affected individuals, most commonly neurological dysfunction, including: ataxia, hereditary sensory motor neuropathy, nystagmus and mild to moderate intellectual disability (Gottschalk et al. 1996;Jenkinson et al. 2012). Perrault syndrome is challenging to diagnose in males or prepubescent females as both groups are likely to present with non-syndromic SNHL (Newman et al. 2014). Perrault syndrome is genetically heterogeneous, as causative biallelic variants in six genes have been identified to date: *HSD17B4* (MIM 233400) (Pierce et al. 2010), *HARS2* (MIM 614926) (Pierce et al. 2011)*, LARS2* (MIM 615300) (Pierce et al. 2013)*, CLPP* (MIM 614129) (Jenkinson et al. 2013), *C10orf2* (MIM 616138) (Morino et al. 2014) and *ERAL1* (MIM 607435) (Chatzispyrou et al. 2017). These six genes do not account for all cases of Perrault syndrome, suggesting that additional genes remain to be identified (Demain et al. 2017;Lerat et al. 2016). Variants in *HSD17B4* are associated with both D-bifunctional protein deficiency, a peroxisomal disorder (Ferdinandusse et al.

2006;McMillan et al. 2012), and Perrault syndrome (Pierce et al. 2010). The other five genes associated with Perrault syndrome are nuclear-encoded mitochondrial proteins and share a common pathology of disrupted mitochondrial protein translation.

We report a novel cause of Perrault syndrome, which shares the common pathology of disrupted mitochondrial translation. Affected individuals in a large consanguineous family are homozygous for a missense variant in *KIAA0391* (MIM 609947), encoding **Pro**teinaceous **R**Nase **P** (PRORP, also known as mitochondrial RNase P protein 3 (MRPP3)), one of the three subunits of the mitochondrial RNase P (mtRNase P) complex. In humans, mtRNase P comprises TRMT10C-SDR5C1-PRORP (also called MRPP1-MRPP2-MRPP3, respectively), and is responsible for cleaving the 5' end of mitochondrial tRNAs from long polycistronic precursor transcripts (Holzmann et al. 2008;Vilardo et al. 2012). We demonstrate that the *KIAA0391* disease-associated variant impairs mtRNase P activity, resulting in the accumulation of unprocessed polycistronic mitochondrial transcripts and leading to a loss of steady-state levels of mitochondrial oxidative phosphorylation (OXPHOS) components. Expression of wild type *KIAA0391* in patient fibroblasts rescued tRNA processing. Finally, immunohistochemistry analyses of mouse auditory sensory epithelium showed prominent levels of PRORP in the efferent synapses and nerve fibres of the auditory hair cells, highlighting a plausible pathology for the sensorineural hearing loss observed in affected individuals.

5.4. Results

5.4.1. Clinical report

A consanguineous Palestinian family of three affected female siblings, two unaffected female siblings, two unaffected male siblings and their unaffected parents were ascertained (Fig. 5.1A). All three affected sisters showed absent middle ear acoustic reflex, despite normal tympanometry, when tested in infancy and subsequent audiology examinations in each revealed profound bilateral SNHL (>90 decibels hearing level at all frequencies) (Fig. 5.1B). The three affected sisters each presented in their late teenage years with primary amenorrhea. Abdominal ultrasound noted the absence of ovaries in all three affected individuals. Hormonal profiles indicated hypergonadotropic hypogonadism (Fig. 5.1C) with otherwise normal endocrine and biochemical tests and a 46, XX

karyotype. The sisters were prescribed estrogen to induce puberty and are currently treated with hormone replacement therapy. Each affected sibling has mild intellectual disability, which is not progressive. The sisters were taught in remedial classes but participate in the full activities of daily living, and one sister has paid employment. Echocardiography for each of the affected sisters was normal. All other physical and neurological examinations were normal and the three sisters each have normal height.

5.4.2. Exome sequencing and variant confirmation

Autozygosity mapping, performed on six siblings, as previously described (Banka et al. 2011), identified three homozygous regions >2Mb shared between the affected individuals, but not with the unaffected individuals (chromosome 14: 34195478-37228220; chromosome 18: 10090808-12264512; and chromosome 22: 21317876-23416005. Genome build: Hg19.). Whole exome sequencing was performed on one affected individual (II-3). After sequence variants in the autozygous regions were filtered to remove variants seen more than once in >800 previously sequenced exomes, three variants remained. Two variants with a minor allele frequency of greater than 1% in the Exome Variant Server (NHLBI GO Exome Sequencing Project (ESP)) and dbSNP frequency (Sherry et al. 2001) respectively were excluded, as they were too common to result in a rare inherited disorder. One variant was novel, *KIAA0391* c.1454C>T; p.(Ala485Val) (Genbank: NM_014672.3).

A

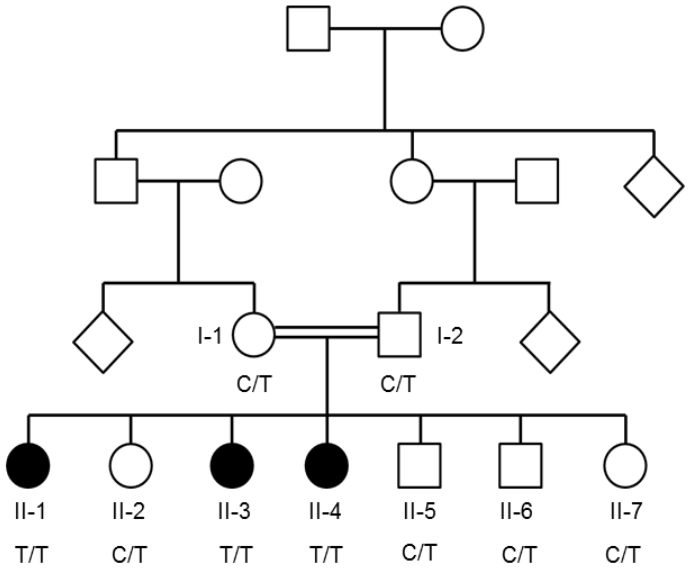

B

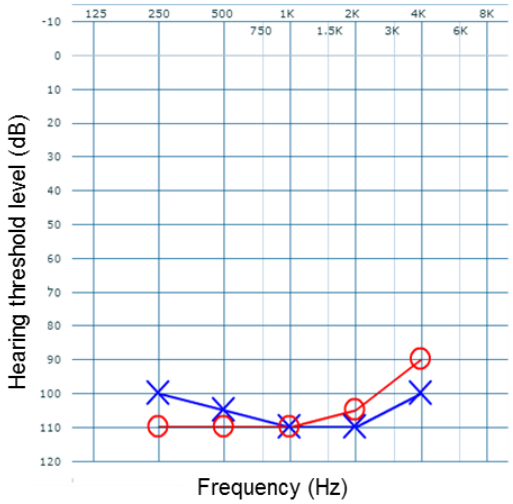

C

	II-1 Age 23 years	II-3 Age 21 years	II-4 Age 19 Years	Postmenopausal Reference Values
Follicle Stimulating Hormone (IU/l)	90.7	53.5	17.7	26.7 - 133.4
Luteinising Hormone (IU/l)	31.8	97.9	75.0	10.4 - 64.6
Estradiol (pmol/l)	14.2	37.3	12.0	36.7 - 102

D

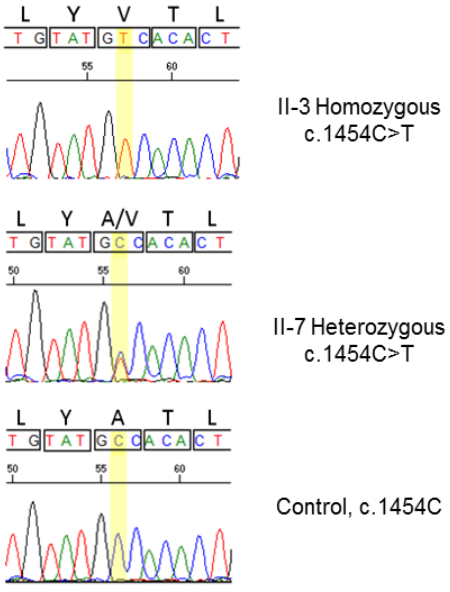

Figure 5.1. The variant *KIAA0391* c.1454 C>T causes sensorineural hearing loss and primary ovarian insufficiency in a large consanguineous family.

Figure legend continued next page.

Figure 5.1. The variant *KIAA0391* c.1454 C>T causes sensorineural hearing loss and primary ovarian insufficiency in a large consanguineous family.

A) The pedigree for the consanguineous Palestinian family with a variant in *KIAA0391*. The pedigree includes genotypes for the variant *KIAA0391* c.1454 C>T. Filled symbols indicate affected individuals. **B**) Audiogram of affected individual II-4. The hearing level of the left ear is represented by the blue crosses and the right ear by red circles. All three affected sisters show a similar audiometric configuration, with profound hearing loss across all tested frequencies. The hearing threshold level of a normal adult is 0-20 dB (Action on Hearing Loss 2017). **C**) Hormone profiles for the three affected sisters, indicative of hypergonadotropic hypogonadism. Patients with hypergonadotropic hypogonadism have levels of follicle stimulating hormone, luteinising hormone and estrogen in the postmenopausal range (Aiman and Smentek 1985). **D**) Sanger sequencing traces for an affected and unaffected member of the family and one control sample at position *KIAA0391* c.1454, highlighted in yellow (NM_014672.3).

KIAA0391 encodes the endonuclease subunit of the mtRNase P complex, PRORP, which catalyses Mg^{2+}-dependent phosphodiester-bond cleavage of 5' extensions of mitochondrial tRNAs (Holzmann et al. 2008). Residue Ala485 is highly conserved in PRORP from multiple species (Appendix IV, Supplemental Fig. SIV.1.). The p.Ala485Val variant is predicted to be deleterious by *in silico* pathogenicity tools, including SIFT (Kumar et al. 2009), PolyPhen2 (Adzhubei et al. 2010) and MutationTaster (Schwarz et al. 2014), and was absent in 100 ethnically matched controls, in the ExAC server (Exome Aggregation Consortium (ExAC)), dbSNP (Sherry et al. 2001) or EVS (NHLBI GO Exome Sequencing Project (ESP)) – comprising a minimum of 70,000 individuals. Of note, homozygous loss of function variants in *KIAA0391* are absent from publically available databases noted above and a cohort of >3,200 British Pakistani individuals (Narasimhan et al. 2016). Segregation of the homozygous variant with the Perrault syndrome phenotype was confirmed via Sanger sequencing (Fig. 5.1A and 5.1D). Sequence analysis of *KIAA0391* in five unrelated individuals with Perrault syndrome (Demain et al. 2017), without a disease-causing variant in the known Perrault syndrome genes, did not identify putative pathogenic variants in a second family.

5.4.3. Patient cells contain normal levels of mtRNase P but display decreased levels of oxidative phosphorylation (OXPHOS) components containing mitochondria-encoded proteins

We investigated the steady-state levels of TRMT10C, SDR5C1 and PRORP in patient fibroblasts by Western blot analysis and found no decrease in the levels of the mtRNase P subunits compared to controls (Fig. 5.2A), suggesting that the p.(Ala485Val) variant does not markedly influence the stability of PRORP or the other mtRNase P subunits. We detected decreased steady-state levels of subunits of respiratory chain complex I (NDUFB8) and complex IV (COXI and COXII) subunits in patient fibroblasts compared to controls – both complexes containing mitochondrial DNA-encoded subunits - with no change of other OXPHOS components observed, most notably complex II, which is entirely nuclear-encoded(Fig. 5.2B). These results indicate a generalised defect of mitochondrial translation in the patient fibroblasts.

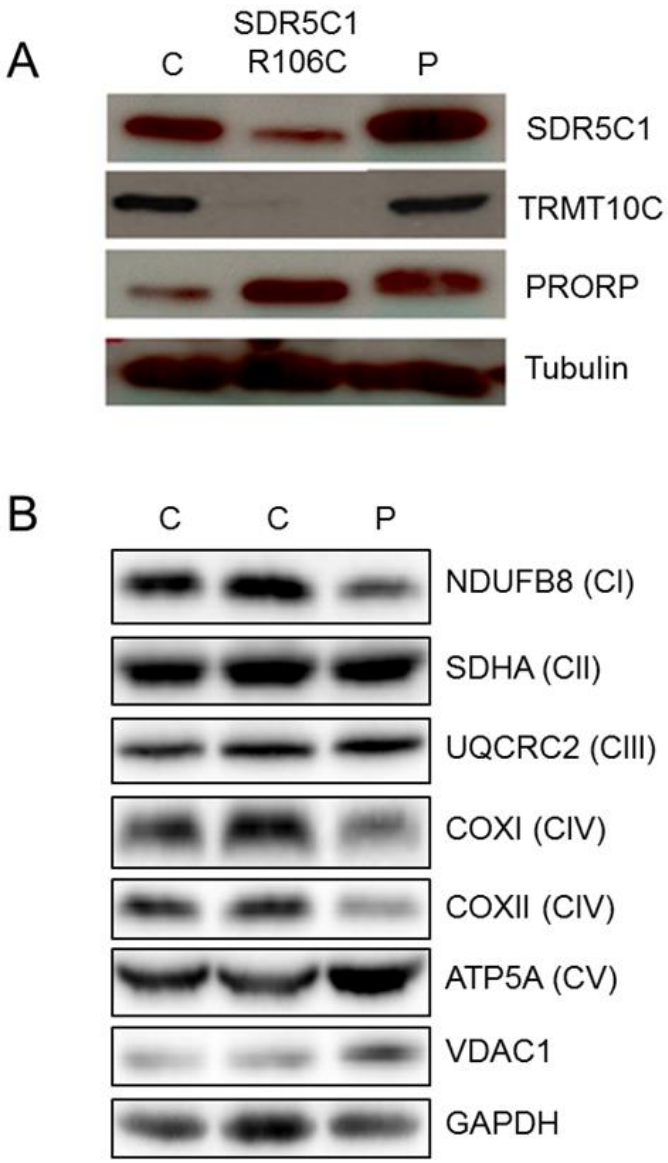

Figure 5.2. Patient fibroblasts show no reduction in subunits of mtRNase P, but show reduced levels of mitochondrial DNA encoded OXPHOS subunits.

A) Western blot analysis of mtRNAse P subunits TRMT10C, SDR5C1 and PRORP in fibroblasts from a healthy control (C); an individual with the R106C pathogenic substitution in SDR5C1 (Deutschmann et al. 2014) and individual II-4 with the p.Ala485Val variant in PRORP (P). Steady state levels of both TRMT10C and SDR5C1 are known to be reduced in patients with HDS10 disease due to the known pathogenic variant in SDR5C1, R106C (Deutschmann et al. 2014). **B**) Western blot analysis of proteins of the five oxidative phosphorylation complexes. Included are two control samples (C) and a patient sample (P), II-4. VDAC1 serves as a mitochondrial loading control.

5.4.4. Patient cells display disrupted mitochondrial RNA processing

The levels of unprocessed mitochondrial transcripts in fibroblasts from individual II-4 were assessed by Northern blot analysis. An *MT-ND1* probe detected an RNA transcript of approximately 2.5 kb in the patient sample not observed in the controls suggesting impaired 5'-end processing of $tRNA^{Leu(UUR)}$ (Fig. 5.3). A larger RNA species appeared on a longer exposure for the *MT-ND1* probe indicating that $tRNA^{Val}$ processing is also decreased. An *MT-ND2* probe detected a large RNA transcript in the patient sample at approximately 4 kb indicating impaired 5'-end processing of $tRNA^{Ile}$, $tRNA^{Met}$ and $tRNA^{Trp}$. A longer exposure revealed multiple bands, indicating the accumulation of transcripts due to the impaired 5'-end processing at multiple tRNA sites. An *MT-CO2* probe showed a transcript of approximately 1.7 kb not detected in the controls suggesting impaired processing of $tRNA^{Lys}$. Multiple bands in a longer exposure using the *MT-CO2* probe indicated decreased processing across multiple tRNA sites. An *MT-ND6* probe detected a transcript at approximately 2.3 kb in the patient sample, which can be explained by impaired 5' processing of $tRNA^{Glu}$. Taken together, the accumulation of various large unprocessed mitochondrial RNA transcripts across multiple tRNA sites indicates a generalised insufficiency of mitochondrial tRNA processing.

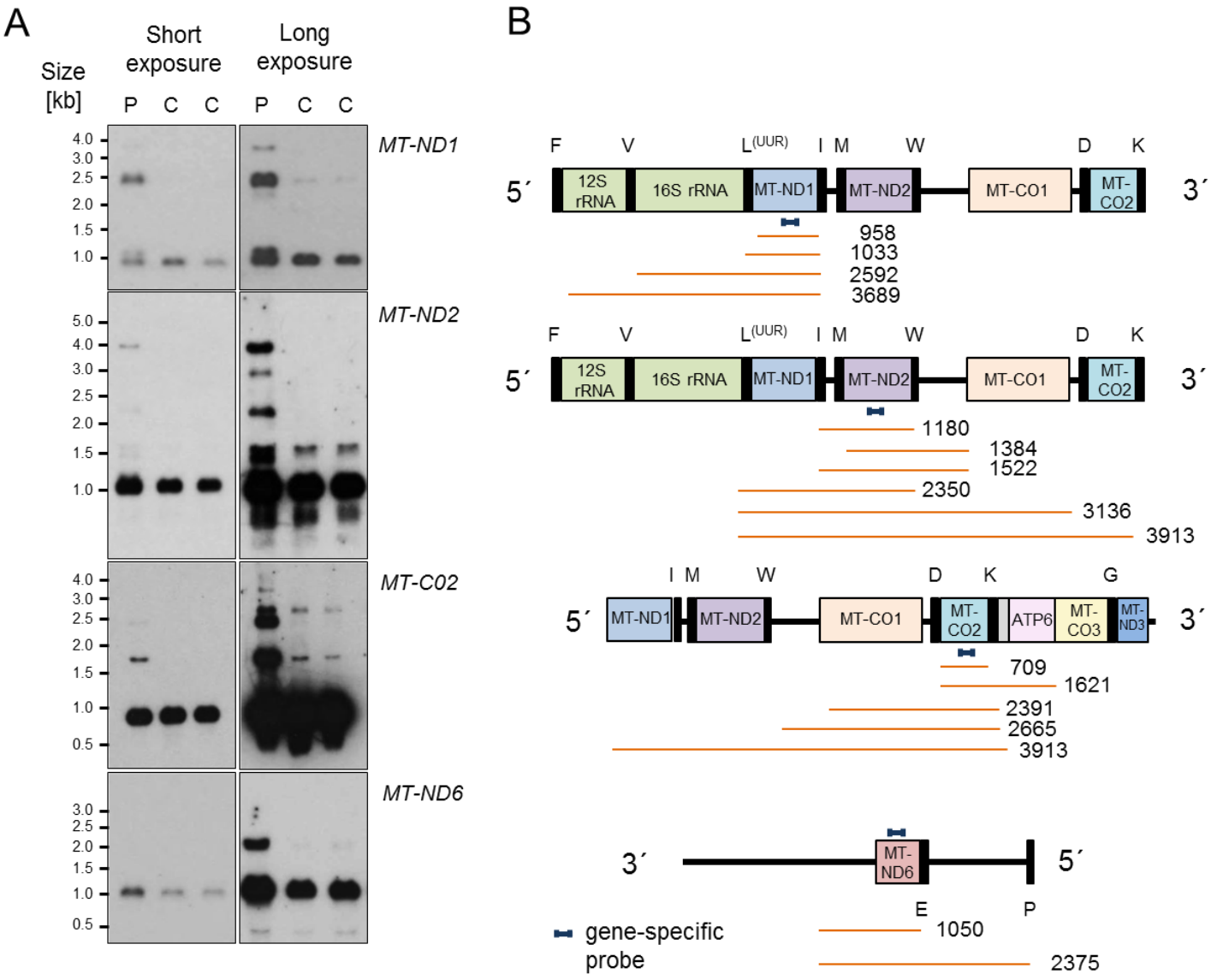

Figure 5.3. Impaired mitochondrial RNA processing is detected in patient fibroblasts.

A) Northern blot assessment of RNA extracted from patient (P) fibroblasts (II-4) and two control (C) samples using strand specific probes designed to complement four different mitochondrial gene transcripts; *MT-ND1*, *MT-ND2*, *MT-CO2* and *MT-ND6*. A long and short exposure of the blots is shown. **B**) Schematic representations of mitochondrial genome regions, the probes (dark blue) and expected fragment sizes in bp (orange) are shown to the right of each blot.

5.4.5. The PRORP p.Ala485Val disease variant displays decreased mtRNase P activity

The disease-associated variant p.Ala485Val is situated in the metallonuclease domain of PRORP, close to four conserved aspartate residues implicated in metal ion binding (Fig. 5.4A and 5.4B) (Howard et al. 2012). Replacing the conserved alanine at residue 485 with the bulkier valine could distort the active site and impair catalysis by interfering with proper coordination of the metal ions, thereby reducing the endonucleolytic activity of PRORP. To determine whether the p.Ala485Val variant alters the catalytic activity of PRORP, we compared the enzymatic activity of the disease-associated isoform and the wild type protein in the RNase P complex.

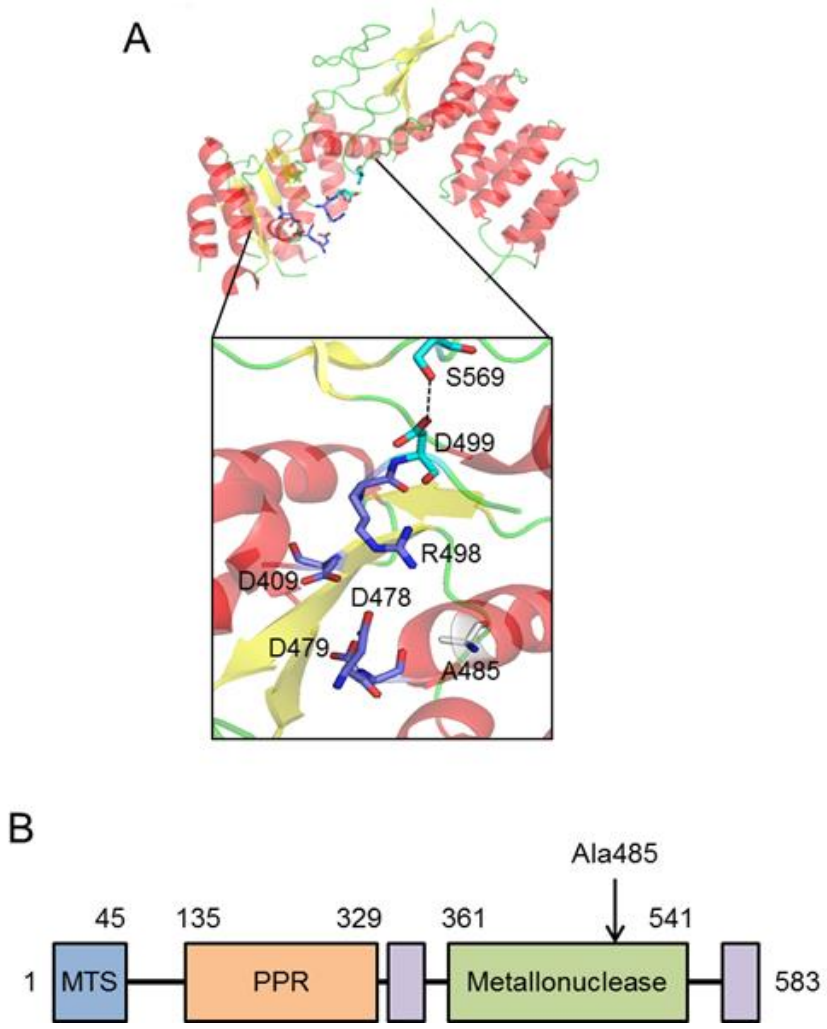

Figure 5.4. The residue Ala485 is situated in the metallonuclease domain of PRORP close to conserved residues.

A) The protein structure of human PRORP; the enlarged region is part of the metallonuclease domain. Residue Ala485 is situated in the centre of the active site close to the conserved aspartate residues that coordinate catalytic magnesium ions. **B**) A bar diagram of the domains of human PRORP (Reinhard et al. 2015). The location of the variant residue Ala485 is noted on the diagram. Mitochondrial targeting sequence, MTS; pentatricopeptide repeat domain, PPR.

The three wild type proteins of the mtRNase P complex TRMT10C, SDR5C1 and PRORP as well as the PRORP p.Ala485Val variant protein were individually produced by recombinant expression in *E.coli* and purified. During the assessment of the recombinant protein PRORP p.Ala485Val we noted that it had a higher melting temperature than wild type PRORP (Appendix IV, Supplemental Fig. SIV.2) suggesting reduced flexibility of the

variant PRORP. Recombinant mtRNase P was reconstituted *in vitro* and 5' end processing assays were performed with radiolabelled precursor tRNA (pre-tRNA) (Fig. 5.5 and Appendix IV Supplemental Fig. SIV.3). Assays were performed with three mitochondrial tRNA substrates. Variants in *HSD17B10* (encoding SDR5C1) causing HSD10 disease (MIM 300438) were reported to affect the accumulation of unprocessed transcripts from the heavy strand, but not those from the light strand (Deutschmann et al. 2014). We therefore selected the heavy strand-encoded pre-tRNA^{Ile} and the light strand-encoded tRNA^{Tyr}. Additionally, Pre-tRNA$^{His\text{-}Ser(AGY)\text{-}Leu(CUN)}$ was selected, because variants in *HARS2* and *LARS2*, which encode mitochondrial histidyl and leucyl aminoacyl synthetases, respectively, cause Perrault syndrome (Pierce et al. 2011;Pierce et al. 2013).
Since mtRNase P is an endonuclease, two fragments result from the cleavage of pre-tRNA^{Tyr} and pre-tRNA^{Ile}: the removed 5'-leader and the 5'-mature tRNA (Fig. 5.5A and 5.5C; Appendix IV Supplemental Fig. SIV.3A). From the pre-tRNA transcript containing three tRNAs, the combination of two mtRNase P sites produces five possible fragments (Rossmanith 1997) (Fig. 5.5B, 5.5D and 5.5E). The variant mtRNase P complex generated markedly less processed tRNA than the wild type complex across all time points and reactions. Quantitative phosphorimaging revealed a diminution of cleavage products by ~35-45% ($p<0.01$) depending on the pre-tRNA substrate used (Fig. 5.5F, 5.5G, 5.5H, and Appendix IV Supplemental Fig. S3B). There was no significant difference in the reduction of 5'-end processing by PRORP p.Ala485Val-containing mtRNase P between the different pre-tRNA substrates analysed ($p>0.05$), consistent with the accumulation of both heavy and light-strand transcripts seen in patient fibroblasts (Fig. 5.3).

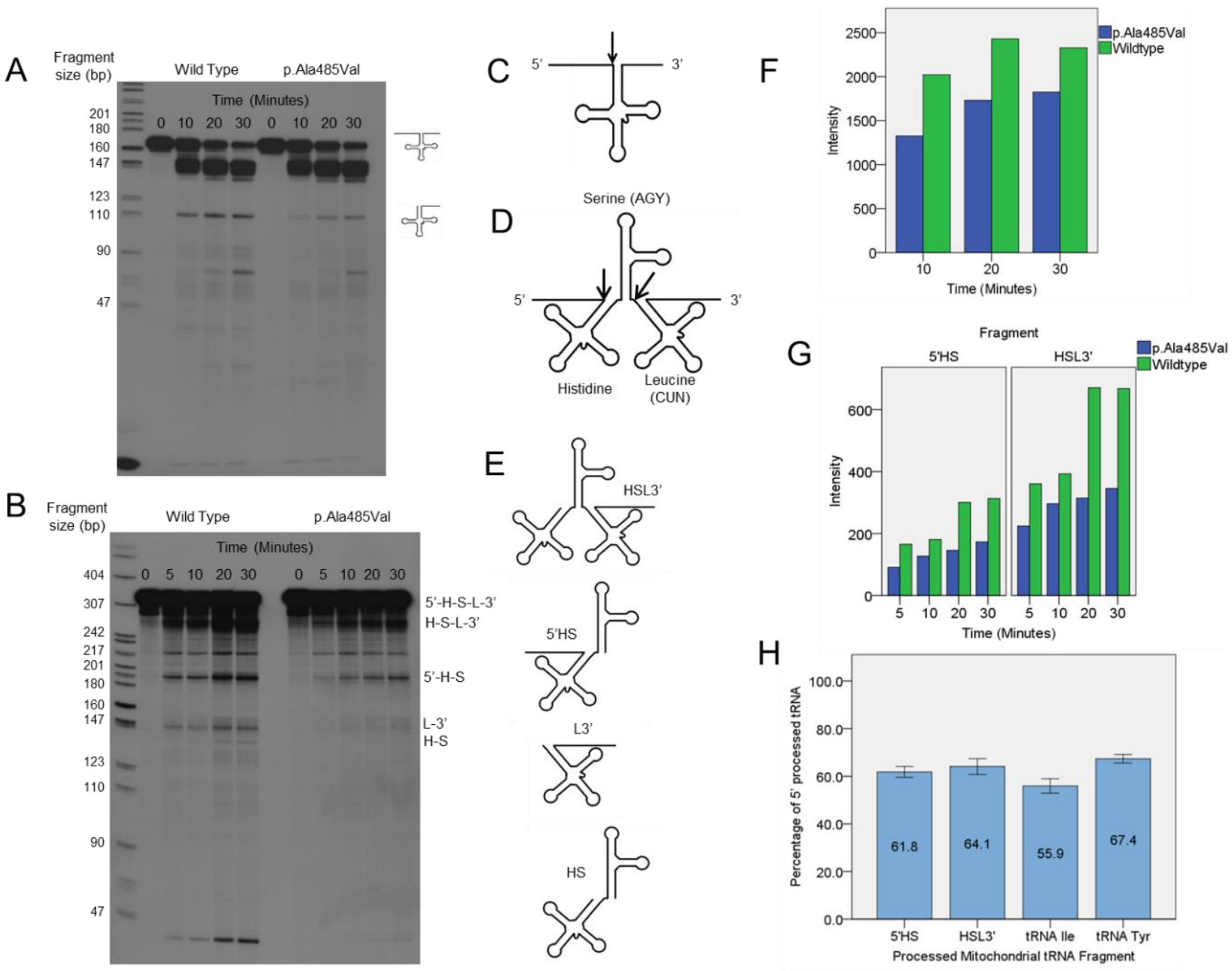

Figure 5.5. *In vitro* mtRNase processing assays show the variant p.Ala485Val PRORP produces significantly less 5' end processed tRNA than wild type PRORP.

Figure legend continued next page.

Figure 5.5. *In vitro* mtRNase processing assays show the variant p.Ala485Val PRORP produces significantly less 5' end processed tRNA than wild type PRORP.

A) Mitochondrial pre-tRNA^{Tyr} was subjected to cleavage by reconstituted recombinant mtRNase P containing either wild type or p.Ala485Val PRORP. Aliquots were removed from the reactions and stopped at the time points indicated, and resolved by urea-PAGE. **B**) Mitochondrial pre-tRNA$^{His\text{-}Ser(AGY)\text{-}Leu(CUN)}$ was subjected to cleavage by reconstituted recombinant mtRNase P containing either wild type or p.Ala485Val PRORP. Processing as in (**A**) with an additional time point added at 5 minutes. See (**E**) for fragment labelling. **C**) A simplified drawing of pre-tRNA; the arrow indicates the site of mtRNase P processing. **D**) A drawing of pre-tRNA$^{His\text{-}Ser(AGY)\text{-}Leu(CUN)}$, (Rossmanith 1997). The arrows indicate the sites of mtRNase P processing. **E**) The fragments produced from pre-tRNA$^{His\text{-}Ser(AGY)Leu\text{-}(CUN)}$ by mtRNase P processing listed in order of descending size; the 5'-end fragment not included. **F**) Quantitative analysis of pre-tRNA^{Tyr} processing experiment shown in (**A**). There was significant difference between the p.Ala485Val and wild type mtRNaseP over three replicate experiments (n = 9 paired wild type and equivalent variant time points across 3 replicate experiments, $P<0.01$). **G**) Quantitative analysis of pre-tRNA$^{His\text{-}Ser(AGY)\text{-}Leu(CUN)}$ processing experiment shown in (**B**), only the fragments HSL3'and 5'HS are shown. The HSL3' fragment at 30 minutes shows reduction compared to the fragment at 20 minutes likely because of further processing to produce the HS fragment. There was significant difference between the p.Ala485Val and the wild type mt RNaseP (HSL3'; n = 12 paired time points across 3 replicate experiments, $P< 0.01$ and 5'HS; n = 12 paired time points across 3 replicate experiments, $P< 0.01$). **H**) The average tRNA processing of the four major fragments from the three substrates as compared to the wild type processing. Wild type is set to 100%. Data presented as the mean of 3 replicate experiments (all time points included) +/- SEM.

5.4.6. tRNA processing in patient cells can be rescued by expression of wild type *KIAA0391*

Rescue experiments were used to connect the accumulation of unprocessed RNA transcripts seen in the patient cells to the variant PRORP p.(Ala485Val). Patient fibroblasts were transfected with a plasmid containing the wild type *KIAA0391* sequence. Unprocessed RNA transcripts were quantified by qPCR across processing sites (Fig.5.6A). In untransfected patient cells there was a greater than 6-fold increase in both pre-tRNA^{Leu} and pre-tRNA^{Val} transcripts in comparison to controls. When the patient cells were transfected with wild type PRORP, this increase was reduced to about 3-fold for pre-tRNA^{Leu}, and pre-tRNA^{Val} levels came back close to the control. Transfection efficiency,

which is 70% maximum, could account for tRNA processing not achieving wild type levels in transfected patient cells.

5.4.7. PRORP is present in hair cell synapses and neurons of the mouse organ of Corti

To understand why the variant in PRORP, p.Ala485Val, could be associated with hearing loss in the affected family, we undertook localisation studies of PRORP in the mouse organ of Corti. The organs of Corti from C57/BJ6 mice at postnatal (P) day 4 (P4), P16 and P24, were immunofluorescently stained to reveal the localisation of endogenous PRORP. The samples were also counterstained with a presynaptic membrane marker SNAP25 (synaptosome-associated protein 25), and DAPI, a fluorescent stain for double-stranded DNA that highlights the cell nucleus.

In mice, the onset of hearing occurs at approximately P12-P14 (Ehret 1976). At P4, the organ of Corti is not fully mature and low levels of SNAP25 protein are detected at presynaptic hair cell membranes (Figure 5.6b) (Sendin et al. 2007). At P4, diffuse PRORP staining at low levels is observed. Shortly after the onset of hearing at P16, the outer hair cell (OHC) efferent synapses and the inner hair cell (IHC) nerve fibres are highlighted by SNAP25. At P16 PRORP signal is detected around the base of inner hair cells where afferent and efferent synapses are situated. At the same time, we observed low levels of PRORP in the hair cell bodies and in the efferent synapses of OHCs. By P24, PRORP immunoreactivity is increased at the efferent synapses of OHCs and around the base of inner hair cells. PRORP partially co-localises with SNAP25 staining around IHCs (see P16 images), suggesting that PRORP could be present not only in the mitochondria of efferent synapses but possibly afferent synapses and nerve fibres around the IHCs. Low levels of PRORP signal is present in OHC bodies at P24 alongside the more intense signal seen at the OHC synapses and IHC base. At P24, the mitochondrial marker Tom20 labels mitochondria mainly within hair cell bodies and does not show increased signal in mitochondria within the supporting cells or efferent synaptic buttons (Appendix IV Supplementary Fig. S4), arguing for structurally different mitochondria with different protein compositions present in different cell types (Lesus et al. 2017;Lysakowski and Goldberg 1997). It is likely that the high levels of PRORP found in the subset of mitochondria associated with the synapses and neurons of the organ of Corti hair cells

reflect those cells' increased demand for genes involved in mitochondrial tRNA processing and translation.

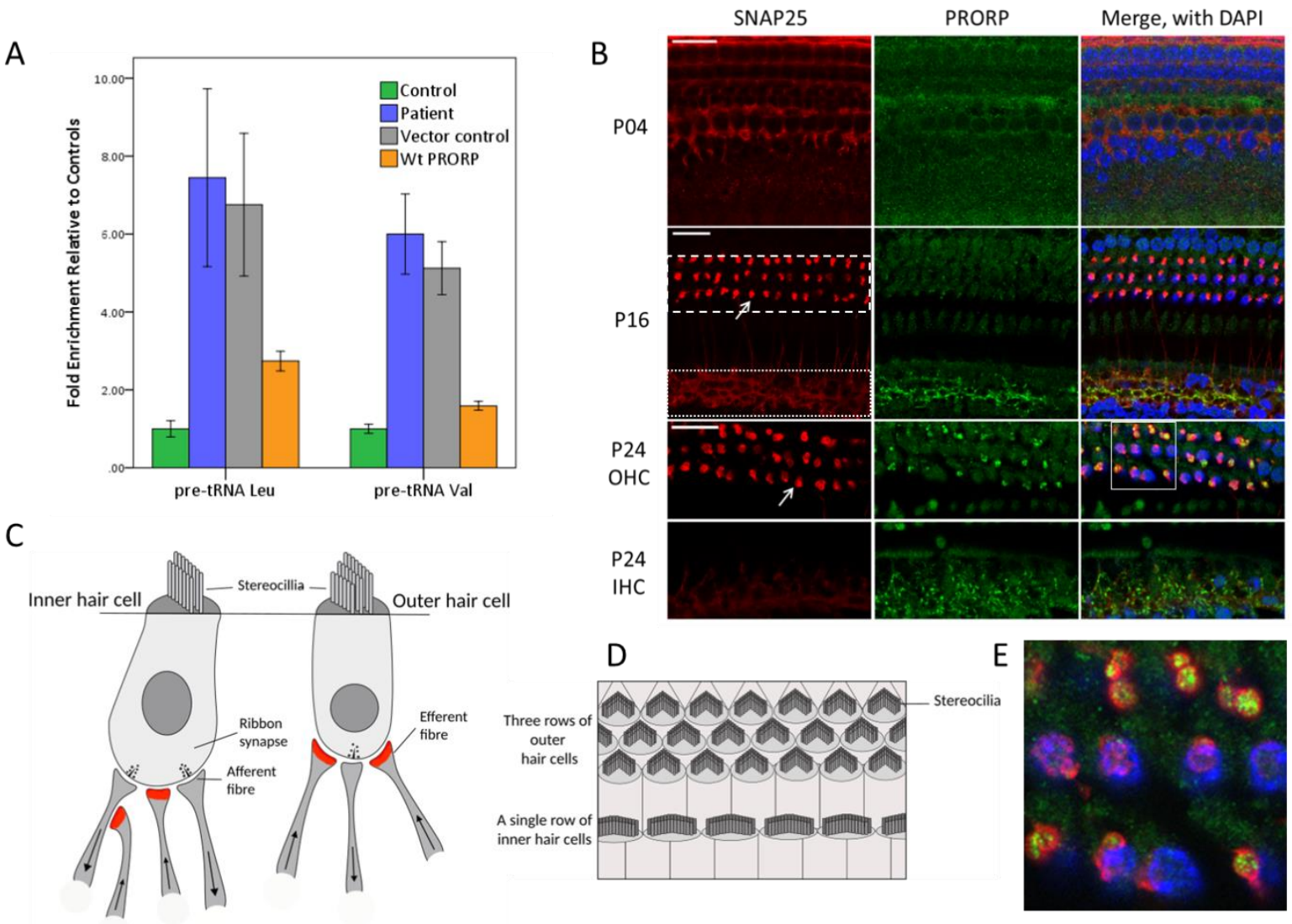

Figure 5.6. Expression of wild type *KIAA0391* encoding PRORP rescues tRNA processing and localisation in the mouse organ of Corti shows high levels of PRORP in the synapses and nerve fibres of hair cells.

Figure legend continued next page.

Figure 5.6. Expression of wild type *KIAA0391* encoding PRORP rescues tRNA processing and localisation in the mouse organ of Corti shows high levels of PRORP in the synapses and nerve fibres of hair cells.

A) Mitochondrial precursor transcripts containing $tRNA^{Val}$ and $tRNA^{Leu}$ were quantified in control and patient fibroblasts using real time PCR. The patient samples are presented as a relative fold increase of the relevant controls. The precursor transcripts in patient samples were measured in non-transfected cells, cells transfected with the empty vector and in cells transfected with the vector containing the wild type *KIAA0391* sequence. For the control samples non-transfected fibroblasts were quantified. Fibroblast cell cultures of three different healthy donors served as controls. (mean ± SEM). Untransfected patient cells showed a greater than 5 fold increase in both pre-$tRNA^{Leu}$ and pre-$tRNA^{Val}$ transcripts compared to controls. Transfection of patient cells with wild type *KIAA0391* reduced precursor transcripts by ~75% for pre-$tRNA^{Leu}$ and ~ 65% pre-$tRNA^{Val}$, rescuing tRNA processing. **B**) Confocal fluorescence microscopy optical sections of the whole mount organ of Corti samples from C57/BJ6 mice at postnatal days 4, 16 and 24 (P4,P16 and P24, correspondingly) showing localization of PRORP protein (green). Samples were counterstained with DAPI (nuclear DNA marker, blue) to visualize the nuclei of hair cells and SNAP25 (presynaptic membrane marker, red) to visualize efferent synapses at the base of OHCs and nerve fibres and synaptic buttons at the base and around IHCs. In the panels for P4 and P16 the dashed white line outlines the area of the outer hair cells (OHC) at the nuclear level and the dotted white line outlines the area around the inner hair cell nuclei (IHC). The white arrows point to one of the OHC efferent presynaptic buttons. The two panels at P24 represent two optical sections through the same organ of Corti sample at different focal plains to visualize OHC synaptic area (top) and IHC synaptic area (bottom). The scale bar is 20μm. **C**) An illustration of the innervation of inner hair cells and outer hair cells. Arrows in the nerve fibres indicate the direction of transmission. The area of SNAP25 staining is shown in red. **D**) An illustration of the arrangement of hair cells in the organ of Corti in the same orientation as shown in Panel **B**. **E)** An enlarged view of the area inside the white box in Panel **B** showing the co-localisation of SNAP25 (red) and PRORP (green) with the OHC nuclei shown in blue.

5.5. Discussion

In this report we provide evidence that Perrault syndrome is caused by a novel homozygous variant in *KIAA0391,* a gene not previously implicated in this disorder. *KIAA0391* is the nuclear gene encoding PRORP, the catalytic subunit of the mtRNase P complex (Holzmann et al. 2008). *In vitro* tRNA processing assays supported the *in silico* predictions that the amino acid substitution in PRORP p.Ala485Val, the expected result of

the nucleotide alteration c.1454C>T, would be damaging by impairing the processing of mitochondrial tRNAs. The absence of variants in *KIAA0391* in other known cases of Perrault syndrome suggests that variants in *KIAA0391* are not a common cause of this heterogeneous condition. However, our discovery provides further important insights into the pathogenesis of hearing loss and ovarian insufficiency. The functional work reported here indicates the mitochondrial respiratory chain deficiency seen in this family can be attributed to a variant in *KIAA0391*. An independent family would provide additional data linking variants in *KIAA0391* with Perrault syndrome as would recapitulation of the Perrault syndrome phenotype in an animal model of the p.Ala485Val substitution in PRORP.

The mtRNase P complex is composed of three proteins, TRMT10C-SDR5C1-PRORP, each encoded by the nuclear genome and post-translationally imported into the mitochondria matrix via an N-terminal mitochondrial targeting sequence (Holzmann et al. 2008;Vilardo et al. 2012). Mitochondrial tRNAs are processed at the 5' end by mtRNase P (Holzmann et al. 2008) and at the 3' end by mtRNase Z, encoded by *ELAC2* (Brzezniak et al. 2011;Rossmanith 2011). This tRNA processing excises most of the RNA species from the polycistronic mitochondrial precursor transcripts according to the tRNA punctuation model (Ojala et al. 1981;Rossmanith 2012).

We observed normal levels of PRORP in patient fibroblasts (Fig. 5.2A), which contrasts with the reduction of the other two subunits of mtRNase P, SDR5C1 (Deutschmann et al. 2014;Zschocke 2012) and TRMT10C (Metodiev et al. 2016) in patients with inherited deficiencies of those proteins. Accumulation of multiple unprocessed transcripts in patient fibroblasts indicated a generalised defect in mitochondrial tRNA processing (Fig. 5.3), leading to a mild but observable downstream effect on mitochondrial protein synthesis as evidenced by decreased steady-state levels of complex I and complex IV subunits (Fig. 5.2B). A similar, but more pronounced, OXPHOS defect was also observed in patients with pathogenic variants in *TRMT10C* (Metodiev et al. 2016) and *HSD17B10* (encoding SDR5C1) (Chatfield et al. 2015). OXPHOS deficiency has also been associated with Perrault syndrome in patients with variants in *ERAL1* (Chatzispyrou et al. 2017). The pattern of OXPHOS deficiency in patients with Perrault syndrome due to *ERAL1* variants is similar to that seen in our patient, suggesting that they may share a common pathogenesis.

Biallelic variants, which are predicted to result in complete loss of function, have not been identified in any of the three subunits of the mtRNase P complex. All three mtRNase P complex genes are among the core set of genes essential for the survival of cells in tissue culture (Blomen et al. 2015;Wang et al. 2015). There are no knockout mouse models for *trmt10c* and the homozygous knockout of *hsd17b10* results in an early embryonic lethal phenotype (Rauschenberger et al. 2010). Knockout of *1110008L16Rik* (*KIAA0391* homolog) is embryonic lethal, but cardiac and skeletal muscle specific *1110008L16Rik* conditional knockout mice have been produced (Rackham et al. 2016). These mice die at 11 weeks due to cardiomyopathy. The conditional knockout mice showed a significant reduction in the synthesis of mitochondrial encoded proteins with no alteration in nuclear encoded proteins. The reduction in mitochondrial-encoded proteins was accompanied by a significant reduction in mitochondrial respiration (Rackham et al. 2016). The mice also showed an accumulation of unprocessed mitochondrial RNA transcripts, but in contrast to patients with defects in subunits of mtRNase P, the mice had no mature transcripts (Rackham et al. 2016). The lack of mature mitochondrial transcripts may be the result of the complete loss of PRORP protein function in mice in comparison to patients with predicted hypomorphic variants in *TRMT10C*, *HSD17B10* or *KIAA0391*.

Despite the similarities in defective mitochondrial tRNA processing, variants in the three subunits of mtRNase P result in markedly differing clinical phenotypes. Pathogenic variants in *TRMT10C* cause a lethal, childhood multisystem disorder characterised by muscular hypotonia, SNHL and metabolic acidosis (Metodiev et al. 2016). Pathogenic variants in *HSD17B10*, encoding SDR5C1 (protein also known as HSD10, HADH2, MRPP2 or ABAD), cause HSD10 disease, which manifests as a severe, infantile-onset neurodegenerative condition with cardiomyopathy (Zschocke 2012;Vilardo and Rossmanith 2015). The clinical presentation of Perrault syndrome is less severe than of individuals with TRMT10C (Metodiev et al. 2016) and SDR5C1-associated diseases (Zschocke 2012). The tissue specific phenotype of Perrault syndrome (SNHL and POI) in comparison to the more systemic presentations of TRMT10C- and SDR5C1-associated phenotypes may be accounted for by the differing function of the proteins. TRMT10C and SDR5C1 are also important for methylation at position 9 of mitochondrial tRNAs, which stabilises the tertiary L-shaped structure of some tRNAs (Vilardo et al. 2012),whereas

PRORP is required for the nuclease function of mtRNase P only (Holzmann et al. 2008;Vilardo et al. 2012). It is possible that more deleterious variants in *KIAA0391* would result in further reduction in PRORP activity and a more severe multisystem disorder, similar to that seen in individuals with *LARS2* variants (Riley et al. 2015). Conversely, hypomorphic alleles in *KIAA0391* could result in milder degrees of SNHL or POI only.

Immunohistochemistry of the mouse organ of Corti revealed the localisation of PRORP in hair cells with higher levels associated with the efferent synapses of the outer hair cells and nerve fibres of the inner hair cells. This particular pattern of PRORP localisation becomes apparent after the onset of hearing and involves only mitochondria of some cell types. It seems likely that a subpopulation of mitochondria associated with neurons in the organ of Corti are enriched for PRORP and may require a higher level of mitochondrial translation, after hearing onset.

Recently, the expression levels of hearing loss genes were examined in different areas of the mouse cochlea. Four of the six genes associated with Perrault syndrome were examined, and it was found that they showed higher expression levels in the spiral ganglion neurons than in other parts of the cochlea, including the organ of Corti (Nishio et al. 2017). This pattern of expression correlates with our immunohistochemistry results, as the cell bodies of the nerve fibres with efferent synapses that terminate at the base of OHC and IHC are in the brainstem, and IHC afferent synapses and their nerve fibres originate from the spiral ganglion neurons. Dysfunction of PRORP causing disruption of the hair cell efferent or afferent signalling, in conjunction with malfunctioning mitochondria of hair cell bodies, could be the pathological mechanism behind the hearing loss in the family reported here. The gene expression patterns from other Perrault syndrome genes suggest that they may share a similar pathology of neuronal origin with the case presented here (Nishio et al. 2017). Our results together with the results from Nishio *et al* (Nishio et al. 2017) suggest that the neurons in the spiral ganglion and brainstem may have an increased level of mitochondrial translation, perhaps making them vulnerable to disruption of this pathway during sustained sound stimulations after the onset of hearing.

Pathogenic variants resulting in distinct clinical phenotypes have now been identified in all the genes encoding subunits of mtRNase P. It is currently unclear why pathogenic variants in the different subunits of mtRNase P cause distinct clinical phenotypes. Investigation into this could provide insights into differences in the pathogenic mechanisms.

Most genes previously associated with Perrault syndrome (*HARS2, LARS2, C10orf2*, *CLPP* and *ERAL1*) encode proteins implicated in mitochondrial protein translation (Pierce et al. 2011;Pierce et al. 2013;Jenkinson et al. 2013;Morino et al. 2014;Chatzispyrou et al. 2017). Our finding that biallelic variants in *KIAA0391,* encoding PRORP, result in impaired mitochondrial tRNA processing expands the spectrum of genes that can cause Perrault syndrome and provides additional evidence that Perrault syndrome is caused by impaired mitochondrial translation. Further, this discovery lends additional support to the hypothesis that genes involved in mitochondrial translation are candidates for genetically unresolved cases of Perrault syndrome.

5.6. Materials and methods

5.6.1. Ethical approval

All patients provided written informed consent in accordance with local regulations. Ethical approval for this study was granted by the National Health Service Ethics Committee (16/WA/0017) and University of Manchester. The NIH Animal Use Committee approved protocol 1263-15 to T.B.F. for mice.

5.6.2. Autozygosity mapping and whole exome sequencing

Autozygosity mapping was performed on six members of the family (II-1, II-2, II-3, II- 4, II-6 and II-7) using the Affymetrix Genome-wide SNP6.0 arrays as previously described (Banka et al. 2011). Whole exome sequencing was performed on DNA extracted from lymphocytes from individual II-3. The Agilent SureSelect Human All Exon V5 Panel (Agilent Technologies, Santa Clara, CA, USA) was used for library preparation and sequencing was performed on the HiSeq 2500 (Illumina, San Diego, CA, USA) as previously described (Smith et al. 2014).

5.6.3. Confirmation of variants

Variants were confirmed in the family via Sanger sequencing using the ABI big Dye v3.1 (Thermo Fisher Scientific Inc, Waltham, MA, USA) sequencing technology. Primer sequences are available in Appendix I.

5.6.4. Assessment of protein and RNA levels in patient fibroblasts

Western blot analyses for the mtRNase P subunits were performed as previously described (Deutschmann et al. 2014) using cell lysates from dermal fibroblasts (II-4). 30 mg of protein was separated on a 10% SDS-polyacrylamide gel and transferred to a polyvinylidene difluoride membrane (GE Healthcare, Little Chalfont, UK). Membranes were blocked and subsequently incubated with the primary antibodies (Deutschmann et al. 2014) and detected with HRP-conjugated secondary antibodies (Dako, Agilent Technologies, Santa Clara, CA, USA). The blots were developed using the ECL Western Blotting Analysis Detection system (GE Healthcare, Little Chalfont, UK).

Western blots for the respiratory chain complexes (n=3) were performed using fibroblast cell lysates (II-4). Cell lysates were incubated with sample dissociation buffer, separated by 12% SDS–PAGE and immobilized by wet transfer on to PVDF membrane (Immobilon-P, Millipore Corporation, Billerica, USA). Proteins of interest were bound by overnight incubation at 4^{o}C with primary antibodies followed by HRP-conjugated secondary antibodies (Dako Cytomation, Agilent Technologies, Santa Clara, CA, USA) and visualized using ECL-prime (GE Healthcare, Little Chalfont, UK) and Bio-Rad, Hercules, CA, USA ChemiDoc MP with Image Lab software. Antibody details are available in the Supplemental Materials.

Northern blot analysis was performed as previously described (Deutschmann et al. 2014). The NorthernMax kit from Ambion, Thermo Fisher Scientific Inc, Waltham, MA, USA was used. 2–5 µg of total RNA, from fibroblasts (II-4), was separated on a 1% denaturing agarose gel. RNA was then transferred to nylon membrane (Hybond-N + ProteinTech, Manchester, UK) by capillary transfer, UV cross-linked and subjected to hybridization with biotinylated probes. Signals were detected using the BrightStar BioDetect kit (Ambion, Thermo Fisher Scientific Inc, Waltham, MA, USA). A biotinylated RNA size marker (BrightStar RNA Millenium Marker, Ambion, Thermo Fisher Scientific Inc, Waltham, MA,

USA) was used to determine the size of RNA species. Probe sequences as previously described (Deutschmann et al. 2014).

5.6.5. Preparation of the PRORP p.Ala485Val sequence for bacterial expression

The plasmid pET28-b(+) containing the coding sequence for PRORP (Holzmann et al. 2008) was mutagenized as previously described (Kunkel et al. 1987) with the synthetic oligonucleotide PRORP_p.Ala485Val (see 2.10.2 data for oligonucleotide sequence). The potential mutagenized plasmids were extracted using the GenElute HP Plasmid miniprep Kit (Sigma-Aldrich, St. Louis, MO, USA Aldrich) and the variant was confirmed by DNA sequencing.

5.6.6. Recombinant expression and purification of TRMT10C, SDR5C1 and PRORP (wt and p.Ala485Val)

The templates for recombinant expression of *TRMT10C, SDR5C1 and PRORP* were as detailed in (Holzmann et al. 2008) and above. Expression was induced in *E.coli* Rosetta2 DE3 (Novagen, Merck, Kenilworth, NJ, USA) using Overnight Express medium (Novagen, Merck, Kenilworth, NJ, USA). Affinity chromatography of the His-tagged proteins was performed as previously described (Holzmann et al. 2008). Their purity was assessed by SDS-PAGE. Aliquots of purified proteins were dialysed overnight at 4°C in 20 mM Tris-Cl pH 7.4, 100 mM NaCl, 15% glycerol, then flash frozen and stored at -80°C.

5.6.7. Preparation of mitochondrial pre-tRNA transcripts

The templates for pre-tRNA^{Tyr} and pre-tRNA^{Ile} were as described in (Holzmann et al. 2008). The template for the pre-tRNA$^{His\text{-}Ser(AGY)\text{-}Leu(CUN)}$ was as described in section 2.13.8. Run off *in vitro* transcription to produce body labelled pre-tRNA substrate was performed as previously described (O'Keefe et al. 1996).

5.6.8. Pre-tRNA processing assays

Pre-tRNA processing assays were performed as previously described (Rossmanith et al. 1995;Holzmann et al. 2008). The TRMT10C, SDR5C1 and PRORP proteins were mixed in a 2:4:1 molar ratio as described (Holzmann et al. 2008). 6% (w/v) acrylamide 8M urea gels were used to resolve substrate and cleavage products. Dried gels were exposed to X-ray

film at -80°C or exposed to a phosphorimaging screen to detect assay precursors, intermediates and products..

5.6.9. Real-time PCR

Real-time PCR and analysis was performed as previously described (Deutschmann et al. 2014). Total RNA was isolated from patient and control dermal fibroblasts and treated with DNase. Reverse transcription was performed using tRNA specific primers containing an adaptor sequence for subsequent real-time PCR. Primers sequences are as previously described (Deutschmann et al. 2014). Real time PCR was performed using standard conditions (60°C elongation, 40 cycles) and relative expression of precursor transcripts in patient fibroblasts was calculated using the ct value for the appropriate transcript from three different healthy controls. Ubiquitin B expression served as the reference for both patient samples and controls.

5.6.10. Rescue experiments

The coding sequence of wild type *KIAA0391* was cloned in an expression vector as described previously (Deutschmann et al. 2014). The coding sequence was verified by Sanger sequencing. Patient dermal fibroblasts (2.0×10^5) were seeded in 25 cm^2 flasks and cultivated in 4 ml MEM medium. The next day cells were transfected using 3µg plasmid DNA (PRORP-vector and empty vector as transfection control) and 7.5 µl Turbofect transfection reagent and cultured for additional 48 hours. The cells were then harvested and precursor tRNAs were quantified by real-time PCR as described previously (Deutschmann et al. 2014).

5.6.11. Localisation of PRORP in the mouse organ of Corti

The NIH Animal Use Committee approved protocol 1263-15 to T.B.F. for mice. C57/BJ6 mice at ages P4, P16 and P24 were euthanised, the cochlear capsule was removed and fixed with 4% paraformaldehyde in PBS for 2 hours. The samples were microdissected and the organ of Corti was permeabilised with 1% Triton X-100 in PBS for 30 min followed by three 10 min washes with 1X PBS. Nonspecific binding sites were blocked with 5% normal goat serum and 2% BSA in PBS for 1 h at room temperature. Samples were incubated for 2 h with rabbit polyclonal PRORP antibody (MRPP3, Proteintech, Manchester, UK -

Catalog number: 20959-1-AP) at 1µg/ml and mouse monoclonal SNAP25 antibody (Santa Cruz Biotechnology, Dallas, TX, USA, sc-136267) at 1µg/ml followed by several rinses with PBS. Samples were incubated with goat anti-rabbit IgG Alexa Fluor 488 conjugated secondary antibody and goat anti-mouse Alexa Fluor 568 conjugated secondary antibody (Molecular Probes, Invitrogen, Carlsbad, CA, USA) for 30 min. Samples were washed several times with PBS and were mounted with ProLongGold Antifade staining reagent with DAPI (Molecular Probes, Invitrogen, Carlsbad, CA, USA) and examined using LSM780 confocal microscope (Zeiss Inc, Oberkochen, Germany Inc) equipped with 63X, 1.4 N.A. objective.

5.6.12. Statistical analysis

The Wilcoxon paired test (N=<20) was used with a significance value of 0.05 to test for differences between the wild type and p.Ala485Val pairs for each pre-tRNA substrate.

To test for differences in the percentage reduction in the tRNA output of the p.Ala485Val variant between substrates the data was determined to be normally distributed using the Shapiro-Wilk test. One-way ANOVA with a significance value of 0.05 was used to test for differences.

5.6.13. Funding

This study was supported by Action on Hearing Loss; Action Medical Research; the Wellcome Centre for Mitochondrial Research (203105/Z/16/Z to RWT); the Medical Research Council (MRC) Centre for Translational Research in Neuromuscular Disease (G0601943 to RWT); the UK NHS Highly Specialised “Rare Mitochondrial Disorders of Adults and Children” Service (RWT); and The Lily Foundation (RWT and KT); Austrian Science Fund (FWF) P25983 (WR) and the Intramural Research Program of the NIH, NIDCD (DC000039 to TBF).

5.7. Acknowledgements

We would like to thank the family for their participation.

5.8. Author Contributions

Conceptualisation, I.H., W.G.N. and R.T.O.; Methodology, W.G.N., R.T.O., L.A.M.D., I.H., J.O., A.J.D., W.R., A.A., S.O., W.W.Y., J.Z., I.B., T.B.F., and R.W.T.; Software, S.G.W. and S.S.B.; Formal Analysis, S.G.W., S.S.B., L.A.M.D., J.E.U. and J.O.; Investigation, W.G.N, R.T.O., L.A.M.D., I.H., J.E.U, J.O., A.J.D., A.A., S.D, N.A., Z.B., S.Y., S.O., K.T, W.W.Y., J.Z., I.A.B, M.B., and R.W.T.; Writing – original draft, L.A.M.D and W.G.N; Writing – review and additional input, all; Visualisation, I.H., L.A.M.D, A.J.D., A.A., Z.B., S.O., K.T, W.W.Y., J.Z., R.W.T., I.B. and R.T.O.; Supervision, K.J.M, T.B.F, W.G.N. and R.T.O.

5.9. Conflict of Interest Statement

The authors declare no conflicts of interest.

5.10. References

Action on Hearing Loss. (2017). *Levels of hearing loss* [Online]. Action on hearing loss. Available: https://www.actiononhearingloss.org.uk/your-hearing/about-deafness-and-hearing-loss/glossary/levels-of-hearing-loss.aspx [Accessed 12/06 2017].

Adzhubei, I. A., Schmidt, S., Peshkin, L., Ramensky, V. E., Gerasimova, A., Bork, P., Kondrashov, A. S. & Sunyaev, S. R. (2010). A method and server for predicting damaging missense mutations. *Nat Methods,* 7(4)**,** 248-9.

Aiman, J. & Smentek, C. (1985). Premature ovarian failure. *Obstet Gynecol,* 66(1)**,** 9-14.

Banka, S., Blom, H. J., Walter, J., Aziz, M., Urquhart, J., Clouthier, C. M., Rice, G. I., de Brouwer, A. P., Hilton, E., Vassallo, G., Will, A., Smith, D. E., Smulders, Y. M., Wevers, R. A., Steinfeld, R., Heales, S., Crow, Y. J., Pelletier, J. N., Jones, S. & Newman, W. G. (2011). Identification and characterization of an inborn error of metabolism caused by dihydrofolate reductase deficiency. *Am J Hum Genet,* 88(2)**,** 216-25.

Blomen, V. A., Majek, P., Jae, L. T., Bigenzahn, J. W., Nieuwenhuis, J., Staring, J., Sacco, R., van Diemen, F. R., Olk, N., Stukalov, A., Marceau, C., Janssen, H., Carette, J. E., Bennett, K. L., Colinge, J., Superti-Furga, G. & Brummelkamp, T. R. (2015). Gene essentiality and synthetic lethality in haploid human cells. *Science,* 350(6264)**,** 1092-6.

Brzezniak, L. K., Bijata, M., Szczesny, R. J. & Stepien, P. P. (2011). Involvement of human ELAC2 gene product in 3' end processing of mitochondrial tRNAs. *RNA Biol,* 8(4)**,** 616-26.

Chatfield, K. C., Coughlin, C. R., Friederich, M. W., Gallagher, R. C., Hesselberth, J. R., Lovell, M. A., Ofman, R., Swanson, M. A., Thomas, J. A., Wanders, R. J. A., Wartchow, E. P. & Van Hove, J. L. K. (2015). Mitochondrial energy failure in HSD10 disease is due to defective mtDNA transcript processing. *Mitochondrion,* 21**,** 1-10.

Chatzispyrou, I. A., Alders, M., Guerrero-Castillo, S., Zapata Perez, R., Haagmans, M. A., Mouchiroud, L., Koster, J., Ofman, R., Baas, F., Waterham, H. R., Spelbrink, J. N., Auwerx, J., Mannens, M. M., Houtkooper, R. H. & Plomp, A. S. (2017). A homozygous missense mutation in ERAL1, encoding a mitochondrial rRNA chaperone, causes Perrault syndrome. Hum Mol Genet, 26(13), 2541-2550..

Demain, L. A., Urquhart, J. E., O'Sullivan, J., Williams, S. G., Bhaskar, S. S., Jenkinson, E. M., Lourenco, C. M., Heiberg, A., Pearce, S. H., Shalev, S. A., Yue, W. W., Mackinnon, S., Munro, K. J., Newbury-Ecob, R., Becker, K., Kim, M. J., RT, O. K. & Newman, W. G. (2017). Expanding the genotypic spectrum of Perrault syndrome. *Clin Genet,* 91(2)**,** 302-312.

Deutschmann, A. J., Amberger, A., Zavadil, C., Steinbeisser, H., Mayr, J. A., Feichtinger, R. G., Oerum, S., Yue, W. W. & Zschocke, J. (2014). Mutation or knock-down of 17beta-hydroxysteroid dehydrogenase type 10 cause loss of MRPP1 and impaired processing of mitochondrial heavy strand transcripts. *Hum Mol Genet,* 23(13)**,** 3618-28.

Ehret, G. (1976). Development of absolute auditory thresholds in the house mouse (Mus musculus). *J Am Audiol Soc,* 1(5)**,** 179-84.

Exome Aggregation Consortium (ExAC). *Exome Aggregation Consortium (ExAC)* [Online]. Cambridge, MA. Available: http://exac.broadinstitute.org [Accessed 08/07 2017].

Ferdinandusse, S., Denis, S., Mooyer, P. A., Dekker, C., Duran, M., Soorani-Lunsing, R. J., Boltshauser, E., Macaya, A., Gartner, J., Majoie, C. B., Barth, P. G., Wanders, R. J. & Poll-The, B. T. (2006). Clinical and biochemical spectrum of D-bifunctional protein deficiency. *Ann Neurol,* 59(1)**,** 92-104.

Gottschalk, M. E., Coker, S. B. & Fox, L. A. (1996). Neurologic anomalies of Perrault syndrome. *Am J Med Genet,* 65(4)**,** 274-6.

Holzmann, J., Frank, P., Loffler, E., Bennett, K. L., Gerner, C. & Rossmanith, W. (2008). RNase P without RNA: identification and functional reconstitution of the human mitochondrial tRNA processing enzyme. *Cell,* 135(3)**,** 462-74.

Howard, M. J., Lim, W. H., Fierke, C. A. & Koutmos, M. (2012). Mitochondrial ribonuclease P structure provides insight into the evolution of catalytic strategies for precursor-tRNA 5' processing. *Proc Natl Acad Sci U S A,* 109(40)**,** 16149-54.

Jenkinson, E. M., Clayton-Smith, J., Mehta, S., Bennett, C., Reardon, W., Green, A., Pearce, S. H. S., De Michele, G., Conway, G. S., Cilliers, D., Moreton, N., Davis, J. R. E., Trump, D. & Newman, W. G. (2012). Perrault syndrome: Further evidence for genetic heterogeneity. *J Neurol,* 259(5)**,** 974-976.

Jenkinson, E. M., Rehman, A. U., Walsh, T., Clayton-Smith, J., Lee, K., Morell, R. J., Drummond, M. C., Khan, S. N., Naeem, M. A., Rauf, B., Billington, N., Schultz, J. M., Urquhart, J. E., Lee, M. K., Berry, A., Hanley, N. A., Mehta, S., Cilliers, D., Clayton, P. E., Kingston, H., Smith, M. J., Warner, T. T., Black, G. C., Trump, D., Davis, J. R. E., Ahmad, W., Leal, S. M., Riazuddin, S., King, M. C., Friedman, T. B. & Newman, W. G. (2013). Perrault syndrome is caused by recessive mutations in CLPP, encoding a mitochondrial ATP-dependent chambered protease. *Am J Hum Genet,* 92(4)**,** 605-613.

Kumar, P., Henikoff, S. & Ng, P. C. (2009). Predicting the effects of coding non-synonymous variants on protein function using the SIFT algorithm. *Nat Protoc,* 4(7)**,** 1073-81.

Kunkel, T. A., Roberts, J. D. & Zakour, R. A. (1987). Rapid and efficient site-specific mutagenesis without phenotypic selection. *Methods Enzymol,* 154**,** 367-382.

Lerat, J., Jonard, L., Loundon, N., Christin-Maitre, S., Lacombe, D., Goizet, C., Rouzier, C., Van Maldergem, L., Gherbi, S., Garabedian, E. N., Bonnefont, J. P., Touraine, P., Mosnier, I., Munnich, A., Denoyelle, F. & Marlin, S. (2016). An Application of NGS for Molecular Investigations in Perrault Syndrome: Study of 14 Families and Review of the Literature. *Hum Mutat,* 37(12)**,** 1354-1362.

Lesus, J., Perkins, G. & Lysakowski, A. (2017). Structural Analysis of Inner Ear Hair Cell Mitochondria Near the Striated Organelle. *The FASEB Journal,* 31(1 Supplement)**,** 740.18-740.18.

Lysakowski, A. & Goldberg, J. M. (1997). A regional ultrastructural analysis of the cellular and synaptic architecture in the chinchilla cristae ampullares. *J Comp Neurol,* 389(3)**,** 419-43.

McMillan, H. J., Worthylake, T., Schwartzentruber, J., Gottlieb, C. C., Lawrence, S. E., Mackenzie, A., Beaulieu, C. L., Mooyer, P. A., Consortium, F. C., Wanders, R. J., Majewski, J., Bulman, D. E., Geraghty, M. T., Ferdinandusse, S. & Boycott, K. M. (2012). Specific combination of compound heterozygous mutations in 17beta-hydroxysteroid dehydrogenase type 4 (HSD17B4) defines a new subtype of D-bifunctional protein deficiency. *Orphanet J Rare Dis,* 7**,** 90.

Metodiev, M. D., Thompson, K., Alston, C. L., Morris, A. A., He, L., Assouline, Z., Rio, M., Bahi-Buisson, N., Pyle, A., Griffin, H., Siira, S., Filipovska, A., Munnich, A., Chinnery, P. F., McFarland, R., Rotig, A. & Taylor, R. W. (2016). Recessive Mutations in TRMT10C Cause Defects in Mitochondrial RNA Processing and Multiple Respiratory Chain Deficiencies. *Am J Hum Genet,* 98(5)**,** 993-1000.

Morino, H., Pierce, S. B., Matsuda, Y., Walsh, T., Ohsawa, R., Newby, M., Hiraki-Kamon, K., Kuramochi, M., Lee, M. K., Klevit, R. E., Martin, A., Maruyama, H., King, M. C. & Kawakami, H. (2014). Mutations in Twinkle primase-helicase cause Perrault syndrome with neurologic features. *Neurology,* 83(22)**,** 2054-61.

Narasimhan, V. M., Hunt, K. A., Mason, D., Baker, C. L., Karczewski, K. J., Barnes, M. R., Barnett, A. H., Bates, C., Bellary, S., Bockett, N. A., Giorda, K., Griffiths, C. J., Hemingway, H., Jia, Z., Kelly, M. A., Khawaja, H. A., Lek, M., McCarthy, S., McEachan, R., O'Donnell-Luria, A., Paigen, K., Parisinos, C. A., Sheridan, E., Southgate, L., Tee, L., Thomas, M., Xue, Y., Schnall-Levin, M., Petkov, P. M., Tyler-Smith, C., Maher, E. R., Trembath, R. C., MacArthur, D. G., Wright, J., Durbin, R. & van Heel, D. A. (2016). Health and population effects of rare gene knockouts in adult humans with related parents. *Science,* 352(6284)**,** 474-77.

Newman, W. G., Friedman, T. B. & Conway, G. S. (2014). Perrault Syndrome. *In:* Pagon RA, A. M., Ardinger HH, et al., editors (ed.) *GeneReviews® [Internet].* University of Washington, Seattle.

NHLBI GO Exome Sequencing Project (ESP). *Exome Variant Server* [Online]. Seattle, WA. Available: http://evs.gs.washington.edu/EVS/ [Accessed 09/07 2016].

Nishio, S. Y., Takumi, Y. & Usami, S. I. (2017). Laser-capture micro dissection combined with next-generation sequencing analysis of cell type-specific deafness gene expression in the mouse cochlea. *Hear Res,* 348**,** 87-97.

O'Keefe, R. T., Norman, C. & Newman, A. J. (1996). The Invariant U5 snRNA Loop 1 Sequence Is Dispensable for the First Catalytic Step of pre-mRNA Splicing in Yeast. *Cell,* 86(4)**,** 679-689.

Ojala, D., Montoya, J. & Attardi, G. (1981). tRNA punctuation model of RNA processing in human mitochondria. *Nature,* 290(5806)**,** 470-4.

Pallister, P. D. & Opitz, J. M. (1979). The Perrault syndrome: autosomal recessive ovarian dysgenesis with facultative, non-sex-limited sensorineural deafness. *Am J Med Genet,* 4(3)**,** 239-46.

Pierce, S. B., Chisholm, K. M., Lynch, E. D., Lee, M. K., Walsh, T., Opitz, J. M., Li, W., Klevit, R. E. & King, M. C. (2011). Mutations in mitochondrial histidyl tRNA synthetase HARS2 cause ovarian dysgenesis and sensorineural hearing loss of Perrault syndrome. *Proc Natl Acad Sci U S A,* 108(16)**,** 6543-8.

Pierce, S. B., Gersak, K., Michaelson-Cohen, R., Walsh, T., Lee, M. K., Malach, D., Klevit, R. E., King, M. C. & Levy-Lahad, E. (2013). Mutations in LARS2, encoding mitochondrial leucyl-tRNA synthetase, lead to premature ovarian failure and hearing loss in Perrault syndrome. *Am J Hum Genet,* 92(4)**,** 614-620.

Pierce, S. B., Walsh, T., Chisholm, K. M., Lee, M. K., Thornton, A. M., Fiumara, A., Opitz, J. M., Levy-Lahad, E., Klevit, R. E. & King, M. C. (2010). Mutations in the DBP-Deficiency Protein HSD17B4 Cause Ovarian Dysgenesis, Hearing Loss, and Ataxia of Perrault Syndrome. *Am J Hum Genet,* 87(2)**,** 282-8.

Rackham, O., Busch, J. D., Matic, S., Siira, S. J., Kuznetsova, I., Atanassov, I., Ermer, J. A., Shearwood, A. M., Richman, T. R., Stewart, J. B., Mourier, A., Milenkovic, D., Larsson, N. G. & Filipovska, A. (2016). Hierarchical RNA Processing Is Required for Mitochondrial Ribosome Assembly. *Cell Rep,* 16(7)**,** 1874-90.

Rauschenberger, K., Schöler, K., Sass, J. O., Sauer, S., Djuric, Z., Rumig, C., Wolf, N. I., Okun, J. G., Kölker, S., Schwarz, H., Fischer, C., Grziwa, B., Runz, H., Nümann, A., Shafqat, N., Kavanagh, K. L., Hämmerling, G., Wanders, R. J. A., Shield, J. P. H., Wendel, U., Stern, D., Nawroth, P., Hoffmann, G. F., Bartram, C. R., Arnold, B., Bierhaus, A., Oppermann, U., Steinbeisser, H. & Zschocke, J. (2010). A non-enzymatic function of 17β-hydroxysteroid dehydrogenase type 10 is required for mitochondrial integrity and cell survival. *EMBO Mol Med,* 2(2)**,** 51-62.

Reinhard, L., Sridhara, S. & Hallberg, B. M. (2015). Structure of the nuclease subunit of human mitochondrial RNase P. *Nucleic Acids Res,* 43(11)**,** 5664-72.

Riley, L. G., Rudinger-Thirion, J., Schmitz-Abe, K., Thorburn, D. R., Davis, R. L., Teo, J., Arbuckle, S., Cooper, S. T., Campagna, D. R., Frugier, M., Markianos, K., Sue, C. M., Fleming, M. D. & Christodoulou, J. (2015). LARS2 Variants Associated with Hydrops, Lactic Acidosis, Sideroblastic Anemia, and Multisystem Failure. *JIMD Reports,* 24**,** 1-9.

Rossmanith, W. (1997). Processing of human mitochondrial tRNA(Ser(AGY))(GCU): A novel pathway in tRNA biosynthesis. *J Mol Biol,* 265(4)**,** 365-371.

Rossmanith, W. (2011). Localization of human RNase Z isoforms: dual nuclear/mitochondrial targeting of the ELAC2 gene product by alternative translation initiation. *PLoS One,* 6(4)**,** e19152.

Rossmanith, W. (2012). Of P and Z: mitochondrial tRNA processing enzymes. *Biochim Biophys Acta,* 1819(9-10)**,** 1017-26.

Rossmanith, W., Tullo, A., Potuschak, T., Karwan, R. & Sbisa, E. (1995). Human mitochondrial tRNA processing. *J Biol Chem,* 270(21)**,** 12885-12891.

Schwarz, J. M., Cooper, D. N., Schuelke, M. & Seelow, D. (2014). MutationTaster2: mutation prediction for the deep-sequencing age. *Nat Methods,* 11(4)**,** 361-2.

Sendin, G., Bulankina, A. V., Riedel, D. & Moser, T. (2007). Maturation of ribbon synapses in hair cells is driven by thyroid hormone. *J Neurosci,* 27(12)**,** 3163-73.

Sherry, S. T., Ward, M. H., Kholodov, M., Baker, J., Phan, L., Smigielski, E. M. & Sirotkin, K. (2001). dbSNP: the NCBI database of genetic variation. *Nucleic Acids Res,* 29(1)**,** 308-311.

Smith, M. J., Beetz, C., Williams, S. G., Bhaskar, S. S., O'Sullivan, J., Anderson, B., Daly, S. B., Urquhart, J. E., Bholah, Z., Oudit, D., Cheesman, E., Kelsey, A., McCabe, M. G., Newman, W. G. & Evans, D. G. (2014). Germline mutations in SUFU cause Gorlin syndrome-associated childhood medulloblastoma and redefine the risk associated with PTCH1 mutations. *J Clin Oncol,* 32(36)**,** 4155-61.

Vilardo, E., Nachbagauer, C., Buzet, A., Taschner, A., Holzmann, J. & Rossmanith, W. (2012). A subcomplex of human mitochondrial RNase P is a bifunctional methyltransferase-extensive moonlighting in mitochondrial tRNA biogenesis. *Nucleic Acids Res,* 40(22)**,** 11583-11593.

Vilardo, E. & Rossmanith, W. (2015). Molecular insights into HSD10 disease: impact of SDR5C1 mutations on the human mitochondrial RNase P complex. *Nucleic Acids Res,* 43(10)**,** 5112-9.

Wang, T., Birsoy, K., Hughes, N. W., Krupczak, K. M., Post, Y., Wei, J. J., Lander, E. S. & Sabatini, D. M. (2015). Identification and characterization of essential genes in the human genome. *Science,* 350(6264)**,** 1096-101.

Zschocke, J. (2012). HSD10 disease: clinical consequences of mutations in the HSD17B10 gene. *JIMD,* 35(1)**,** 81-9.

Chapter 6: Biallelic Variants in Nucleolar protein NOP14 are associated with Perrault syndrome and highlight that NOP14 is important for mitochondrial homeostasis

Biallelic Variants in Nucleolar protein NOP14 are associated with Perrault syndrome and highlight that NOP14 is important for mitochondrial homeostasis

Leigh A. M. Demain,[1,2] Jill E. Urquhart, [1,2] James O'Sullivan, [1,2] Liam M. Jones,[3] Inna A. Belyantseva,[4] Melanie Barzik, [5] Simon G. Williams,[1,2] Sanjeev S. Bhaskar,[1,2] Emma M. Jenkinson,[1] Thomas B. Friedman,[4] Kevin J. Munro,[5,6] Raymond T. O'Keefe,[3,] William G. Newman[1,1,]

[1] Division of Evolution and Genomic Sciences, Faculty of Biology, Medicine and Health, School of Biological Sciences, University of Manchester, Manchester, UK

[2] Manchester Centre for Genomic Medicine, Central Manchester University Hospitals NHS Foundation Trust, Manchester, UK

[3] Division of Cellular & Molecular Function, Faculty of Biology, Medicine and Health, University of Manchester, Manchester, UK

[4] Laboratory of Molecular Genetics, National Institute on Deafness and Other Communication Disorders, National Institutes of Health, Bethesda, MD, USA

[5] School of Health Sciences, University of Manchester, Manchester, UK

[6] Central Manchester University Hospitals NHS Foundation Trust, Manchester Academic Health Science Centre, Manchester, UK

6.1. Abstract

Perrault syndrome is a rare autosomal recessive condition characterised by sensorineural hearing loss in both sexes and primary ovarian insufficiency in females with a normal karyotype. Six genes have been found to cause Perrault syndrome to date: *HSD17B4*, *HARS2*, *LARS2*, *CLPP*, *C10orf2* and *ERAL1*. Five of the genes which cause Perrault syndrome function in mitochondrial translation and in some cases of Perrault syndrome the underlying pathology has been shown to be a defect of mitochondrial translation. Using a combination of whole exome sequencing and autozygosity mapping in a large consanguineous family we identified a homozygous putative pathogenic variant in a novel Perrault syndrome gene, *NOP14*. Nucleolar protein 14 (NOP14) is part of a sub-complex responsible for the processing of 18S rRNA and the formation of the nuclear ribosomal 40S subunit. Both haploinsufficiency and overexpression of NOP14 was found to be detrimental to cells suggesting that expression of NOP14 is tightly controlled. We found that knockout of one copy of NOP14 orthologue, NOP14p, in diploid yeast causes the cells to slowly lose their mitochondria. In the mouse organ of Corti Nop14 showed a very specific, non-nucleolar expression pattern exclusive to sensory hair cells, which becomes apparent after the onset of hearing. Here we present the data that biallelic variants in *NOP14* are likely associated with Perrault syndrome and that NOP14 is not exclusively localised to the nucleolus and may have a role in mitochondrial function either directly or through nuclear-mitochondrial communication.

6.2. Introduction

Perrault syndrome, characterised by sensorineural hearing loss (SNHL) in both sexes and primary ovarian insufficiency (POI) in females with a normal karyotype, is a rare autosomal recessive condition (MIM 233400) (Pallister and Opitz 1979). In some families with Perrault syndrome neurological phenotypes are present including intellectual disability, ataxia and motor sensory neuropathy (Fiumara et al. 2004;Gottschalk et al. 1996). Six genes are associated with Perrault syndrome to date: *HSD17B4* (MIM 233400) (Pierce et al. 2010), *HARS2* (MIM 614926) (Pierce et al. 2011), *LARS2* (MIM 615300) (Pierce et al. 2013), *CLPP* (MIM 614129) (Jenkinson et al. 2013), *C10orf2* (MIM 616138) (Morino et al. 2014) and *ERAL1* (MIM 607435) (Chatzispyrou et al. 2017). Of these genes, the latter five function in the mitochondrial translation pathway and recently it has

become apparent that at least some cases of Perrault syndrome are due to defects of mitochondrial translation (Chapter 5) (Chatzispyrou et al. 2017).

Here we present a single consanguineous family comprising three sisters with Perrault syndrome due to variants in a novel Perrault syndrome gene *NOP14*. Whole exome sequencing used in conjunction with autozygosity mapping revealed four rare homozygous variants in the affected siblings of which *NOP14* c.1160A>G p.(Glu387Gly) was the most promising candidate for the Perrault syndrome phenotype.

NOP14 is part of a sub-complex involved in the processing of nuclear 18S rRNA and the biogenesis of the 40s small ribosomal subunit (Liu and Thiele 2001;Warda et al. 2016). NOP14 was shown to be essential for the biogenesis of the 40s ribosomal subunit with knockdown of NOP14 in cells resulting in the accumulation of pre-18S rRNA and the depletion of mature 18s rRNA and the 40S ribosomal subunit (Warda et al. 2016).

Our data revealed that NOP14 may have functions in addition to its role in nuclear ribosome biogenesis. In diploid yeast the knockout of one copy of the NOP14 gene resulted in the slow loss of mitochondria from these cells. In HeLa cells overexpression of NOP14 appeared detrimental to the cells. Localisation of Nop14 in the mouse organ of Corti revealed a unique localisation pattern in the sensory hair cells outside the nucleus which appeared after the onset of hearing. Here we have identified *NOP14* as a putative novel Perrault syndrome gene and provide the initial evidence for a role for NOP14 in mitochondrial homeostasis.

6.3. Materials and methods

6.3.1. Ethical approval

All patients provided written informed consent in accordance with local regulations. Ethical approval for this study was granted by the National Health Service Ethics Committee (16/WA/0017) and University of Manchester. The NIH Animal Use Committee approved protocol 1263-15 to T.B.F. for mice.

6.3.2. Autozygosity mapping and whole exome sequencing

Autozygosity mapping was performed on five individuals from the family (III-1, III-2, III-3, III-4 and III-5) using the Affymetrix Genome-wide SNP6.0 arrays and analysed in AutoSNPa

(http://dna.leeds.ac.uk/autosnpa/) (Carr et al. 2006). Whole exome sequencing was performed on DNA extracted from lymphocytes from individual III-4. The Agilent Technologies, Santa Clara, CA, USA SureSelect Human All Exon V5 Panel was used for library preparation and sequencing was performed on the SOLiD 4 sequencer previously detailed (Mitchell et al. 2012).

6.3.4. Confirmation of variants

Variants were confirmed in the family via Sanger sequencing using the ABI big Dye v3.1 (Thermo Fisher Scientific Inc, Waltham, MA, USA) sequencing technology. Primer sequences are available in Appendix I.

6.3.5. Prediction of variant pathogenicity

The following resources were used in the prediction of variant pathogenicity;

Exome Variant Server (EVS) (NHLBI GO Exome Sequencing Project (ESP)), http://evs.gs.washington.edu/EVS/
ExAC (Exome Aggregation Consortium (ExAC)), http://exac.broadinstitute.org/
Polyphen2 (Adzhubei et al. 2010), http://genetics.bwh.harvard.edu/pph2/
SIFT (Kumar et al. 2009), http://sift.jcvi.org/
Mutation Taster (Schwarz et al. 2014), http://www.mutationtaster.org/

6.3.6. Conservation mapping

Sequences were mapped using Clustal Omega (http://www.ebi.ac.uk/Tools/msa/clustalo/) (Sievers et al. 2011). The reference sequences are as follows; Human, NP_001278907. Chimpanzee, ENSPTRT00000029596.5. Rat, ENSRNOT00000082612.1. Mouse, NP_083554. Platypus, ENSOANT00000029290.2. Chicken, ENSGALT00000025234.6. Xenopus, ENSXETT00000032248.3. Tetradon, ENSTNIT00000022183.1. Zebrafish, ENSDART00000165357.1. Fruitfly, NP_652040.2. C. Elegans, NP_740774. S. Cerevisiae NP_010133.

6.3.7. Mitochondrial targeting sequence prediction

Mitofates (http://mitf.cbrc.jp/MitoFates/cgi-bin/top.cgi) (Fukasawa et al. 2015) was used to predict if proteins contained a mitochondrial targeting sequence.

6.3.8. Prediction of functional domains

The following online software was used to predict the functional domains of proteins using the protein reference sequence NP_001278907.

SMART (http://smart.embl-heidelberg.de/) (Letunic et al. 2015)

NCBI conserved domains (https://www.ncbi.nlm.nih.gov/Structure/cdd/wrpsb.cgi) (Marchler-Bauer et al. 2015)

Interpro (https://www.ebi.ac.uk/interpro) (Jones et al. 2014)

6.3.9. Yeast Strains

The *Saccharomyces cerevisiae* strains used in this report are shown in Table 6.1. All knockout strains are diploid with one copy of NOP14 ablated. Yeast cells were grown in standard YPD media or on standard YPD agar plates unless otherwise indicated. The strain containing the plasmid was grown on Synthetic defined (SD)-URA plates. YP-Ethanol, YP-Acetate and YP-Glycerol plates were used as a non-fermentable carbon source. Yeast were always grown at 30°C. Plasmids were transformed into yeast using the one-step transformation method (Chen et al. 1992).

Strain	**Genotype**
BY4743_NOP14Δ	BY4743; *MATa/MATα; ura3Δ0/ura3Δ0; leu2Δ0/leu2Δ0; his3Δ1/his3Δ1; met15Δ0/MET15; LYS2/lys2Δ0; YDL148c/YDL148c::kanMX4*
YPH501	*MAT*a/*MAT*α *ura3-52/ura3-52 lys2-801_amber/lys2-801_amber ade2-101_ochre/ade2-101_ochre trp1-Δ63/trp1-Δ63 his3-Δ200/his3-Δ200 leu2-Δ1/leu2-Δ1*
YPH501_NOP14Δ	YPH501 YDL148C::KanMX4/YDL148C
YPH501_NOP14Δ Mouse Nop14	YPH501_NOP14Δ pSF-STE5-MouseNop14

Table 6.1. *Saccharomyces cerevisiae* NOP14 yeast strains

6.3.10. Cell culture

HeLa cells were cultured in Dulbecco Modified Eagle Medium (DMEM) media with 10% (v/v) foetal bovine serum (FBS) and 2mM Glutamax at 37C in 10% CO^2.

6.3.11. Cell transfection and staining

HeLa cells were transfected with the plasmids Nop14-EGFP and Nop14-TurboGFP using Lipofectamine 3000 (Thermo Fisher Scientific Inc, Waltham, MA, USA) Briefly $10x4^5$ cells were seeded into each well of a six well plate in the morning for a transfection in the afternoon. When attached, the cells were transfected according to the manufacturer protocol using 1.6-1.75 ug of plasmid DNA per 2.5ul of lipofetamine 3000 reagent. The transfected cells were incubated overnight at 37°C with 10% CO^2. For the imaging of cells using the confocal microscope HeLa cells were seeded onto glass bottom plates prepared with fibronectin. The cells were incubated for approximately 4 hours (3-5) until optimum cell density and attachment was achieved then fixed in the following solution for 15 minutes at room temperature, 4% paraformaldehyde, 2% sucrose in PBS. After fixation the cells were washed 3 times in PBS and stored at 4°C until staining.

Cells were permeabilised and blocked in the 0.2% Triton X and 10% normal goat serum in PBS solution at room temperature. After permeabilisation/blocking the samples were washed 3 times in PBS. Cells were incubated with the primary antibodies (Table 6.2) in blocking solution (blocking solution - 2% normal goat serum in PBS) for 1-2 hours at room temperature. Samples were washed 3 times in PBS. The samples were incubated in Secondary antibody solution (Phalloidin Alexa 647, Hoechst (2.5µg/ml) and secondary antibody in blocking solution (Table 6.2) for 2 hours at room temperature with gentle agitation. After incubation with the secondary antibody solution the cell were washed 3 times in PBS and stored at 4°C in PBS to be imaged within 24 hours. Cells were imaged using a LSM780 confocal microscope (Zeiss Inc, Oberkochen, Germany Inc) equipped with 63X, 1.4 N.A. objective.

Antibody Name	Supplier and details	Concentration/dilution used
NOP14-Sigma	NOP14 rabbit polyclonal antibody- Sigma-Aldrich, St. Louis, MO, USA - Cat no. HPA039596	HeLa Cells -0.2µg/ml, organ of Corti - 5µg/ml
NOP14-SantaCruz	NOP14 mouse monoclonal antibody- Santa Cruz Biotechnology, Dallas, TX, USA - Cat no. sc-398724	HeLa Cells - 0.4µg/ml
NIFK	NIFK mouse monoclonal antibody - Abcam, Cambridge, UK- Cat no. ab211871	HeLa Cells - 2µg/ml
SNAP25	SNAP 25mouse monoclonal antibody - Santa Cruz Biotechnology, Dallas, TX, USA - Cat no. sc-136267	organ of Corti - 1µg/ml
Cytoskeletal staining	Alexa fluor 647 phalloidin or rhodamine phalloidin, Thermo Fisher Scientific Inc, Waltham, MA, USA	HeLa Cells - 1:50, organ of Corti- 1:100
Mouse secondary antibody	Goat anti-mouse - Alexa fluor 568, Thermo Fisher Scientific Inc, Waltham, MA, USA	HeLa Cells - 1:250, organ of Corti 1:400
Rabbit secondary antibody	Goat anti-rabbit - Alexa fluor 488, goat anti-rabbit Alexa fluor 568, Thermo Fisher Scientific Inc, Waltham, MA, USA	HeLa Cells - 1:250, organ of Corti 1:400

Table 6.2. Antibody details and concentrations.

Details and concentrations for the antibodies and staining reagents used in this report. Two different NOP14 antibodies were used to localise NOP14 in HeLa cells. The antibody used will be specified in the appropriate figure legend.

6.3.12. Plasmids

The plasmid Nop14-TurboGFP (Origene, Rockville, MD, USA, cat no. MG210980, Accession NM_029278) was used as provided by the manufacturer. The plasmid Nop14-EGFP was created by cloning the mouse ORF cDNA (BC043043) Nop14 into a C-terminal pEGFP-N1 vector (Clontech, Mountain View, CA, USA-discontinued). Briefly the Mouse ORF cDNA minus the stop codon was amplified using the primers below from the plasmid 5701430 (Dharmacon, Lafayette, CO, USA -MMM1013-202858876).

Nop14_infusion_1: TACCGGACTCAGATCTATGGGGAAAGCCAAG

Nop14_infusion_2: CGCGGTACCGTCGACTGCAGTTTTTTGAACTTTTTCCTCT

The pEGFP-N1 vector was digested with BglII and PstI. The ORF was inserted into the digested vector using the In-Fusion HD Plus EcoDry Cloning System (Clontech, Mountain View, CA, USA) according to manufacturer instructions.

The plasmid pRS-STE5-Nop14 was created by cloning the mouse ORF cDNA (BC043043) Nop14 into a pSF-STE5-URA3 yeast expression vector (Oxford Genetics, Oxford, UK-OG535). Briefly the Mouse ORF cDNA was amplified using the primers below from the plasmid 5701430 (Dharmacon, Lafayette, CO, USA -MMM1013-202858876).

MoNOP14-F(NcoI) – GCGCGCCCATGGGGAAAGCCAAGCGGAC

MoNOP14-B(XbaI) – GGGGGTCTAGATTATTTTTTGAACTTTTTCCTC

Both the cloned ORF and the vector were digested with NcoI and XbaI and ligated using T4 ligase. All inserts were confirmed via Sanger sequencing using the ABI big Dye v3.1 (Thermo Fisher Scientific Inc, Waltham, MA, USA) sequencing technology before use. Plasmid maps and sequencing primers are available in Appendix I.

6.3.13. Localisation of PRORP in the mouse organ of Corti

The NIH Animal Use Committee approved protocol 1263-15 to T.B.F. for mice. C57/BJ6 mice at ages Postnatal day 3 (P3), P10, P14, P18 and P30 were euthanised, the cochlear capsule was removed and fixed with 4% paraformaldehyde in PBS for 2 hours. The samples were microdissected and the organ of Corti was permeabilised with 1% Triton X-100 in PBS for 30 min followed by three 10 min washes with 1X PBS. Nonspecific binding sites were blocked with 5% normal goat serum and 2% BSA in PBS for 1 h at room temperature. Samples were incubated for 2 h with primary antibodies (Table 6.2) in blocking solution, followed by several rinses with PBS. Samples were incubated with secondary antibodies (Table 6.2) for 30 min. Samples were washed several times with PBS and were mounted with ProLongGold Antifade staining reagent with DAPI (Molecular Probes, Invitrogen, Carlsbad, CA, USA) and examined using LSM780 confocal microscope (Zeiss Inc, Oberkochen, Germany Inc) equipped with 63X, 1.4 N.A. objective.

6.3.14. Gene Gun transfection of organ of Corti

Inner-ear sensory epithelium cultures were prepared from organ of Corti of P1 C57Bl/6 mice and transfected with plasmid DNA using the gene gun method as described in Belyantseva (2016). Briefly the organ of corti spiral was dissected in Leibowitz cell culture

medium (Invitrogen, Carlsbad, CA, USA) and was attached to a glass-bottom Petri dish (MatTek, Ashland, MA, USA) coated with Rat tail collagen and maintained at 37°C and 5% CO2 in DMEM supplemented with 7% FBS for 1–3 days. Cultures were then transfected by using a Helios gene gun (Bio-Rad, Hercules, CA, USA). Gold particles of 1.0-µm diameter (Bio-Rad, Hercules, CA, USA) were coated with Nop14-TurboGFP plasmid DNA at a ratio of 2 µg of plasmid DNA to 1 mg of gold particles and precipitated onto the inner wall of Tefzel tubing, which was cut into individual cartridges containing approximately 1µg of plasmid DNA. Samples were bombarded with the gold particles from one cartridge per culture by using 110 psi of helium. After an additional 8 h to 4 days in culture, samples were fixed in 4% paraformaldehyde and stained using the same method as the tissue samples above.

6.4. Results

6.4.1. Clinical Report

Detailed phenotypes for the three affected siblings in this family have been reported previously (Mehdipour et al. 1999). Briefly, the family is consanguineous and of Iranian descent. There are three affected sisters, two unaffected male siblings and their unaffected parents (Fig 6.1). Progressive bilateral SNHL was present in all three siblings with onset at two years of age in the eldest affected sibling. At the latest assessment the hearing loss was severe to profound in the two elder affected siblings and moderate to profound at higher frequencies in the youngest affected sibling. All three affected sisters achieved a normal height and tests indicated thyroid function was normal. The three sisters also presented with primary amenorrhea and lacked secondary sexual characteristics. Ultrasound showed hypoplasic uterus and small or streak ovaries for all affected siblings. Cytogenetic testing confirmed a 46, XX karyotype in all affected patients. Follicle stimulating hormones and luteinising hormones were in the postmenopausal range for all sisters and all had no response to the progesterone challenge (indicating low levels of estradiol) confirming a diagnosis of hypergonadotropic hypogonadism. The proband had a mild intellectual disability with the second sister having a normal IQ and the youngest affected sibling having a borderline intellectual disability. No other

neurological phenotypes were reported in this family and the CT scans for the three affected sisters were normal (Mehdipour et al. 1999).

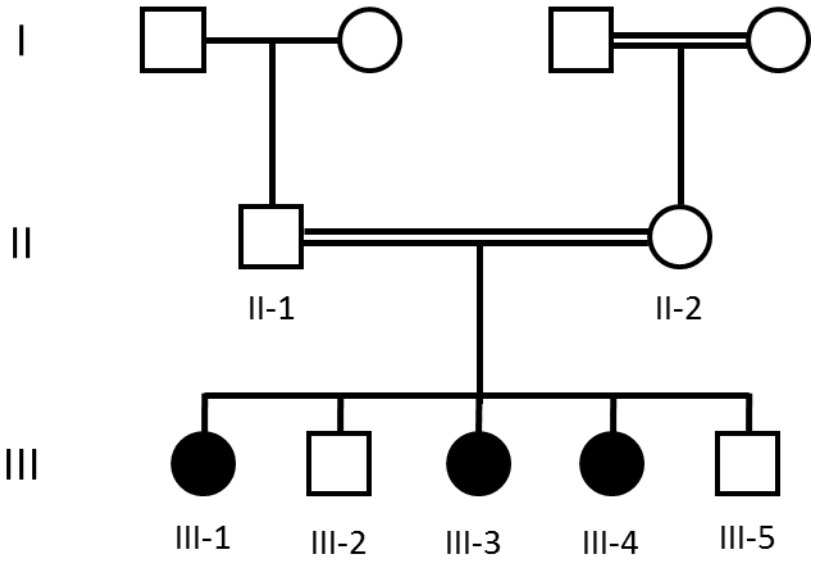

Figure 6.1. Pedigree of a consanguineous Iranian family with Perrault syndrome. Filled icons indicate affected individuals. Adapted from (Mehdipour et al. 1999).

6.4.2. Exome sequencing, Filtering and Variant confirmation

Whole exome sequencing was performed on affected individual III-4 as previously detailed (Mitchell et al. 2012). Autozygosity mapping was performed on five individuals from the family (III-1, III-2, III-3, III-4 and III-5) as previously described (Banka et al. 2011). Four regions of homozygosity above 2mb were identified which were shared by affected individuals but not unaffected individuals (Table 6.3).

Chromosome	Position	Size
4	0-7,192,960	7.2Mb
8	100,801,200-103,148,200	2.3Mb
11	116,148,900-121,051,700	4.9Mb
14	101,774,000-108,671,300	6.9Mb

Table 6.3. Regions of homozygosity shared in affected individuals.

Regions of homozygosity above 2Mb shared between affected individuals (III-1, III-2, and III-4) but not unaffected individuals (III-3, III-5).

Four homozygous variants were detected in the regions of homozygosity with a frequency less than 1% in the Exome variant server (EVS) (NHLBI GO Exome Sequencing Project (ESP)).

Gene	UVSSA	NOP14	HMBS	ZNF839
Variant	c.17C>T p.(Ser6Leu)	c.1160A>G p.(Glu387Gly)	c.664G>A p.(Val222Met)	c.2027C>T p.(Pro676Leu)
Transcript	NM_020894	NM_001291978	NM_000190	NM_018335
Variant annotation	rs138607842	N	CM980985	rs544983444
EVS MAF	0.0769	N	N	N
ExAC MAF	0.0009243	N	N	0.03
Polyphen	Possibly damaging (0.92)	Benign (0.026)	Probably damaging (0.98)	Benign (0.307)
SIFT	Deleterious (0.02)	Tolerated (0.33)	Deleterious (0.01)	Tolerated (0.28)
Mutation Taster	Polymorphism (1)	Disease causing (1)	Disease causing (1)	Polymorphism (1)

Table 6.4. Rare homozygous variants identified in regions of homozygosity in individual III-4.

Variants with a minor allele frequency (MAF) less than 1% in EVS seen in the exome data from individual III-4, filtered to only include the regions of homozygosity (Table 6.3). N, not present.

UVSSA encodes UV-stimulated scaffold protein A which functions in the nucleotide excision repair pathway (Nakazawa et al. 2012). Biallelic variants in *UVSSA* are associated with UV-sensitive syndrome characterised by cutaneous photosensitivity and cutaneous

pigmentation. The cells of affected individuals show depressed recovery of transcription after UV irradiation (Itoh et al. 1994;Nakazawa et al. 2012). As the patients in this family showed no sign of photosensitivity the variant in *UVSSA* was excluded as the cause of Perrault syndrome.

HMBS encodes porphobilinogen deaminase an enzyme in the heme synthesis pathway. Heterozygous variants in *HMBS* are associated with autosomal dominant acute intermittent porphyria characterised by recurrent attacks of neurological dysfunction which may include gastrointestinal disturbances and nervous system dysfunction (Grandchamp et al. 1989;Chen et al. 1994). Biallelic variants in *HMBS* have been associated with a more severe phenotype with one child displaying porencephaly and severe developmental retardation. In this case both parents had shown an acute intermittent porphyria phenotype either clinically or biochemically (Beukeveld et al. 1990). In another unrelated child a homozygous change in *HMBS* as shown to cause with hepatosplenomegaly, mild intellectual disability, yellow-brown teeth, and dark red urine. The parents in this case were both heterozygous for the variant and asymptomatic making this a true case of a recessive phenotype due to variants in *HMBS* (Hessels et al. 2004). Although the software has predicted the variant to be pathogenic the phenotype associated with this gene does not match the Perrault syndrome phenotype especially in light of the more severe presentation associated with biallelic variants in *HMBS*.

The function of *ZNF839* is not well characterised. A single nucleotide polymorphism in *ZNF839* has been shown to be associated with survival rates in colorectal cancer through microRNA binding (Yang et al. 2017). Although rare this variant has been seen as a homozygous change in one individual in ExAC (Exome Aggregation Consortium (ExAC)). As the ExAC population is in theory unaffected by genetic syndromes it is unlikely that this variant is responsible for the Perrault syndrome phenotype in the affected family.

NOP14 encodes NOP14 a nucleolar protein involved in the biogenesis of the 40s ribosomal subunit (Liu and Thiele 2001). There have been no genetic disorders reported to be associated with variants in *NOP14*. There are no reported homozygous loss of function variants in this gene, including in a large consanguineous population comprising over 3200 healthy individuals (Narasimhan et al. 2016), suggesting it may be essential for life. The variant *NOP14* c.1160A>G p.(Glu387Gly) is also absent from Gnomad (Lek et al. 2016). With the exclusion of the other candidate variants the variant *NOP14* c.1160A>G

p.(Glu387Gly) appeared a promising candidate for the cause of Perrault syndrome in this family.

The variant *NOP14* c.1160A>G p.(Glu387Gly) was confirmed via Sanger sequencing. All three affected siblings were homozygous for the variant while the two unaffected siblings and the unaffected parents were heterozygous for the variant (Fig. 6.2a). Six families with genetically unresolved Perrault syndrome without a known genetic cause were screened for *NOP14* but no putative pathogenic variants were identified.

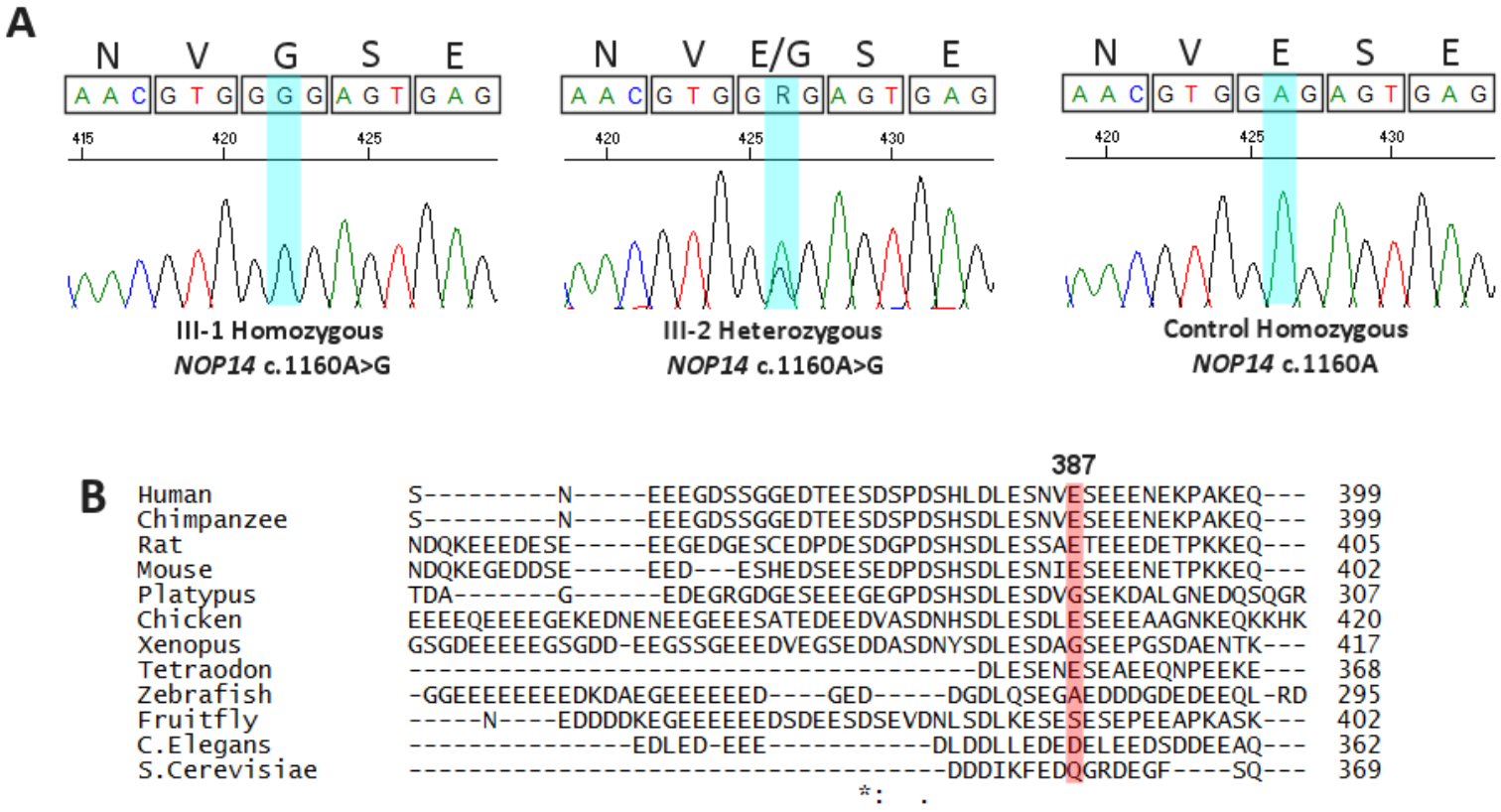

Figure 6.2. Affected individuals are homozygous for the variant *NOP14* c.1160A>G and the residue NOP14 p.387 is moderately conserved.

A) Sanger sequencing traces from affected individual III-1, her unaffected sibling (III-2) and a control sample. The affected residue is highlighted in blue. The affected individual is homozygous for the variant c.1160A>G, the unaffected sibling is heterozygous c.1160A>G and the control sample is wild type at this position. B) Conservation of NOP14 p.387 across multiple species. The variant residue in this family, NOP14 p.387, is highlighted in red.

The residue NOP14 p.E387 is moderately conserved but is a glycine in both platypus and in xenopus (Fig 6.2b). There are no known functional domains in Yeast Nop14p (Liu and Thiele 2001). We performed an analysis of the human protein (NP_001278907) using SMART (http://smart.embl-heidelberg.de/) (Letunic et al. 2015), NCBI conserved domains (https://www.ncbi.nlm.nih.gov/Structure/cdd/wrpsb.cgi) (Marchler-Bauer et al. 2015) and Interpro (https://www.ebi.ac.uk/interpro) (Jones et al. 2014) but no functional domains or known motifs were identified. It has been reported that Nop14p was detected on a western using an antibody for Noc2p. The authors suggested this was due to tertiary structure similarities rather than sequence homology (Milkereit et al. 2003). This could mean that any functional domains in NOP14 may share structural but not sequence homology to known domains making them difficult to identify using traditional prediction tools. With no identifiable domains and no 3D structure available it is difficult to predict the likely effect of the variant *NOP14* c.1160A>G p.(Glu387Gly).

6.4.3. The loss of one copy of Nop14p in diploid yeast causes the slow loss of mitochondria

The genetic data suggested *NOP14* was the most likely causative gene for Perrault syndrome in this family but NOP14 has no known function in mitochondria. As such *NOP14* does not associate with the other Perrault syndrome genes and there may be a different pathogenic mechanism for the SNHL and POI in this family. We undertook investigations in the yeast *Saccharomyces cerevisiae* to examine the pathology of Perrault syndrome due to variants in *NOP14*.

The orthologue of human NOP14 in Saccharomyces cerevisiae is NOP14p, it shares ~25% sequence homology with the human protein and the function in ribosomal biogenesis has been shown to be conserved (Liu and Thiele 2001). Analysis of the Yeast orthologue NOP14p with Mitofates (http://mitf.cbrc.jp/MitoFates/cgi-bin/top.cgi) (Fukasawa et al. 2015) revealed a degenerate mitochondrial targeting sequence. Both the yeast and mouse orthologues of NOP14 have shown to be localised to the mitochondria using mass spectrometry (Sickmann et al. 2003;Calvo et al. 2016) Analysis of human NOP14 (NP_001278907) with Mitofates predicted the protein does not have a mitochondrial

targeting sequence and human NOP14 has not been found to be part of the human mitochondrial proteome (Fukasawa et al. 2015;Calvo et al. 2016).

NOP14 is an essential gene in yeast and complete knockout is lethal. We obtained a diploid strain with one copy of NOP14 removed. This was confirmed by PCR. Given the predicted mitochondrial targeting sequence we wanted to test the mitochondrial function in this strain. When the NOP14 knockout strain was grown on a non-fermentable carbon source, which forces yeast to use their mitochondria for respiration, the strain was not viable indicating non-functional mitochondria. This suggested the loss of even one copy of NOP14 was detrimental to mitochondrial function so we produced a NOP14 knockout in the diploid YPH501 strain. The YPH501 strain contains a variant in ADE2 which causes cells with functioning mitochondria to produce a red pigment allowing mitochondrial function to be monitored (Dorfman 1969). It was noted that over time colonies of the diploid knockout for Nop14 would lose their red colour and thus their mitochondrial function. This was apparent on standard YPD plates. There was no initial growth defect on a non-fermentable carbon source. This indicates that loss of even one copy of NOP14 causes the loss of functional mitochondria but this process is not immediate and may take a number of generations to become apparent.

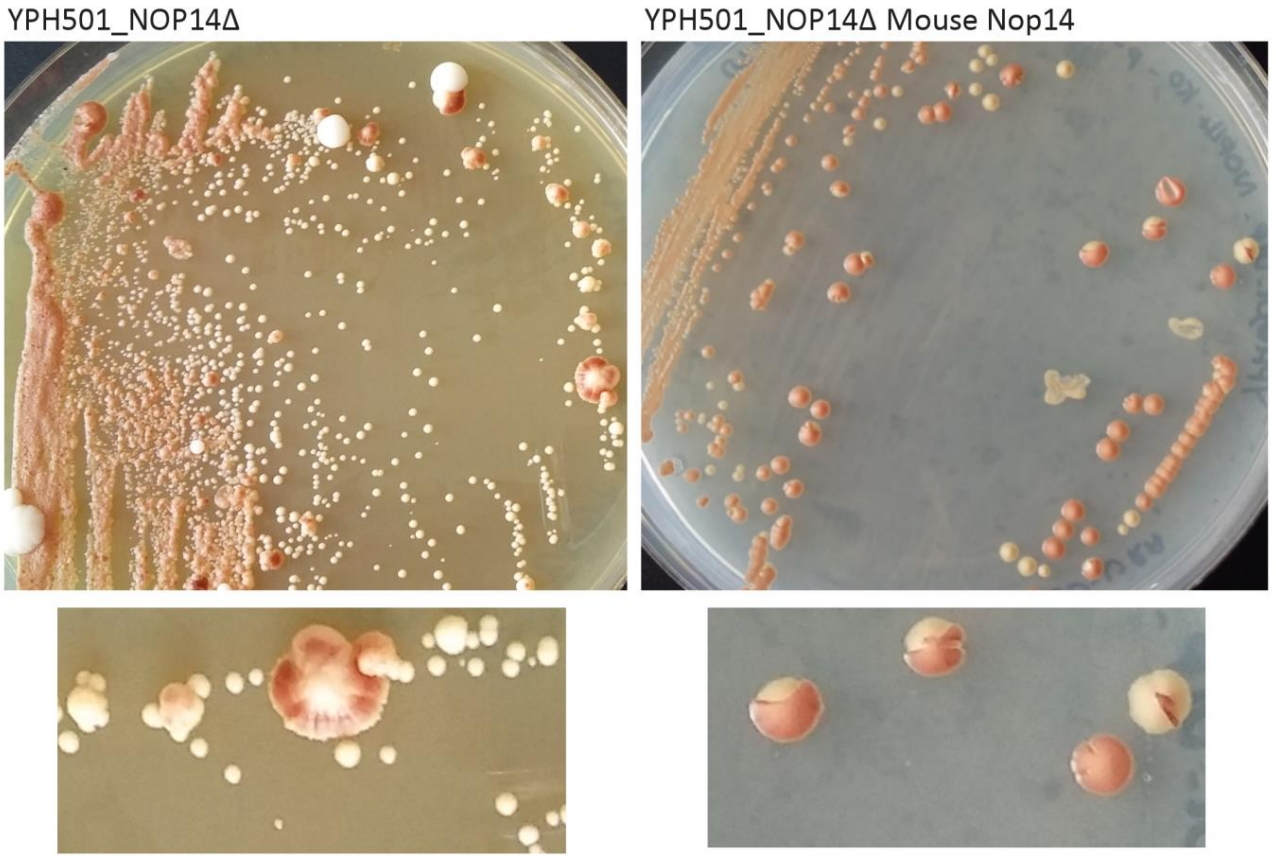

Figure 6.3. The loss of one copy of NOP14 causes the gradual loss of mitochondrial function in yeast which is not rescued by Mouse Nop14.

Images of two strains YPH501_NOP14Δ and YPH501_NOP14Δ transformed with pSF-STE5-Nop14Mouse. Some cells have lost mitochondrial function indicated by the loss of red pigment. In the enlarged view you can see the loss of mitochondria the colonies occurring in sectors. This sectoring is commonly seen in strains with the ADE2 variants when genetic defects cause mitochondrial loss (Wang et al. 2007).

6.4.4. Complementation with Mouse Nop14 does not rescue mitochondrial loss

In order to perform yeast complementation assays we inserted the mouse Nop14 sequence (BC043043) into a plasmid containing a yeast STE5 (low activity) promotor. The plasmid was transformed into the YPH501_NOP14Δ strain for sporulation to produce haploid cells with either yeast NOP14 or the plasmid containing mouse Nop14. These cells failed to sporulate and when examined by light microscopy had stalled during sporulation. We can assume that over-expression of murine Nop14 in yeast cells is detrimental for sporulation as the diploid knockout had previously sporulated normally. It was also noted that the cells transformed with the plasmid were losing mitochondria function (Fig 6.3) and so the insertion of the Nop14 mouse gene did not rescue the mitochondrial loss in these cells.

6.4.5. Localisation of NOP14 in Hela cells

Experiments in yeast showed that NOP14p has an influence over mitochondrial function so we were interested to see if NOP14 had additional localisations outside the nucleolus. Using antibody staining we confirmed the localisation of endogenous NOP14 in Hela cells to the nucleolus (Fig 6.4). There appeared to be no additional localisations for endogenous NOP14 in Hela cells.

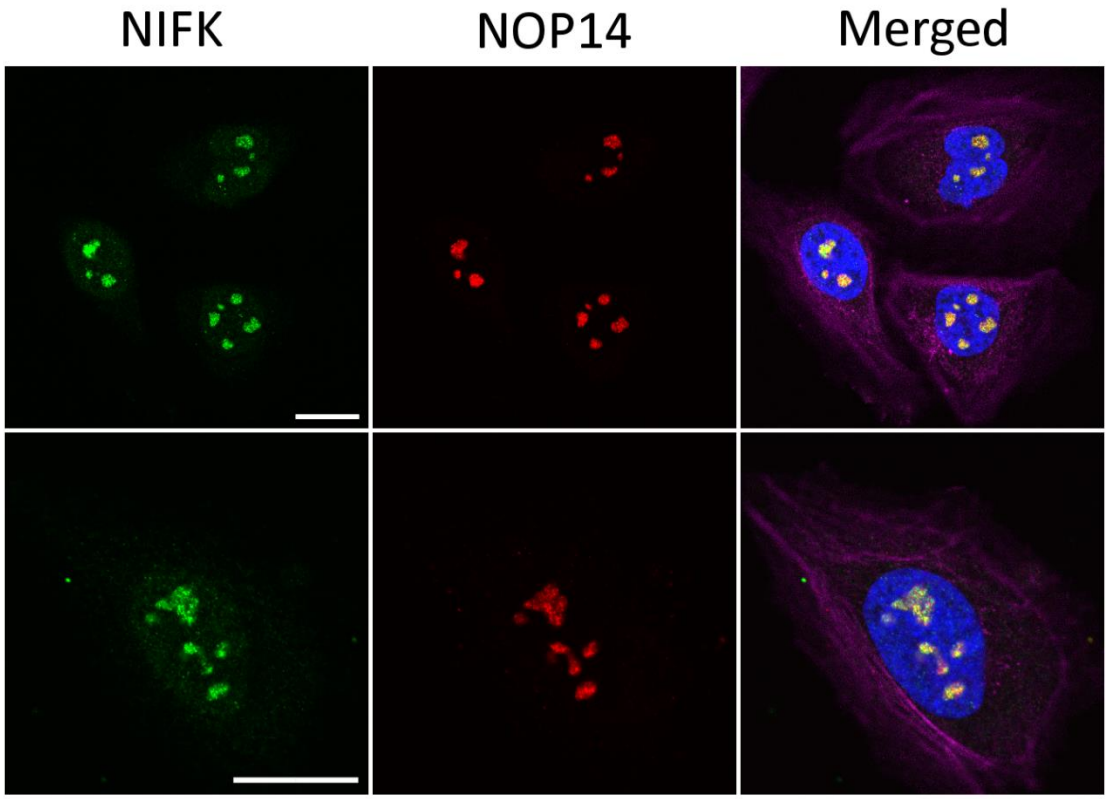

Figure 6.4. In HeLa cells endogenous NOP14 localises to the nucleolus

Confocal fluorescence microscopy of HeLa cells showing localisation of NOP14 protein (NOP14-Sigma, red). Cells were counterstained with Hoechst (nuclear marker, blue) to visualise the nuclei, NIFK (nucleolar marker, green) to visualise the nucleolus and Phalloidin (F-actin marker, pink) to visualise the cytoskeleton. The scale bar is 20µm.

To assess the effect of overexpression of NOP14 we produced a plasmid containing the mouse cDNA for Nop14 (Accession - BC043043) with a C-terminal EGFP tag. The C-terminal tag was chosen as to not disrupt targeting sequences located at the N-terminus of the protein. We transfected Hela cells with this construct (Fig.6.5). In contrast to the localisation of endogenous NOP14 we noted two distinct localisations for Nop14-EGFP. In some cells large spots of nucleolar staining was seen with additional staining at nuclear foci (Fig.6.5A and 6.5D). It is possible that the EGFP tag is causing the protein to aggregate on the surface of the nucleoli either directly or through reduced associated with co-factors required for nucleolar localisation. The use of mouse Nop14 may also reduce association with these co-factors such as such as NOC4L (Warda et al. 2016), which is essential for the nucleolar localisation of NOP14. The aggregation of protein at nuclear foci has been seen in cells where EMG1 (NOP14 co-factor) and the variant EMG1 D86G were overexpressed. In these cases the EMG1 was localised to these foci for proteasome degradation (Armistead et al. 2009;Warda et al. 2016). It seems likely that Nop14 is also localised to foci for proteasome degradation as the saturation of proteins required for the localisation of NOP14 to the nucleolus, could prevent complete nucleolar localisation.
In other cells diffuse nuclear staining was noted (Fig. 6.5B and 6.5C). In these cells there was a high level of NOP14 antibody staining in what appeared to be the nucleolus. It may be that some of the Nop14 has lost the EGFP tag and thus preventing the aggregation of Nop14-EGFP on the nucleoli as seen in panel A. It is not clear why some cells show these differing patterns of Nop14-EGFP expression, it may relate to the levels of expression of the construct.

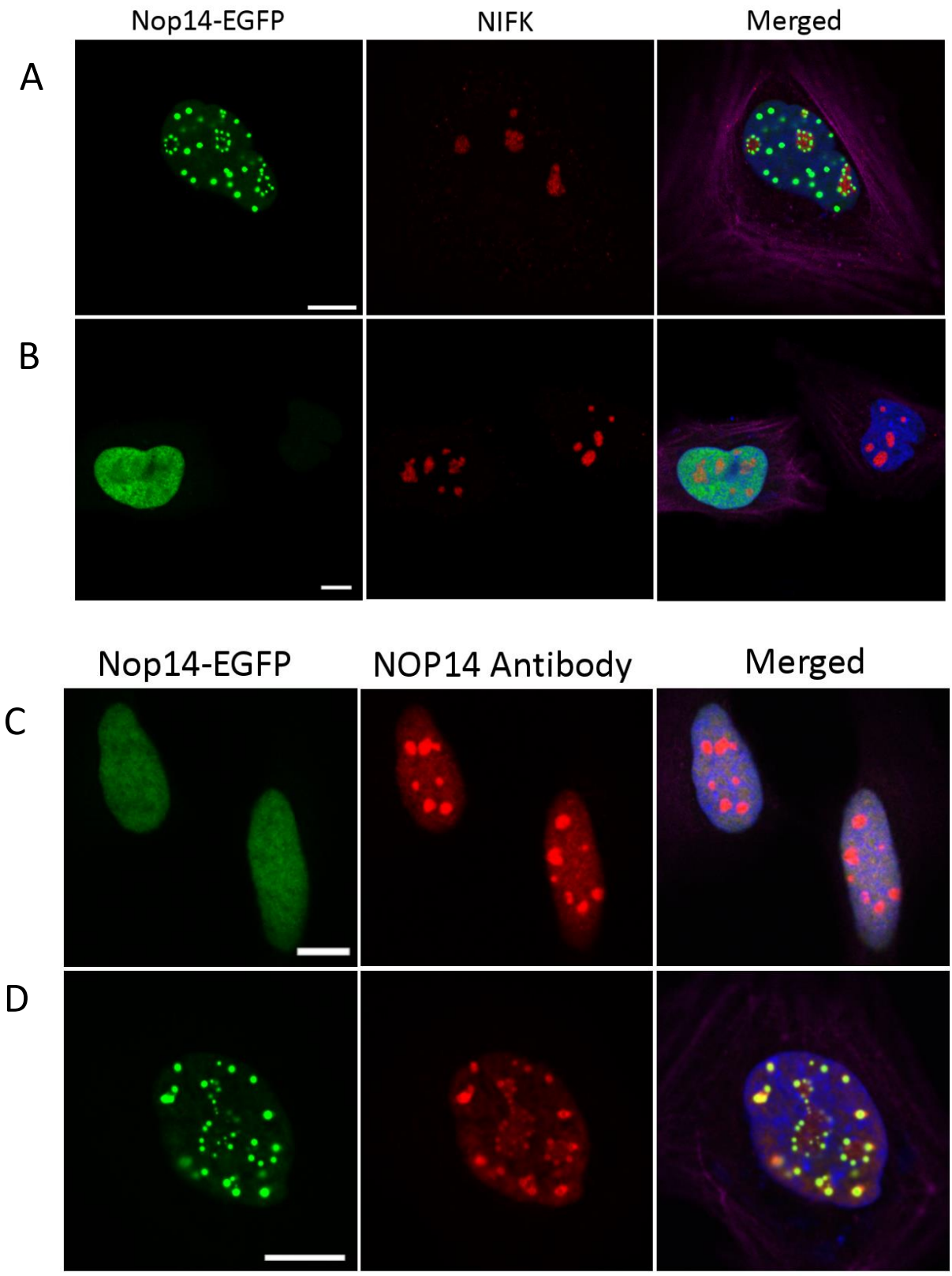

Figure 6.5. Nop14-EGFP shows two distinct patterns of localisation

Confocal fluorescence microscopy of HeLa cells showing localisation of Nop14 with a c-terminal EGFP tag (green). A & B) Cells were counterstained with Hoechst (nuclear DNA

marker, blue) to visualise the nuclei, NIFK (nucleolar marker, red) to visualise the nucleolus and Rhodamine-Phalloidin (F-actin marker, pink) to visualise the cytoskeleton. The scale bar is 20µm. C & D) Cells were counterstained with Hoechst (nuclear DNA marker, blue) to visualise the nuclei, NOP14 antibody (Santa Cruz Biotechnology, Dallas, TX, USA, red) and Phalloidin (F-actin marker, pink) to visualise the cytoskeleton. The scale bar is 20µm.

HeLa cells were also transfected with a construct containing Nop14 c-terminally labelled with turbo GFP (Origene Rockville, MD, USA, Accession NM_029278.2). These cells showed the same dual localisation patterns as the EGFP tagged Nop14. In contrast this construct was able to enter the nucleolus (Fig 6.6) suggesting that the aggregation on the nucleolar surface (Fig 6.5A and 6.5D) is due to the EGFP tag. There was also some Nop14-TurboGFP localised to the cytoplasm which is likely due to overexpression saturating import into the nucleus or the Turbo-GFP tag causing slight interference to nuclear import.

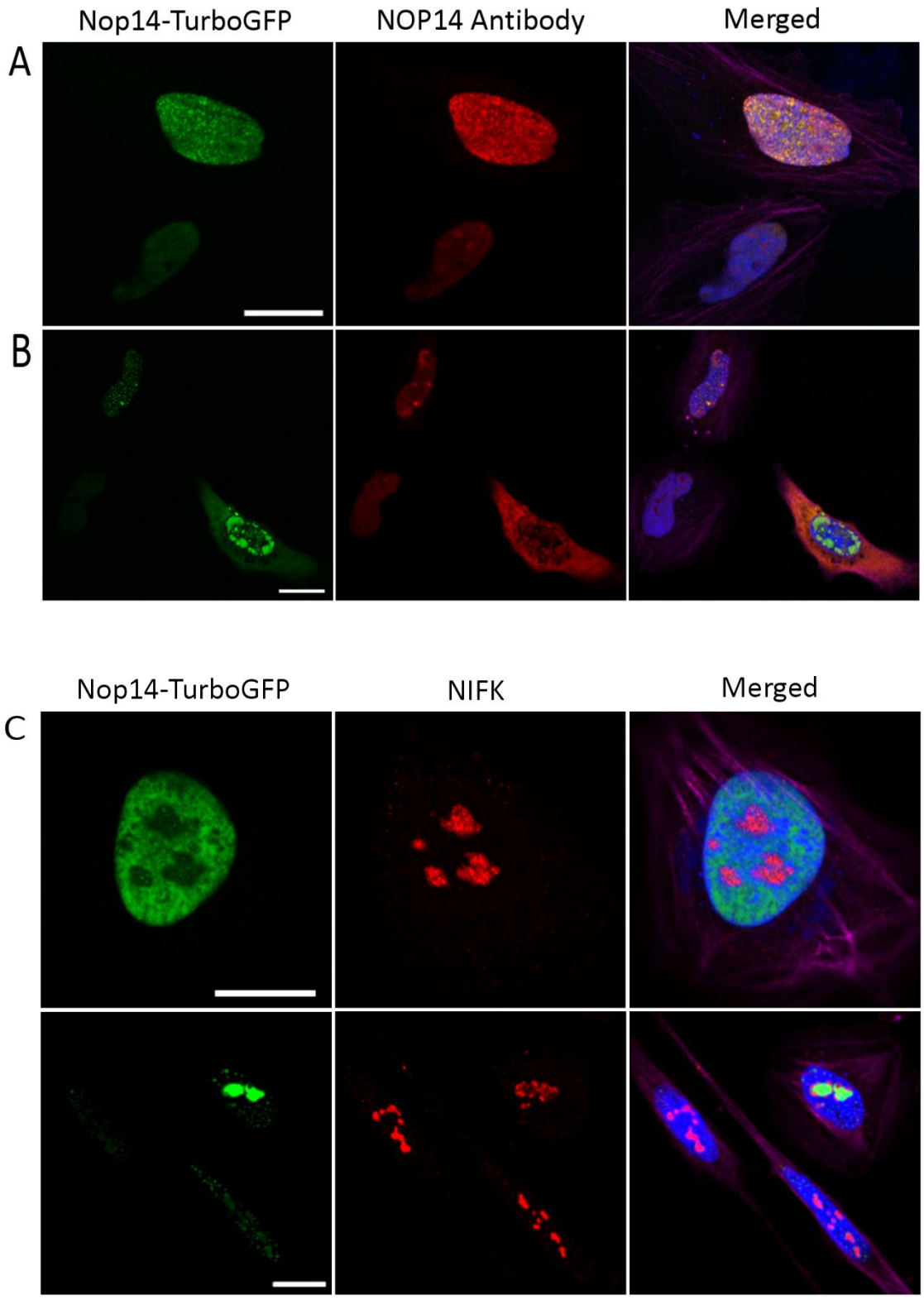

Figure 6.6. Nop14-TurboGFP shows two distinct patterns of localisation in HeLa cells.

Confocal fluorescence microscopy of HeLa cells showing localisation of Nop14 with a c-terminal TurboGFP tag (green). A & B) Cells were counterstained with NOP14 (Sigma, Red), Hoechst (nuclear DNA marker, blue) to visualise the nuclei and phalloidin (F-actin

marker, pink) to visualise the cytoskeleton. The scale bar is 20µm. C) Cells were counterstained with Hoechst (nuclear DNA marker, blue) to visualise the nuclei, NIFK (nucleolar marker, red) and Phalloidin (F-actin marker, pink) to visualise the cytoskeleton. The scale bar is 20µm.

Some cells transfected with NOP14-turboGFP showed nuclear blebbing and malformation (Fig 6.7). A notable number of cells were seen with this defect. It appears overexpression of NOP14-turboGFP is detrimental to Hela cells.

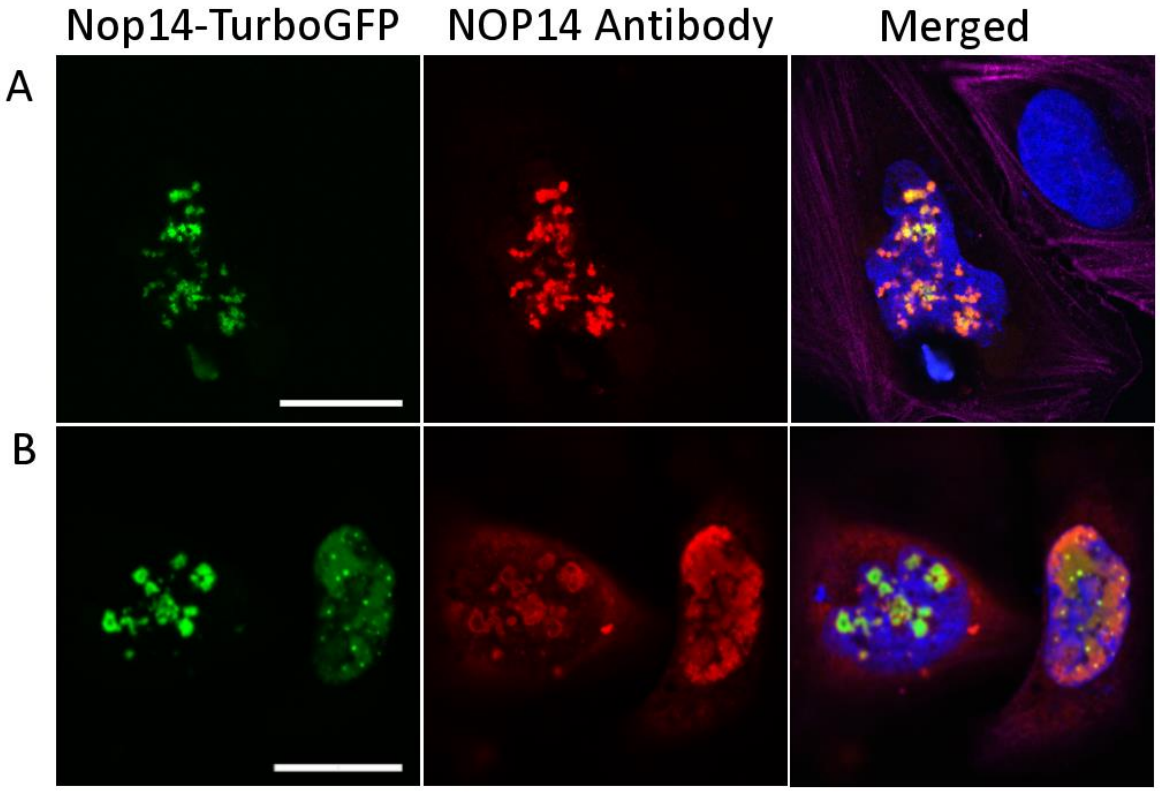

Figure 6.7. Overexpression of Nop14-TurboGFP has a detrimental effect on HeLa cells

Confocal fluorescence microscopy of HeLa cells showing localisation of Nop14 with a c-terminal GFP tag (green). Cells were counterstained with Hoechst (nuclear DNA marker, blue) to visualise the nuclei and Phalloidin (F-actin marker, pink) to visualise the cytoskeleton. Panel A was conterstained with NOP14-Santa Cruz Biotechnology, Dallas, TX, USA and panel B with NOP14-Sigma. The scale bar is 20µm.

6.4.6. NOP14 has a specific non-nucleolar localisation in mouse auditory hair cells

Although it appears that NOP14 may have an uncharacterised function affecting mitochondria we did not see any specific non-nucleolar localisation of endogenous NOP14 or overexpressed Nop14 in HeLa cells. We considered that NOP14 may have tissue specific expression which might not be apparent in tissue culture cells. To investigate this potential tissue specific expression and the pathological mechanism behind the hearing loss in the affected family we undertook localisation of Nop14 in the mouse organ of Corti. The organ of Corti from mice aged postnatal day 3 (P3) to P30 were removed and fixed before endogenous Nop14 was localised using a NOP14 antibody (Sigma, green). Samples were also counterstained using a nuclear marker (DAPI, blue), a cytoskeletal marker (localises f-actin, rhodamine-phalloidin in panel A, red. Phalloidin in panel C and E, pink) and in panel c a presynaptic membrane marker SNAP25 synaptosome-associated protein 25).

At P3 we see low levels of Nop14, which is likely background staining, in the mouse organ of Corti (Fig 6.8A). The distinct nucleolar staining seen in HeLa cells is not seen here and it is likely that if the hair cells are expressing Nop14 it is at low levels. At P3 the organ of Corti is not fully developed and the mice cannot hear, the onset of hearing occurs at approximately P12-P14 (Ehret 1976). At P14 we see a distinct pattern of Nop14 localisation with staining in both the outer hair cells and at the base of the inner hair cells. In the outer hair cells the location and pattern of expression suggest Nop14 localises to the outer hair cells synapses. In the inner hair cells there appears to be a single foci of Nop14 per cell, which does not localise to nucleus. By P18 localisation of Nop14 is no longer seen in outer hairs cells but there is increased Nop14 localised to the base of the inner hair cells (Fig. 6.8C and 6.8D). This localisation persists into adult mice (P30, Fig 6.8E). We did not see significant nuclear localisation of Nop14 in the mouse organ of Corti at any age. The pattern of Nop14 localisation seen in the organ of Corti is markedly different than that seen in HeLa cells. It appears Nop14 is not exclusively localised to the nucleolus and as such may have additional tissue specific localisation.

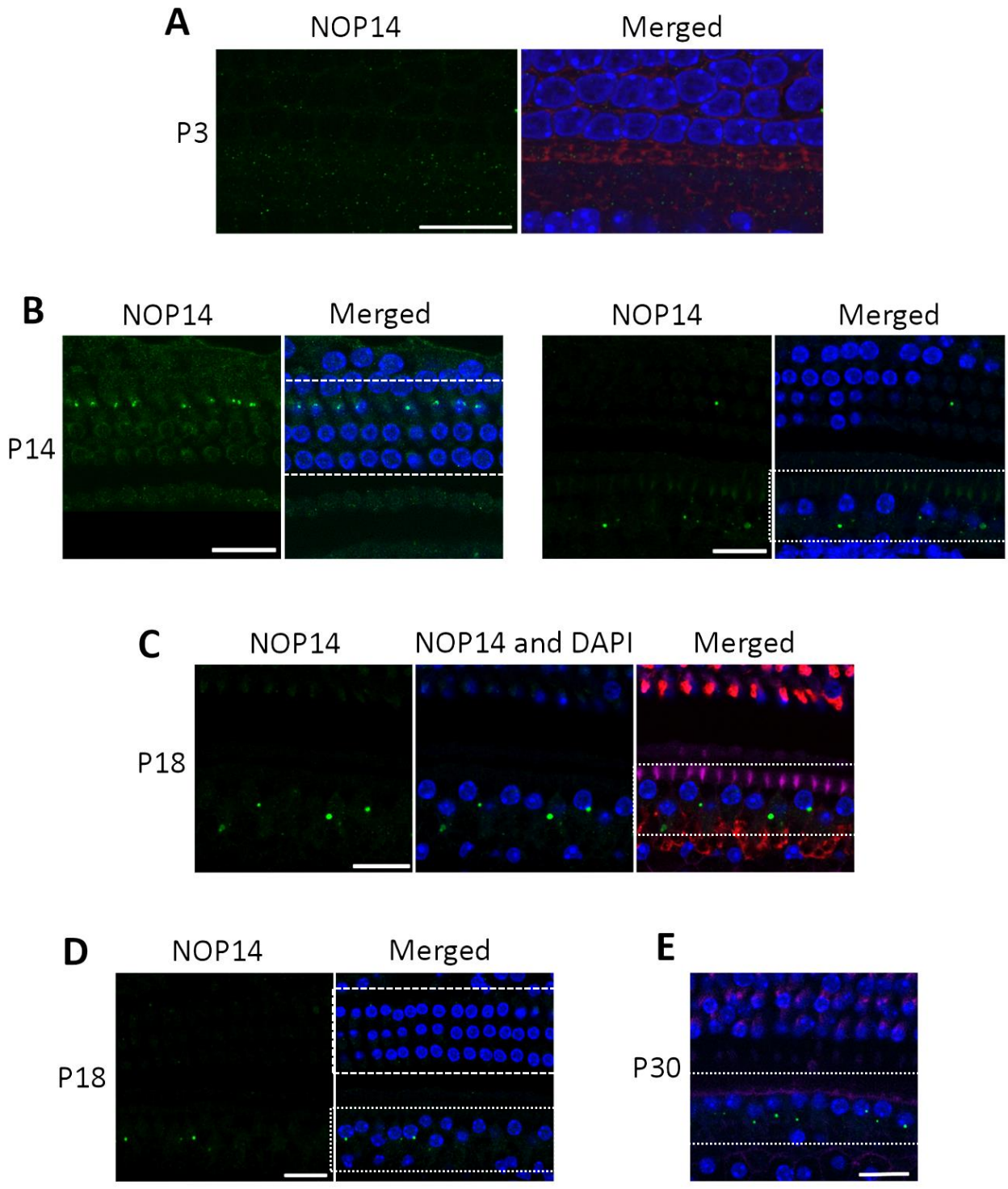

Figure 6.8. Nop14 has a specific non-nucleolar localisation pattern in the mouse organ of Corti

Confocal fluorescence microscopy optical sections of the whole mount organ of Corti samples from C57/BJ6 mice at postnatal days 3, 14 and 18 and 30 (P3, P14, P18 and P30, correspondingly) showing localisation of Nop14 (green). All samples were counterstained with DAPI (nuclear DNA marker, blue) to visualize the nuclei of hair cells. Panel A was also counterstained with rhodamine-phalloidin (cytoskeletal marker, red). Panel C and E were

counterstained with phalloidin (cytoskeletal marker, pink). Panel C was also stained for SNAP25 (presynaptic membrane marker, red), to visualize efferent synapses at the base of outer hair cells (OHCs) and nerve fibres and synaptic buttons at the base and around IHCs. Panel B shows different focal planes within a sample to visualise both the OHC (left) and IHC (right) areas. The dashed white line outlines the area of the outer hair cells (OHC) at the nuclear level and the dotted white line outlines the area around the inner hair cell nuclei (IHC). The scale bar is 20µm.

To determine if the pattern of Nop14 localisation in the organ of corti is age specific we transfected organ of corti explants from C57/BJ6 mice at P3 with Nop14-TurboGFP using the gene gun method (Fig 6.9). Transfected hair cells showed the same pattern of expression as HeLa cells suggesting that the endogenous pattern of expression seen above is age specific and cannot be induced by the overexpression of Nop14 in mice before the onset of hearing. It also suggests that at this age Nop14 does localise to the nucleolus if it is produced.

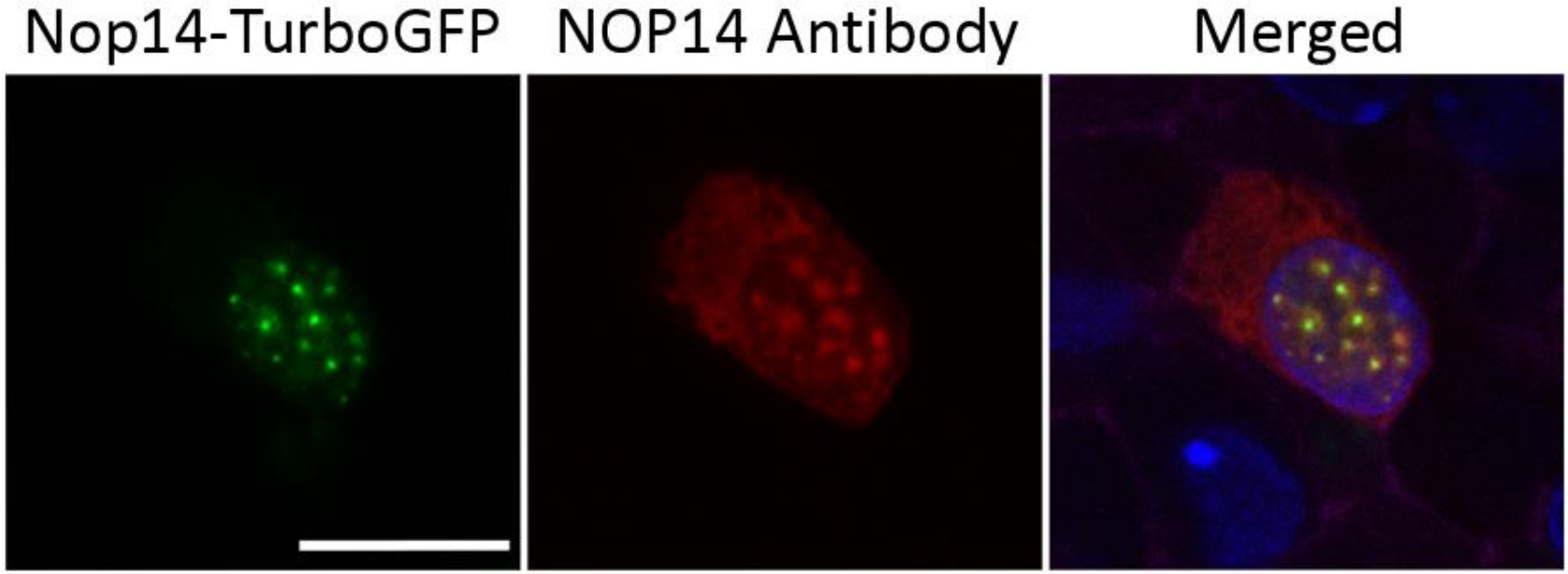

Figure 6.9. Hair cells from P3 mice transfected with Nop14-TurboGFP show a nucleolar pattern of Nop14 localisation.

Confocal fluorescence microscopy optical section of the whole mount organ of Corti sample from a C57/BJ6 mouse at P3 which was gene gun transfected with the plasmid Nop14-TurboGFP (green). The sample was counterstained with NOP14 (Sigma, red), DAPI (nuclear DNA marker, blue) and phalloidin (cytoskeletal marker, pink). The transfected cell is an outer hair cell. The scale bar is 20µm.

6.5. Discussion

We have identified a putative novel Perrault syndrome gene, *NOP14*, in a single consanguineous family. NOP14 is involved in nuclear ribosomal formation and as such does not fit the hypothesis that Perrault syndrome genes will be involved in the mitochondrial translation pathway. Initially the variant in NOP14 appeared like it may represent an alternate non-mitochondrial pathology for Perrault syndrome. When we performed investigations in yeast it became clear that NOP14 had an influence over mitochondrial function. Localisation in the mouse organ of Corti showed that NOP14 has a tissue specific expression pattern and is not always localised to the nucleolus. This localisation indicates that NOP14 may have an additional non-nucleolar function and influences mitochondrial function.

NOP14 is part of a sub-complex involved in the processing of 18S rRNA (Liu and Thiele 2001;Warda et al. 2016). The sub-complex comprises UTP14A, NOC4L, NOP14 and EMG1. The complex is assembled in a hierarchical manner as shown in figure 6.10 with all of the preceding subunits required for the nucleolar localisation of the subsequent protein (Warda et al. 2016). NOP14 forms a stable heterodimer with NOC4L and is likely co-regulated (Milkereit et al. 2003). It is possible that NOC4L and NOP14 are recruited into the sub-complex as a heterodimer but this has yet to be shown experimentally. EMG1 is a methyltransferase responsible for a post-transcriptional modification of 18s RNA, which is not essential for ribosome biogenesis (Meyer et al. 2011). The sub-complex also has an additional role in ribosomal biogenesis which has not been fully elucidated but likely involves processing of the 18s RNA (Liu and Thiele 2001;Meyer et al. 2011). Knockdown of any of the four subunits of the sub-complex resulted in the accumulation of pre-18S rRNA and depletion of mature 18S RNA and the 40S ribosomal subunit (Warda et al. 2016).

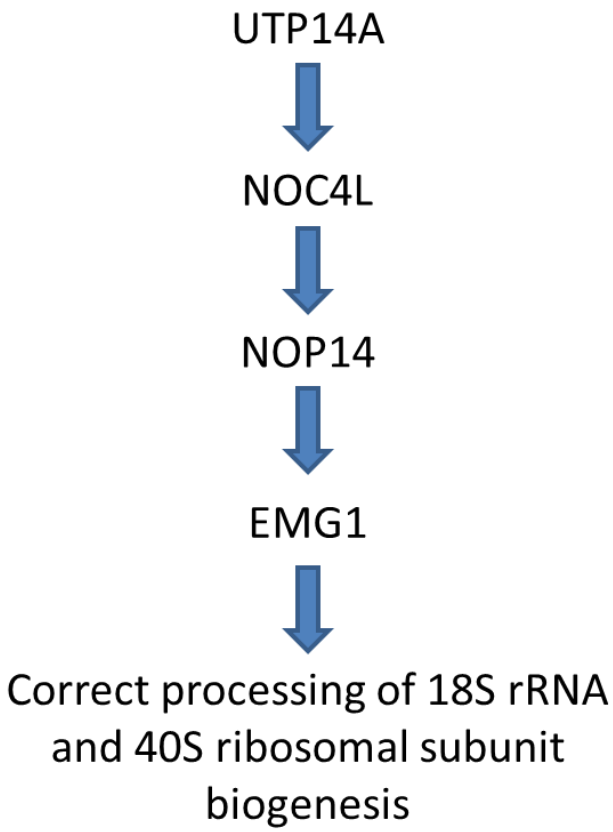

Figure 6.10. The hierarchical assembly of the ribosomal biogenesis sub-complex containing NOP14.

The preceding subunit is required for the recruitment of each subsequent protein to the nucleolus and the complete complex is required for the biogenesis of the 40S ribosomal subunit (Warda et al. 2016).

A single homozygous variant in EMG1, D86G, causes Bowen-Conradi syndrome (Armistead et al. 2009). Bowen Conradi syndrome is a severe infantile disorder which presents as growth retardation, micrognathia, microcephaly, joint abnormalities and severe psychomotor delay with affected children rarely surviving beyond the age of one year (Lowry et al. 2003;Armistead et al. 2009). The reported variant causes protein instability and a severe reduction in the amount of EMG1 localising to the nucleolus (Armistead et al. 2009). There are no reported genetic syndromes associated with the other three subunits of the complex.

The family reported here did not have the features of Bowen-Conradi syndrome, caused by variants in *EMG1*. Not having features of Bowen-Conradi syndrome may have been due to the milder defect of NOP14 in this family or the additional function of EMG1 as a

methyltransferase (Meyer et al. 2011). Our functional work suggested that there may be another reason. When we investigated further it became apparent that NOP14 had more in common with other Perrault syndrome proteins than initially thought.

Haploinsufficiency of NOP14p in yeast caused the loss of mitochondria indicating that NOP14p either has an essential mitochondrial function or is an essential component of mitochondrial and nuclear communication (mitonuclear communication). Mitochondrial-nuclear communication is vital for mitochondrial homeostasis and occurs through a bidirectional pathway with anterograde (nuclear to mitochondrial) and retrograde (mitochondrial to nuclear) signalling. While the pathway is bidirectional, anterograde signalling is mainly responsible for homeostasis and the retrograde pathway often signals mitochondrial stress (Quiros et al. 2016). Anterograde mitonuclear communication is controlled via the expression of nuclear encoded mitochondrial proteins that are involved in the expression of mitochondrial DNA or the regulation of the mitochondrial proteome. We could predict if NOP14 was affecting mitonuclear communications it may function in the anterograde pathway given its localisation in the nucleolus and the fact that the knockout yeast lost their mitochondria under normal non-stress conditions suggesting mitochondrial homeostasis was disrupted.

We also saw indications that NOP14 may have additional functions outside the nucleus. We found that mouse Nop14 has a very specific localisation pattern in the sensory hair cells of the organ of Corti. The localisation was seen from the onset of hearing and was seen in the outer hair cells (OHC) and inner hair cells (IHC) only. At P14 we saw localisation of Nop14 in the body of the OHCs. The pattern was suggestive of synaptic localisation and was no longer apparent at P18. In contrast from P14 we saw localisation of Nop14 to single foci towards the base of the inner hair cells. This localisation persisted into adulthood and was still present at the latest age examined (P30). This localisation pattern showed similarities to another Perrault syndrome gene, MRPP3, which after the onset of hearing showed localisation to the OHC synapses and the IHC synaptic area. It would be useful to co-localise Nop14 in the organ of Corti with the hair cell synapses as it appears to localise to the OHC synapses at P14 and the single foci of Nop14 in the IHC bodies may correspond to the synaptic bouton of the IHCs. A defect of the hair cell synapses could explain the hearing loss seen in this family with Perrault syndrome.

NOP14 appears to be a vital gene with no homozygous loss of function variants reported in online databases. Variants in *NOP14* have not been previously associated with any form of genetic disease. The complete loss of NOP14p is lethal in yeast with haploinsufficiency causing mitochondrial dysfunction. The overexpression of NOP14 in Hela cells was detrimental to the cells. This lethality following NOP14 overexpression suggests that the expression of NOP14 is likely tightly controlled in normal functioning cells with NOP14 appearing to have specific tissue and developmental localisation patterns. It would be useful to assess the localisation of NOP14 in additional tissues with focus on possible mitochondrial localisation. This may help elucidate the role of NOP14 in mitochondrial homeostasis.

The homozygous variant *NOP14* c.1160A>G p.(Glu387Gly) is the likely cause of Perrault syndrome in this reported family. There have been no additional families identified with Perrault syndrome due to variants in *NOP14* but this is not unexpected given the high genetic heterogeneity seen in Perrault syndrome and the rarity of cases. We have submitted this case to GeneMatcher (https://genematcher.org/), an online tool which connects individuals with interest in the same gene to solve unsolved exomes (Sobreira et al. 2015). It is important to identify a second family with Perrault syndrome and causative variants in *NOP14* to confirm pathogenicity. It appears that this case of Perrault syndrome may have a similar pathology of mitochondrial dysfunction as other cases of Perrault syndrome (Chatzispyrou et al. 2017). It is currently unknown whether NOP14 functions in mitonuclear communication or has a role within the mitochondria itself. It is clear that the disruption of NOP14 disrupts mitochondrial homeostasis which is the likely pathological mechanism for the sensorineural hearing loss and primary ovarian insufficiency of Perrault syndrome.

6.6. References

Adzhubei, I. A., Schmidt, S., Peshkin, L., Ramensky, V. E., Gerasimova, A., Bork, P., Kondrashov, A. S. & Sunyaev, S. R. (2010). A method and server for predicting damaging missense mutations. *Nat Methods,* 7(4)**,** 248-9.

Armistead, J., Khatkar, S., Meyer, B., Mark, B. L., Patel, N., Coghlan, G., Lamont, R. E., Liu, S., Wiechert, J., Cattini, P. A., Koetter, P., Wrogemann, K., Greenberg, C. R., Entian, K. D., Zelinski, T. & Triggs-Raine, B. (2009). Mutation of a gene essential for ribosome biogenesis, EMG1, causes Bowen-Conradi syndrome. *Am J Hum Genet,* 84(6)**,** 728-39.

Banka, S., Blom, H. J., Walter, J., Aziz, M., Urquhart, J., Clouthier, C. M., Rice, G. I., de Brouwer, A. P., Hilton, E., Vassallo, G., Will, A., Smith, D. E., Smulders, Y. M., Wevers, R. A., Steinfeld, R., Heales, S., Crow, Y. J., Pelletier, J. N., Jones, S. & Newman, W. G. (2011). Identification and characterization of an inborn error of metabolism caused by dihydrofolate reductase deficiency. Am J Hum Genet, 88(2), 216-25.

Belyantseva, I. A. (2016). Helios® Gene Gun-Mediated Transfection of the Inner Ear Sensory Epithelium: Recent Updates. *In:* Sokolowski, B. (ed.) *Auditory and Vestibular Research: Methods and Protocols.* New York, NY: Springer New York.

Beukeveld, G. J., Wolthers, B. G., Nordmann, Y., Deybach, J. C., Grandchamp, B. & Wadman, S. K. (1990). A retrospective study of a patient with homozygous form of acute intermittent porphyria. *J Inherit Metab Dis,* 13(5)**,** 673-83.

Calvo, S. E., Clauser, K. R. & Mootha, V. K. (2016). MitoCarta2.0: an updated inventory of mammalian mitochondrial proteins. *Nucleic Acids Res,* 44(D1)**,** D1251-7.

Carr, I. M., Flintoff, K. J., Taylor, G. R., Markham, A. F. & Bonthron, D. T. (2006). Interactive visual analysis of SNP data for rapid autozygosity mapping in consanguineous families. *Hum Mutat,* 27(10)**,** 1041-6.

Chatzispyrou, I. A., Alders, M., Guerrero-Castillo, S., Zapata Perez, R., Haagmans, M. A., Mouchiroud, L., Koster, J., Ofman, R., Baas, F., Waterham, H. R., Spelbrink, J. N., Auwerx, J., Mannens, M. M., Houtkooper, R. H. & Plomp, A. S. (2017). A homozygous missense mutation in ERAL1, encoding a mitochondrial rRNA chaperone, causes Perrault syndrome. *Hum Mol Genet,* 26(13)**,** 2541-2550.

Chen, C. H., Astrin, K. H., Lee, G., Anderson, K. E. & Desnick, R. J. (1994). Acute intermittent porphyria: identification and expression of exonic mutations in the hydroxymethylbilane synthase gene. An initiation codon missense mutation in the housekeeping transcript causes "variant acute intermittent porphyria" with normal expression of the erythroid-specific enzyme. *J Clin Invest,* 94(5)**,** 1927-37.

Chen, D. C., Yang, B. C. & Kuo, T. T. (1992). One-step transformation of yeast in stationary phase. *Curr Genet,* 21(1)**,** 83-4.

Dorfman, B. Z. (1969). The isolation of adenylosuccinate synthetase mutants in yeast by selection for constitutive behavior in pigmented strains. *Genetics,* 61(2)**,** 377-89.

Ehret, G. (1976). Development of absolute auditory thresholds in the house mouse (Mus musculus). *J Am Audiol Soc,* 1(5)**,** 179-84.

Exome Aggregation Consortium (ExAC). *Exome Aggregation Consortium (ExAC)* [Online]. Cambridge, MA. Available: http://exac.broadinstitute.org [Accessed 01/07 2017].

Fiumara, A., Sorge, G., Toscano, A., Parano, E., Pavone, L. & Opitz, J. M. (2004). Perrault syndrome: Evidence for progressive nervous system involvement. *Am J Med Genet,* 128A(3)**,** 246-249.

Fukasawa, Y., Tsuji, J., Fu, S. C., Tomii, K., Horton, P. & Imai, K. (2015). MitoFates: improved prediction of mitochondrial targeting sequences and their cleavage sites. *Mol Cell Proteomics,* 14(4)**,** 1113-26.

Gottschalk, M. E., Coker, S. B. & Fox, L. A. (1996). Neurologic anomalies of Perrault syndrome. *Am J Med Genet,* 65(4)**,** 274-6.

Grandchamp, B., Picat, C., Kauppinen, R., Mignotte, V., Peltonen, L., Mustajoki, P., Romeo, P. H., Goossens, M. & Nordmann, Y. (1989). Molecular analysis of acute intermittent porphyria in a Finnish family with normal erythrocyte porphobilinogen deaminase. *Eur J Clin Invest,* 19(5)**,** 415-8.

Hessels, J., Voortman, G., van der Wagen, A., van der Elzen, C., Scheffer, H. & Zuijderhoudt, F. M. (2004). Homozygous acute intermittent porphyria in a 7-year-old boy with massive excretions of porphyrins and porphyrin precursors. *J Inherit Metab Dis,* 27(1)**,** 19-27.

Itoh, T., Ono, T. & Yamaizumi, M. (1994). A new UV-sensitive syndrome not belonging to any complementation groups of xeroderma pigmentosum or Cockayne syndrome: siblings showing biochemical characteristics of Cockayne syndrome without typical clinical manifestations. *Mutat Res,* 314(3)**,** 233-48.

Jenkinson, E. M., Rehman, A. U., Walsh, T., Clayton-Smith, J., Lee, K., Morell, R. J., Drummond, M. C., Khan, S. N., Naeem, M. A., Rauf, B., Billington, N., Schultz, J. M., Urquhart, J. E., Lee, M. K., Berry, A., Hanley, N. A., Mehta, S., Cilliers, D., Clayton, P. E., Kingston, H., Smith, M. J., Warner, T. T., Black, G. C., Trump, D., Davis, J. R. E., Ahmad, W., Leal, S. M., Riazuddin, S., King, M. C., Friedman, T. B. & Newman, W. G. (2013). Perrault syndrome is caused by recessive mutations in CLPP, encoding a mitochondrial ATP-dependent chambered protease. *Am J Hum Genet,* 92(4)**,** 605-613.

Jones, P., Binns, D., Chang, H. Y., Fraser, M., Li, W., McAnulla, C., McWilliam, H., Maslen, J., Mitchell, A., Nuka, G., Pesseat, S., Quinn, A. F., Sangrador-Vegas, A., Scheremetjew, M., Yong, S. Y., Lopez, R. & Hunter, S. (2014). InterProScan 5: genome-scale protein function classification. *Bioinformatics,* 30(9)**,** 1236-40.

Kumar, P., Henikoff, S. & Ng, P. C. (2009). Predicting the effects of coding non-synonymous variants on protein function using the SIFT algorithm. *Nat Protoc,* 4(7)**,** 1073-81.

Lek, M., Karczewski, K. J., Minikel, E. V., Samocha, K. E., Banks, E., Fennell, T., O'Donnell-Luria, A. H., Ware, J. S., Hill, A. J., Cummings, B. B., Tukiainen, T., Birnbaum, D. P., Kosmicki, J. A., Duncan, L. E., Estrada, K., Zhao, F., Zou, J., Pierce-Hoffman, E., Berghout, J., Cooper, D. N., Deflaux, N., DePristo, M., Do, R., Flannick, J., Fromer, M., Gauthier, L., Goldstein, J., Gupta, N., Howrigan, D., Kiezun, A., Kurki, M. I., Moonshine, A. L., Natarajan, P., Orozco, L., Peloso, G. M., Poplin, R., Rivas, M. A., Ruano-Rubio, V., Rose, S. A., Ruderfer, D. M., Shakir, K., Stenson, P. D., Stevens, C., Thomas, B. P., Tiao, G., Tusie-Luna, M. T., Weisburd, B., Won, H. H., Yu, D., Altshuler, D. M., Ardissino, D., Boehnke, M., Danesh, J., Donnelly, S., Elosua, R., Florez, J. C., Gabriel, S. B., Getz, G., Glatt, S. J., Hultman, C. M., Kathiresan, S., Laakso, M., McCarroll, S., McCarthy, M. I., McGovern, D., McPherson, R., Neale, B. M., Palotie, A., Purcell, S. M., Saleheen, D., Scharf, J. M., Sklar, P., Sullivan, P. F., Tuomilehto, J., Tsuang, M. T., Watkins, H. C., Wilson, J. G., Daly, M. J., MacArthur, D. G. & Exome Aggregation, C. (2016). Analysis of protein-coding genetic variation in 60,706 humans. *Nature,* 536(7616)**,** 285-91.

Letunic, I., Doerks, T. & Bork, P. (2015). SMART: recent updates, new developments and status in 2015. *Nucleic Acids Res,* 43(Database issue)**,** D257-60.

Liu, P. C. C. & Thiele, D. (2001). Novel stress-responsive genes EMG1 and NOP14 encode conserved, interacting proteins required for 40S ribosome biogenesis. *Mol Biol Cell,* 12(11)**,** 3644-3657.

Lowry, R. B., Innes, A. M., Bernier, F. P., McLeod, D. R., Greenberg, C. R., Chudley, A. E., Chodirker, B., Marles, S. L., Crumley, M. J., Loredo-Osti, J. C., Morgan, K. & Fujiwara, T. M. (2003). Bowen-Conradi syndrome: a clinical and genetic study. *Am J Med Genet A,* 120A(3)**,** 423-8.

Marchler-Bauer, A., Derbyshire, M. K., Gonzales, N. R., Lu, S., Chitsaz, F., Geer, L. Y., Geer, R. C., He, J., Gwadz, M., Hurwitz, D. I., Lanczycki, C. J., Lu, F., Marchler, G. H., Song, J. S., Thanki, N., Wang, Z., Yamashita, R. A., Zhang, D., Zheng, C. & Bryant, S. H. (2015). CDD: NCBI's conserved domain database. *Nucleic Acids Res,* 43(Database issue)**,** D222-6.

Mehdipour, P., Karimi, A. R. & Bastanhagh, M. M. (1999). Perrault's syndrome: a clinical and genetic investigation of three sisters. *Acta Med Iran,* 37(2)**,** 78-85.

Meyer, B., Wurm, J. P., Kotter, P., Leisegang, M. S., Schilling, V., Buchhaupt, M., Held, M., Bahr, U., Karas, M., Heckel, A., Bohnsack, M. T., Wohnert, J. & Entian, K. D. (2011). The Bowen-Conradi syndrome protein Nep1 (Emg1) has a dual role in eukaryotic ribosome biogenesis, as an essential assembly factor and in the methylation of Psi1191 in yeast 18S rRNA. *Nucleic Acids Res,* 39(4)**,** 1526-37.

Milkereit, P., Strauss, D., Bassler, J., Gadal, O., Kuhn, H., Schutz, S., Gas, N., Lechner, J., Hurt, E. & Tschochner, H. (2003). A Noc complex specifically involved in the formation and nuclear export of ribosomal 40 S subunits. *J Biol Chem,* 278(6)**,** 4072-81.

Mitchell, K., O'Sullivan, J., Missero, C., Blair, E., Richardson, R., Anderson, B., Antonini, D., Murray, J. C., Shanske, A. L., Schutte, B. C., Romano, R. A., Sinha, S., Bhaskar, S. S., Black, G. C., Dixon, J. & Dixon, M. J. (2012). Exome sequence identifies RIPK4 as the Bartsocas-Papas syndrome locus. *Am J Hum Genet,* 90(1)**,** 69-75.

Morino, H., Pierce, S. B., Matsuda, Y., Walsh, T., Ohsawa, R., Newby, M., Hiraki-Kamon, K., Kuramochi, M., Lee, M. K., Klevit, R. E., Martin, A., Maruyama, H., King, M. C. & Kawakami, H. (2014). Mutations in Twinkle primase-helicase cause Perrault syndrome with neurologic features. *Neurology,* 83(22)**,** 2054-61.

Nakazawa, Y., Sasaki, K., Mitsutake, N., Matsuse, M., Shimada, M., Nardo, T., Takahashi, Y., Ohyama, K., Ito, K., Mishima, H., Nomura, M., Kinoshita, A., Ono, S., Takenaka, K., Masuyama, R., Kudo, T., Slor, H., Utani, A., Tateishi, S., Yamashita, S., Stefanini, M., Lehmann, A. R., Yoshiura, K. & Ogi, T. (2012). Mutations in UVSSA cause UV-sensitive syndrome and impair RNA polymerase IIo processing in transcription-coupled nucleotide-excision repair. *Nat Genet,* 44(5)**,** 586-92.

Narasimhan, V. M., Hunt, K. A., Mason, D., Baker, C. L., Karczewski, K. J., Barnes, M. R., Barnett, A. H., Bates, C., Bellary, S., Bockett, N. A., Giorda, K., Griffiths, C. J., Hemingway, H., Jia, Z., Kelly, M. A., Khawaja, H. A., Lek, M., McCarthy, S., McEachan, R., O'Donnell-Luria, A., Paigen, K., Parisinos, C. A., Sheridan, E., Southgate, L., Tee, L., Thomas, M., Xue, Y., Schnall-Levin, M., Petkov, P. M., Tyler-Smith, C., Maher, E. R., Trembath, R. C., MacArthur, D. G., Wright, J., Durbin, R. & van Heel, D. A. (2016). Health and population effects of rare gene knockouts in adult humans with related parents. *Science,* 352(6284)**,** 474-77.

NHLBI GO Exome Sequencing Project (ESP). *Exome Variant Server* [Online]. Seattle, WA. Available: http://evs.gs.washington.edu/EVS/ [Accessed 09/07 2015].

Pallister, P. D. & Opitz, J. M. (1979). The Perrault syndrome: autosomal recessive ovarian dysgenesis with facultative, non-sex-limited sensorineural deafness. *Am J Med Genet,* 4(3)**,** 239-46.

Pierce, S. B., Chisholm, K. M., Lynch, E. D., Lee, M. K., Walsh, T., Opitz, J. M., Li, W., Klevit, R. E. & King, M. C. (2011). Mutations in mitochondrial histidyl tRNA synthetase HARS2 cause ovarian dysgenesis and sensorineural hearing loss of Perrault syndrome. *Proc Natl Acad Sci U S A,* 108(16)**,** 6543-8.

Pierce, S. B., Gersak, K., Michaelson-Cohen, R., Walsh, T., Lee, M. K., Malach, D., Klevit, R. E., King, M. C. & Levy-Lahad, E. (2013). Mutations in LARS2, encoding mitochondrial leucyl-tRNA synthetase, lead to premature ovarian failure and hearing loss in Perrault syndrome. *Am J Hum Genet,* 92(4)**,** 614-620.

Pierce, S. B., Walsh, T., Chisholm, K. M., Lee, M. K., Thornton, A. M., Fiumara, A., Opitz, J. M., Levy-Lahad, E., Klevit, R. E. & King, M. C. (2010). Mutations in the DBP-Deficiency Protein HSD17B4 Cause Ovarian Dysgenesis, Hearing Loss, and Ataxia of Perrault Syndrome. *Am J Hum Genet,* 87(2)**,** 282-8.

Quiros, P. M., Mottis, A. & Auwerx, J. (2016). Mitonuclear communication in homeostasis and stress. *Nat Rev Mol Cell Biol,* 17(4)**,** 213-26.

Schwarz, J. M., Cooper, D. N., Schuelke, M. & Seelow, D. (2014). MutationTaster2: mutation prediction for the deep-sequencing age. *Nat Methods,* 11(4)**,** 361-2.

Sickmann, A., Reinders, J., Wagner, Y., Joppich, C., Zahedi, R., Meyer, H. E., Schonfisch, B., Perschil, I., Chacinska, A., Guiard, B., Rehling, P., Pfanner, N. & Meisinger, C. (2003). The proteome of Saccharomyces cerevisiae mitochondria. *Proc Natl Acad Sci U S A,* 100(23)**,** 13207-12.

Sievers, F., Wilm, A., Dineen, D., Gibson, T. J., Karplus, K., Li, W., Lopez, R., McWilliam, H., Remmert, M., Soding, J., Thompson, J. D. & Higgins, D. G. (2011). Fast, scalable generation of high-quality protein multiple sequence alignments using Clustal Omega. *Mol Syst Biol,* 7**,** 539.

Sobreira, N., Schiettecatte, F., Valle, D. & Hamosh, A. (2015). GeneMatcher: a matching tool for connecting investigators with an interest in the same gene. *Hum Mutat,* 36(10)**,** 928-30.

Wang, Y., Singh, U. & Mueller, D. M. (2007). Mitochondrial genome integrity mutations uncouple the yeast Saccharomyces cerevisiae ATP synthase. *J Biol Chem,* 282(11)**,** 8228-36.

Warda, A. S., Freytag, B., Haag, S., Sloan, K. E., Gorlich, D. & Bohnsack, M. T. (2016). Effects of the Bowen-Conradi syndrome mutation in EMG1 on its nuclear import, stability and nucleolar recruitment. *Hum Mol Genet,* 25(24)**,** 5353-5364.

Yang, Y. P., Ting, W. C., Chen, L. M., Lu, T. L. & Bao, B. Y. (2017). Polymorphisms in MicroRNA Binding Sites Predict Colorectal Cancer Survival. *Int J Med Sci,* 14(1)**,** 53-57.

Chapter 7: Variants in mitochondrial ribosomal protein DAP3 are causative of Perrault syndrome without a defect of mitochondrial translation

Variants in mitochondrial ribosomal protein DAP3 are causative of Perrault syndrome without a defect of mitochondrial translation

Leigh A. M. Demain,[1,2] Jill E. Urquhart, [1,2] James O'Sullivan, [1,2] Jamie M. Ellingford, [1,2] Christian Beetz,[3] Walid Omara, [4] Liam M. Jones,[4] Robyn Bell,[4] Inna A. Belyantseva,[5] Melanie Barzik, [5] Monika Olahova,[6] Ruth Glasgow,[6] Simon G. Williams,[1,2] Sanjeev S. Bhaskar,[1,2] Emma M. Jenkinson,[1] Robert W. Taylor,[6] Thomas B. Friedman,[5] Kevin J. Munro,[7,8] Raymond T. O'Keefe,[4,] William G. Newman[1,2]

[1] Division of Evolution and Genomic Sciences, Faculty of Biology, Medicine and Health, School of Biological Sciences, University of Manchester, Manchester, UK

[2] Manchester Centre for Genomic Medicine, Central Manchester University Hospitals NHS Foundation Trust, Manchester, UK

[3] Department of Clinical Chemistry and Laboratory Medicine, Jena University Hospital, Jena 07745, Germany

[4] Division of Cellular & Molecular Function, Faculty of Biology, Medicine and Health, University of Manchester, Manchester, UK

[5] Laboratory of Molecular Genetics, National Institute on Deafness and Other Communication Disorders, National Institutes of Health, Bethesda, MD, USA

[6] Wellcome Centre for Mitochondrial Research, Institute of Neuroscience, Newcastle University, Medical School, Newcastle upon Tyne, UK

[7] School of Health Sciences, University of Manchester, Manchester, UK

[8] Central Manchester University Hospitals NHS Foundation Trust, Manchester Academic Health Science Centre, Manchester, UK

7.1. Abstract

Perrault syndrome is a rare autosomal recessive condition characterised by sensorineural hearing loss in both sexes and primary ovarian insufficiency in 46, XX karyotype females. Other features, most commonly neurological are present in some cases. Six genes have been associated with Perrault syndrome to date: *HSD17B4*, *HARS2*, *LARS2*, *CLPP*, *C10orf2* and *ERAL1,* the latter five of which function in mitochondrial translation. Here we have identified a novel Perrault syndrome gene, *DAP3*. The proband in this case was the only child of a non-consanguineous family. Whole exome sequencing identified a hemizygous variant *DAP3* c.1184G>A p.(Cys395Tyr) and large deletion encompassing the entire *DAP3* gene. *DAP3* encodes death associated protein 3 (DAP3), which was initially identified as a pro-apoptotic factor. DAP3 also functions as part of the 28S mitochondrial ribosomal subunit and has a role in mitochondrial fission through regulation of the Drp, the mitochondrial fission protein. When the yeast orthologue of DAP3, RSM23, is knocked out yeast rapidly lose their mitochondria. We localised endogenous Dap3 in the mouse organ of Corti. We saw little endogenous Dap3 localised to the mitochondria, with high levels of Dap3 seen in a diffuse cytoplasmic localisation. Not all cells showed Dap3 localisation which can be associated with cell damage. The patient fibroblasts did not show a mitochondrial translational defect suggesting the pathological mechanisms of this case of Perrault syndrome may differ from those of previously reported cases with defects of mitochondrial translation. Dysfunction in a non-mitochondrial translation function of DAP3, either mitochondrial dynamics or apoptosis, may explain the Perrault syndrome phenotype in this case. While mitochondrial dysfunction explains many cases of Perrault syndrome, the underlying pathology may not be the same in all cases.

7.2. Introduction

Perrault syndrome is a rare autosomal recessive condition which is characterised by sensorineural hearing loss (SNHL) in both sexes and primary ovarian insufficiency (POI) in 46, XX karyotype females (Pallister and Opitz 1979). Fertility in males is presumed to be normal (Newman et al. 1993-2016). Neurological features and dysmorphia can also present in some cases including; nystagmus, intellectual disability, ataxia, sensory motor neuropathy and marfanoid proportions (Fiumara et al. 2004;Jacob et al. 2007). Six genes are associated with Perrault syndrome to date: *HSD17B4* (MIM 233400) (Pierce et al. 2010), *HARS2* (MIM 614926) (Pierce et al. 2011), *LARS2* (MIM 615300) (Pierce et al. 2013), *CLPP* (MIM 614129) (Jenkinson et al. 2013), *C10orf2* (MIM 616138) (Morino et al. 2014) and *ERAL1* (MIM 607435) (Chatzispyrou et al. 2017). Of these genes, the latter five function in the mitochondrial translation pathway and it is likely most cases of Perrault syndrome are the result of mitochondrial dysfunction. Variants in *PRORP* (Chapter 5) and *ERAL1* (Chatzispyrou et al. 2017) have a generalised defect of mitochondrial translation. Here we present a single case of Perrault syndrome associated with a novel Perrault syndrome gene *DAP3*. The proband in this case has congenital hearing loss, POI and progressive late onset ataxia. Using whole exome sequencing we found the proband was hemizygous for a maternally inherited missense change, *DAP3* c.1184G>A p.(Cys395Tyr), *in trans* with a 135Kb deletion which included the whole *DAP3* gene.

DAP3 encodes death associated protein 3 (DAP3). DAP3 was initially identified as a pro-apoptotic factor but its exact role in apoptosis is disputed (Kissil et al. 1995;Mukamel and Kimchi 2004;Kim et al. 2007). siRNA repression of *DAP3* was shown to reduce cell sensitivity to apoptotic signals with over-expression of DAP3 shown to sensitise cells to apoptotic signals (Kim et al. 2007;Mukamel and Kimchi 2004). DAP3 localises predominantly to the mitochondrial matrix and has two known functions in mitochondria in addition to the role in apoptosis (Xiao et al. 2015). DAP3 is also known as mitochondrial 28S ribosomal Protein S29 (MRPS29) and is the GTPase subunit of the mitochondrial ribosomal 28S subunit, essential for mitochondrial translation (Cavdar Koc et al. 2001;Xiao et al. 2015). Knockout of the yeast *DAP3* orthologue RSM23 caused rapid mitochondrial loss (Berger et al. 2000). DAP3 also functions in mitochondrial fission via the phosphorylation of Drp1, a mitochondrial fission protein (Xiao et al. 2015). Knockout

of DAP3 has been shown to be embryonic lethal in mice, with mitochondria in these embryos showing morphological defects (Kim et al. 2007).

Irretrievable loss of mitochondrial function in a yeast RSM23 knockout might explain why we could not rescue the knockout with human DAP3. The expression of the human DAP3 gene in yeast resulted in a growth defect which was exacerbated by the variant DAP3 p.Cys395Tyr. Although hard to interpret given the lack of mitochondrial function, this suggests that the variant may be deleterious.

In the mouse organ of Corti we saw little endogenous Dap3 localised to mitochondria. High levels of Dap3 were seen in a diffuse cytoplasmic localisation, with not all cells affected equally. Some cells with high levels of Dap3 localisation appeared damaged. When overexpressed in the mouse organ of Corti Dap3 did localise to the mitochondria but overexpression of Dap3 did not seem to cause cell damage or the diffuse cytoplasmic localisation, suggesting the high level of endogenous Dap3 may be the result of, not the cause of, the cellular damage. We had previously seen that candidate Perrault syndrome genes showed distinctive localisation in the mouse organ of Corti, often to co-localising to regions of synapses and nerve fibres (Chapter 5 and 6). This distinctive localisation pattern was not seen for Dap3.

Unlike previously reported cases of Perrault syndrome the patient cells did not show a mitochondrial translational defect suggesting the mechanisms behind this case of Perrault syndrome may differ from those of previously reported cases (Chapter 5) (Chatzispyrou et al. 2017). The data suggests a defect of mitochondrial translation may not explain this case of Perrault syndrome, which is surprising given the essential role of DAP3 in the mitochondrial ribosome. Although it appears that most cases of Perrault syndrome result from mitochondrial dysfunction these data suggest that all cases may not have the same mitochondrial pathology.

7.3. Materials and Methods

7.3.1. Ethical approval

All patients provided written informed consent in accordance with local regulations. Ethical approval for this study was granted by the National Health Service Ethics Committee (16/WA/0017) and University of Manchester. The NIH Animal Use Committee

approved protocol 1263-15 to T.B.F. for mice.

7.3.2. Whole exome sequencing

Whole exome sequencing was performed on DNA extracted from lymphocytes from individual II-1. The Agilent Technologies, Santa Clara, CA, USA SureSelect Human All Exon V5 Panel was used for library preparation and sequencing was performed on the HiSeq 2500 Illumina, San Diego, CA, USA as previously described (Smith et al. 2014).

7.3.3. Identification and confirmation of the deletion

A 135Kb deletion encompassing the DAP3 gene was identified using the ExomeDepth v1.1.6 software package as previously described (Plagnol et al. 2012;Ellingford et al. 2017). Briefly the read depth around the area of the possible deletion was compared to a reference aggregated set of exome read depths for this region. The read depth was approximately 0.5 times the aggregated depth indicating a single allele deletion.

The fusion product and the breakpoint region of the deletion were confirmed in the proband by Sanger sequencing using the ABI big Dye v3.1 (Thermo Fisher Scientific Inc, Waltham, MA, USA) sequencing technology. The primers were designed around areas of slight polymorphism between the two segmental duplications where the deletion breakpoints were situated.

7.3.4. Primers for the amplification of the fusion product

DAP3_BP-SeqInt_f 5’ TGGCAGAGTTAGCCGATGC 3’

DAP3_BP-SeqInt_r 5’ CCATTGGGAATGGATTTGACC 3’

7.3.5. Confirmation of the missense variant

The variant was confirmed in the proband and unaffected mother via Sanger sequencing using the ABI big Dye v3.1 (Thermo Fisher Scientific Inc, Waltham, MA, USA) sequencing technology. Primer sequences are available in the appendix.

7.3.6. Prediction of variant pathogenicity

The following resources were used in the prediction of variant pathogenicity;

Exome Variant Server (EVS) (NHLBI GO Exome Sequencing Project (ESP)), http://evs.gs.washington.edu/EVS/

ExAC (Exome Aggregation Consortium (ExAC)), http://exac.broadinstitute.org/

Polyphen2 (Adzhubei et al. 2010), http://genetics.bwh.harvard.edu/pph2/

SIFT (Kumar et al. 2009), http://sift.jcvi.org/

Mutation Taster (Schwarz et al. 2014), http://www.mutationtaster.org/

7.3.7. Conservation mapping

Sequences were mapped using Clustal Omega (http://www.ebi.ac.uk/Tools/msa/clustalo/) (Sievers et al. 2011). The reference sequences are as follows; Human, NP_001186778.1. Chimpanzee, ENSPTRT00000002635.4. Dog, ENSCAFG00000016941. Rat, NP_001011950.2. Mouse, NP_001158005.1. Chicken, ENSGALG00000019796. Xenopus, ENSXETT00000063437.1. Zebrafish, NP_001092207.1. Tetraodon, ENSTNIT00000021716.1. Fruitfly , NP_523811.1 *Caenorhabditis elegans*, NP_496280.1. *Saccharomyces cerevisiae*, NP_011386.2.

7.3.8. Dermal fibroblast Cell culture

Patient dermal fibroblasts were cultured in Eagle's minimal essential medium supplemented with 10% (v/v) foetal calf serum, 1 × non-essential amino acids, 1 mm sodium pyruvate and 50 μg/ml uridine, humidified at 37 °C and 5% CO_2.

7.3.9. Dermal fibroblast Cell culture for stress conditions

The cells were cultured under the conditions above prior to seeding. Cells were seeded at 4,000 cells per well in a TPP 96 well plate with modified glucose media. After 24 hours, the media was removed from all wells. Modified glucose media was added to half the wells of each cell line, and galactose media added to the other half. The plate was imaged, and confluence measured, every 2 hours for a period of 5 days using an Incucyte live cell imager.

7.3.10. Cell lyses and western blotting

Cultured fibroblasts were harvested and lysed in 50 mm Tris-HCl pH 7.5, 130 mm NaCl, 2 mm $MgCl_2$, 1 mm phenylmethanesulfonyl fluoride (PMSF), 1% Nonidet P-40 (v/v) and 1

× EDTA free protease inhibitor cocktail (Pierce). Protein lysates (40 µg) were separated according to size on 12% gels by sodium dodecyl sulphate—polyacrylamide gel electrophoresis (SDS-PAGE) and electrophoretically transferred to a PVDF membrane (Immobilon-P). Immunoblotting was performed using primary and HRP-conjugated secondary antibodies.

7.3.11. Immunoblotting

The following primary antibodies were used for immunoblotting: NDUFA9 (Molecular Probes, Invitrogen, Carlsbad, CA, USA, A21344), NDUFB8 (Abcam, Cambridge, UK, ab110242), SDHA (MitoSciences, Eugene, OR, USA, MS204), UQCRC2 (Abcam, Cambridge, UK, ab14745), COX1 (Abcam, Cambridge, UK, ab14705) and COX2 (Molecular Probes, Invitrogen, Carlsbad, CA, USA, A6404), DAP3 (Abcam, Cambridge, UK, ab11928), MRPL3 (Invitrogen, Carlsbad, CA, USA, PA5-18107), MRPS26 (Proteintech, Manchester, UK, 15989-1-AP), MRPS27 (Proteintech, Manchester, UK, 17280-1-AP), beta-actin (Sigma, A1978). All antibodies were diluted 1:1000 in 5% milk in TBS-Tween, except beta-actin which was diluted 1:10 000

HRP-conjugated anti-mouse or anti-rabbit secondary antibodies were used (P0260 and P0399 respectively; Dako, Glostrup, Denmark). Chemiluminescence ECL Prime Kit (Amersham, GE Healthcare, Little Chalfont, UK) and ChemiDocMP Imaging System (Bio-Rad, Hercules, CA, USA) were used for signal detection and Image lab 4.0.1 (Bio-Rad, Hercules, CA, USA) software for analysis.

7.3.12. Yeast Strains

The *Saccharomyces cerevisiae* strains used in this report are shown in Table 7.1. Yeast cells were grown in standard YPD media or on standard YPD agar plates unless otherwise indicated. The strain containing the plasmid was grown on Synthetic defined (SD)-URA plates. YP-Ethanol, YP-Acetate and YP-Glycerol plates were used as a non-fermentable carbon source. Yeast were grown at 30°C unless otherwise indicated. Plasmids were transformed into yeast using the high efficiency yeast transformation method (Gietz and Schiestl 2007).

Strain	Genotype
BY4742	*MATα: ura3Δ0; leu2Δ0; his3Δ1; lys2Δ0*
BY4742_RSM23Δ	BY4742 YGL129C::KanMX4
RSM23Δ_ Vector	BY4742 RSM23Δ + p426GPD
RSM23Δ_ DAP3	BY4742 RSM23Δ + p426GPD-DAP3
RSM23Δ_ DAP3C395Y	BY4742 RSM23Δ + p426GPD-DAP3C395Y
YPH500	MATα ura3-52 lys2-801_amber ade2-101_ochre trp1-Δ63 his3-Δ200 leu2-Δ1
YPH500_RSM23Δ	YPH500_ YGL129C::KanMX4

Table 7.1. *Saccharomyces cerevisiae* yeast strains used in this report.

7.3.13. Yeast expression Plasmids

The plasmid p426GPD-DAP3 was created by cloning the Human ORF cDNA (NM_001199849) of DAP3 into a yeast expression plasmid with a strong promotor p426GPD (ATCC, Manassas, VA, USA - 87361). Briefly the Human ORF cDNA was amplified from human cDNA.

The p426GPD vector was digested with HindIII. The ORF was inserted into the digested vector using Gibson assembly molecular cloning technique (Gibson et al. 2009). The plasmid p426GPD-DAP3C395Y was created by mutagenizing the plasmid p426GPD-DAP3 as previously described (Kunkel et al. 1987) with the synthetic oligonucleotide DAP3_p.Cys395Tyr (see 2.12.2 for oligonucleotide sequence). All plasmids were extracted using the GenElute HP Plasmid miniprep Kit (Sigma-Aldrich, St. Louis, MO, USA) and inserts were confirmed via Sanger sequencing using the ABI big Dye v3.1 (Thermo Fisher Scientific Inc, Waltham, MA, USA) sequencing technology. Plasmid maps and sequencing primers are available in Appendix I.

7.3.14. Primers for the amplification of Human ORF cDNA (NM_001199849)

hDAP3_FWD: CTGCAGGAATTCGATATCAATGATGCTGAAAGGAATAACAAGGCT

hDAP3_REV: GGTCGACGGTATCGATATTAGAGGTAGGCACAGTGCCG

7.3.15. Yeast knockout in the YPH500 strain

The deletion module containing the selectable marker, KanMX4, was amplified by PCR from a plasmid template. The primers contained sequence complementary to the deletion module at the 3' end and sequence complementary to the sequencing flanking the appropriate yeast gene at the 5' end for homologous recombination. The PCR product was assessed my agarose gel electrophoresis as in section 2.7.3 and purified using the QIAquick PCR Purification Kit (Qiagen, Hilden, Germany) according to manufacturer instruction. 35-50 µl of the deletion module was transformed into yeast using the High efficiency transformation protocol (Gietz and Schiestl 2007). The transformed cells were plated onto YPD and incubated overnight at 30°C. Colonies were transferred to selective medium and incubated for 2-3 days at 30°C. Gene knockout was confirmed using PCR and agarose gel electrophoresis.

7.3.16. HeLa Cell culture

HeLa cells were cultured in DMEM media with 10% (v/v) foetal bovine serum (FBS) and 2mM Glutamax at 37°C in 10% CO_2.

7.3.17 Cell transfection and staining

HeLa cells were transfected with the plasmid Dap3-EGFP using Lipofectamine 3000 (Thermo Fisher Scientific Inc, Waltham, MA, USA). Briefly $10x4^5$ cells were seeded into each well of a six well plate in the morning for a transfection in the afternoon. When attached, the cells were transfected according to the manufacturer protocol using 1.6-1.75 ug of plasmid DNA per 2.5ul of lipofetamine 3000 reagent. The transfected cells were incubated overnight at 37°C with 10% CO_2. For the imaging of cells using the confocal microscope HeLa cells were seeded onto glass bottom plates prepared with fibronectin. The cells were incubated for approximately 4 hours (3-5) until optimum cell density and attachment was achieved then fixed in the following solution for 15 minutes at room temperature, 4% paraformaldehyde, 2% sucrose in 1X PBS. After fixation the cells were washed 3 times in 1X PBS and stored at 4°C until staining.

Cells were permeabilised and blocked in the 0.2% Triton X and 10% normal goat serum in PBS solution at room temperature. After permeabilisation/blocking the samples were washed 3 times in PBS. Cells were incubated with the primary antibodies (Table 7.2) in

blocking solution (blocking solution - 2% normal goat serum in PBS) for 1-2 hours at room temperature. Samples were washed 3 times in PBS. The samples were incubated in Secondary antibody solution (Phalloidin Alexa 647, Hoechst (2.5µg/ml) and secondary antibody in blocking solution (Table 7.2) for 2 hours at room temperature with gentle agitation. After incubation with the secondary antibody solution the cell were washed 3 times in PBS and stored at 4°C in PBS to be imaged within 24 hours. Cells were imaged using a LSM780 confocal microscope (Zeiss Inc, Oberkochen, Germany Inc) equipped with 63X, 1.4 N.A. objective.

Antibody Name	**Supplier and details**	**Concentration/dilution used**
DAP3	DAP3 mouse monoclonal antibody - BDbiosciences, San Jose, CA,USA - Cat no. 610660	HeLa Cells -0.5µg/ml, organ of Corti – 2.5µg/ml
TOM20	TOM20 rabbit polyclonal antibody - Santa Cruz Biotechnology, Dallas, TX, USA - Cat no. sc-11415	HeLa Cells -0.4µg/ml, organ of Corti – 2µg/ml
Cytoskeletal staining	Alexa fluor 647 phalloidin or rhodamine phalloidin, Thermo Fisher Scientific Inc, Waltham, MA, USA	HeLa Cells - 1:50, organ of Corti- 1:100
Mouse secondary antibody	Goat anti-mouse - Alexa fluor 488, Thermo Fisher Scientific Inc, Waltham, MA, USA	HeLa Cells - 1:250, organ of Corti 1:400
Rabbit secondary antibody	Goat anti-rabbit Alexa fluor 568, Thermo Fisher Scientific Inc, Waltham, MA, USA	HeLa Cells - 1:250, organ of Corti 1:400

Table 7.2. Antibody details and concentrations.

Details and concentrations for the antibodies and staining reagents used in this report.

7.3.18. EGFPpPlasmids

The plasmid Dap3-EGFP was created by cloning the mouse ORF cDNA Dap3 (BC019566) into a C-terminal pEGFP-N1 vector (Clontech, Mountain View, CA, USA-discontinued). Briefly the Mouse ORF cDNA minus the stop codon was amplified using the primers below from the plasmid 4235517 (Dharmacon, Lafayette, CO, USA - MMM1013-202765774).

DAP3_infusion_1 TACCGGACTCAGATCTATGCTGACAGGAATAACAA

DAP3_infusion_2 CGCGGTACCGTCGACTGCAGCAGCGAGGCACAGAGC

The pEGFP-N1 vector was digested with BglII and PstI. The ORF was inserted into the digested vector using the In-Fusion HD Plus EcoDry Cloning System (Clontech, Mountain View, CA, USA) according to manufacturer instructions.

All inserts were confirmed via Sanger sequencing using the ABI big Dye v3.1 (Thermo Fisher Scientific Inc, Waltham, MA, USA) sequencing technology before use. Plasmid maps and sequencing primers are available in appendix I and appendix II.

7.3.19. Localisation of Dap3 in the mouse organ of Corti

The NIH Animal Use Committee approved protocol 1263-15 to T.B.F. for mice. C57/BJ6 mice at ages Postnatal day 3 (P3), P10, P14 and P30 were euthanised, the cochlear capsule was removed and fixed with 4% paraformaldehyde in PBS for 2 hours. The samples were microdissected and the organ of Corti was permeabilised with 1% Triton X-100 in PBS for 30 min followed by three 10 min washes with 1X PBS. Nonspecific binding sites were blocked with 5% normal goat serum and 2% BSA in PBS for 1 h at room temperature. Samples were incubated for 2 h with primary antibodies (Table 7.2) in blocking solution, followed by several rinses with PBS. Samples were incubated with secondary antibodies (Table 7.2) for 30 min. Samples were washed several times with PBS and were mounted with ProLongGold Antifade staining reagent with DAPI (Molecular Probes, Invitrogen, Carlsbad, CA, USA) and examined using LSM780 confocal microscope (Zeiss Inc, Oberkochen, Germany Inc) equipped with 63X, 1.4 N.A. objective.

7.3.20. Gene Gun transfection of organ of Corti

Inner-ear sensory epithelium cultures were prepared from organ of Corti of P1 C57Bl/6 mice and transfected with plasmid DNA using the gene gun method as described in Belyantseva (2016). Briefly the organ of corti spiral was dissected in Leibowitz cell culture medium (Invitrogen, Carlsbad, CA, USA) and was attached to a glass-bottom Petri dish (MatTek, Ashland, MA, USA) coated with rat tail collagen and maintained at 37°C and 5% CO_2 in DMEM supplemented with 7% FBS for 1–3 days. Cultures were then transfected by using a Helios gene gun (Bio-Rad, Hercules, CA, USA). Gold particles of 1.0-µm diameter (Bio-Rad, Hercules, CA, USA) were coated with Dap3-EGFP plasmid DNA at a ratio of 2 µg

of plasmid DNA to 1 mg of gold particles and precipitated onto the inner wall of Tefzel tubing, which was cut into individual cartridges containing approximately 1µg of plasmid DNA. Samples were bombarded with the gold particles from one cartridge per culture by using 120 psi of helium. After an additional 8 hours to 4 days in culture, samples were fixed in 4% paraformaldehyde and stained using the same method as the tissue samples above.

7.4. Results

7.4.1. Clinical Report

The proband is the only child of non-consanguineous British parents (Fig. 7.1). The mother of the proband is unaffected, the father is deceased from a condition unrelated to Perrault syndrome. The proband was born at 40 weeks and spent 2 weeks intensive care because of hypoxia at birth. By the age of 1 year profound SNHL was noted which was initially believed to be caused by hypoxia. She communicates effectively by lip reading. At 14 years of age the proband presented with primary amenorrhea with absent secondary sexual characteristics, raised gonadotrophins. Ovarian biopsy showed a small vestigial uterus and streak ovaries with ovarian stroma and no follicles. The proband received hormone replacement therapy. The diagnosis was initially Turner syndrome which was revised to Perrault syndrome when the proband was found to have a 46,XX karyotype Recently the proband presented with progressive late onset ataxia but is still able to walk unaided. She has also reported intermittent episodes of dizziness and nausea. The proband has short stature but has no dysmorphic features.

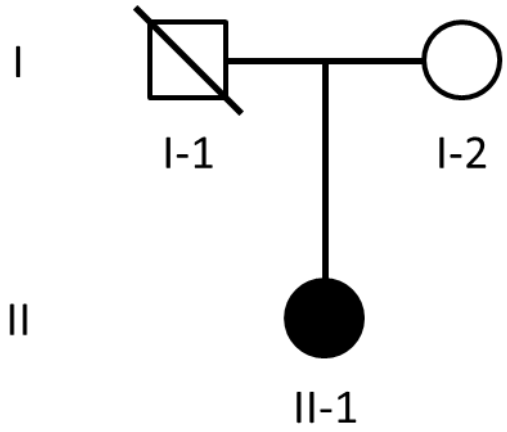

Figure 7.1. Pedigree of the family with Perrault syndrome

Filled icon indicates the affected individual.

7.4.2. Identification of the variant *DAP3* c.1184G>A p.(Cys395Tyr)

Whole exome sequencing was performed on the proband as previously detailed (Smith et al. 2014). No putative pathogenic variants were identified in known Perrault syndrome genes. The data was filtered to exclude variants seen more than once in our in house database of over 500 exomes and variants seen with a frequency of >1% in EVS (NHLBI GO Exome Sequencing Project (ESP)), ExAC (Exome Aggregation Consortium (ExAC)) and dbSNP (Sherry et al. 2001). An autosomal recessive model was applied and heterozygous variants with no additional rare variants were also excluded as well as variants in highly variable genes such as HLA genes (appendix III). Using prediction software and assessment of potential gene function the homozygous variant *DAP3* c.1184G>A p.(Cys395Tyr) (Accession- NM_001199849) was selected as the most likely cause of Perrault syndrome in this individual. Candidate variants and a list of highly variable genes excluded are available in appendix III. The variant *DAP3* c.1184G>A p.(Cys395Tyr) was confirmed as homozygous in the proband and as heterozygous in the unaffected mother by Sanger sequencing. A sample was not available from the father.

DAP3 c.1184G>A p.(Cys395Tyr) is absent from EVS and dbSNP. It has been seen once as a heterozygous variant in a European (non-Finnish) population in ExAC and Gnomad (Lek et al. 2016). *DAP3* c.1184G>A p.(Cys395Tyr) was predicted to be deleterious by Polyphen2

(0.996) (Adzhubei et al. 2010) , Mutation Taster (0.999) (Schwarz et al. 2014) and SIFT(0) (Kumar et al. 2009). *DAP3* encodes Death association protein 3 (DAP3) which was identified as a pro-apoptotic factor but also has roles in mitochondrial fission, and most relevant to Perrault syndrome, is an essential protein of the mitochondrial ribosome (Kissil et al. 1995;Cavdar Koc et al. 2001;Xiao et al. 2015). DAP3 is therefore a key component of the proposed Perrault syndrome pathway of mitochondrial translation.

7.4.3 Identification of a 135Kb deletion encompassing *DAP3*.

Given the rarity of Perrault syndrome and the fact the family is non-consanguineous it was thought unlikely that the ultra-rare variant *DAP3* c.1184G>A p.(Cys395Tyr) was homozygous in the proband and instead was potentially hemizygous *in trans* with a deletion. Whole exome depth coverage analysis was performed as previously described (Ellingford et al. 2017;Plagnol et al. 2012). Reduced exome depth coverage was found surrounding the *DAP3* region and the data suggested that this individual was heterozygous for a large deletion encompassing the region of chr1:155,581,680-155,717,258 (GRCh37.p8). There are two segmental duplications located at chr1:155573392-155587902 and chr1:155711167-155723605 (hg19). It was thought that non-allelic homologous recombination had occurred between these duplications resulting in the deletion seen in the exome data. To verify this deletion, PCR was performed with the primers designed around a region where a number of bases differed between the segmental duplications. This PCR approach meant the fusion product would be identifiable as it would contain unique variants from the 5' and 3' segmental duplications in the same sequence. The fusion product (Fig. 7.2A) was sequenced and was 478bp in length (full sequence in appendix III).This sequencing narrowed down the breakpoint of the recombination to chr1:155747068-155747546 and chr1:155611487-155611965. The deleted region is approximately 135kb and includes the entire *DAP3* gene as well as *YY1AP1* and part of *MST01*. There were no variants found in either *YY1AP1* or *MST01* in the exome data. It appears in the proband a non-allelic homologous recombination event produces a complete loss of one copy of *DAP3*. As a paternal sample was not available we cannot confirm whether this deletion is paternally inherited or *de novo*.

The variant *DAP3* c.1184G>A p.(Cys395Tyr) should be the only allele expressed in the proband. The residue DAP3 Cys395 is relatively well conserved (Fig. 7.2A) with only

chicken and fruitfly showing an alternate residue at this loci, which is not glycine in either case. The residue is not located in the GTP or nucleotide binding regions of DAP3 but is located in a possible prenylation sequence, CAYL, with the cysteine the residue being modified (Cavdar Koc et al. 2001). Prenylation adds lipids to the C-terminus of a protein, making it hydrophobic, and is thought to be important for the attachment of proteins to lipid membranes and protein-protein interactions (Wang and Casey 2016). It is possible that the substitution of cysteine at residue 395 for glycine removes a prenylation site which may affect the interaction of DAP3 with a membrane or binding partner. This CAYL site was shown not to be prenylated in bovine ribosomal mitochondria under normal metabolic conditions (Cavdar Koc et al. 2001) but may be modified under different physiological conditions.

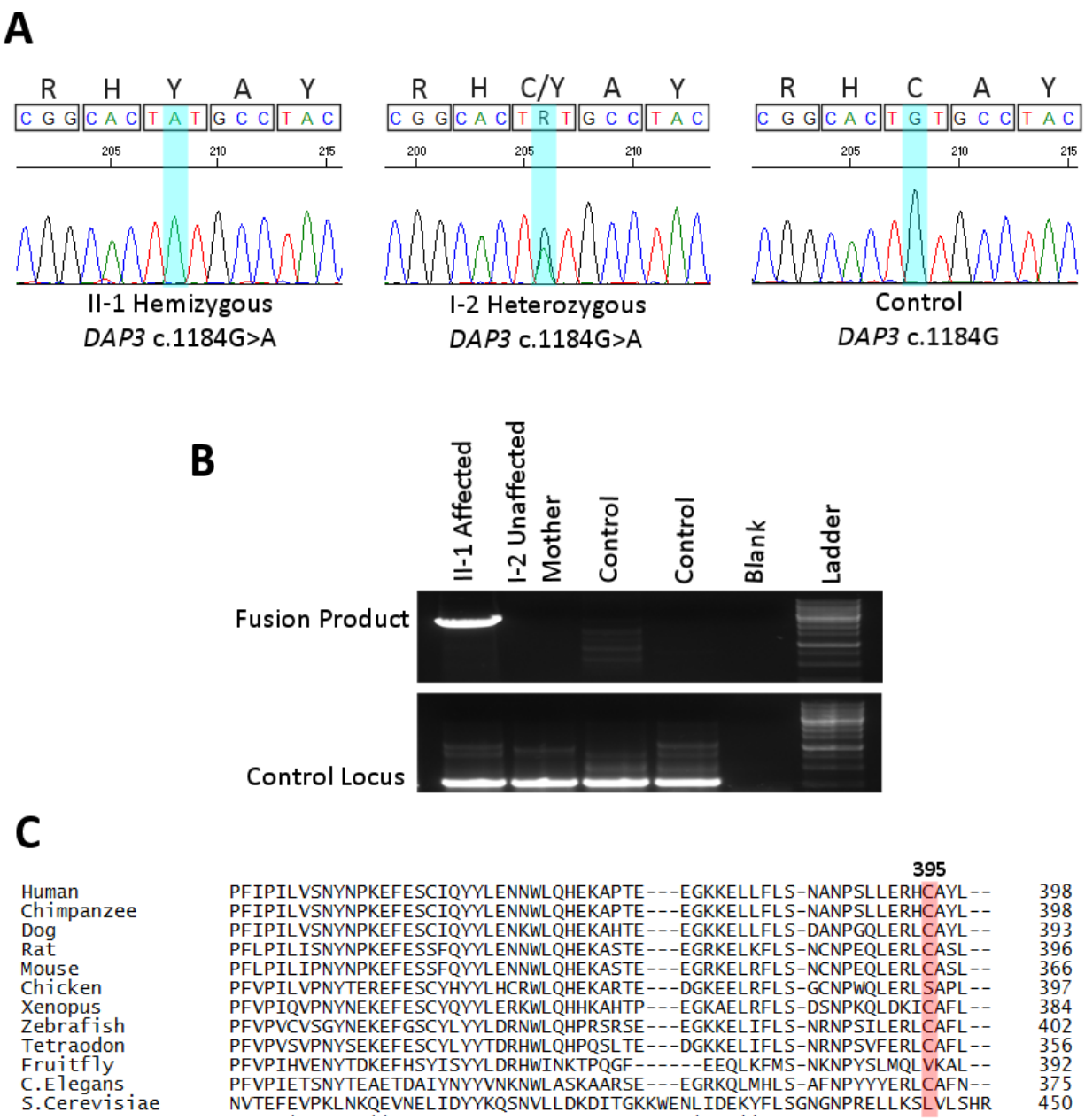

Figure 7.2. The proband is hemizygous for a the variant *DAP3* c.1184G>A p.(Cys395Tyr)

A) Sanger sequencing traces for the position *DAP3* c.1184. The proband is hemizygous for the variant *DAP3* c.1184G>A (NM_001199849), her unaffected mother is heterozygous for the variant and the control is wildtype at position c.1184. The blue box indicates *DAP3* c.1184. B) Fusion product for the large 135Kb deletion. The fusion product is seen in the proband but not in her unaffected mother or the control samples. The control locus verified the quality of the DNA samples. C) The conservation of *DAP3* p.C395 in multiple species. The residue corresponding to the human residue p.C395 is highlighted in red.

7.4.4. Patient fibroblasts do not show depletion of DAP3 or diminution of components of the mitochondrial oxidative phosphorylation pathway.

The mitochondrial encoded subunits of the oxidative phosphorylation (OXPHOS) pathway have been shown to be reduced in patients with Perrault syndrome with variants in *PRORP* (chapter 5) and *ERAL1* (Chatzispyrou et al. 2017) indicating defects of mitochondrial translation. As DAP3 has a vital role in the mitochondrial ribosome we performed western blots on patient dermal fibroblasts to assess the steady state levels of DAP3 and components of the OXPHOS pathway. Surprisingly there appeared to be no reduction in either DAP3 or the subunits of the OXPHOS pathway in the proband (Fig. 7.3). The single remaining copy of *DAP3* is therefore able to maintain physiologically normal levels of DAP3 and it is unlikely that haploinsufficiency is contributing to the Perrault syndrome phenotype in this patient. The steady state levels of both mitochondrial encoded components of the OXPHOS complex such as COXII and COXIII as well as nuclear encoded components such as SDHA do not show differences from the control samples indicating mitochondrial translation is not affected by the variant in DAP3 p.C395Y.

Two components of the mitochondrial 28S small ribosomal subunit were also assessed. The bands for MRPS26 are faint and hard to interpret but the steady state levels of MRPS27, which is a predicted interaction partner of DAP3 (Cavdar Koc et al. 2001), are not reduced.

There did appear to be some increase in CORE2 in patient cells and in MRPL3. CORE2 (also known as Ubiquinol-Cytochrome-C Reductase Complex Core Protein 2) is a nuclear encoded subunit of complex III, MRPL3 is a component of the mitochondrial large ribosomal subunit. Both are nuclear encoded genes but not all nuclear encoded genes show increased steady state protein levels. The reason for the increase in these two proteins is unclear but it is unlikely that this increase in CORE2 and MRPL3 levels is a compensational increase of mitochondrial load as theorised in patients with variants in *PRORP* (Chapter 5).

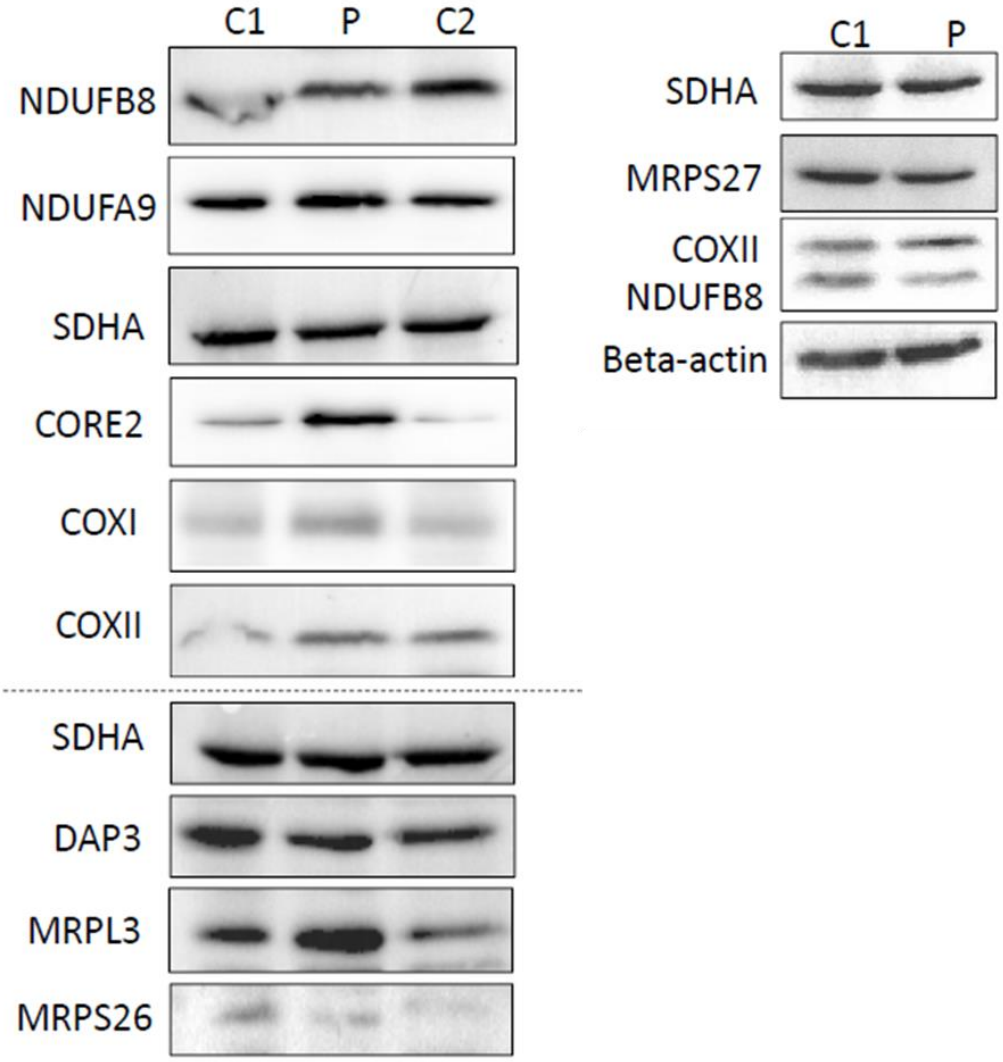

Figure 7.3. Patient cells do not show any reduction in DAP3 or mitochondrial encoded components of the OXPHOS pathway.

Western blot analysis of DAP3, proteins of the five oxidative phosphorylation complexes and mitochondrial ribosomal proteins. Included are two control samples (C1 and C2) and the patient sample (P), II-1.

7.4.5. Patient Dermal fibroblasts do not show any growth defects in response to stress

Defects of the OXPHOS pathway can produce a growth reduction in cells under stress conditions (Hofhaus et al. 1996). We considered if there was an OXPHOS defect in this patient that was only apparent under stress conditions. We assessed the growth of patient fibroblasts in comparison to control fibroblasts under stress conditions. Cells grown in modified glucose media were either transferred to modified galactose media (stress conditions) or maintained in glucose media and growth over 5 days compared (Fig. 7.4).

In glucose media the patient cells showed similar growth to the control samples. In the stress conditions (galactose media) the patient cells showed slightly better growth than the control cells. Therefore, the patient fibroblasts do not have a growth defect in stress conditions re-enforcing that there is no OXPHOS deficiency in the patient.

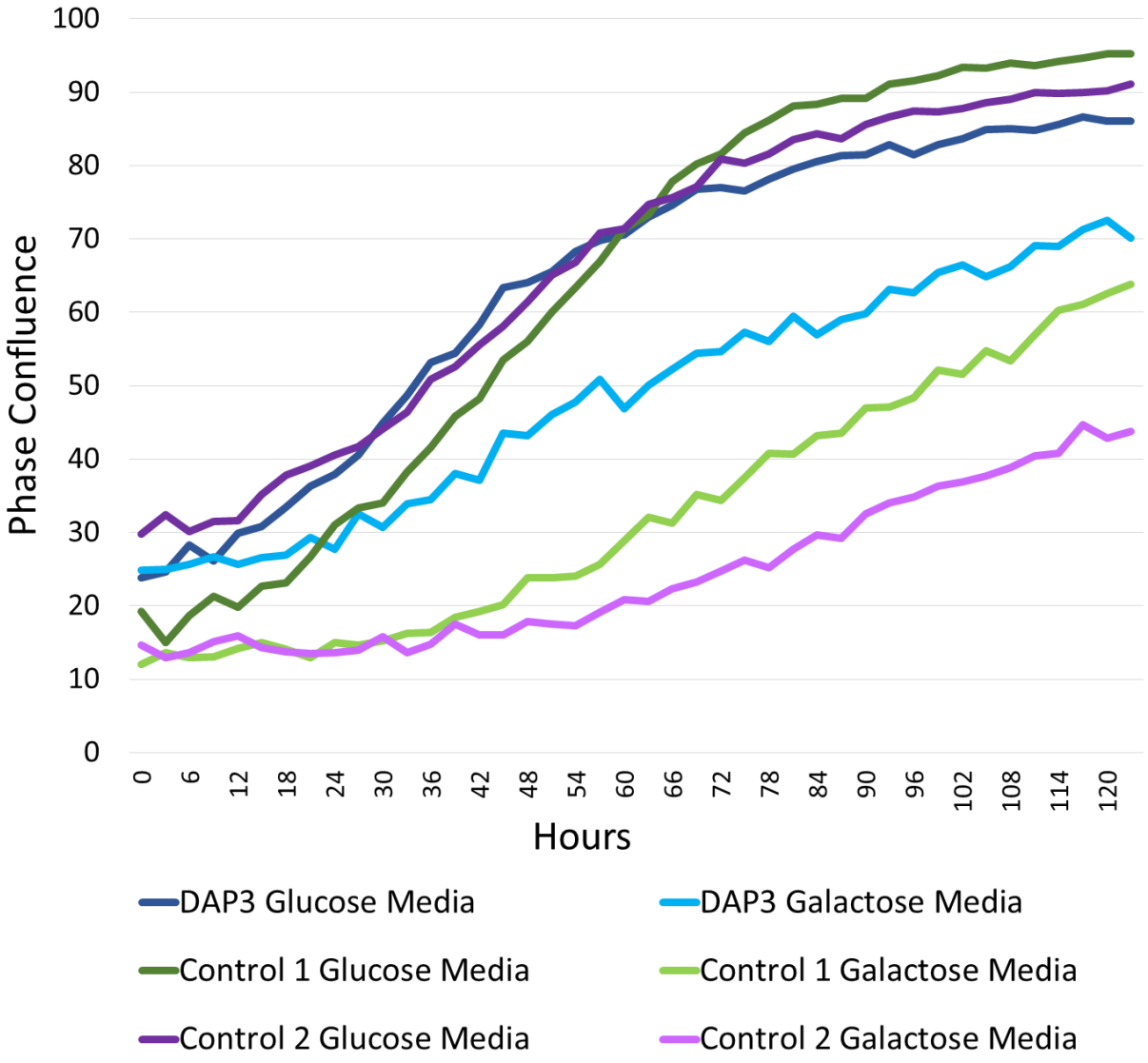

Figure 7.4. Patient cells do not exhibit a stress induced growth defect

A growth curve of fibroblasts under normal (glucose media) and stress conditions (galactose media). Samples labelled DAP3 are patient samples. Samples were assessed over 5 days with confluence measured at the times (hours) indicated on the X-axis.

7.4.6. Knockout of the yeast orthologue of DAP3, RSM23, causes the rapid loss of mitochondria

To assess the effect of the variant DAP3 p.Cys395Tyr we planned to use yeast complementation assays. It has been shown that the human gene complements the yeast orthologue, RSM23 (Berger et al. 2000). We found that knockout of the yeast RSM23 did not affect growth on normal YPD media but the strain was not viable on a non-

fermentable carbon source, which forces yeast to use mitochondria for respiration (Fig. 7.5). The mitochondrial defect in the knockout is concordant with previous results (Berger et al. 2000).

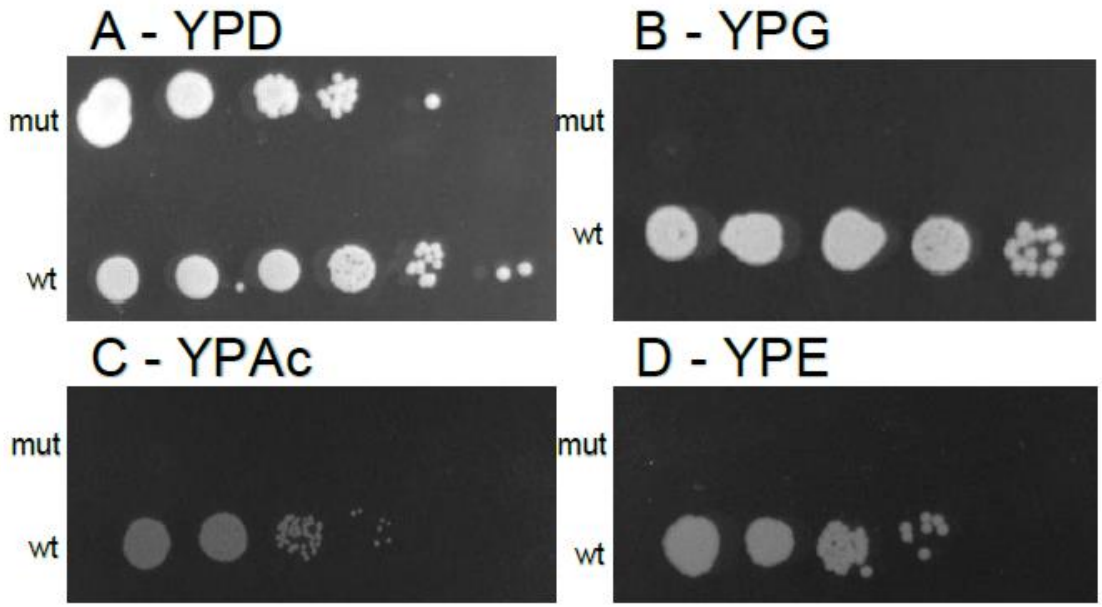

Figure 7.5. The yeast strain BY4742_RSM23Δ shows a growth defect on a non-fermentable carbon sources.

Growth competency analysis of wild type BY4742 (wt) and BY4742_RSM23Δ (mut) yeast on (A) fermentable glucose (YPD) as well as (B) non-fermentable glycerol (YPG), (C) acetate (YPAc) and (D) ethanol (YPE) carbon sources. Yeast cultures were grown overnight then 1:10 serial dilutions spotted onto the indicated plates.

To assess the impact of the variant DAP3 p.C395Y we complemented the yeast knockout RSM23 with the human gene DAP3 and the variant DAP3 p.C395Y cloned into yeast expression vectors. These transformed strains were not viable on a non-fermentable carbon source most likely because the knockout strain has already irretrievably lost mitochondrial function. When grown on standard media yeast transformed with the human DAP3 gene showed growth defects (Fig. 7.6) with the variant C395Y having a greater negative effect on growth than the wild type human DAP3. These results are interesting but difficult to interpret given the lack of functioning mitochondria in this strain. To assess the rate of mitochondrial loss we knocked out the RSM23 gene in a strain with an ADE2 variant, YPH500. Strains with ADE2 variants produce red pigment if

mitochondrial function is normal (Dorfman 1969). The YPH500_RSM23Δ yeast were white indicating that mitochondrial loss occurred very rapidly after gene knockout.

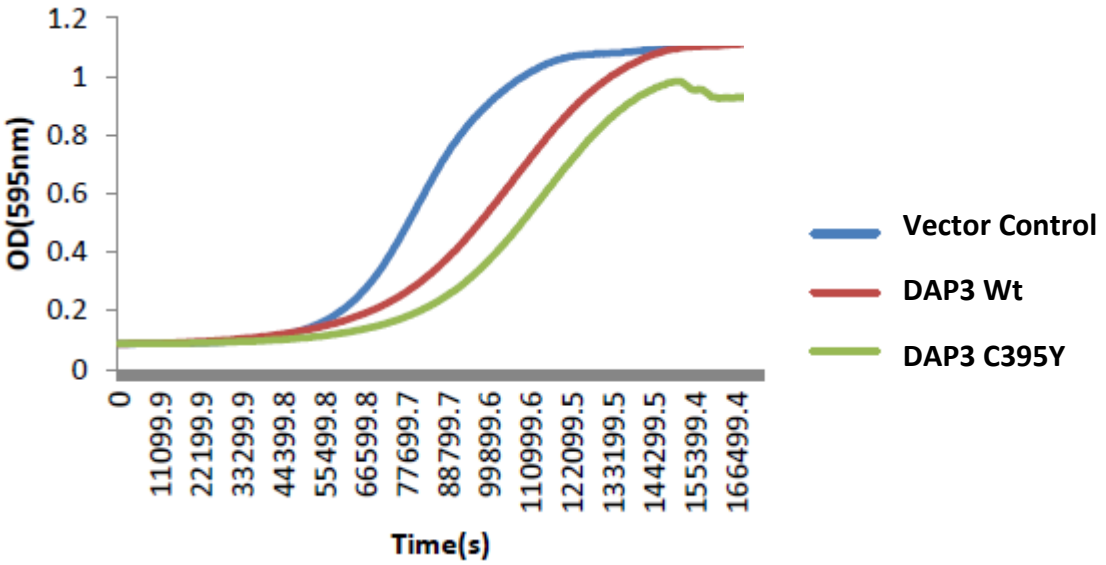

Figure 7.6. The strains RSM23Δ_DAP3 and RSM23Δ_ DAP3C395Y show growth defects in standard media

Growth curves for the yeast strains RSM23Δ_Vector (Vector control), RSM23Δ_ DAP3 (DAP3 Wt) and RSM23Δ_ DAP3C395Y (DAP3 C395Y) in YPD media. Optical Density (OD measurements were performed over 48 hours.

7.4.7. DAP3 localises to mitochondria in HeLa cells but overexpression has no effect on mitochondrial morphology

We localised endogenous DAP3 in HeLa cells (Fig. 7.7A) and saw, as in previous reports, DAP3 localised to mitochondria (Xiao et al. 2015;Mukamel and Kimchi 2004). Unlike previous reports there was no apparent cytosolic pool of DAP3 (Miyazaki et al. 2002;Miyazaki and Reed 2001). To assess overexpression of DAP3 we produced a C-terminal EGFP tagged plasmid containing the mouse cDNA for Dap3 (Accession-BC019566). The C-terminal tag was chosen so not to disrupt targeting sequences located at the N-terminus of the protein. We transfected Hela cells with this construct (Fig. 7.7b). The construct localised to the mitochondria with some diffuse additional staining in the cytoplasm and nucleus, likely as a result of overexpression. The construct Dap3-EGFP did not appear detrimental to HeLa cells nor did it noticeably affect the morphology of the mitochondria in the transfected cells. DAP3 overexpression is not detrimental to HeLa

which concordant with the results of Xiao et al. (2015) but conflicts with the results of Mukamel and Kimchi (2004) who found overexpression of DAP3 caused apoptosis in cells. One possible reason given for the differing results around DAP3 overexpression was varying expression levels between the constructs used (Xiao et al. 2015).

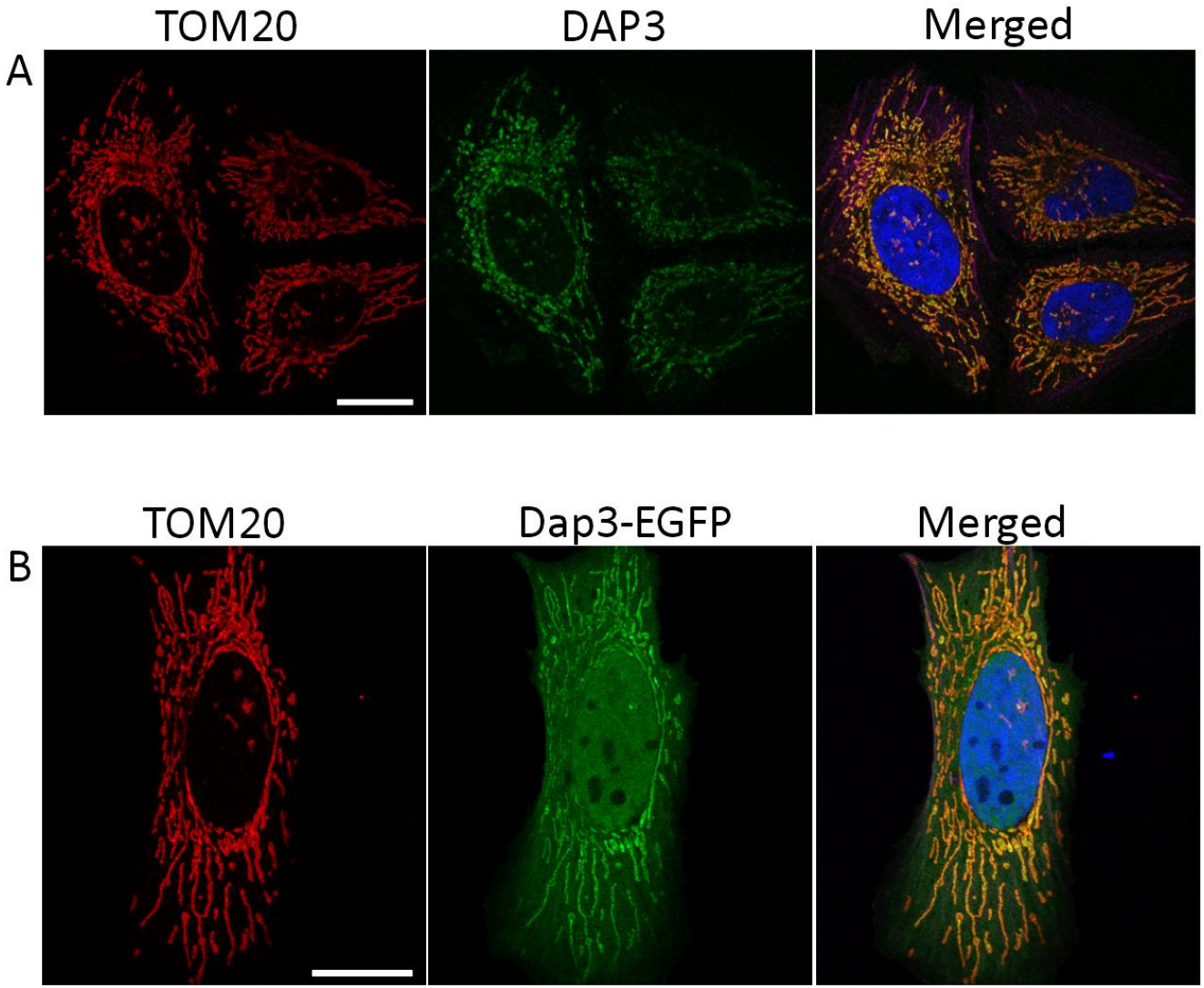

Figure 7.7. DAP3 localises to mitochondria in HeLa cells.

A) Confocal fluorescence microscopy of HeLa cells showing endogenous localisation of DAP3 (green). Cells were counterstained with Hoechst (nuclear marker, blue) to visualise the nuclei, TOM20 (mitochondrial marker, red) to visualise the mitochondria. B) Confocal fluorescence microscopy of HeLa cells showing localisation of Dap3-EGFP (green). Cells were counterstained with Hoechst (nuclear marker, blue) to visualise the nuclei, TOM20 (mitochondrial marker, red) to visualise the mitochondria. The scale bar is 10µm.

Two Perrault syndrome genes, NOP14 and PRORP, have shown very specific but similar localisation in the organ of Corti, which was distinct from their localisation in HeLa cells (Chapter 5 and 6). We were interested to see if Dap3 had any unexpected localisation in the mouse organ of Corti. The organs of Corti from C57/BJ6 mice at postnatal day 3 (P3) – P30 were immunofluorescently stained to reveal the localisation of endogenous Dap3. The samples were also counterstained with a mitochondrial marker (TOM20, mitochondrial membrane protein), and DAPI (fluorescent stain for double-stranded DNA that highlights the cell nucleus).

We saw little endogenous Dap3 localised to the mitochondria in the mouse organ of Corti at multiple ages (P3-P30). We did see high expression of DAP3 in certain cells which may be associated with cell damage or stress. At P3 (Fig. 7.8a) we saw high levels of Dap3 in individual cells, with not all cells showing this pattern of localisation. The Dap3 localisation was seen in the body of the cell and the cells appeared to be damaged (Fig. 7.8b) with misshapen nuclei. This localisation of Dap3 was seen also at P10 and after the onset of hearing (Ehret 1976) at P14 (Fig. 7.9).

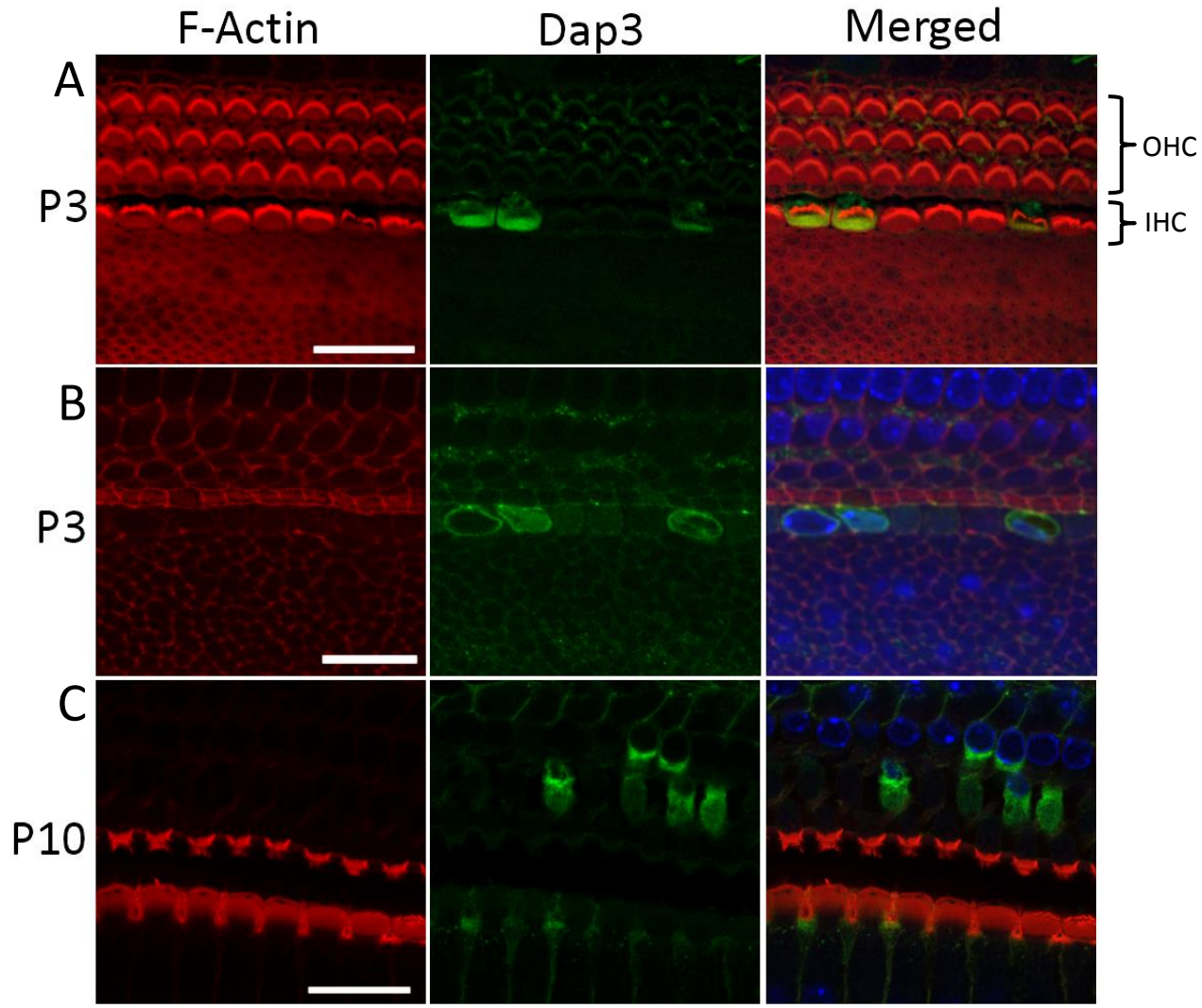

Figure 7.8. Dap3 shows irregularly distributed localisation in the mouse organ of Corti, prior to the onset of hearing.

Confocal fluorescence microscopy optical sections of the whole mount organ of Corti samples from C57/BJ6 mice at postnatal days 3, 10 (P3 and P10 respectively) showing localisation of Dap3 (green). All samples were counterstained with DAPI (nuclear DNA marker, blue) to visualize the nuclei of hair cells and rhodamine-phalloidin (F-actin, red) to visualise the cytoskeleton and auditory stereocilia. Panels A and B shows different focal planes within a sample to visualise both the stereocilia (A) cell bodies (B). The rows of outer hair cells (OHC) and inner hair cells (IHC) are indicated in panel A. The scale bar is 20µm.

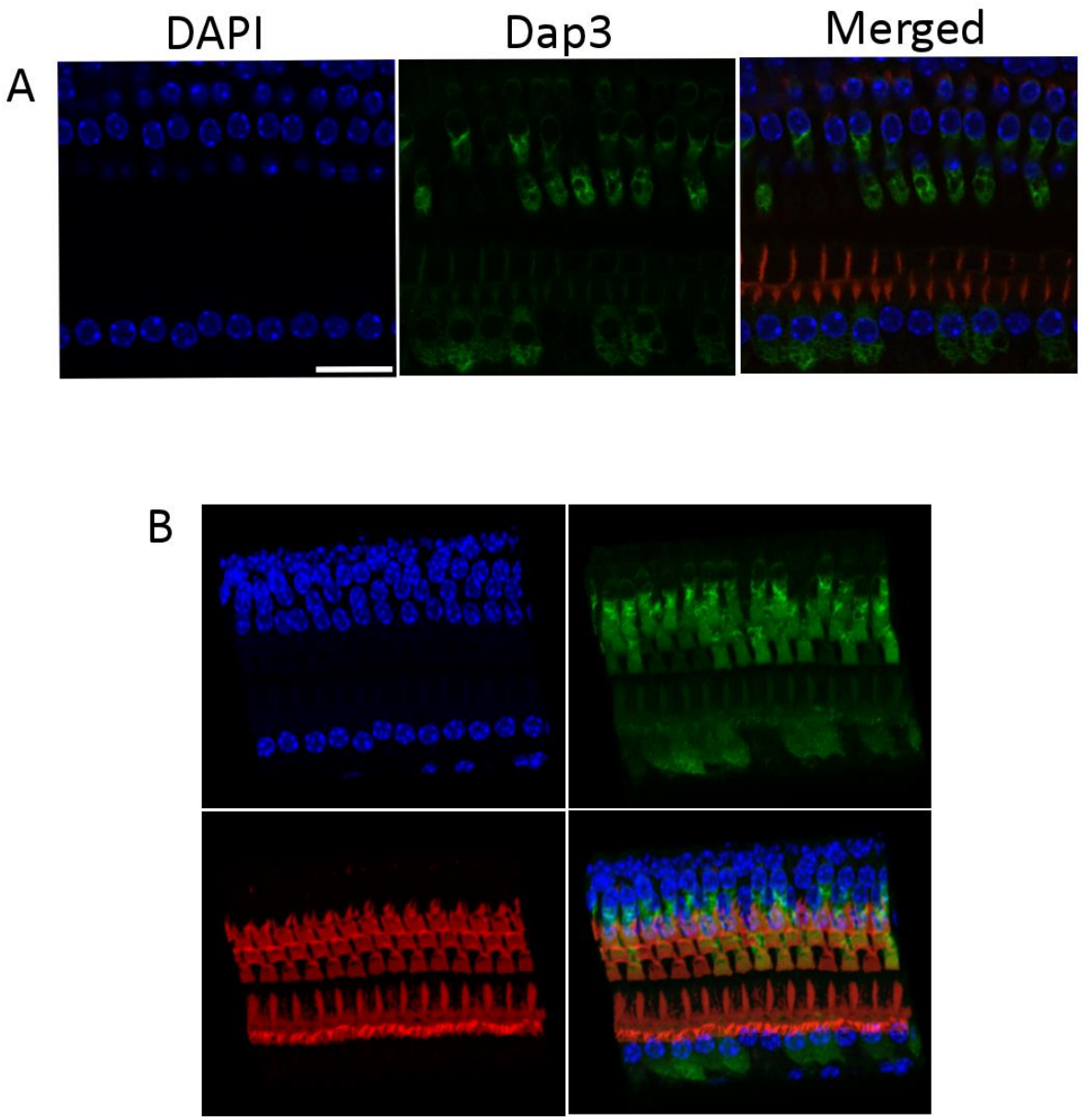

Figure 7.9. Dap3 shows irregularly distributed localisation in the mouse organ of Corti after the onset of hearing.

Confocal fluorescence microscopy optical sections of the whole mount organ of Corti samples from a C57/BJ6 mouse at postnatal days 14 (P14) showing localisation of Dap3 (green). The sample was counterstained with DAPI (nuclear DNA marker, blue) to visualize the nuclei of hair cells and rhodamine-phalloidin (F-actin, red) to visualise the cytoskeleton and auditory stereocilia. Panel A shows a single optical section and B shows a 3D rendering of multiple optical sections from the sample from panel A. The scale bar is 20µm.

To examine the overexpression of Dap3 in the organ of Corti we used a gene gun to transfect cells with Dap3-EGFP. Unlike with the endogenous protein we saw a similar localisation pattern in the transfected cells as the HeLa cells. In transfected and HeLa cells Dap3-EGFP co-localised with mitochondrial marker TOM20 with some diffuse staining in the cell body. We also saw that there were no signs of cellular damage in the transfected cells suggesting like in the HeLa cells that the overexpression of Dap3-EGFP alone is not enough to induce cell damage.

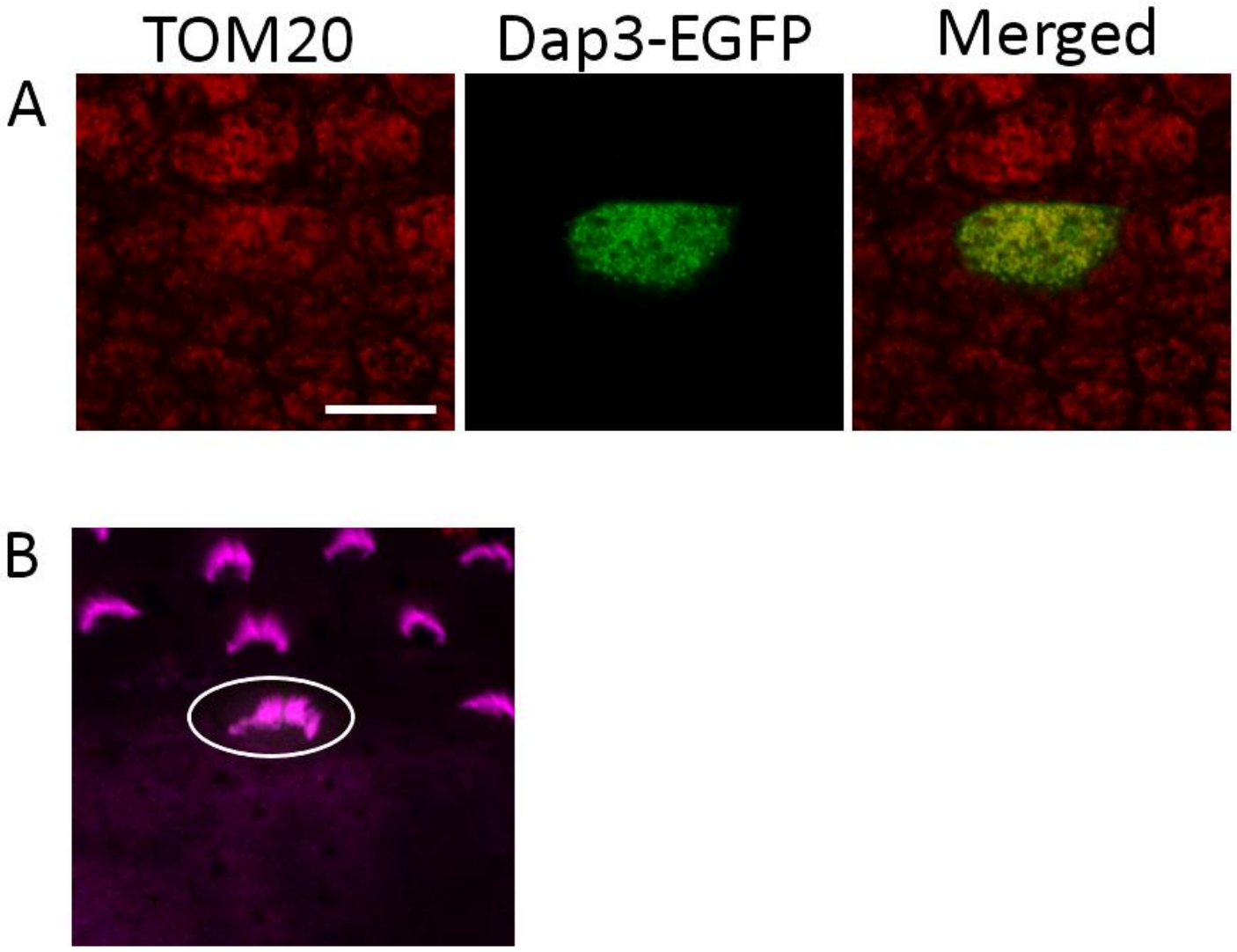

Figure 7.10. Dap3-EGFP localises to the mitochondria of hair cells and the overexpression of Dap3 does not cause cell damage.

Confocal fluorescence microscopy optical section of the whole mount organ of Corti sample from a C57/BJ6 mouse at P3 which was gene gun transfected with the plasmid Dap3-EGFP (green). The sample was counterstained with TOM20 (mitochondrial marker, red) and phalloidin (cytoskeletal marker, pink). Panel A and B show different focal planes within a sample to visualise the cell body (A) and the stereocilia (B) The transfected cell is circled in B and is an outer hair cell. The scale bar is 10µm.

7.5. Discussion

Here we have identified a putative novel Perrault syndrome gene, *DAP3*, in a single affected individual. After filtering the exome data for rare variants, in line with the extremely low incidence of Perrault syndrome, we identified the variant *DAP3* c.1184G>A p.(Cys395Tyr) as the most promising candidate gene for the cause of Perrault syndrome in this patient. This variant was subsequently found to be in *trans* to a 135Kb deletion encompassing the whole *DAP3* gene. This is the first large whole gene deletion associated with Perrault syndrome. Previous variants have included frameshift variants and smaller deletions which have caused a similar the loss of protein product (Pierce et al. 2013;Theunissen et al. 2016). It is possible large deletions in *trans* with other variants may explain some of the genetically unresolved cases of Perrault syndrome. Deletions are difficult to detect using next generation sequencing panels and whole exome sequencing unless specific data analysis techniques are applied. This case suggests it may be worth examining the whole exome data of genetically unresolved cases of Perrault syndrome for copy number variations.

DAP3 was identified initially as a pro-apoptotic factor (Kissil et al. 1995) and has been reported to act as a mediator of apoptosis through the extrinsic Tumour Necrosis Pathways and Interferon pathways (Kissil et al. 1995;Miyazaki and Reed 2001;Miyazaki et al. 2004); and the intrinsic pathway (Xiao et al. 2015). The exact role of DAP3 in any of these pathways has not been resolved. It has been demonstrated that the loss of DAP3 desensitises cells to death stimuli (Kissil et al. 1995) and overexpression of DAP3 can cause apoptosis (Mukamel and Kimchi 2004).

DAP3 has two roles additional to its function in apoptosis: as part of the mitochondrial ribosome (Cavdar Koc et al. 2001) and as a mediator of mitochondrial fission (Xiao et al. 2015;Mukamel and Kimchi 2004). DAP3, also known as mitochondrial ribosomal protein small subunit 29 (MRPS29), is the GTPase subunit of the mitochondrial 28S small ribosomal subunit (Cavdar Koc et al. 2001). The exact role of DAP3 in the mitoribosome is unknown but it has been suggested that Dap3 is involved in tethering the ribosome to the mitochondrial inner matrix (O'Brien et al. 2005;Tang et al. 2009) and possibly interacts with mitochondrial translational initiation factor 3 (Haque et al. 2011). The knockdown of

DAP3 causes defects of mitochondrial translation in cells (Xiao et al. 2015) and reduces oxygen consumption (Kim et al. 2007).

The exact role of DAP3 in mitochondrial fission is also unknown but it seems to modulate mitochondrial fission by altering the activation of the mitochondrial fission protein, dynamin related protein 1 (Drp1) (Xiao et al. 2015). Drp1 causes mitochondrial fission by forming spirals around the mitochondrial membrane and constricting until a membrane scission event occurs (Hoppins et al. 2007). The phosphorylation of Drp1 at Ser^{637} is an important modification that regulates its role in mitochondrial fission with de-phosphorylation by calcineurin resulting in Drp1 recruitment to the mitochondria and activation of fission (Cereghetti et al. 2008), and phosphorylation by cyclic AMP-dependant kinase (PKA) inactivating Drp1 (Chang and Blackstone 2007). Knockdown of DAP3 decreased Drp1 phosphorylation at Ser^{637} and resulted in an increase in cells with fragmented mitochondria. The fragmented mitochondria phenotype was rescued by the addition of a PKA activator suggesting DAP3 modulates mitochondrial fission via the PKA-calcineurin pathway (Xiao et al. 2015).

DAP3 has a vital and conserved role in mitochondrial function (Berger et al. 2000;Kim et al. 2007;Xiao et al. 2015). When we overexpressed the human DAP3 gene in the BY4742_RSM23Δ strain it could not rescue mitochondrial function indicating that these yeast have permanently loss their mitochondria. It has been shown that knockout of RSM23 in yeast causes the loss of mitochondrial DNA (Berger et al. 2000) which would account for the permanent loss of mitochondria. The human gene had a dominant negative effect on cell growth which was exacerbated by the variant DAP3 p Cys395Tyr. Although this suggests the variant seen in the proband may be deleterious caution should be used in interpreting these results as these cells had no mitochondrial function and both the wild type and variant human genes were overexpressed.

When we localised endogenous DAP3 in Hela cells we saw only mitochondrial localisation and not cytoplasmic localisation as had been previously reported (Miyazaki et al. 2002). There have been conflicting reports about the localisation of DAP3 (Berger et al. 2000), as the methods and the cell and tissue types used differed (Miyazaki et al. 2002). When we overexpressed Dap3-EGFP in HeLa cells we saw some cytoplasmic localisation which is likely because of overexpression. This cytoplasmic staining upon overexpression was seen previously in HeLa cells when we transfected them with the Nop14-TurboGFP construct.

The overexpression of Dap3-EGFP did not result in changes to mitochondrial morphology or any apparent cellular damage. Our results regarding the overexpression of DAP3 in cells are concordant with the work of (Xiao et al. 2015) but are contradictory to others who found that the overexpression of DAP3 caused fragmented mitochondria (Mukamel and Kimchi 2004). Varying levels of construct overexpression was suggested to account for the differences seen with DAP3 overexpression (Xiao et al. 2015). DAP3 overexpression in vectors with different promotor strengths could help resolve this contradiction. There is no consensus on the localisation or results of overexpression of DAP3 but the knockdown or knockout of DAP3 is always reported as deleterious (Kim et al. 2007;Berger et al. 2000;Kissil et al. 1995).

For previous Perrault candidate genes, *PRORP* and *NOP14* we have seen distinct localisation patterns in the mouse organ of Corti which appear similar and may have some localisation to, or relationship with, the synapses and nerve fibres of the auditory hair cells (chapter 5 and 6). We do not see a similar pattern of endogenous Dap3 localisation. Dap3 shows very little endogenous localisation to the mitochondria. Dap3 does show high levels of diffuse cytoplasmic staining in an irregular pattern with not all cells having localisation. This localisation may be linked to cell damage and apoptosis which is concordant with the role of Dap3 as a pro-apoptotic factor (Kissil et al. 1995;Miyazaki and Reed 2001). There is some increase in the number of cells with high Dap3 at P10 and P14 in comparison to P3. This increased number of cells with high Dap3 could be explained by damage from hypoxia as mice over the age of P9 were euthanized using CO_2 while mice aged P9 or below are resistant to the effects of CO_2 and were euthanized using alternate methods.

When organ of corti explants were transfected with Dap3-GFP we saw mitochondria localisation showing Dap3 can localise to the mitochondria in hair cells if expressed. We could theorise that as overexpression of DAP3 did not induce cell damage the cytoplasmic localisation may be the result of release or production of DAP3 upon cellular damage rather than the expression DAP3 itself causing damage.

The variant *DAP3* c.1184G>A p.(Cys395Tyr) does not cause a defect of mitochondrial translation in the patient fibroblasts. The cells did not show reductions in either mitochondrial or nuclear encoded components of the OXPHOS pathway or any reduction in the level of DAP3. There was no growth defect in patient fibroblasts under stress

conditions which would have indicated an OXPHOS defect (Hofhaus et al. 1996). No loss in proteins of the mitochondrial ribosome was found. It appears the variant *DAP3* c.1184G>A p.(Cys395Tyr) it may affect a non-translational function of DAP3. The *DAP3* c.1184G>A p.(Cys395Tyr) variant therefore likely affects the pro-apoptotic or mitochondrial fission functions of DAP3. When mitochondrial translation was inhibited there was no effect on mitochondrial morphology (Xiao et al. 2015) suggesting that the function of DAP3 in the ribosome may be discrete from its function in modulating mitochondrial fission. The pro-apoptotic role of DAP3 may be performed by a cytosolic pool of DAP3 (Miyazaki et al. 2002). Our data did not provide evidence as to which function of Dap3 may be affected. It would be informative to examine the mitochondrial morphology of patient cells and to test patient cell responses to pro-apoptotic factors to further define the pathology in this case of Perrault syndrome. A reasonable theory to explore is that the variant DAP3 p.Cys395Tyr abolishes a prenylation site which is important for a function of DAP3 which is discrete from its mitochondrial ribosomal function. This prenylation linked function of Dap3 could explain why none of the DAP3 isolated from the bovine ribosome was prenylated (Cavdar Koc et al. 2001). If the theory that the CAYL prenylation site which is important for a function of DAP3 which is discrete from its mitochondrial ribosomal function is correct the variant DAP3 p.Cys395Tyr could help us explore the non-translational roles of DAP3 in more detail.

We have submitted this case to GeneMatcher, an online tool which connects individuals with interest in the same gene to solve unsolved exomes (Sobreira et al. 2015). As Perrault syndrome is so rare it is often difficult to find a second family for new genes. Using GeneMatcher (https://genematcher.org/) we can contact with both researchers and clinicians who have a patient with putative pathogenic variants in *DAP3*. Additional individuals with pathogenic variants in *DAP3* may have a more severe phenotype as we have seen with variants in *LARS2* and *CLPP* (Riley et al. 2016;Theunissen et al. 2016).

The data we have generated suggests the molecular mechanisms of Perrault syndrome may differ between this case of Perrault syndrome and previously reported cases highlighting the importance of investigating the molecular mechanisms of Perrault syndrome. Our work demonstrates that while Perrault syndrome is a disease of mitochondrial dysfunction this is not limited to the dysfunction of mitochondrial translation as previously theorised. This potential difference in molecular mechanisms for

Perrault syndrome makes genetic diagnosis particularly important as this proband showed no clinical features which would differentiate her case from other cases of Perrault syndrome. If there are different molecular categories of Perrault syndrome then correct molecular diagnosis might aid clinical intervention or prognosis.

References

Adzhubei, I. A., Schmidt, S., Peshkin, L., Ramensky, V. E., Gerasimova, A., Bork, P., Kondrashov, A. S. & Sunyaev, S. R. (2010). A method and server for predicting damaging missense mutations. *Nat Methods,* 7(4)**,** 248-9.

Belyantseva, I. A. (2016). Helios® Gene Gun-Mediated Transfection of the Inner Ear Sensory Epithelium: Recent Updates. *In:* Sokolowski, B. (ed.) *Auditory and Vestibular Research: Methods and Protocols.* New York, NY: Springer New York.

Berger, T., Brigl, M., Herrmann, J. M., Vielhauer, V., Luckow, B., Schlondorff, D. & Kretzler, M. (2000). The apoptosis mediator mDAP- 3 is a novel member of a conserved family of mitochondrial proteins. *J Cell Sci,* 113(20)**,** 3603-3612.

Cavdar Koc, E., Ranasinghe, A., Burkhart, W., Blackburn, K., Koc, H., Moseley, A. & Spremulli, L. L. (2001). A new face on apoptosis: death-associated protein 3 and PDCD9 are mitochondrial ribosomal proteins. *FEBS Lett,* 492(1-2)**,** 166-70.

Cereghetti, G. M., Stangherlin, A., Martins de Brito, O., Chang, C. R., Blackstone, C., Bernardi, P. & Scorrano, L. (2008). Dephosphorylation by calcineurin regulates translocation of Drp1 to mitochondria. *Proc Natl Acad Sci U S A,* 105(41)**,** 15803-8.

Chang, C. R. & Blackstone, C. (2007). Cyclic AMP-dependent protein kinase phosphorylation of Drp1 regulates its GTPase activity and mitochondrial morphology. *J Biol Chem,* 282(30)**,** 21583-7.

Chatzispyrou, I. A., Alders, M., Guerrero-Castillo, S., Zapata Perez, R., Haagmans, M. A., Mouchiroud, L., Koster, J., Ofman, R., Baas, F., Waterham, H. R., Spelbrink, J. N., Auwerx, J., Mannens, M. M., Houtkooper, R. H. & Plomp, A. S. (2017). A homozygous missense mutation in ERAL1, encoding a mitochondrial rRNA chaperone, causes Perrault syndrome. *Hum Mol Genet,* 26(13)**,** 2541-2550.

Dorfman, B. Z. (1969). The isolation of adenylosuccinate synthetase mutants in yeast by selection for constitutive behavior in pigmented strains. *Genetics,* 61(2)**,** 377-89.

Ehret, G. (1976). Development of absolute auditory thresholds in the house mouse (Mus musculus). *J Am Audiol Soc,* 1(5)**,** 179-84.

Ellingford, J. M., Campbell, C., Barton, S., Bhaskar, S., Gupta, S., Taylor, R. L., Sergouniotis, P. I., Horn, B., Lamb, J. A., Michaelides, M., Webster, A. R., Newman, W. G., Panda, B., Ramsden, S. C. & Black, G. C. (2017). Validation of copy number variation analysis for next-generation sequencing diagnostics. *Eur J Hum Genet,* 25(6)**,** 719-724.

Exome Aggregation Consortium (ExAC). *Exome Aggregation Consortium (ExAC)* [Online]. Cambridge, MA. Available: http://exac.broadinstitute.org [Accessed 10/08 2017].

Fiumara, A., Sorge, G., Toscano, A., Parano, E., Pavone, L. & Opitz, J. M. (2004). Perrault syndrome: Evidence for progressive nervous system involvement. *Am J Med Genet,* 128A(3)**,** 246-249.

Gibson, D. G., Young, L., Chuang, R. Y., Venter, J. C., Hutchison, C. A., 3rd & Smith, H. O. (2009). Enzymatic assembly of DNA molecules up to several hundred kilobases. *Nat Methods,* 6(5)**,** 343-5.

Gietz, R. D. & Schiestl, R. H. (2007). High-efficiency yeast transformation using the LiAc/SS carrier DNA/PEG method. *Nat Protoc,* 2(1)**,** 31-4.

Haque, M. E., Koc, H., Cimen, H., Koc, E. C. & Spremulli, L. L. (2011). Contacts between mammalian mitochondrial translational initiation factor 3 and ribosomal proteins in the small subunit. *Biochim Biophys Acta,* 1814(12)**,** 1779-84.

Hofhaus, G., Johns, D. R., Hurko, O., Attardi, G. & Chomyn, A. (1996). Respiration and growth defects in transmitochondrial cell lines carrying the 11778 mutation associated with Leber's hereditary optic neuropathy. *J Biol Chem,* 271(22)**,** 13155-61.

Hoppins, S., Lackner, L. & Nunnari, J. (2007). The machines that divide and fuse mitochondria. *Annu Rev Biochem,* 76**,** 751-80.

Jacob, J. J., Paul, T. V., Mathews, S. S. & Thomas, N. (2007). Perrault Syndrome with Marfanoid Habitus in Two Siblings. *J Pediatr Adolesc Gynecol,* 20(5)**,** 305-308.

Jenkinson, E. M., Rehman, A. U., Walsh, T., Clayton-Smith, J., Lee, K., Morell, R. J., Drummond, M. C., Khan, S. N., Naeem, M. A., Rauf, B., Billington, N., Schultz, J. M., Urquhart, J. E., Lee, M. K., Berry, A., Hanley, N. A., Mehta, S., Cilliers, D., Clayton, P. E., Kingston, H., Smith, M. J., Warner, T. T., Black, G. C., Trump, D., Davis, J. R. E., Ahmad, W., Leal, S. M., Riazuddin, S., King, M. C., Friedman, T. B. &

Newman, W. G. (2013). Perrault syndrome is caused by recessive mutations in CLPP, encoding a mitochondrial ATP-dependent chambered protease. *Am J Hum Genet,* 92(4)**,** 605-613.
Kim, H.-R., Chae, H.-J., Thomas, M., Miyazaki, T., Monosov, A., Monosov, E., Krajewska, M., Krajewski, S. & Reed, J. C. (2007). Mammalian dap3 is an essential gene required for mitochondrial homeostasis in vivo and contributing to the extrinsic pathway for apoptosis. *FASEB J,* 21(1)**,** 188.
Kissil, J. L., Deiss, L. P., Bayewitch, M., Raveh, T., Khaspekov, G. & Kimchi, A. (1995). Isolation of DAP3, a novel mediator of interferon-gamma-induced cell death. *J Biol Chem,* 270(46)**,** 27932-6.
Kumar, P., Henikoff, S. & Ng, P. C. (2009). Predicting the effects of coding non-synonymous variants on protein function using the SIFT algorithm. *Nat Protoc,* 4(7)**,** 1073-81.
Kunkel, T. A., Roberts, J. D. & Zakour, R. A. (1987). Rapid and efficient site-specific mutagenesis without phenotypic selection. *Methods Enzymol,* 154**,** 367-382.
Lek, M., Karczewski, K. J., Minikel, E. V., Samocha, K. E., Banks, E., Fennell, T., O'Donnell-Luria, A. H., Ware, J. S., Hill, A. J., Cummings, B. B., Tukiainen, T., Birnbaum, D. P., Kosmicki, J. A., Duncan, L. E., Estrada, K., Zhao, F., Zou, J., Pierce-Hoffman, E., Berghout, J., Cooper, D. N., Deflaux, N., DePristo, M., Do, R., Flannick, J., Fromer, M., Gauthier, L., Goldstein, J., Gupta, N., Howrigan, D., Kiezun, A., Kurki, M. I., Moonshine, A. L., Natarajan, P., Orozco, L., Peloso, G. M., Poplin, R., Rivas, M. A., Ruano-Rubio, V., Rose, S. A., Ruderfer, D. M., Shakir, K., Stenson, P. D., Stevens, C., Thomas, B. P., Tiao, G., Tusie-Luna, M. T., Weisburd, B., Won, H. H., Yu, D., Altshuler, D. M., Ardissino, D., Boehnke, M., Danesh, J., Donnelly, S., Elosua, R., Florez, J. C., Gabriel, S. B., Getz, G., Glatt, S. J., Hultman, C. M., Kathiresan, S., Laakso, M., McCarroll, S., McCarthy, M. I., McGovern, D., McPherson, R., Neale, B. M., Palotie, A., Purcell, S. M., Saleheen, D., Scharf, J. M., Sklar, P., Sullivan, P. F., Tuomilehto, J., Tsuang, M. T., Watkins, H. C., Wilson, J. G., Daly, M. J., MacArthur, D. G. & Exome Aggregation, C. (2016). Analysis of protein-coding genetic variation in 60,706 humans. *Nature,* 536(7616)**,** 285-91.
Miyazaki, T., Kim, H.-R., Godzik, A., Krajewski, S. & Reed, J. C. (2002). Response to 'Interaction of DAP3 and FADD only after cellular disruption'. *Nat Immunol,* 3(1)**,** 4-5.
Miyazaki, T. & Reed, J. C. (2001). A GTP-binding adapter protein couples TRAIL receptors to apoptosis-inducing proteins. *Nat Immunol,* 2(6)**,** 493-500.
Miyazaki, T., Shen, M., Fujikura, D., Tosa, N., Kim, H. R., Kon, S., Uede, T. & Reed, J. C. (2004). Functional role of death-associated protein 3 (DAP3) in anoikis. *J Biol Chem,* 279(43)**,** 44667-72.
Morino, H., Pierce, S. B., Matsuda, Y., Walsh, T., Ohsawa, R., Newby, M., Hiraki-Kamon, K., Kuramochi, M., Lee, M. K., Klevit, R. E., Martin, A., Maruyama, H., King, M. C. & Kawakami, H. (2014). Mutations in Twinkle primase-helicase cause Perrault syndrome with neurologic features. *Neurology,* 83(22)**,** 2054-61.
Mukamel, Z. & Kimchi, A. (2004). Death-associated protein 3 localizes to the mitochondria and is involved in the process of mitochondrial fragmentation during cell death. *J Biol Chem,* 279(35)**,** 36732-8.
Newman, W. G., Friedman, T. B. & Conway, G. S. (1993-2016). Perrault Syndrome. *In:* Pagon, R. A., Adam, M. P., Ardinger, H. H., Wallace, S. E., Amemiya, A., Bean, L. J. H., Bird, T. D., Fong, C. T., Mefford, H. C., Smith, R. J. H. & Stephens, K. (eds.) *GeneReviews(R).* Seattle (WA).
NHLBI GO Exome Sequencing Project (ESP). *Exome Variant Server* [Online]. Seattle, WA. Available: http://evs.gs.washington.edu/EVS/ [Accessed 09/07 2015].
O'Brien, T. W., O'Brien, B. J. & Norman, R. A. (2005). Nuclear MRP genes and mitochondrial disease. *Gene,* 354**,** 147-51.
Pallister, P. D. & Opitz, J. M. (1979). The Perrault syndrome: autosomal recessive ovarian dysgenesis with facultative, non-sex-limited sensorineural deafness. *Am J Med Genet,* 4(3)**,** 239-46.
Pierce, S. B., Chisholm, K. M., Lynch, E. D., Lee, M. K., Walsh, T., Opitz, J. M., Li, W., Klevit, R. E. & King, M. C. (2011). Mutations in mitochondrial histidyl tRNA synthetase HARS2 cause ovarian dysgenesis and sensorineural hearing loss of Perrault syndrome. *Proc Natl Acad Sci U S A,* 108(16)**,** 6543-8.
Pierce, S. B., Gersak, K., Michaelson-Cohen, R., Walsh, T., Lee, M. K., Malach, D., Klevit, R. E., King, M. C. & Levy-Lahad, E. (2013). Mutations in LARS2, encoding mitochondrial leucyl-tRNA synthetase, lead to premature ovarian failure and hearing loss in Perrault syndrome. *Am J Hum Genet,* 92(4)**,** 614-620.
Pierce, S. B., Walsh, T., Chisholm, K. M., Lee, M. K., Thornton, A. M., Fiumara, A., Opitz, J. M., Levy-Lahad, E., Klevit, R. E. & King, M. C. (2010). Mutations in the DBP-Deficiency Protein HSD17B4 Cause Ovarian Dysgenesis, Hearing Loss, and Ataxia of Perrault Syndrome. *Am J Hum Genet,* 87(2)**,** 282-8.
Plagnol, V., Curtis, J., Epstein, M., Mok, K. Y., Stebbings, E., Grigoriadou, S., Wood, N. W., Hambleton, S., Burns, S. O., Thrasher, A. J., Kumararatne, D., Doffinger, R. & Nejentsev, S. (2012). A robust model for read count data in exome sequencing experiments and implications for copy number variant calling. *Bioinformatics,* 28(21)**,** 2747-54.

Riley, L. G., Rudinger-Thirion, J., Schmitz-Abe, K., Thorburn, D. R., Davis, R. L., Teo, J., Arbuckle, S., Cooper, S. T., Campagna, D. R., Frugier, M., Markianos, K., Sue, C. M., Fleming, M. D. & Christodoulou, J. (2016). LARS2 Variants Associated with Hydrops, Lactic Acidosis, Sideroblastic Anemia, and Multisystem Failure. *JIMD reports,* 28**,** 49-57.

Schwarz, J. M., Cooper, D. N., Schuelke, M. & Seelow, D. (2014). MutationTaster2: mutation prediction for the deep-sequencing age. *Nat Methods,* 11(4)**,** 361-2.

Sherry, S. T., Ward, M. H., Kholodov, M., Baker, J., Phan, L., Smigielski, E. M. & Sirotkin, K. (2001). dbSNP: the NCBI database of genetic variation. *Nucleic Acids Res,* 29(1)**,** 308-311.

Sievers, F., Wilm, A., Dineen, D., Gibson, T. J., Karplus, K., Li, W., Lopez, R., McWilliam, H., Remmert, M., Soding, J., Thompson, J. D. & Higgins, D. G. (2011). Fast, scalable generation of high-quality protein multiple sequence alignments using Clustal Omega. *Mol Syst Biol,* 7**,** 539.

Smith, M. J., Beetz, C., Williams, S. G., Bhaskar, S. S., O'Sullivan, J., Anderson, B., Daly, S. B., Urquhart, J. E., Bholah, Z., Oudit, D., Cheesman, E., Kelsey, A., McCabe, M. G., Newman, W. G. & Evans, D. G. (2014). Germline mutations in SUFU cause Gorlin syndrome- associated childhood medulloblastoma and redefine the risk associated with PTCH1 mutations. *J Clin Oncol,* 32(36)**,** 4155-61.

Tang, T., Zheng, B., Chen, S. H., Murphy, A. N., Kudlicka, K., Zhou, H. & Farquhar, M. G. (2009). hNOA1 interacts with complex I and DAP3 and regulates mitochondrial respiration and apoptosis. *J Biol Chem,* 284(8)**,** 5414-24.

Theunissen, T. E., Szklarczyk, R., Gerards, M., Hellebrekers, D. M., Mulder-Den Hartog, E. N., Vanoevelen, J., Kamps, R., de Koning, B., Rutledge, S. L., Schmitt-Mechelke, T., van Berkel, C. G., van der Knaap, M. S., de Coo, I. F. & Smeets, H. J. (2016). Specific MRI Abnormalities Reveal Severe Perrault Syndrome due to CLPP Defects. *Front Neurol,* 7**,** 203.

Wang, M. & Casey, P. J. (2016). Protein prenylation: unique fats make their mark on biology. *Nat Rev Mol Cell Biol,* 17(2)**,** 110-22.

Xiao, L., Xian, H., Lee, K. Y., Xiao, B., Wang, H., Yu, F., Shen, H. M. & Liou, Y. C. (2015). Death-associated Protein 3 Regulates Mitochondrial-encoded Protein Synthesis and Mitochondrial Dynamics. *J Biol Chem,* 290(41)**,** 24961-74.

Chapter 8: Discussion

8.1. Realisation of Project Aims

The aims of this project were to:

- Undertake mapping and sequencing studies in families with Perrault syndrome for the identification of novel Perrault syndrome genes.
- Undertake functional characterisation of variants in novel disease causing genes.
- Further define the molecular cause of Perrault syndrome.

Over the course of this project three putative novel Perrault syndrome genes were identified, *PRORP*, *NOP14* and *DAP3*. We characterised these variants which led to some surprising results. We showed that patients with a variant in *PRORP* had an accumulation of unprocessed mitochondrial RNA and a reduction in the function of PRORP by ~40%. A loss of mitochondrial DNA encoded OXPHOS subunits highlighted a defect of mitochondrial translation in these patients. This pattern of OXPHOS deficiency had also been seen in Perrault syndrome patients with variants in *ERAL* (Chatzispyrou et al. 2017*)* suggesting that these cases of Perrault syndrome share a common pathology of defective mitochondrial translation. We found that NOP14 may have a role in mitochondria. NOP14 is characterised as a nucleolar protein but we found that NOP14 knockout yeast lose their mitochondria. Nop14 also has a distinctive non-nucleolar localisation in the mouse organ of corti. We found no OXPHOS defect in DAP3 patient cells showing the pathology of Perrault syndrome in this case is not a defect of mitochondrial translation. This lack of OXPHOS defect is surprising given the role of DAP3 in the mitochondrial ribosome. We have further defined the molecular pathology of Perrault syndrome by identifying a second gene, *PRORP*, which causes Perrault syndrome due to dysfunction of mitochondrial translation. Contrary to previous data we found that there may be additional causative molecular mechanisms, therefore, more work is needed to fully understand the pathology of Perrault syndrome.

8.2. Improving Perrault syndrome diagnosis

Part of the aim of this project was to provide data which may improve Perrault syndrome diagnosis. The identification of three novel Perrault syndrome genes will help improve diagnostic rates. Next generation sequencing is becoming more prevalent as a diagnostic test and including Perrault syndrome genes on hearing loss panels will improve the

diagnosis rate of males and pre-pubescent females who present with apparent non-syndromic hearing loss. The identification of new Perrault syndrome genes will also improve the diagnostic rate of individuals who undergo whole exome sequencing, as we have seen for the patients with neurological phenotypes who have Perrault syndrome due to variants in *CLPP* (Ahmed et al. 2015;Demain et al. 2017b;Theunissen et al. 2016). The identification of the large deletion in the case of Perrault syndrome caused by variants in *DAP3* also highlights the usefulness of copy number variation analysis on genetically unresolved cases of Perrault syndrome and may improve genetic diagnosis.

Looking at variants in known Perrault syndrome genes is important for genotype-phenotype links and because Perrault syndrome is so rare reporting new variants may help genetic diagnosis either via the exact variants seen in other affected individuals or highlighting Perrault syndrome hotspot regions as we see in *CLPP*. We made some genotype-phenotype links in Perrault syndrome which could help improve diagnosis. We provided evidence for a link between the variant *LARS2* c.1565C>A p.(Thr522Asn) and low frequency sensorineural hearing loss. In patients with the variant *LARS2* c.1565C>A p.(Thr522Asn), either homozygous or in trans with an additional *LARS2* variant, we saw a distinctive pattern of hearing loss which was more severe at lower frequencies and progressed to a flat type loss over time. *LARS2* is the only gene to be associated with autosomal recessive low frequency sensorineural hearing loss to date and it is the only *LARS2* variant c.1565C>A p.(Thr522Asn) which produces the low frequency loss (Demain et al. 2017b). The mechanisms behind this unusual pattern of hearing loss are not understood although it likely affects the organ of Corti from the apex, where the lowest frequency sounds are heard, progressing towards the base (Stakhovskaya et al. 2007). Low frequency hearing loss could be a useful indicator of Perrault syndrome in an individual with apparent non-syndromic hearing loss and an inheritance pattern consistent with autosomal recessive inheritance.

We provided in depth clinical assessment of our families and found that marfanoid proportions are a non-specific feature of Perrault syndrome (Zerkaoui et al. 2017). A milder form of the marfanoid proportion phenotype is arachnodactyly or high arched palate. These features have been seen in both known genes and in genetically unresolved cases of Perrault syndrome. Therefore, marfanoid habitus and associated dysmorphic

features are likely non-specific features of Perrault syndrome. Reporting new cases of Perrault syndrome is important to further clarify the phenotypic spectrum.

Perrault syndrome has a large clinical heterogeneity which has not been explained. Variation in other mitochondrial proteins such as those involved in mitochondrial proteostasis could account for some of this heterogeneity (Jenkinson et al. 2013). I suggest that variants in mitochondrial DNA may influence the phenotype. Variants in mitochondrial rRNA and tRNA could be especially applicable in cases of Perrault syndrome due to variants in *PRORP*, *LARS2* and *HARS2* as the mitochondrial RNA directly interacts with the affected protein in these instances. The heteroplasmy of mitochondrial DNA for variants could account for some of the intra-familial clinical variation.

8.3. The molecular mechanisms of Perrault syndrome

In chapters 4, 5 and 6 we investigated the molecular mechanisms of variants in three novel Perrault syndrome genes; *PRORP*, *NOP14* and *DAP3*.

We identified variants in *PRORP* in a single family with Perrault syndrome . Fibroblasts from an affected patient showed a defect of mitochondrial translation. We demonstrated an accumulation of unprocessed mitochondrial RNA but no apparent reduction in mature RNA transcripts. The underlying mechanism of the defect of mitochondrial translation in the PRORP case is currently unknown, but data from both PRORP conditional knockout mice and from patients with defects in SDR5C1 suggest that the Perrault syndrome phenotype in this family may be due to dysfunction of mitochondria ribosomal biogenesis. Knockout of PRORP is embryonic lethal but cardiac and skeletal muscle specific PRORP conditional knockout mice have been produced (Rackham et al. 2016). These mice die at 11 weeks from cardiomyopathy. The conditional knockout mice showed a significant reduction in the synthesis of mitochondrial encoded proteins with the nuclear encoded proteins unaffected. The reduction in mitochondrial encoded proteins was accompanied by a significant reduction in mitochondrial respiration (Rackham et al. 2016). The mice showed an accumulation of unprocessed mitochondrial RNA transcripts but, in contrast to patients with defects in subunits of mtRNAse P, the mice showed no mature transcripts (Rackham et al. 2016). This is likely due to the more deleterious knockout in mice in comparison to the patients with variants in TRMT10C, SDR5C1 or

PRORP. Rackham et al. (2016) showed that ribosomal formation was severely impaired in the conditional knockout mice with some ribosomal subunits attempting to form around the unprocessed transcripts. There appears to be no phenotypic overlap between the conditional knockout mice and the family reported here. The PRORP knockout in these mice was tissue specific to skeletal and cardiac muscle and, as such, it is unlikely they would display a hearing or fertility phenotype. In light of the cardiac phenotype in the conditional knockout mice our patients were tested for heart defects using echocardiogram, the results of which were normal. The knockout of PRORP in the conditional knockout mice was a more severe defect than the missense variant in the family reported here. We might expect the mice would show a phenotype in all knockout tissues where our milder affected family would only show a phenotype in the tissue most sensitive to defects in mitochondrial translation. The conditional knockout mouse, for reasons discussed above, does not recapitulate the phenotype seen in the Perrault syndrome family reported here. Many of the molecular defects were similar to those seen in this family and as such the conditional knockout mice may provide insights into the molecular mechanisms behind the pathology of defects in PRORP in humans.

The accumulation of unprocessed mitochondrial RNA transcripts rather than a deficit in mature RNA may be the pathogenic mechanism in patients with defects in SDR5C1 (Deutschmann et al. 2014). Patients with Perrault syndrome caused by *ERAL1* variants have reduced mitoribosome formation affecting mitochondrial translation (Chatzispyrou et al. 2017). PRORP conditional knockout mice also have severely reduced mitoribosome formation and it was reported in these mice that mitoribosomes had attempted to form around the unprocessed transcripts in the absence of the fully processed ribosomal RNA (Rackham et al. 2016). It may be that unprocessed mitochondrial RNA transcripts are interfering with mitoribosome formation in patients with defects in subunits of mtRNase P, although there is no evidence at this time as to the pathogenic mechanisms in humans.

The theory that dysfunction of the mitochondrial ribosome causes Perrault syndrome would also correlate well with the characterised role of CLPP in mitochondrial ribosomal biogenesis (Dennerlein et al. 2010) and I would suggest that a number of cases of Perrault syndrome may be caused by mitochondrial ribosome dysfunction. It would be informative

to investigate mitoribosome assembly and function in cases where variants in *PRORP* and *CLPP* cause Perrault syndrome.

NOP14 functions in the processing of 18S rRNA and the biogenesis of the 40S ribosomal subunit (Liu and Thiele 2001). The known function NOP14 does not fit in the Perrault syndrome pathway of mitochondrial translation, nor do the patients with *NOP14* variants present with typical ribosomopathy phenotypes which often include bone marrow, craniofacial or skeletal defects (Narla and Ebert 2010). We show that haploinsufficiency of NOP14 in yeast causes the slow loss of mitochondrial function. We have presented data which suggests a second function for NOP14, which is currently uncharacterised but likely mitochondrial or involved in mito-nuclear communication. This possible second function for *NOP14* indicates that the pathology of Perrault syndrome may be more similar to the other cases of Perrault syndrome than initially thought and is likely to involve mitochondrial dysfunction.

DAP3 is the GTPase subunit of the mitochondrial ribosome (Cavdar Koc et al. 2001) and, as such, functions in the Perrault syndrome pathway of mitochondrial translation. Unlike previous Perrault syndrome cases there were no defects in the OXPHOS pathway in patient cells under either normal or stress conditions. We had previously expected that cases of Perrault syndrome due to variants in novel genes would show the same defect of mitochondrial translation as seen in the cases due to variants in *PRORP* or *ERAL1* (Chatzispyrou et al. 2017). The pathological mechanism of the *DAP3* c.1184G>A p.(Cys395Tyr) variant remain unclear, although it is likely related to the role of DAP3 as a pro-apoptotic factor or regulator of mitochondrial fission (Cavdar Koc et al. 2001;Xiao et al. 2015). Interestingly, the function affected by the DAP3 variant Cys395Tyr seems discrete from the mitochondrial ribosomal function of DAP3 meaning this variant may be informative in studying the role of DAP3 in either apoptosis or mitochondrial fission. We predicted that the variant Cys395Tyr could abolish a post-translational modification site and affect the interaction of DAP3 with either a lipid membrane or a binding partner. The residue Cys395 is not modified in the bovine mitochondrial ribosome under normal conditions (Cavdar Koc et al. 2001), but it may be modified either in non-ribosomal DAP3 or in other conditions. It could be informative to assess the whole cellular pool of DAP3 in patient and control cells to detect post-translational modification at residue 395. It could

be variants in other regions of *DAP3* cause Perrault syndrome through mitochondrial ribosome dysfunction.

Defects of the mitochondrial translation pathway are known to be associated with hearing loss (Xing et al. 2007). The exact pathological mechanisms behind this tissue specific phenotype are not well understood. Our immunohistochemistry data suggests some proteins involved in mitochondrial translation have specific localisation in the organ of Corti. We found that PRORP in particular associated with the synapses and nerve fibres of the organ of Corti after the onset of hearing. The work of Nishio et al. (2017) found that some of the genes associated with Perrault syndrome are highly expressed in the spiral ganglion which connects auditory input to the central auditory system in the brain. We suggest that the neurons in the spiral ganglion and brainstem may have an increased level of mitochondrial translation, perhaps making them vulnerable to disruption of this pathway during sustained sound stimulations after the onset of hearing. This could go some way to explaining the tissue specific phenotype of hearing loss in cases of Perrault syndrome. Defects of mitochondrial translation are often associated with primary ovarian insufficiency (Demain et al. 2017a) and there may be a similar mechanism at work here. Our data highlights that mitochondria are not homogenous organelles and have specific cell, tissue and developmental patterns of protein expression and localisation which should be taken into account when considering the often tissue specific pathology of mitochondrial disorders.

8.5 Future work

The three novel putative Perrault syndrome genes reported here were all identified in single families. Despite screening five additional families with genetically unresolved Perrault syndrome we did not find an additional affected family for any case. Perrault syndrome is an incredibly rare condition with few affected individuals worldwide. A second Perrault syndrome family with variants in *HARS2* was not identified until five years after the initial report and was reported by a different group (Pierce et al. 2011;Lerat et al. 2016). It, therefore, may be some time before the second family is identified in these cases.

To ascertain a second family for each novel Perrault syndrome gene we have submitted these variants to GeneMatcher (https://genematcher.org/). GeneMatcher is an online tool which connects individuals with interest in the same gene to resolve the genetic basis of human genetic disease. In this way we hope to find additional families with pathogenic variants in *PRORP*, *NOP14* and *DAP3* to complete the evidence of pathogenicity for these genes.

In these cases of Perrault syndrome genes with a single affected family, recapitulating the phenotype in mice using the CRISPR genome editing technology (Cong et al. 2013) would bridge the evidence gap which is left without a second family. These mouse models would also provide more data on the molecular causes of the pathology at a tissue level which we have seen may be important as Perrault syndrome genes have tissue and cell specific expression patterns in the organ of Corti. As most of the genes involved in Perrault syndrome are essential for life, creating the exact putative pathogenic variants is important as knockout mice are unavailable or non-viable in most cases. Tissue specific knockout mice have been produced for PRORP (Rackham et al. 2016). These models are often not particularly informative about Perrault syndrome as the ear and ovaries are not usually affected and the knockout phenotype will likely be more severe than the Perrault syndrome phenotype where the defect is generally mild. CRISPR mice (Cong et al. 2013) would be particularly useful cases where a variant has a specific phenotype associated with it such as in the *LARS2* variant associated with low frequency SNHL. CRISPR technology (Cong et al. 2013) could also prove useful in creating a variant cell line in the cases where patient cells are not available.

Where patient fibroblast cells are available assessment of the mitochondrial OXPHOS complexes should be performed. If there are cases of Perrault syndrome with a different molecular pathology than a defect of mitochondrial translation then this would help stratify them quickly. In the cases where there is a defect of mitochondrial translation I would suggest assessing mitochondrial ribosomal biogenesis and function as this a may be a common dysfunction in some cases of Perrault syndrome.

The genetic and molecular assessment of each case of Perrault syndrome is important in facilitating new gene discovery and elucidating genotype-phenotype links, both of which

improve the diagnosis rate of Perrault syndrome. Improving the diagnosis rate of Perrault syndrome will increase the clinical data available about the syndrome and may help to address some of the unanswered questions surrounding the syndrome including the sex-biased aspects.

8.6. Conclusion

In the past few years the knowledge of Perrault has greatly improved. In the age of diagnosis via next generation sequencing it is even more important to identify Perrault syndrome genes. We have seen this demonstrated through next generation sequencing of *CLPP* diagnosed cases of Perrault syndrome.(Ahmed et al. 2015;Demain et al. 2017b;Theunissen et al. 2016). Alongside achieving the project aims in identifying and characterising three novel Perrault syndrome genes we have also identified a possible mechanism behind defects of mitochondrial translation and hearing loss and identified that NOP14 has a vital role in mitochondrial function. I also anticipate that the variant in DAP3 will provide insight into the function of DAP3 in apoptosis or mitochondrial fission. Although Perrault syndrome is a rare disease we have also shown here that investigating Perrault syndrome has applications beyond the immediate diagnosis of patients in both identifying the pathogenic mechanisms behind mitochondrial related hearing loss and infertility and in providing insight into the function of proteins like NOP14 and DAP3.

References

Action on Hearing Loss. (2017). *Levels of hearing loss* [Online]. Action on hearing loss. Available: https://www.actiononhearingloss.org.uk/your-hearing/about-deafness-and-hearing-loss/glossary/levels-of-hearing-loss.aspx [Accessed 12/06 2017].

Adzhubei, I. A., Schmidt, S., Peshkin, L., Ramensky, V. E., Gerasimova, A., Bork, P., Kondrashov, A. S. & Sunyaev, S. R. (2010). A method and server for predicting damaging missense mutations. *Nat Methods,* 7(4)**,** 248-9.

Ahmed, S., Jelani, M., Alrayes, N., Mohamoud, H. S. A., Almramhi, M. M., Anshasi, W., Ahmed, N. A. B., Wang, J., Nasir, J. & Al-Aama, J. Y. (2015). Exome analysis identified a novel missense mutation in the CLPP gene in a consanguineous Saudi family expanding the clinical spectrum of Perrault Syndrome type-3. *J Neurol Sci,* 353(1-2)**,** 149–154.

Aiman, J. & Smentek, C. (1985). Premature ovarian failure. *Obstetrics and gynecology,* 66(1)**,** 9-14

Aittomäki, K., Dieguez Lucena, J., Pakarinen, P., Sistonen, P., Tapanainen, J., Gromoll, J., Kaskikari, R., Sankila, E. M., Lehväslaiho, H., Reyes Engel, A., Nieschlag, E., Huhtaniemi, I. & de la Chapelle, A. (1995). Mutation in the follicle- stimulating hormone receptor gene causes hereditary hypergonadotropic ovarian failure. *Cell,* 82(6)**,** 959-968.

Ameen, K. H. N. & Pinninti, R. (2012). A rare cause for primary amenorrhea: Sporadic perrault syndrome. *Indian J Endocrinol Metab,* 16(5)**,** 843-845.

Anderson, S., Bankier, A. T., Barrell, B. G., de Bruijn, M. H., Coulson, A. R., Drouin, J., Eperon, I. C., Nierlich, D. P., Roe, B. A., Sanger, F., Schreier, P. H., Smith, A. J., Staden, R. & Young, I. G. (1981). Sequence and organization of the human mitochondrial genome. *Nature,* 290(5806)**,** 457-65.

Bamshad, M. J., Ng, S. B., Bigham, A. W., Tabor, H. K., Emond, M. J., Nickerson, D. A. & Shendure, J. (2011). Exome sequencing as a tool for Mendelian disease gene discovery. *Nat Rev Genet,* 12(11)**,** 745-755.

Bayat, V., Thiffault, I., Jaiswal, M., Tetreault, M., Donti, T., Sasarman, F., Bernard, G., Demers-Lamarche, J., Dicaire, M. J., Mathieu, J., Vanasse, M., Bouchard, J. P., Rioux, M. F., Lourenco, C. M., Li, Z. H., Haueter, C., Shoubridge, E. A., Graham, B. H., Brais, B. & Bellen, H. J. (2012). Mutations in the Mitochondrial Methionyl- tRNA Synthetase Cause a Neurodegenerative Phenotype in Flies and a Recessive Ataxia (ARSAL) in Humans. *PLOS BIOLOGY,* 10(3).

Belostotsky, R., Ben-Shalom, E., Rinat, C., Becker-Cohen, R., Feinstein, S., Frishberg, Y., Zeligson, S., Segel, R., Elpeleg, O. & Nassar, S. (2011). Mutations in the mitochondrial Seryl- tRNA synthetase cause hyperuricemia, pulmonary hypertension, renal failure in infancy and alkalosis, HUPRA syndrome. *Am J Hum Genet,* 88(2)**,** 193-200.

Belyantseva, I. A. (2016). Helios® Gene Gun-Mediated Transfection of the Inner Ear Sensory Epithelium: Recent Updates. *In:* Sokolowski, B. (ed.) *Auditory and Vestibular Research: Methods and Protocols.* New York, NY: Springer New York.

Boycott, K. M., Vanstone, M. R., Bulman, D. E. & MacKenzie, A. E. (2013). Rare-disease genetics in the era of next- generation sequencing: Discovery to translation. *Nat Rev Genet,* 14**,** 681-691.

Carr, I. M., Flintoff, K. J., Taylor, G. R., Markham, A. F. & Bonthron, D. T. (2006). Interactive visual analysis of SNP data for rapid autozygosity mapping in consanguineous families. *Hum Mutat,* 27(10)**,** 1041-6.

Cavdar Koc, E., Ranasinghe, A., Burkhart, W., Blackburn, K., Koc, H., Moseley, A. & Spremulli, L. L. (2001). A new face on apoptosis: death-associated protein 3 and PDCD9 are mitochondrial ribosomal proteins. *FEBS Lett,* 492(1-2)**,** 166-70.

Chatzispyrou, I. A., Alders, M., Guerrero-Castillo, S., Zapata Perez, R., Haagmans, M. A., Mouchiroud, L., Koster, J., Ofman, R., Baas, F., Waterham, H. R., Spelbrink, J. N., Auwerx,

J., Mannens, M. M., Houtkooper, R. H. & Plomp, A. S. (2017). A homozygous missense mutation in ERAL1, encoding a mitochondrial rRNA chaperone, causes Perrault syndrome. *Hum Mol Genet,* 26(13)**,** 2541-2550.

Check Hayden, E. (2014). Is the $1,000 genome for real? *Nature News* [Online]. Available: http://www.nature.com/news/is-the-1-000-genome-for-real-1.14530 [Accessed 19/11/2014].

Chen, D. C., Yang, B. C. & Kuo, T. T. (1992). One-step transformation of yeast in stationary phase. *Curr Genet,* 21(1)**,** 83-4.

Chinnery, P. F. (2014). Mitochondrial Disorders Overview. *In:* Pagon, R. A., Adam, M. P., Ardinger, H. H., Wallace, S. E., Amemiya, A., Bean, L. J. H., Bird, T. D., Fong, C. T., Mefford, H. C., Smith, R. J. H. & Stephens, K. (eds.) *GeneReviews(R).* Seattle (WA).

Chittka, L. & Brockmann, A. (2005). Perception Space—The Final Frontier (Primer). *PLoS Biology,* 3(4)**,** e137.

Cong, L., Ran, F. A., Cox, D., Lin, S., Barretto, R., Habib, N., Hsu, P. D., Wu, X., Jiang, W., Marraffini, L. A. & Zhang, F. (2013). Multiplex genome engineering using CRISPR/Cas systems. *Science,* 339(6121)**,** 819-23.

Dallabona, C., Diodato, D., Kevelam, S., Haack, T., Wong, L.-J., Salomons, G., Baruffini, E., Melchionda, L., Mariotti, C. & Strom, T. (2014). Novel (ovario) leukodystrophy related to AARS2 mutations. *Neurology,* 82(23)**,** 2063-2071.

de Launoit, Y. & Adamski, J. (1999). Unique multifunctional HSD17B4 gene product: 17 beta-hydroxysteroid dehydrogenase 4 and D-3-hydroxyacyl-coenzyme A dehydrogenase hydratase involved in Zellweger syndrome. *J Mol Endocrinol,* 22(3)**,** 227-240.

Demain, L. A., Conway, G. S. & Newman, W. G. (2017a). Genetics of mitochondrial dysfunction and infertility. *Clin Genet,* 91(2)**,** 199-207.

Demain, L. A., Urquhart, J. E., O'Sullivan, J., Williams, S. G., Bhaskar, S. S., Jenkinson, E. M., Lourenco, C. M., Heiberg, A., Pearce, S. H., Shalev, S. A., Yue, W. W., Mackinnon, S., Munro, K. J., Newbury-Ecob, R., Becker, K., Kim, M. J., RT, O. K. & Newman, W. G. (2017b). Expanding the genotypic spectrum of Perrault syndrome. *Clin Genet,* 91(2)**,** 302-312.

Dennerlein, S., Rozanska, A., Wydro, M., Chrzanowska-Lightowlers, Z. M. & Lightowlers, R. N. (2010). Human ERAL1 is a mitochondrial RNA chaperone involved in the assembly of the 28S small mitochondrial ribosomal subunit. *Biochem J,* 430(3)**,** 551-8.

Deutschmann, A. J., Amberger, A., Zavadil, C., Steinbeisser, H., Mayr, J. A., Feichtinger, R. G., Oerum, S., Yue, W. W. & Zschocke, J. (2014). Mutation or knock-down of 17beta-hydroxysteroid dehydrogenase type 10 cause loss of MRPP1 and impaired processing of mitochondrial heavy strand transcripts. *Hum Mol Genet,* 23(13)**,** 3618-28.

Diodato, D., Ghezzi, D. & Tiranti, V. (2014a). The Mitochondrial Aminoacyl tRNA Synthetases: Genes and Syndromes. *Int J Cell Biol,* 2014.

Diodato, D., Melchionda, L., Haack, T. B., Dallabona, C., Baruffini, E., Donnini, C., Granata, T., Ragona, F., Balestri, P., Margollicci, M., Lamantea, E., Nasca, A., Powell, C. A., Minczuk, M., Strom, T. M., Meitinger, T., Prokisch, H., Lamperti, C., Zeviani, M. & Ghezzi, D. (2014b). VARS2 and TARS2 Mutations in Patients with Mitochondrial Encephalomyopathies. *Hum Mutat,* 35(8)**,** 983-989.

Dursun, F., Mohamoud, H. S., Karim, N., Naeem, M., Jelani, M. & Kirmizibekmez, H. (2016). A Novel Missense Mutation in the CLPP Gene Causing Perrault Syndrome Type 3 in a Turkish Family. *J Clin Res Pediatr Endocrinol,* 8(4)**,** 472-477.

Edvardson, S., Shaag, A., Einbinder, T., Saada, A., Elpeleg, O., Gomori, J. M., Kolesnikova, O. & Tarassov, I. (2007). Deleterious mutation in the mitochondrial arginyl- transfer RNA synthetase gene is associated with pontocerebellar hypoplasia. *Am J Hum Genet,* 81(4)**,** 857-862.

Eisen, M. D. & Ryugo, D. K. (2007). Hearing molecules: contributions from genetic deafness. *Cell Mol Life Sci,* 64(5)**,** 566-80.

Ellingford, J. M., Campbell, C., Barton, S., Bhaskar, S., Gupta, S., Taylor, R. L., Sergouniotis, P. I., Horn, B., Lamb, J. A., Michaelides, M., Webster, A. R., Newman, W. G., Panda, B., Ramsden, S. C. & Black, G. C. (2017). Validation of copy number variation analysis for next-generation sequencing diagnostics. *Eur J Hum Genet,* 25(6)**,** 719-724.

Elo, J. M., Euro, L., Isohanni, P., Götz, A., Carroll, C. J., Tyynismaa, H., Suomalainen, A., Paetau, A., Yadavalli, S. S., Caruso, E. M., Ibba, M., Pihko, H., Valanne, L., Alkuraya, F. S. & Uusimaa, J. (2012). Mitochondrial phenylalanyl- trna synthetase mutations underlie fatal infantile alpers encephalopathy. *Hum Mol Genet,* 21(20)**,** 4521-4529.

European Commission DG Health & Consumers. (2014). *Rare diseases Policy* [Online]. European Commission. Available: http://ec.europa.eu/health/rare_diseases/policy/index_en.htm [Accessed 08/12/2014 2014].

Exome Aggregation Consortium (ExAC). *Exome Aggregation Consortium (ExAC)* [Online]. Cambridge, MA. Available: http://exac.broadinstitute.org [Accessed 08/07 2015].

Faridi, R., Rehman, A. U., Morell, R. J., Friedman, P. L., Demain, L., Zahra, S., Khan, A. A., Tohlob, D., Assir, M. Z., Beaman, G., Khan, S. N., Newman, W. G., Riazuddin, S. & Friedman, T. B. (2017). Mutations of SGO2 and CLDN14 collectively cause coincidental Perrault syndrome. *Clin Genet,* 91(2)**,** 328-332.

Ferdinandusse, S., Majoie, C. B. L. M., Barth, P. G., Wanders, R. J. A., Poll-The, B. T., Denis, S., Mooyer, P. A. W., Dekker, C., Duran, M., Soorani-Lunsing, R. J., Boltshauser, E., Macaya, A. & Gärtner, J. (2006a). Clinical and biochemical spectrum of D-bifunctional protein deficiency. *Annals of Neurology,* 59(1)**,** 92-104.

Ferdinandusse, S., Ylianttila, M. S., Gloerich, J., Koski, M. K., Oostheim, W., Waterham, H. R., Hiltunen, J. K., Wanders, R. J. A. & Glumoff, T. (2006b). Mutational Spectrum of d-Bifunctional Protein Deficiency and Structure-Based Genotype-Phenotype Analysis. *Am J Hum Genet,* 78(1)**,** 112-124.

Fiumara, A., Sorge, G., Toscano, A., Parano, E., Pavone, L. & Opitz, J. M. (2004). Perrault syndrome: Evidence for progressive nervous system involvement. *Am J Med Genet,* 128A(3)**,** 246-249.

Fortnum, H. M., Summerfield, A. Q., Marshall, D. H., Davis, A. C., Bamford, J. M., Davis, A., Yoshinaga-Itano, C. & Hind, S. (2001). Prevalence of permanent childhood hearing impairment in the united kingdom and implications for universal neonatal hearing screening: questionnaire based ascertainment study commentary: universal newborn hearing screening: implications for coordinating and developing services for deaf and hearing impaired children. *BMJ,* 323(7312)**,** 536.

Fratter, C. M., Gorman, G. S. M., Stewart, J. D. P., Buddles, M. P., Smith, C. P., Evans, J. P., Seller, A. P., Poulton, J. D., FRCPCH, Roberts, M. F., Hanna, M. G. F., Rahman, S. P., FRCPCH, Omer, S. E. F., Klopstock, T. M., Schoser, B. M., Kornblum, C. M., Czermin, B. P., Lecky, B. M., FRCP, Blakely, E. L. P., Craig, K. P., Chinnery, P. F. P., FRCP, Turnbull, D. M. P., FRCP, Horvath, R. M. & Taylor, R. W. P. (2010). The clinical, histochemical, and molecular spectrum of PEO1 (Twinkle)-linked adPEO. *Neurology,* 74(20)**,** 1619-1626.

Fukasawa, Y., Tsuji, J., Fu, S. C., Tomii, K., Horton, P. & Imai, K. (2015). MitoFates: improved prediction of mitochondrial targeting sequences and their cleavage sites. *Mol Cell Proteomics,* 14(4)**,** 1113-26.

Geethalakshmi, S., Geethalakshmi, V. & Narendrakumar, V. (2015). Perrault syndrome – A rare case report. *J Clin Diagn Res,* 9(3)**,** OD01-OD02.

Gibson, D. G., Young, L., Chuang, R. Y., Venter, J. C., Hutchison, C. A., 3rd & Smith, H. O. (2009). Enzymatic assembly of DNA molecules up to several hundred kilobases. *Nat Methods,* 6(5)**,** 343-5.

Gispert, S., Parganlija, D., Klinkenberg, M., Dröse, S., Wittig, I., Mittelbronn, M., Grzmil, P., Koob, S., Hamann, A., Walter, M., Büchel, F., Adler, T., Angelis, M. H. d., Busch, D. H., Zell, A.,

Reichert, A. S., Brandt, U., Osiewacz, H. D., Jendrach, M. & Auburger, G. (2013). Loss of mitochondrial peptidase Clpp leads to infertility, hearing loss plus growth retardation via accumulation of CLPX, mtDNA and inflammatory factors. *Hum Mol Genet,* 22(24)**,** 4871-4887.

Gottschalk, M. E., Coker, S. B. & Fox, L. A. (1996). Neurologic anomalies of Perrault syndrome. *Am J Med Genet,* 65(4)**,** 274-6.

Götz, A., Tyynismaa, H., Euro, L., Hämäläinen, R. H., Tyni, T., Suomalainen, A., Ellonen, P., Hyötyläinen, T., Oresic, M., Ojala, T., Tommiska, J., Raivio, T., Karikoski, R., Paetau, A., Tammela, O. & Simola, K. O. J. (2011). Exome sequencing identifies mitochondrial alanyl-tRNA synthetase mutations in infantile mitochondrial cardiomyopathy. *Am J Hum Genet,* 88(5)**,** 635-642.

Gravholt, C. H. (2004). Epidemiological, endocrine and metabolic features in Turner syndrome. *Eur J Endocrinol,* 151**,** 657–687.

Hearing Link. (2017). *What do different audiograms look like?* [Online]. Hearing Link. Available: https://www.hearinglink.org/your-hearing/hearing-tests-audiograms/what-do-different-audiograms-look-like/ [Accessed 12/06 2017].

Hinson , J. T., Fantin , V. R., Schönberger , J., Breivik , N., Siem , G., McDonough , B., Sharma , P., Keogh , I., Godinho , R., Santos , F., Esparza , A., Nicolau , Y., Selvaag , E., Cohen , B. H., Hoppel , C. L., Tranebjærg , L., Eavey , R. D., Seidman , J. G. & Seidman , C. E. (2007). Missense Mutations in the BCS1L Gene as a Cause of the Björnstad Syndrome. *New England Journal of Medicine,* 356(8)**,** 809-819.

Holzmann, J., Frank, P., Loffler, E., Bennett, K. L., Gerner, C. & Rossmanith, W. (2008). RNase P without RNA: identification and functional reconstitution of the human mitochondrial tRNA processing enzyme. *Cell,* 135(3)**,** 462-74.

Illumina. (2017). *Illumina Sequencing Introduction* [Online]. Available: https://www.illumina.com/content/dam/illumina-marketing/documents/products/illumina_sequencing_introduction.pdf [Accessed 16/09/17 2017].

Janitz, M. (2011). *Next-generation genome sequencing: towards personalized medicine*: John Wiley & Sons.

Jenkinson, E. M., Clayton-Smith, J., Mehta, S., Bennett, C., Reardon, W., Green, A., Pearce, S. H. S., De Michele, G., Conway, G. S., Cilliers, D., Moreton, N., Davis, J. R. E., Trump, D. & Newman, W. G. (2012). Perrault syndrome: Further evidence for genetic heterogeneity. *J Neurol,* 259(5)**,** 974-976.

Jenkinson, E. M., Rehman, A. U., Walsh, T., Clayton-Smith, J., Lee, K., Morell, R. J., Drummond, M. C., Khan, S. N., Naeem, M. A., Rauf, B., Billington, N., Schultz, J. M., Urquhart, J. E., Lee, M. K., Berry, A., Hanley, N. A., Mehta, S., Cilliers, D., Clayton, P. E., Kingston, H., Smith, M. J., Warner, T. T., Black, G. C., Trump, D., Davis, J. R. E., Ahmad, W., Leal, S. M., Riazuddin, S., King, M. C., Friedman, T. B. & Newman, W. G. (2013). Perrault syndrome is caused by recessive mutations in CLPP, encoding a mitochondrial ATP-dependent chambered protease. *Am J Hum Genet,* 92(4)**,** 605-613.

Jones, P., Binns, D., Chang, H. Y., Fraser, M., Li, W., McAnulla, C., McWilliam, H., Maslen, J., Mitchell, A., Nuka, G., Pesseat, S., Quinn, A. F., Sangrador-Vegas, A., Scheremetjew, M., Yong, S. Y., Lopez, R. & Hunter, S. (2014). InterProScan 5: genome-scale protein function classification. *Bioinformatics,* 30(9)**,** 1236-40.

Josso, N. (1963). Familial Turner's Syndrome. Study of 2 Families with Xo and Xx Karyotypes. *Ann Pediatr (Paris),* 10**,** 163–167.

Kang, S. G., Dimitrova, M. N., Ortega, J., Ginsburg, A. & Maurizi, M. R. (2005). Human Mitochondrial ClpP Is a Stable Heptamer That Assembles into a Tetradecamer in the Presence of ClpX. *J Biol Chem,* 280(42)**,** 35424-35432.

Kim, M. J., Kim, S. J., Kim, J., Chae, H., Kim, M. & Kim, Y. (2013). Genotype and Phenotype Heterogeneity in Perrault Syndrome. *J Pediatr Adolesc Gynecol,* 26(1)**,** e25-e27.

Kochhar, A., Hildebrand, M. S. & Smith, R. J. H. (2007). Clinical aspects of hereditary hearing loss. *Genet Med,* 9(7)**,** 393-408.

Konovalova, S. & Tyynismaa, H. (2013). Mitochondrial aminoacyl- tRNA synthetases in human disease. *Mol Genet Metab,* 108(4)**,** 206-211.

Kumar, P., Henikoff, S. & Ng, P. C. (2009). Predicting the effects of coding non-synonymous variants on protein function using the SIFT algorithm. *Nat Protoc,* 4(7)**,** 1073-81.

Kunkel, T. A., Roberts, J. D. & Zakour, R. A. (1987). Rapid and efficient site-specific mutagenesis without phenotypic selection. *Methods Enzymol,* 154**,** 367-382.

Laercio, O., Pedalini, M. E. B. & Caropreso, C. A. (1992). Sensorineural hearing loss associated to gonadal dysgenesis in sisters: Perrault's syndrome. *Am J Otol,* 13(1)**,** 82-83.

Lek, M., Karczewski, K. J., Minikel, E. V., Samocha, K. E., Banks, E., Fennell, T., O'Donnell-Luria, A. H., Ware, J. S., Hill, A. J., Cummings, B. B., Tukiainen, T., Birnbaum, D. P., Kosmicki, J. A., Duncan, L. E., Estrada, K., Zhao, F., Zou, J., Pierce-Hoffman, E., Berghout, J., Cooper, D. N., Deflaux, N., DePristo, M., Do, R., Flannick, J., Fromer, M., Gauthier, L., Goldstein, J., Gupta, N., Howrigan, D., Kiezun, A., Kurki, M. I., Moonshine, A. L., Natarajan, P., Orozco, L., Peloso, G. M., Poplin, R., Rivas, M. A., Ruano-Rubio, V., Rose, S. A., Ruderfer, D. M., Shakir, K., Stenson, P. D., Stevens, C., Thomas, B. P., Tiao, G., Tusie-Luna, M. T., Weisburd, B., Won, H. H., Yu, D., Altshuler, D. M., Ardissino, D., Boehnke, M., Danesh, J., Donnelly, S., Elosua, R., Florez, J. C., Gabriel, S. B., Getz, G., Glatt, S. J., Hultman, C. M., Kathiresan, S., Laakso, M., McCarroll, S., McCarthy, M. I., McGovern, D., McPherson, R., Neale, B. M., Palotie, A., Purcell, S. M., Saleheen, D., Scharf, J. M., Sklar, P., Sullivan, P. F., Tuomilehto, J., Tsuang, M. T., Watkins, H. C., Wilson, J. G., Daly, M. J., MacArthur, D. G. & Exome Aggregation, C. (2016). Analysis of protein-coding genetic variation in 60,706 humans. *Nature,* 536(7616)**,** 285-91.

Lerat, J., Jonard, L., Loundon, N., Christin-Maitre, S., Lacombe, D., Goizet, C., Rouzier, C., Van Maldergem, L., Gherbi, S., Garabedian, E. N., Bonnefont, J. P., Touraine, P., Mosnier, I., Munnich, A., Denoyelle, F. & Marlin, S. (2016). An Application of NGS for Molecular Investigations in Perrault Syndrome: Study of 14 Families and Review of the Literature. *Hum Mutat,* 37(12)**,** 1354-1362.

Letunic, I., Doerks, T. & Bork, P. (2015). SMART: recent updates, new developments and status in 2015. *Nucleic Acids Res,* 43(Database issue)**,** D257-60.

Lieber, D. S., Hershman, S. G., Slate, N. G., Calvo, S. E., Sims, K. B., Schmahmann, J. D. & Mootha, V. K. (2014). Next generation sequencing with copy number variant detection expands the phenotypic spectrum of HSD17B4-deficiency. *BMC Med Genet,* 15**,** 30.

Lines, M. A., Jobling, R., Brady, L., Marshall, C. R., Scherer, S. W., Rodriguez, A. R., Lee, L., Lang, A. E., Mestre, T. A., Wanders, R. J., Ferdinandusse, S. & Tarnopolsky, M. A. (2014). Peroxisomal D-bifunctional protein deficiency: Three adults diagnosed by whole-exome sequencing. *Neurology,* 82(11)**,** 963-8.

Liu, P. C. C. & Thiele, D. (2001). Novel stress-responsive genes EMG1 and NOP14 encode conserved, interacting proteins required for 40S ribosome biogenesis. *Mol Biol Cell,* 12(11)**,** 3644-3657.

Llano, E., Gomez, R., Gutierrez-Caballero, C., Herran, Y., Sanchez-Martin, M., Vazquez-Quinones, L., Hernandez, T., de Alava, E., Cuadrado, A., Barbero, J. L., Suja, J. A. & Pendas, A. M. (2008). Shugoshin-2 is essential for the completion of meiosis but not for mitotic cell division in mice. *Genes Dev,* 22(17)**,** 2400-13.

Luoma, P., Melberg, A., Rinne, J. O., Kaukonen, J. A., Nupponen, N. N., Chalmers, R. M., Oldfors, A., Rautakorpi, I., Peltonen, L., Majamaa, K., Somer, H. & Suomalainen, A. (2004). Parkinsonism, premature menopause, and mitochondrial DNA polymerase gamma mutations: clinical and molecular genetic study. *Lancet,* 364(9437)**,** 875-82.

Marchler-Bauer, A., Derbyshire, M. K., Gonzales, N. R., Lu, S., Chitsaz, F., Geer, L. Y., Geer, R. C., He, J., Gwadz, M., Hurwitz, D. I., Lanczycki, C. J., Lu, F., Marchler, G. H., Song, J. S., Thanki, N., Wang, Z., Yamashita, R. A., Zhang, D., Zheng, C. & Bryant, S. H. (2015). CDD: NCBI's conserved domain database. *Nucleic Acids Res,* 43(Database issue)**,** D222-6.

Marlin, S., Moatti, L., Feldmann, D., Denoyelle, F., Lacombe, D., Jonard, L., Leboulanger, N., Bonneau, D., Goizet, C., Billette De Villemeur, T., Cabrol, S. & Houang, M. (2008). Perrault syndrome: Report of four new cases, review and exclusion of candidate genes. *Am J Med Genet , Part A,* 146(5)**,** 661-664.

Mayr, J. A., Haack, T. B., Freisinger, P., Karall, D., Makowski, C., Koch, J., Feichtinger, R. G., Zimmermann, F. A., Rolinski, B., Ahting, U., Meitinger, T., Prokisch, H. & Sperl, W. (2015). Spectrum of combined respiratory chain defects. *J Inherit Metab Dis,* 38(4)**,** 629-40.

McCarthy, D. J. & Opitz, J. M. (1985). Brief clinical report: Perrault syndrome in sisters. *Am J Med Genet,* 22(3)**,** 629-631.

McMillan, H. J., Worthylake, T., Schwartzentruber, J., Gottlieb, C. C., Lawrence, S. E., Mackenzie, A., Beaulieu, C. L., Mooyer, P. A., Consortium, F. C., Wanders, R. J., Majewski, J., Bulman, D. E., Geraghty, M. T., Ferdinandusse, S. & Boycott, K. M. (2012). Specific combination of compound heterozygous mutations in 17beta-hydroxysteroid dehydrogenase type 4 (HSD17B4) defines a new subtype of D-bifunctional protein deficiency. *Orphanet J Rare Dis,* 7**,** 90.

Mitchell, K., O'Sullivan, J., Missero, C., Blair, E., Richardson, R., Anderson, B., Antonini, D., Murray, J. C., Shanske, A. L., Schutte, B. C., Romano, R. A., Sinha, S., Bhaskar, S. S., Black, G. C., Dixon, J. & Dixon, M. J. (2012). Exome sequence identifies RIPK4 as the Bartsocas-Papas syndrome locus. *Am J Hum Genet,* 90(1)**,** 69-75.

Morimoto, N., Tanaka, T., Taiji, H., Horikawa, R., Naiki, Y., Morimoto, Y. & Kawashiro, N. (2006). Hearing loss in Turner syndrome. *J Pediatr,* 149(5)**,** 697-701.

Morino, H., Pierce, S. B., Matsuda, Y., Walsh, T., Ohsawa, R., Newby, M., Hiraki-Kamon, K., Kuramochi, M., Lee, M. K., Klevit, R. E., Martin, A., Maruyama, H., King, M. C. & Kawakami, H. (2014). Mutations in Twinkle primase-helicase cause Perrault syndrome with neurologic features. *Neurology,* 83(22)**,** 2054-61.

Narla, A. & Ebert, B. L. (2010). Ribosomopathies: human disorders of ribosome dysfunction. *Blood,* 115(16)**,** 3196-205.

Newman, W. G., Friedman, T. B. & Conway, G. S. (2014). Perrault Syndrome. *In:* Pagon RA, A. M., Ardinger HH, et al., editors (ed.) *GeneReviews® [Internet].* University of Washington, Seattle.

NHLBI GO Exome Sequencing Project (ESP). *Exome Variant Server* [Online]. Seattle, WA. Available: http://evs.gs.washington.edu/EVS/ [Accessed 09/07 2015].

Nikali, K., Suomalainen, A., Saharinen, J., Kuokkanen, M., Spelbrink, J. N., Lnnqvist, T. & Peltonen, L. (2005). Infantile onset spinocerebellar ataxia is caused by recessive mutations in mitochondrial proteins Twinkle and Twinky. *Hum Mol Genet,* 14(20)**,** 2981-2990.

Nishi, Y., Hamamoto, K., Kajiyama, M. & Kawamura, I. (1988). The Perrault syndrome: clinical report and review. *Am J Med Genet,* 31(3)**,** 623-9.

Nishio, S. Y., Takumi, Y. & Usami, S. I. (2017). Laser-capture micro dissection combined with next-generation sequencing analysis of cell type-specific deafness gene expression in the mouse cochlea. *Hear Res,* 348**,** 87-97.

Nsengimana, J. & Bishop, D. T. (2012). Design considerations for genetic linkage and association studies. *In:* Elston, R. C., Satagopan, J. M. & Sun, S. (eds.) *Statistical Human Genetics.* XI ed.: Humana Press.

O'Keefe, R. T., Norman, C. & Newman, A. J. (1996). The Invariant U5 snRNA Loop 1 Sequence Is Dispensable for the First Catalytic Step of pre-mRNA Splicing in Yeast. *Cell,* 86(4)**,** 679-689.

Ojala, D., Montoya, J. & Attardi, G. (1981). tRNA punctuation model of RNA processing in human mitochondria. *Nature,* 290(5806)**,** 470-4.

Oldak, M., Ozieblo, D., Pollak, A., Stepniak, I., Lazniewski, M., Lechowicz, U., Kochanek, K., Furmanek, M., Tacikowska, G., Plewczynski, D., Wolak, T., Ploski, R. & Skarzynski, H. (2017). Novel neuro-audiological findings and further evidence for TWNK involvement in Perrault syndrome. *J Transl Med,* 15(1)**,** 25.

Online Mendelian Inheritance in Man OMIM®. Balitmore (MD): McKusick-Nathans Institute of Genetic Medicine, Johns Hopkins University. Available: http://omim.org/ [Accessed 08/07 2015].

Pagliarini, D. J., Calvo, S. E., Chang, B., Sheth, S. A., Vafai, S. B., Ong, S.-E., Walford, G. A., Sugiana, C., Boneh, A., Chen, W. K., Hill, D. E., Vidal, M., Evans, J. G., Thorburn, D. R., Carr, S. A. & Mootha, V. K. (2008). A Mitochondrial Protein Compendium Elucidates Complex I Disease Biology. *Cell,* 134(1)**,** 112-123.

Pallister, P. D. & Opitz, J. M. (1979). The Perrault syndrome: autosomal recessive ovarian dysgenesis with facultative, non-sex-limited sensorineural deafness. *Am J Med Genet,* 4(3)**,** 239-46.

Pandya, A. (2014). Nonsyndromic Hearing Loss and Deafness, Mitochondrial. *In:* Pagon, R. A., Adam, M. P., Ardinger, H. H., Wallace, S. E., Amemiya, A., Bean, L. J. H., Bird, T. D., Fong, C. T., Mefford, H. C., Smith, R. J. H. & Stephens, K. (eds.) *GeneReviews(R).* Seattle (WA).

Perrault, M., Klotz, B. & Housset, E. (1951). [Two cases of Turner syndrome with deaf-mutism in two sisters]. *Bull Mem Soc Med Hop Paris,* 67(3-4)**,** 79-84.

Pierce, S. B., Chisholm, K. M., Lynch, E. D., Lee, M. K., Walsh, T., Opitz, J. M., Li, W., Klevit, R. E. & King, M. C. (2011). Mutations in mitochondrial histidyl tRNA synthetase HARS2 cause ovarian dysgenesis and sensorineural hearing loss of Perrault syndrome. *Proc Natl Acad Sci U S A,* 108(16)**,** 6543-8.

Pierce, S. B., Gersak, K., Michaelson-Cohen, R., Walsh, T., Lee, M. K., Malach, D., Klevit, R. E., King, M. C. & Levy-Lahad, E. (2013). Mutations in LARS2, encoding mitochondrial leucyl-tRNA synthetase, lead to premature ovarian failure and hearing loss in Perrault syndrome. *Am J Hum Genet,* 92(4)**,** 614-620.

Pierce, S. B., Walsh, T., Chisholm, K. M., Lee, M. K., Thornton, A. M., Fiumara, A., Opitz, J. M., Levy-Lahad, E., Klevit, R. E. & King, M. C. (2010). Mutations in the DBP-Deficiency Protein HSD17B4 Cause Ovarian Dysgenesis, Hearing Loss, and Ataxia of Perrault Syndrome. *Am J Hum Genet,* 87(2)**,** 282-8.

Plagnol, V., Curtis, J., Epstein, M., Mok, K. Y., Stebbings, E., Grigoriadou, S., Wood, N. W., Hambleton, S., Burns, S. O., Thrasher, A. J., Kumararatne, D., Doffinger, R. & Nejentsev, S. (2012). A robust model for read count data in exome sequencing experiments and implications for copy number variant calling. *Bioinformatics,* 28(21)**,** 2747-54.

Pujol, R., Nouvian, R. & Lenoir, M. (2016a). *HAIR CELLS: OVERVIEW* [Online]. Available: http://www.cochlea.eu/en/hair-cells [Accessed 12/06 2016].

Pujol, R., Rebillard, G. & Lenoir, M. (2016b). *ORGAN OF CORTI: OVERVIEW* [Online]. Available: http://www.cochlea.eu/en/cochlea/organ-of-corti [Accessed 12/06 2016].

Pyun, J. A., Kim, S., Cha, D. H., Ko, J. J. & Kwack, K. (2012). Epistasis between the HSD17B4 and TG polymorphisms is associated with premature ovarian failure. *Fertil Steril,* 97(4)**,** 968-973.

Rackham, O., Busch, J. D., Matic, S., Siira, S. J., Kuznetsova, I., Atanassov, I., Ermer, J. A., Shearwood, A. M., Richman, T. R., Stewart, J. B., Mourier, A., Milenkovic, D., Larsson, N. G. & Filipovska, A. (2016). Hierarchical RNA Processing Is Required for Mitochondrial Ribosome Assembly. *Cell Rep,* 16(7)**,** 1874-90.

Raimundo, N., Song, L., Shutt, T. E., McKay, S. E., Cotney, J., Guan, M. X., Gilliland, T. C., Hohuan, D., Santos-Sacchi, J. & Shadel, G. S. (2012). Mitochondrial stress engages E2F1 apoptotic signaling to cause deafness. *Cell,* 148(4)**,** 716-26.

Ramalho-Santos, J. & Amaral, S. (2013). Mitochondria and mammalian reproduction. *Mol Cell Endocrinol,* 379(1-2)**,** 74-84.

Raphael, Y. & Altschuler, R. A. (2003). Structure and innervation of the cochlea. *Brain Res Bull,* 60(5-6)**,** 397-422.

Rebar, R. W. (2009). Premature ovarian failure. *Obstet Gynecol,* 113(6)**,** 1355-1363.

Reeve, A. K. & Lightowlers, R. N. (2012). An Introduction to Mitochondria. *In:* Reeve, K. A., Krishnan, J. K., Duchen, R. M. & Turnbull, M. D. (eds.) *Mitochondrial Dysfunction in Neurodegenerative Disorders.* London: Springer London.

Rehman, A. U., Gul, K., Morell, R. J., Lee, K., Ahmed, Z. M., Riazuddin, S., Ali, R. A., Shahzad, M., Jaleel, A., Andrade, P. B., Khan, S. N., Khan, S., Brewer, C. C., Ahmad, W., Leal, S. M. & Friedman, T. B. (2011). Mutations of GIPC3 cause nonsyndromic hearing loss DFNB72 but not DFNB81 that also maps to chromosome 19p. *Hum Genet,* 130(6)**,** 759-65.

Richman, T. R., Rackham, O. & Filipovska, A. (2014). Mitochondria: Unusual features of the mammalian mitoribosome. *Int J Biochem Cell Biol,* 53**,** 115-20.

Riley, L. G., Christodoulou, J., Cooper, S., Hickey, P., Bahlo, M., Rudinger-Thirion, J., Giegé, R., McKenzie, M., Ryan, M. T., Compton, A., Lim, S. C. & Thorburn, D. (2010). Mutation of the mitochondrial tyrosyl- tRNA synthetase gene, YARS2, causes myopathy, lactic acidosis, and sideroblastic anemia - MLASA syndrome. *Am J Hum Genet,* 87(1)**,** 52-59.

Riley, L. G., Rudinger-Thirion, J., Schmitz-Abe, K., Thorburn, D. R., Davis, R. L., Teo, J., Arbuckle, S., Cooper, S. T., Campagna, D. R., Frugier, M., Markianos, K., Sue, C. M., Fleming, M. D. & Christodoulou, J. (2015). LARS2 Variants Associated with Hydrops, Lactic Acidosis, Sideroblastic Anemia, and Multisystem Failure. *JIMD Reports,* 24**,** 1-9.

Riley, L. G., Rudinger-Thirion, J., Schmitz-Abe, K., Thorburn, D. R., Davis, R. L., Teo, J., Arbuckle, S., Cooper, S. T., Campagna, D. R., Frugier, M., Markianos, K., Sue, C. M., Fleming, M. D. & Christodoulou, J. (2016). LARS2 Variants Associated with Hydrops, Lactic Acidosis, Sideroblastic Anemia, and Multisystem Failure. *JIMD reports,* 28**,** 49-57.

Scheper, G. C., Van Der Klok, T., Van Andel, R. J., Van Berkel, C. G. M., Sissler, M., Smet, J., Muravina, T. I., Serkov, S. V., Uziel, G., Bugiani, M., Schiffmann, R., Krägeloh-Mann, I., Smeitink, J. A. M., Florentz, C., Van Coster, R., Pronk, J. C. & Van Der Knaap, M. S. (2007). Mitochondrial aspartyl- tRNA synthetase deficiency causes leukoencephalopathy with brain stem and spinal cord involvement and lactate elevation. *Nat Genet,* 39(4)**,** 534-539.

Schwarz, J. M., Cooper, D. N., Schuelke, M. & Seelow, D. (2014). MutationTaster2: mutation prediction for the deep-sequencing age. *Nat Methods,* 11(4)**,** 361-2.

Sherry, S. T., Ward, M. H., Kholodov, M., Baker, J., Phan, L., Smigielski, E. M. & Sirotkin, K. (2001). dbSNP: the NCBI database of genetic variation. *Nucleic Acids Res,* 29(1)**,** 308-311.

Sievers, F., Wilm, A., Dineen, D., Gibson, T. J., Karplus, K., Li, W., Lopez, R., McWilliam, H., Remmert, M., Soding, J., Thompson, J. D. & Higgins, D. G. (2011). Fast, scalable generation of high-quality protein multiple sequence alignments using Clustal Omega. *Mol Syst Biol,* 7**,** 539.

Simon, M., Richard, E. M., Wang, X., Shahzad, M., Huang, V. H., Qaiser, T. A., Potluri, P., Mahl, S. E., Davila, A., Nazli, S., Hancock, S., Yu, M., Gargus, J., Chang, R., Al-Sheqaih, N., Newman, W. G., Abdenur, J., Starr, A., Hegde, R., Dorn, T., Busch, A., Park, E., Wu, J., Schwenzer, H., Flierl, A., Florentz, C., Sissler, M., Khan, S. N., Li, R., Guan, M. X., Friedman, T. B., Wu, D. K., Procaccio, V., Riazuddin, S., Wallace, D. C., Ahmed, Z. M., Huang, T. & Riazuddin, S. (2015). Mutations of human NARS2, encoding the mitochondrial asparaginyl-tRNA synthetase, cause nonsyndromic deafness and Leigh syndrome. *PLoS Genet,* 11(3)**,** e1005097.

Smith, M. J., Beetz, C., Williams, S. G., Bhaskar, S. S., O'Sullivan, J., Anderson, B., Daly, S. B., Urquhart, J. E., Bholah, Z., Oudit, D., Cheesman, E., Kelsey, A., McCabe, M. G., Newman, W. G. & Evans, D. G. (2014). Germline mutations in SUFU cause Gorlin syndrome-associated childhood medulloblastoma and redefine the risk associated with PTCH1 mutations. *J Clin Oncol,* 32(36)**,** 4155-61.

Smith, R. J. H., Shearer, A. E., Hildebrand, M. S. & Van Camp, G. (2017). Deafness and Hereditary Hearing Loss Overview. *In:* Pagon, R. A., Adam, M. P., Ardinger, H. H., Wallace, S. E.,

Amemiya, A., Bean, L. J. H., Bird, T. D., Ledbetter, N., Mefford, H. C., Smith, R. J. H. & Stephens, K. (eds.) *GeneReviews(R).* Seattle (WA).

Solda, G., Caccia, S., Robusto, M., Chiereghin, C., Castorina, P., Ambrosetti, U., Duga, S. & Asselta, R. (2016). First independent replication of the involvement of LARS2 in Perrault syndrome by whole-exome sequencing of an Italian family. *Journal of human genetics,* 61(4)**,** 295-300.

Spelbrink, J. N., Li, F. Y., Tiranti, V., Nikali, K., Yuan, Q. P., Tariq, M., Wanrooij, S., Garrido, N., Comi, G., Morandi, L., Santoro, L., Toscano, A., Fabrizi, G. M., Somer, H., Croxen, R., Beeson, D., Poulton, J., Suomalainen, A., Jacobs, H. T., Zeviani, M. & Larsson, C. (2001). Human mitochondrial DNA deletions associated with mutations in the gene encoding Twinkle, a phage T7 gene 4-like protein localized in mitochondria. *Nat Genet,* 28(3)**,** 223-231.

Stakhovskaya, O., Sridhar, D., Bonham, B. H. & Leake, P. A. (2007). Frequency map for the human cochlear spiral ganglion: implications for cochlear implants. *J Assoc Res Otolaryngol,* 8(2)**,** 220-33.

Steenweg, M. E., Abbink, T. E. M., Van Berkel, C. G. M., Van Der Knaap, M. S., Ghezzi, D., Zeviani, M., Haack, T., Strom, T. M., Prokisch, H., Martinelli, D., Bley, A., Diogo, L., Grillo, E., Te Water Naudé, J. & Bertini, E. (2012). Leukoencephalopathy with thalamus and brainstem involvement and high lactate (LTBL); caused by EARS2 mutations. *Brain,* 135(5)**,** 1387-1394.

Szczepanowska, K., Maiti, P., Kukat, A., Hofsetz, E., Nolte, H., Senft, K., Becker, C., Ruzzenente, B., Hornig-Do, H. T., Wibom, R., Wiesner, R. J., Kruger, M. & Trifunovic, A. (2016). CLPP coordinates mitoribosomal assembly through the regulation of ERAL1 levels. *EMBO J,* 35(23)**,** 2566-2583.

Theunissen, T. E., Szklarczyk, R., Gerards, M., Hellebrekers, D. M., Mulder-Den Hartog, E. N., Vanoevelen, J., Kamps, R., de Koning, B., Rutledge, S. L., Schmitt-Mechelke, T., van Berkel, C. G., van der Knaap, M. S., de Coo, I. F. & Smeets, H. J. (2016). Specific MRI Abnormalities Reveal Severe Perrault Syndrome due to CLPP Defects. *Front Neurol,* 7**,** 203.

Thorburn, D. R. & Rahman, S. (2014). Mitochondrial DNA-Associated Leigh Syndrome and NARP. *In:* Pagon, R. A., Adam, M. P., Ardinger, H. H., Wallace, S. E., Amemiya, A., Bean, L. J. H., Bird, T. D., Fong, C. T., Mefford, H. C., Smith, R. J. H. & Stephens, K. (eds.) *GeneReviews(R).* Seattle (WA).

Voelkerding, K. V., Dames, S. A. & Durtschi, J. D. (2009). Next- generation sequencing:from basic research to diagnostics. *Clin Chem,* 55(4)**,** 641-658.

Wilcox, E. R., Burton, Q. L., Naz, S., Riazuddin, S., Smith, T. N., Ploplis, B., Belyantseva, I., Ben-Yosef, T., Liburd, N. A., Morell, R. J., Kachar, B., Wu, D. K., Griffith, A. J., Riazuddin, S. & Friedman, T. B. (2001). Mutations in the gene encoding tight junction claudin-14 cause autosomal recessive deafness DFNB29. *Cell,* 104(1)**,** 165-72.

Xiao, L., Xian, H., Lee, K. Y., Xiao, B., Wang, H., Yu, F., Shen, H. M. & Liou, Y. C. (2015). Death-associated Protein 3 Regulates Mitochondrial-encoded Protein Synthesis and Mitochondrial Dynamics. *J Biol Chem,* 290(41)**,** 24961-74.

Xing, G., Chen, Z. & Cao, X. (2007). Mitochondrial rRNA and tRNA and hearing function. *Cell Res,* 17(3)**,** 227-39.

Yan, D., Tekin, M., Blanton, S. H. & Liu, X. Z. (2013). Next- generation sequencing in genetic hearing loss. *Genet Test Mol Biomarkers,* 17(8)**,** 581-587.

Yu-Wai-Man, P., Turnbull, D. M. & Chinnery, P. F. (2002). Leber hereditary optic neuropathy. *J Med Genet,* 39(3)**,** 162-9.

Zerkaoui, M., Demain, L. A. M., Cherkaoui Jaouad, I., Ratbi, I., Amjoud, K., Urquhart, J. E., O'Sullivan, J., Newman, W. G. & Sefiani, A. (2017). Marfanoid habitus is a nonspecific feature of Perrault syndrome. *Clin Dysmorphol,* 26(4)**,** 200-204.

Appendices

Appendix I. Primer details for Sanger Sequencing

Primer name	Sequence 5' to 3'	Annealing temperature °C
C10orf2 exon 1 FWD	GCTGAGGTGGTACTGACGAG	60
C10orf2 exon 1 REV	GTCAGGGCTTTAAAACTGGGG	
CLPP exon 4 FWD	CCTCCCCAGGTTTAGGAGAT	60
CLPP exon 4 REV	GCCCAGTCAGTCCTTCTGTC	
DAP3 exon 13 FWD	TCTTATTGTCACGCATTCACAG	60
DAP3 exon 13 REV	AGTAGCTTGTTGGGGTGAGG	
HSD17B4 exon 1 FWD	TAGATGAACGCAAGGTGTCG	60
HSD17B4 exon 1 REV	TAACAATCGATGCCCACAGA	
HSD17B4 exon 5 FWD	TGTGAGAATTGTTAAAACTTTTGATG	60
HSD17B4 exon 5 REV	TCCATAAAATTGCCACCTCA	
KIAA0391 exon 7 FWD	ACACTGTCCTCTGCCTCTTC	60
KIAA0391 exon 7 REV	TCTAGGACCTGGCTAGTTCC	
LARS2 exon 14 FWD	GATTACAAGCGTGAGCCACC	60
LARS2 exon 14 REV	CTTCTCCCCTTTAATCTGCAC	
LARS2 exon 4 FWD	GTATACATGCAGAGTTCCCAG	60
LARS2 exon 4 REV	GTCCATCTTCAAAGCTGTCC	
NOP14 exon 8 FWD	CAGCCACTGTACACCTTCCA	
NOP14 exon 8 REV	AAAGGGAGGTGAAAGGTA	

Supplemental Table SI.1. Primers for the confirmation of variants.

Plasmid Name	Primer Name	Sequence 5' to 3'
Nop14-EGFP	MB222.NOP14.F1	GGCGAAAACTAACCCAAACC
Nop14-EGFP	MB223.NOP14.F2	GGAGCTCATTGCAAAGTCAA
Nop14-EGFP	MB224.NOP14.F3	TAAAGACGATAGGCGCTTGC
Nop14-EGFP	MB225.NOP14.F4	AGCAACTTTTGGTGGTGGAA
Nop14-EGFP	MB226.NOP14.F5	GGCATCCAGTTGTGACTCCT
Nop14-EGFP	MB227.NOP14.F6	TTGAGCCTGATGAAGCACTG
Nop14-EGFP	MB228.NOP14.F7	GAAAGCGTAAAGTAAAACAGCTTTT
Nop14-EGFP	MB229.NOP14.R1	CACCAAAGTGGGAAGCAGTC
Nop14-EGFP	MB230.NOP14.R2	CGAAGTCTTTCAGCCTCCAG
Nop14-EGFP	MB231.NOP14.R3	CCACCACCAAAAGTTGCTCT
Nop14-EGFP	MB232.NOP14.R4	GCATCTGGCTCATACACAGC
Nop14-EGFP	MB233.NOP14.R5	GCAGTGCCTGATACATGAGC
Nop14-EGFP	MB234.NOP14.R6	CTGCATCCCTTTCCATGATT
Nop14-EGFP	MB235.NOP14.R7	CTCCGCGCCCCAGTC
Dap3-EGFP	MB209.DAP3.F1	ATGCTGACAGGAATAACAA
Dap3-EGFP	MB210.DAP3.R1	CGCTGTTTGTTGTGAGTGGA
Dap3-EGFP	MB211.DAP3.F2	CTAACCCGAGTGAGGAATGC
Dap3-EGFP	MB212.DAP3.R2	TTACAGCGAGGCACAGAGC
Dap3-EGFP	MB213.DAP3.R3	CAACTTCTGGACCCTGGAGA
pSF-STE5-MouseNop14	CYC1	GCGTGAATGTAAGCGTGAC
pSF-STE5-MouseNop14	STE5-NOP14_NOP14-1	TATTCCTGGAGTACGTGTGC
pSF-STE5-MouseNop14	STE5-NOP14_NOP14-2	GAGCCATGAGACTCAGAAGA
pSF-STE5-MouseNop14	STE5-NOP14_NOP14-3	TATGGCCAGTCCTGGCGA
pET28-b(+)PRORP_p.Ala485Val	T7 Terminal	GCTAGTTATTGCTCAGCGG
pre- tRNA transcript histidine-serine(AGY)-leucine(CUN)	M13 (-21) Forward	TGTAAAACGACGGCCAGT
p426GPD-DAP3	RSM23_F	CAAGTATTCATCACGCTAAGTG
p426GPD-DAP3	RSM23_B	TAATCATACATCGGTGGTCCAG
p426GPD-DAP3C395Y	RSM23_F	CAAGTATTCATCACGCTAAGTG
p426GPD-DAP3C395Y	RSM23_B	TAATCATACATCGGTGGTCCAG

Supplemental Table SI.2. Primers for the confirmation inserts in vectors.

Primer name	Sequence 5' to 3'
RSM23_F	CAAGTATTCATCACGCTAAGTG
RSM23_B	TAATCATACATCGGTGGTCCAG
Kan_B	CTGCAGCGAGGAGCCGTAAT
Kan_C	TGATTTTGATGACGAGCGTAAT

Supplemental Table SI.2. Primers for the confirmation of deletion of RSM23.

Appendix II. Construct maps

Maps for EGFP-tagged Construct

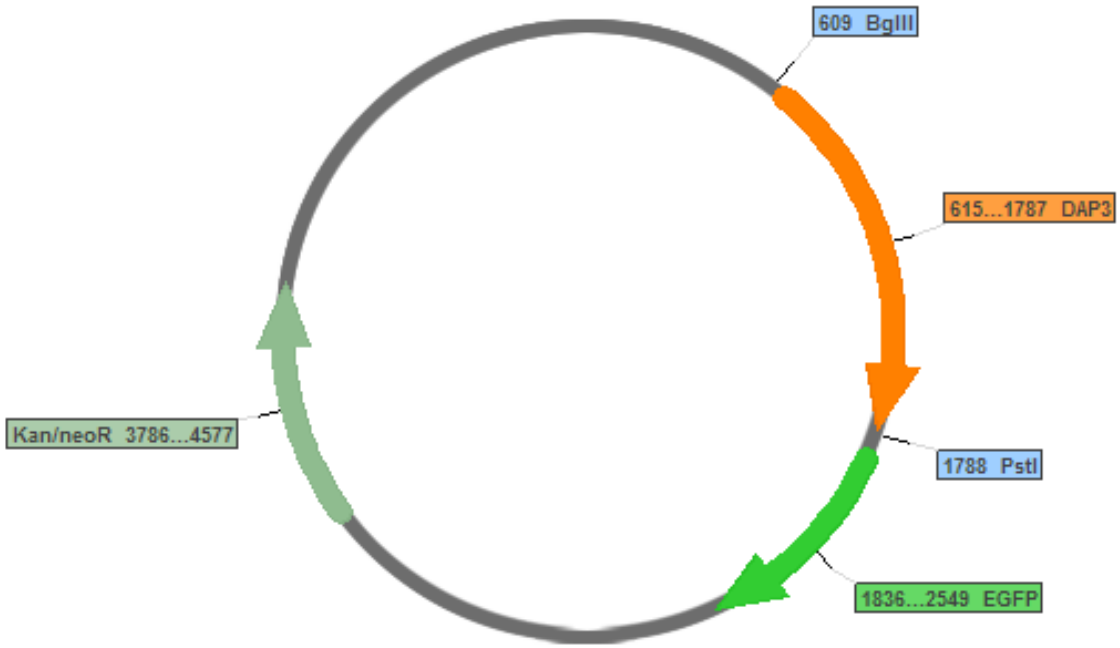

Supplemental Figure SII.1. Construct Map for Dap3-EGFP

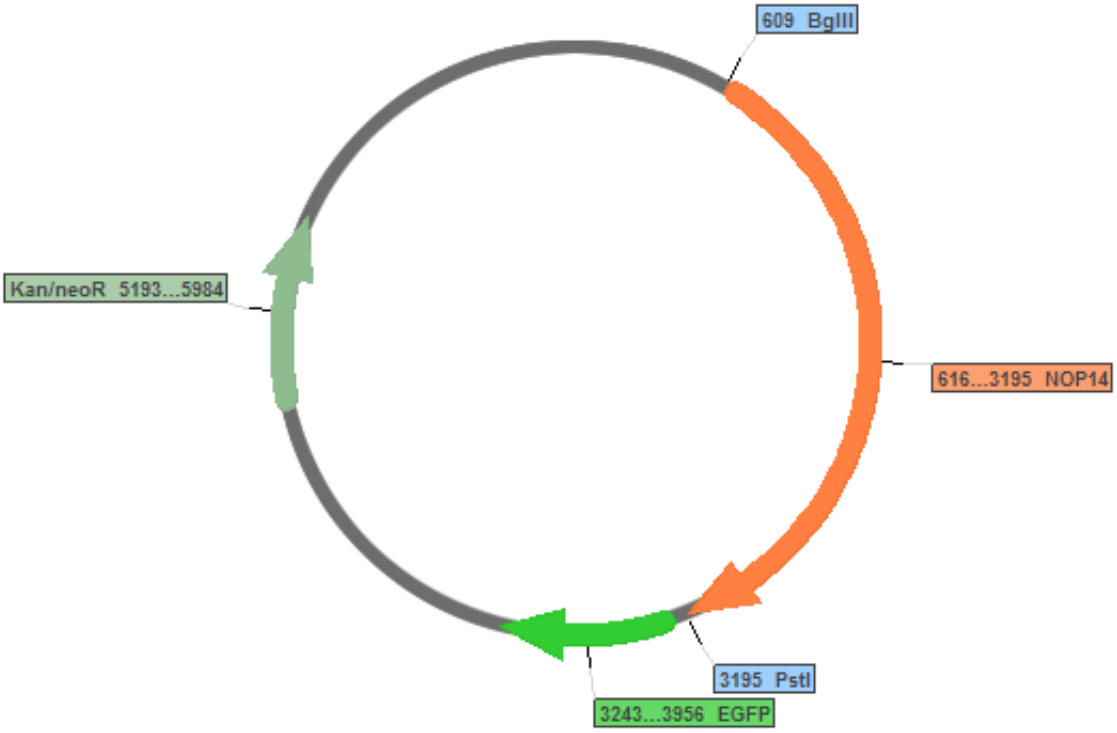

Supplemental Figure SII.2. Construct Map for NOP14-EGFP

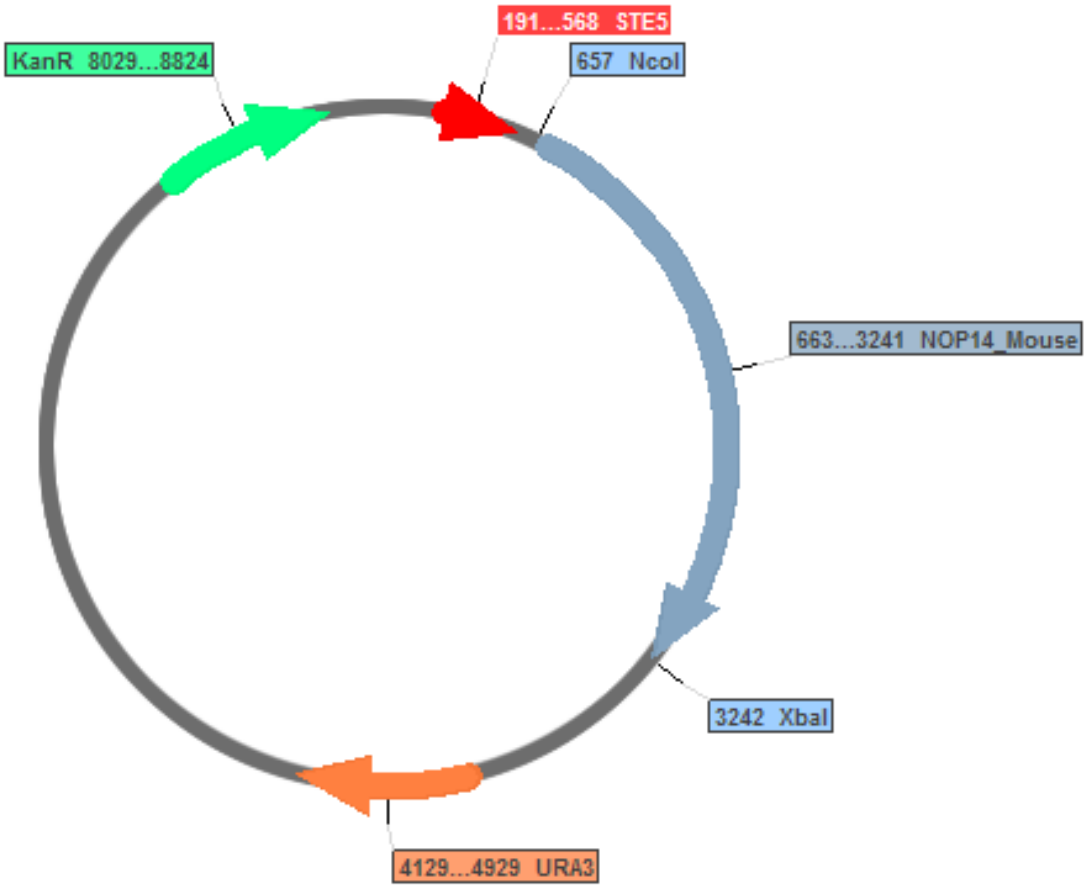

Supplemental Figure SII.3. Construct Map for pSF-STE5-MouseNop14

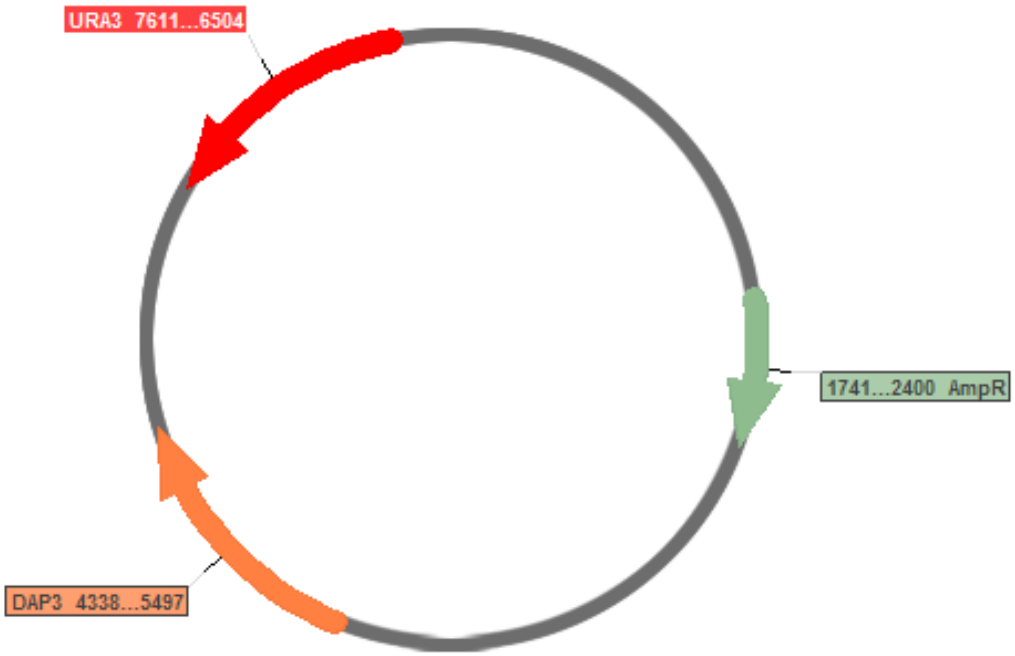

Supplemental Figure SII.4. Construct Map for p426GPD-DAP3

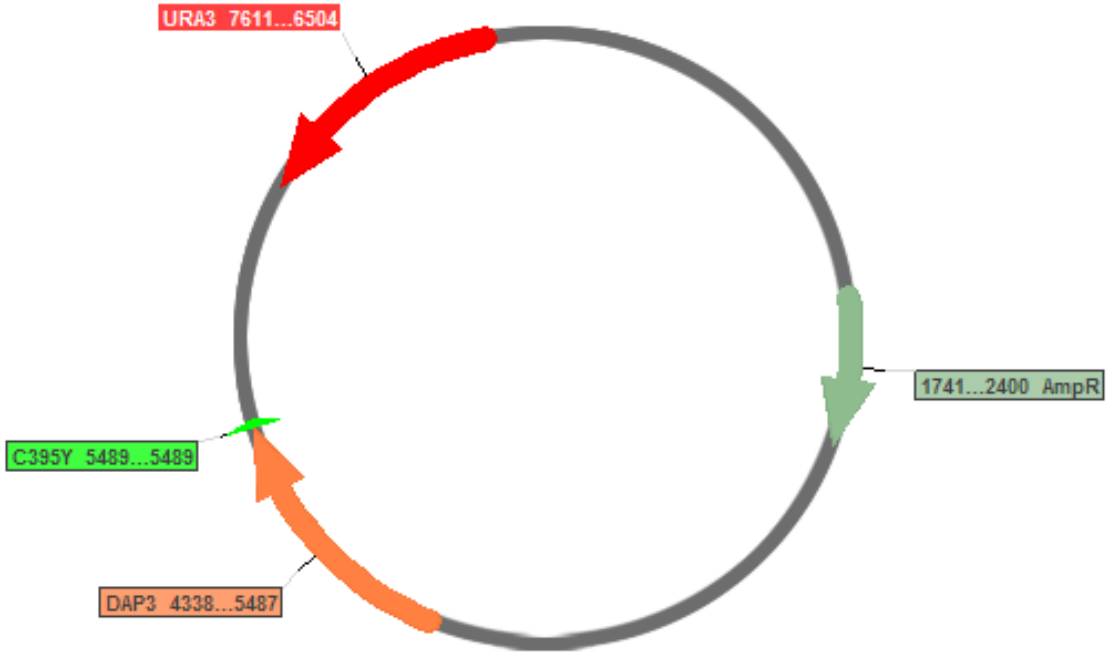

Supplemental Figure SII.5. Construct Map for p426GPD-DAP3 C395Y

Maps for tRNA template Construct

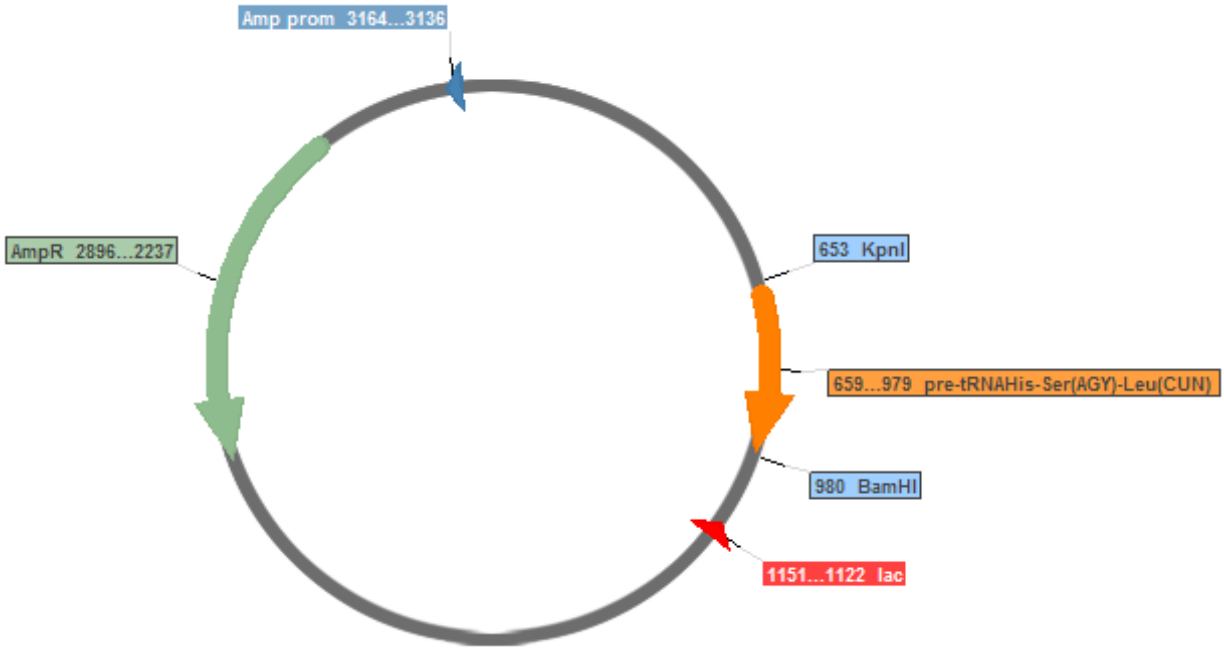

Supplemental Figure SII.5. Construct Map for pBlueScript II SK (+) pre- tRNA transcript histidine-serine(AGY)-leucine(CUN)

Appendix III. Supplemental data for chapter 3, Expanding the genotypic spectrum of Perrault syndrome

Supplementary Figure 1.

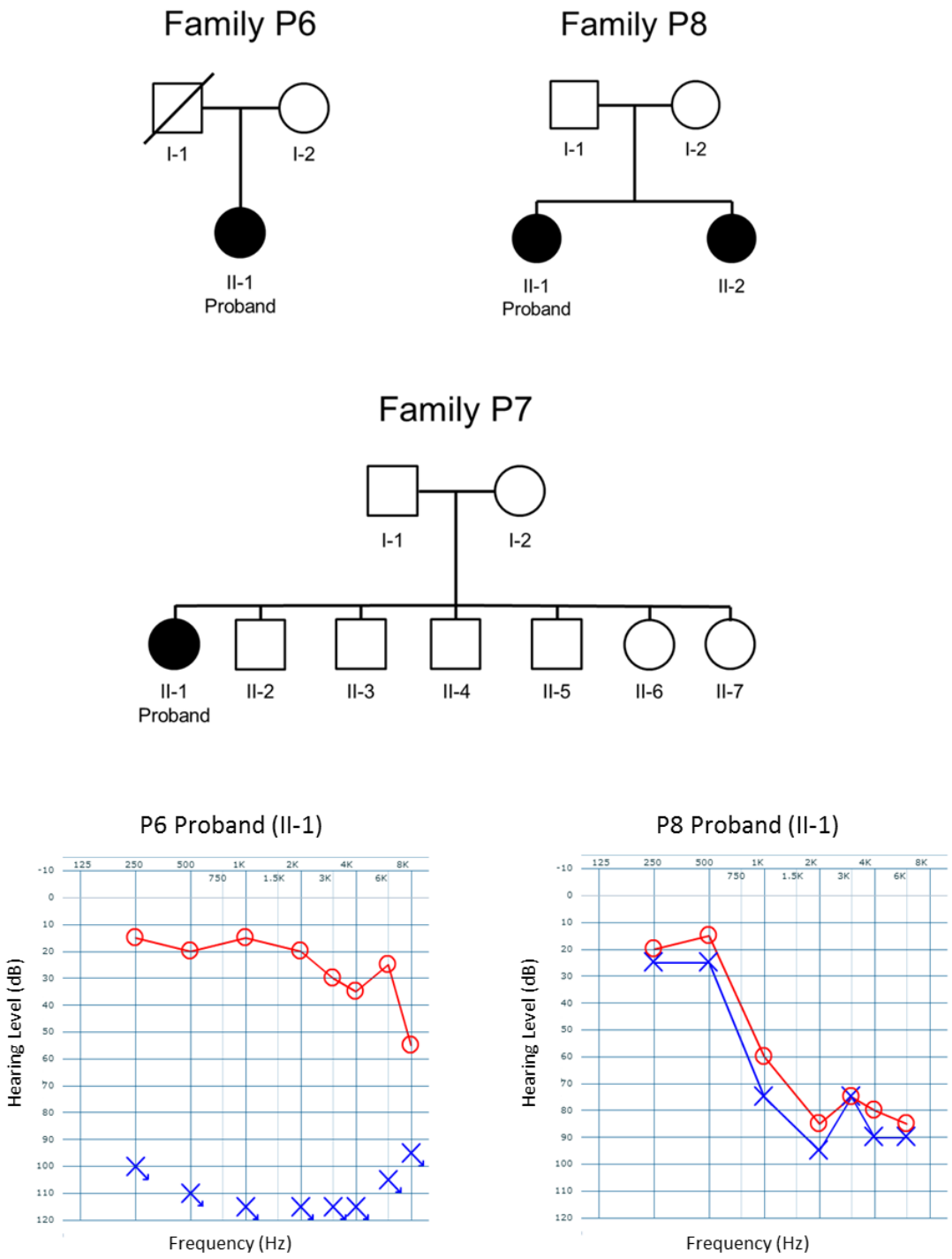

Supplementary Figure 1. Family Pedigrees for families P6-P8 and audiograms for the probands from family P6 and family P8.

In the pedigrees filled icons indicate affected individuals. The hearing level of the left ear is represented by the crosses and the right ear by circles. The arrows indicate no response to stimuli Audiograms were created using the AudGen online tool (version 0.71) (http://audsim.com/audgen/).

Supplementary Figure 2

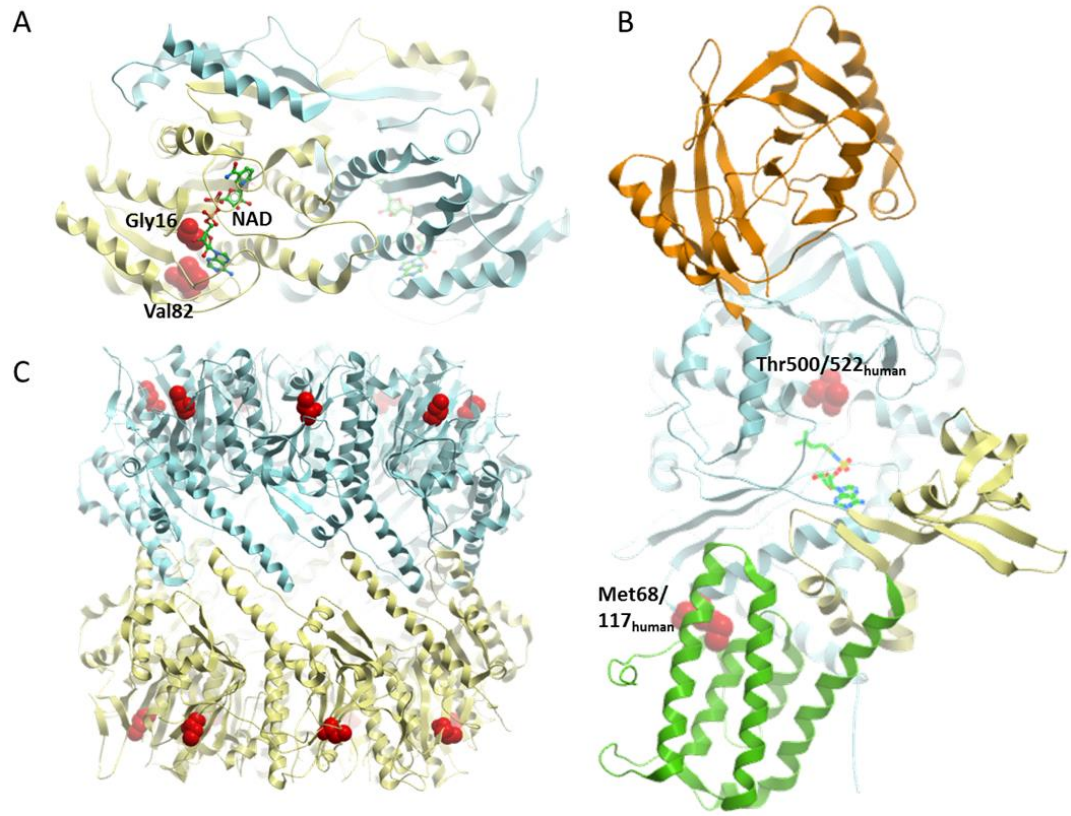

Supplementary Figure 2. Structural prediction of missense mutations in this study.

(A) Structure of human HSD17B4 dehydrogenase domain. The two subunits of a dimer are coloured cyan and yellow. The two sites of mutations (Gly16, Val82) are shown as red spheres. NAD is shown as sticks. (B) Structure of *T. thermophilus* LeuRS, coloured according to functional domains. The two sites of mutations are shown as red spheres. The leucine-adenylate homologue is shown as sticks. (C) Structure of human CLPP, shown as two heptameric rings (cyan, yellow). The site of mutation Cys144 is shown as red spheres in seventeen copies of the homo-oligomer.

Gene
ACTG1
ATP2B2
BDP1
C10orf2
CABP2
CCDC50
CDH23
CEACAM16
CIB2
CLDN14
CLPP
CLRN1
COCH
COL11A2
COL4A6
CRYM
DFNA5
DFNB31
DFNB59
DIABLO
DIAPH1
DIAPH3
EDN3
EDNRB
ESPN
ESRRB
EYA1
EYA4
GIPC3
GJB2
GJB3
GJB6
GPR98
GPSM2
GRHL2
GRXCR1
HARS
HARS2
HGF
HSD17B4
ILDR1
KARS
KCNJ10
KCNQ4
KIT
LARS2
LHFPL5
LOXHD1
LRTOMT
MARVELD2
MIR96
MITF
MSRB3
MYH14
MYH9
MYO15A
MYO3A

MYO6
MYO7A
OSBPL2
OTOA
OTOF
OTOG
P2RX2
PAX3
PCDH15
PDZD7
PNPT1
POU3F4
POU4F3
PRPS1
PTPRQ
RDX
RPGR
SERPINB6
SIX1
SIX5
SLC17A8
SLC26A4
SLC26A5
SLC4A11
SMPX
SNAI2
SOX10
STRC
TECTA
TJP2
TMC1
TMIE
TMPRSS3
TPRN
TRIOBP
USH1C
USH1G
USH2A
WFS1

Table S1. List of hearing loss genes assessed in families P5–P7

Patient	Gene	Variant	Transcript	Zygosity	ExAC Allele Frequency	EVS Minor Allele Frequency	dbSNP Reference
P5 II-1	*CLPP*	c.368-8G>A	NM_006012	Heterozygous	0.0111	0.6468	rs143053584
	DFNB31	c.1040A>T p.(Lys347Met)	NM_001173425	Heterozygous	Not Present	Not Present	Not Present
	GPR98	c.9447+6G>A	NM_032119	Heterozygous	0.0009	0.0510	rs201481219
	MYO15A	c.341_342insC p.(Arg115ProfsTer113)	NM_016239	Heterozygous	0.00001	Not Present	rs536413670
	SLC26A4	c.1790T>C p.Leu(597)Ser	NM_000441	Heterozygous	0.8256	0.6305	rs55638457
	TJP2	c.143C>T p.(Thr48Ile)	NM_001170416	Heterozygous	Not Present	Not Present	Not Present
P6 II-1	*CDH23*	c.509G>A p.(Gly170Asp)	NM_022124	Heterozygous	0.00002	Not Present	rs776354402
	CDH23	c.5737G>A p.(Val1913Ile)	NM_022124	Heterozygous	0.0008	Not Present	rs368828743
	DFNB31	c.668G>A p.(Arg223His)	NM_001173425	Heterozygous	0.0067	0.0923	rs146273185
	GJB2	c.341A>G p.(Glu114Gly)	NM_004004	Heterozygous	0.0146	0.0615	rs2274083
	GPSM2	c.1559_1561delCAA p.(Thr523Del)	NM_013296	Heterozygous	0.0015	Not Present	rs199964596
	OTOA	c.1381A>C p.(Thr461Pro)	NM_170664	Heterozygous	Not Present	Not Present	rs464696
	OTOA	c.1387G>T p.(Glu463Ter)	NM_170664	Heterozygous	Not Present	Not Present	rs200988634
	OTOA	c.92-11C>A -	NM_144672	Homozygous	0.0120	0.0385	rs117553471
	OTOG	c.2026T>C p.Ser676Pro	NM_001292063	Heterozygous	Not Present	Not Present	rs564978061
	OTOG	c.3674G>A p.(Arg1225His)	NM_001292063	Heterozygous	0.0048	Not Present	rs116947228
P8 II-1	*BDP1*	c.4786G>A p.(Glu1596Lys)	NM_018429	Heterozygous	0.000009	Not Present	rs750411430
	CDH23	c.1525C>A p.(Pro509Thr)	NM_052836	Heterozygous	0.0042	0.4808	rs41281304
	DIAPH3	c.1733C>T p.(Pro578Leu)	NM_001258369	Heterozygous	0.0037	0.0495	rs76366906
	GPR98	c.5525-7C>T -	NM_032119	Heterozygous	0.0053	0.4962	rs141528121
	GPSM2	c.57-10A>G -	NM_013296	Heterozygous	0.0001	0.0231	rs184863735
	OTOF	c.4403T>C p.(Val1468Ala)	NM_001287489	Heterozygous	Not Present	Not Present	rs186311765
	SLC26A5	c.609A>G p.(Ile203Met)	NM_198999	Heterozygous	0.000008	Not Present	rs771114775
	SLC4A11	c.2147+7A>G	NM_001174090	Heterozygous	Not Present	Not Present	rs753806855
	SLC4A11	c.2147+11T>G	NM_001174090	Heterozygous	Not Present	Not Present	rs766259194
	SLC4A11	c.2147+15T>G	NM_001174090	Heterozygous	Not Present	Not Present	rs750269299
	USH2A	c.7130A>G p.(Asn2377Ser)	NM_206933	Heterozygous	0.0038	0.3769	rs111033394

Table S2. List of variants in known hearing loss genes present in P5 II-1, P6 II-1 and P7 II-1. Variants previously seen in-house more than five times, and variants present on ExAC (http://exac.broadinstitute.org), EVS (http://evs.gs.washington.edu/EVS/) or dbSNP (http://www.ncbi.nlm.nih.gov/SNP/) with a frequency greater than 1% were removed. Minor allele frequencies are included where applicable

Appendix IV. Supplemental material for chapter 5, A homozygous variant in mitochondrial RNase P subunit PRORP is associated with Perrault syndrome characterized by hearing loss and primary ovarian insufficiency

Supplemental Data

A

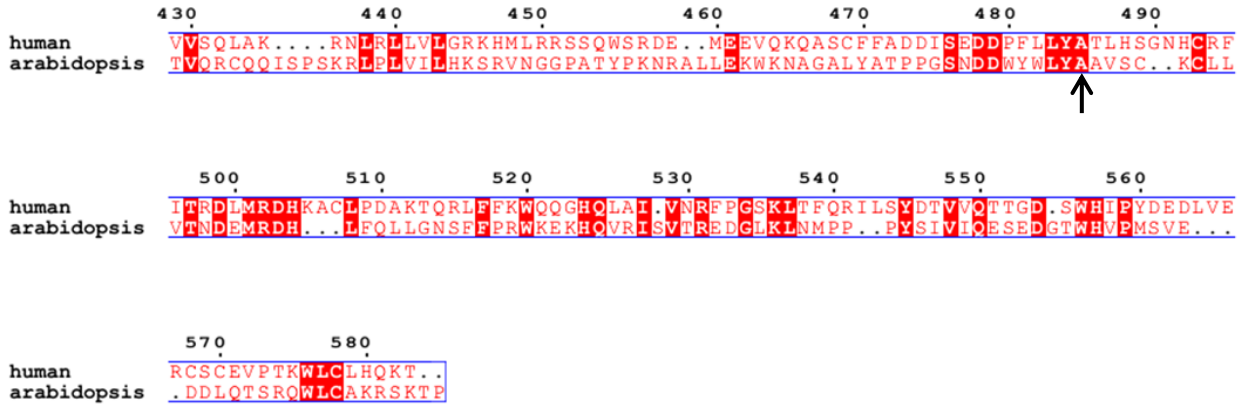

B

Supplemental Figure SIV.1 – Conservation of PRORP p.Ala485

A) The conservation of PRORP between *H. sapiens* and *A. thaliana*. The residue p.Ala485 (in humans) is indicated by the black arrow. **B**) The conservation of PRORP across multiple species. Residue Ala485 is shown in the red box. Numbering relates to the human protein (Genbank: NP_055487.2).

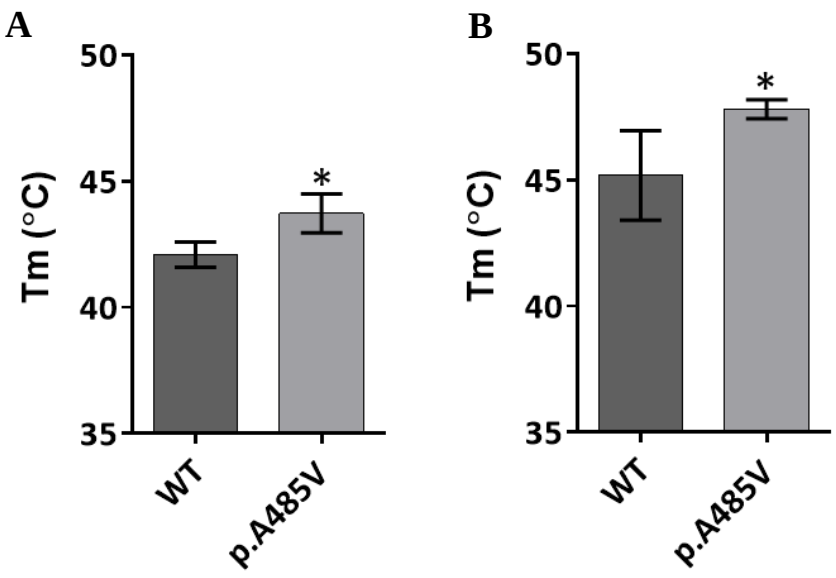

Supplemental Figure SIV.2 – The thermal stability of wild type PRORP and PRORP Ala485Val

The thermal stability of wildtype PRORP and PRORP p.A485V were compared using differential scanning fluorimetry (DSF). Both proteins were applied in the standard buffer used for DSF (graph A) and in a buffer identified to yield the most thermostable PRORP protein (graph B). The variant PRORP p.Ala485Val was more thermostable than the wild type PRORP under both conditions. $n = 3 - 4$. *= P<0.05.

A)

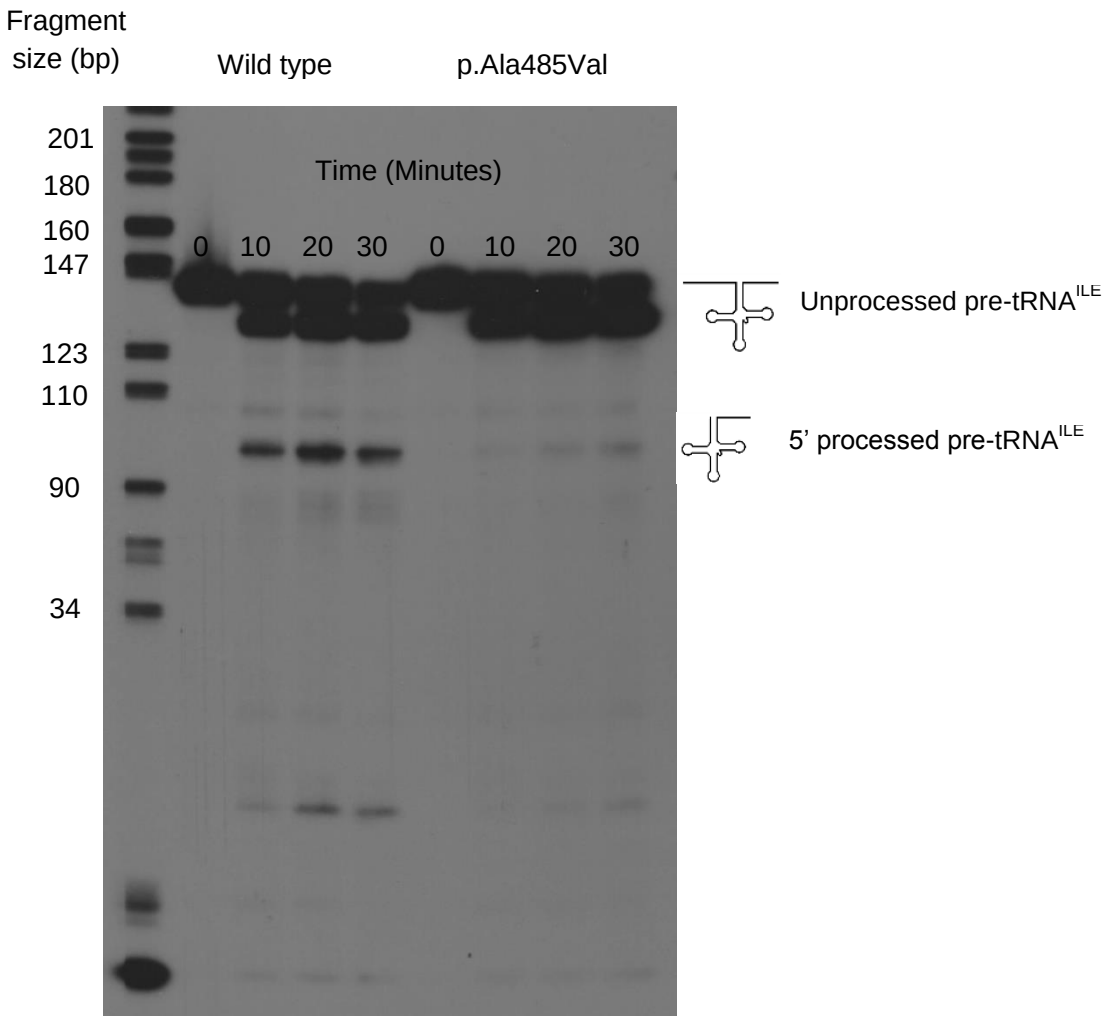

Supplemental Figure SIV.3 – *In vitro* mtRNase P processing assays with wild type and Ala485Val PRORP using pre-tRNA^{Ile}

Continued next page.

B)

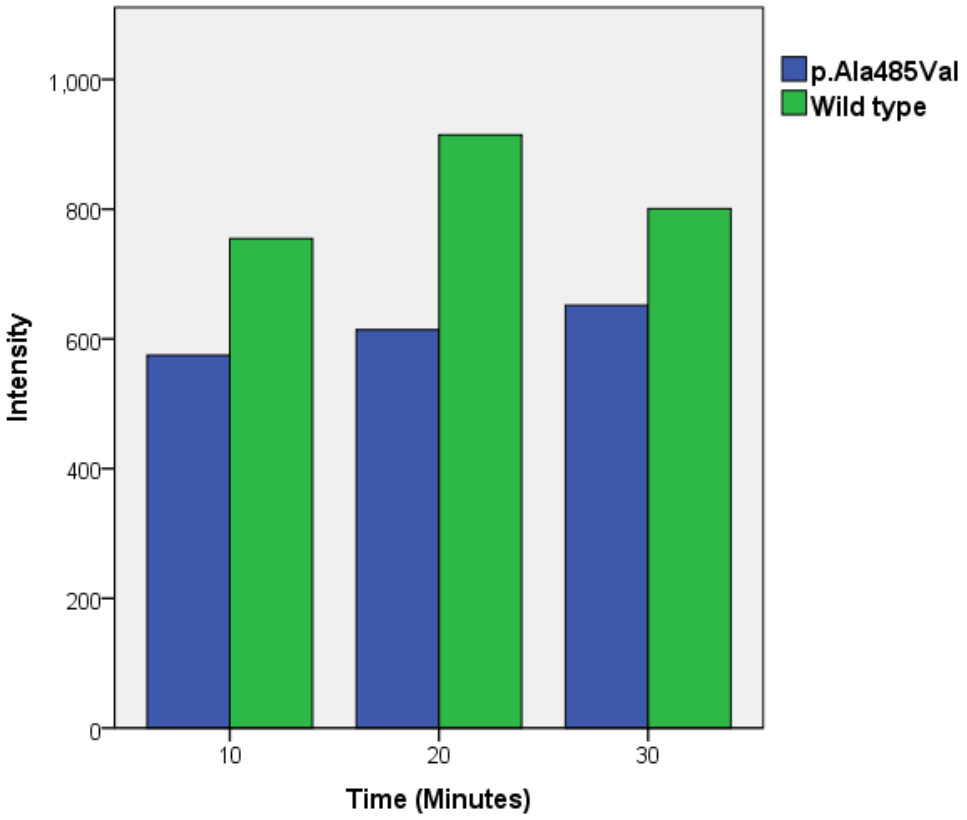

Supplemental Figure SIV.4. – *In vitro* mtRNase P processing assays with wild type and Ala485Val PRORP using pre-tRNA^{Ile}

A) Mitochondrial pre-tRNA^{Ile} was subjected to cleavage by recombinant reconstituted mtRNase P containing either wild type or p.Ala485Val PRORP. Aliquots were removed from the reactions and stopped at the time points indicated, and resolved by urea-PAGE.

B) Quantitative analysis of the 5' processed pre-tRNA^{ILE} bands from the single pre-tRNA^{Ile} processing experiment shown in (A). There was significant difference between the p.Ala485Val and wild type mtRNase P over three replicate experiments (N= 9 paired time points across 3 replicate experiments, evaluated using the Wilcoxon paired test, $P<0.01$).

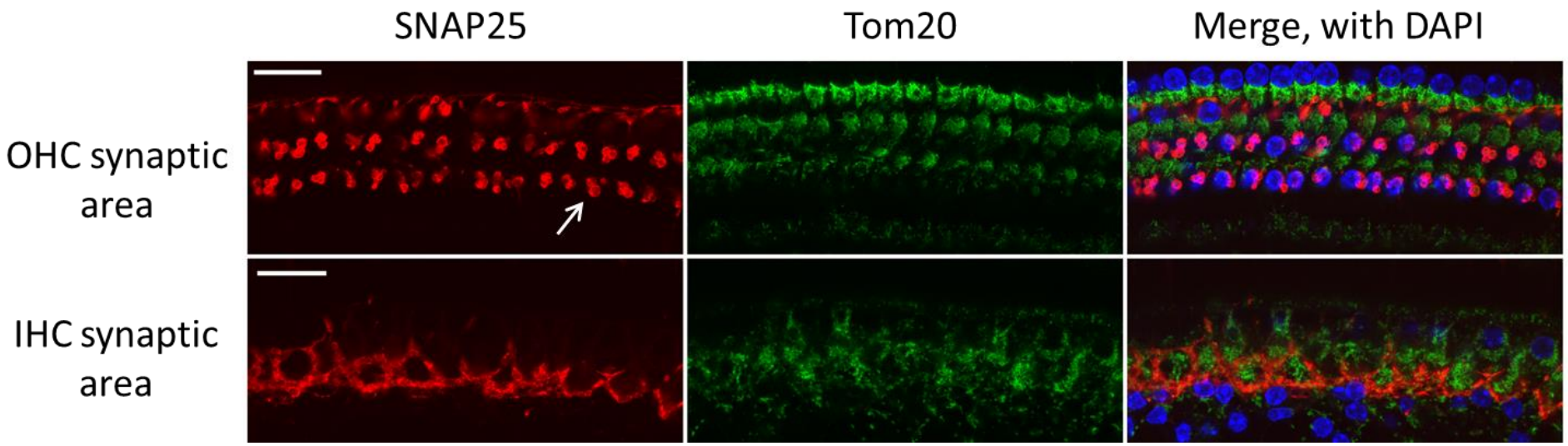

Supplemental Figure SIV.5 – The localisation of mitochondria in the mouse organ of Corti using Tom 20 antibody.

The organ of Corti from C57/BJ6 adult mice at postnatal day 24 (P24) was immunofluorescently stained using mouse monoclonal Tom20 antibody (mitochondrial marker, green) to visualize mitochondria, SNAP25 (presynaptic membrane marker, red) to visualise efferent synaptic buttons and some nerve fibres and. DAPI (nuclear double stranded DNA marker, blue) to visualize hair cell nuclei, The two panels represent optical sections at the OHC and IHC synaptic area of the same organ of Corti sample. The outer hair cell (OHC) synaptic area is shown in the top panels (the arrow points to one of the OHC efferent synaptic button) and the inner hair cell (IHC) synaptic area is shown in the bottom panels. The scale bar is 20µm.

Appendix V. Supplemental material for chapter 7, Variants in mitochondrial ribosomal protein DAP3 are causative of Perrault syndrome without a defect of mitochondrial translation

Variant	Transcript	Consequence	EXaC	dBSNP	Zygosity	SIFT	Polyphen2	EVS_TMAF	Inhouse Count (Het)	Inhouse Count (Hom)
DAP3 c.1061G>A p.(Cys354Tyr)	ENST00000535183	missense	N	N	hom	SIFT=deleterious(0)	PolyPhen=probably_damaging(0.946)	N	0/586	0/586
GPAT2 c.-6-13A>G -	ENST00000439254	splice_region:intron	0.0024/78	rs2579509	hom	-	-	N	1/586	0/586
SYN2 c.251A>G p.(His84Arg)	ENST00000432424	missense	N	rs71624922	hom	SIFT=deleterious(0)	PolyPhen=unknown(0)	N	0/586	0/586
NADK c.725A>G p.(Lys242Arg)	ENST00000344463	missense	N	N	het	SIFT=tolerated(0.52)	PolyPhen=benign(0)	N	0/586	0/586
NADK c.724A>G p.(Lys242Glu)	ENST00000344463	missense	8.56E-05	N	het	SIFT=tolerated(1)	PolyPhen=benign(0)	N	0/586	0/586
NADK c.716C>G p.(Ala239Gly)	ENST00000344463	missense	N	N	het	SIFT=tolerated(0.54)	PolyPhen=benign(0)	N	0/586	0/586
MAP4 c.322A>G p.(Ile108Val)	ENST00000441748	missense	0.000626	rs35736893	het	SIFT=tolerated(0.06)	PolyPhen=probably_damaging(0.995)	C=0.1538	0/586	0/586
MAP4 c.1895G>A p.(Arg632Gln)	ENST00000383736	missense	N	N	het	SIFT=tolerated(0.11)	PolyPhen=probably_damaging(0.998)	T=0.0077	0/586	0/586
PRR23A c.743A>C p.(His248Pro)	ENST00000383163	missense	N	N	het	SIFT=tolerated(0.14)	PolyPhen=unknown(0)	N	1/586	0/586
PRR23A c.737A>C p.(His246Pro)	ENST00000383163	missense	N	N	het	SIFT=tolerated(0.27)	PolyPhen=unknown(0)	N	0/586	0/586
GRID2IP c.2263A>C p.(Ser755Arg)	ENST00000457091	missense	N	N	het	SIFT=deleterious(0)	PolyPhen=benign(0.121)	N	0/586	0/586
GRID2IP c.2261T>C p.(Leu754Pro)	ENST00000457091	missense	N	N	het	SIFT=tolerated(0.12)	PolyPhen=probably_damaging(0.982)	N	0/586	0/586
PABPC1 c.833C>A p.(Phe278Leu)	ENST00000519100	missense	N	N	het	SIFT=tolerated(0.07)	PolyPhen=benign(0.002)	N	0/586	0/586
PABPC1 c.829A>T p.(Tyr277Phe)	ENST00000519100	missense	0.005886	rs146200489	het	SIFT=tolerated(0.16)	PolyPhen=benign(0.014)	N	1/586	0/586
ADAMTSL1 c.1177G>A p.(Gly393Arg)	ENST00000276935	missense	5.93E-05	rs199787607	het	SIFT=deleterious(0)	PolyPhen=probably_damaging(0.992)	A=0.0154	0/586	0/586
ADAMTSL1 c.2770G>A p.(Val924Ile)	ENST00000380548	missense	0.0003736	rs199730614	het	SIFT=tolerated(0.17)	PolyPhen=benign(0.013)	A=0.103	0/586	0/586
LDB3 c.1318T>C p.(Ser440Pro)	ENST00000361373	missense	N	N	het	SIFT=deleterious(0.02)	PolyPhen=probably_damaging(0.957)	N	1/586	0/586

Supplemental Table SV.1. Filtered Variants from Exome data

Continued next page.

Variant	Transcript	Consequence	EXaC	dBSNP	Zygosity	SIFT	Polyphen2	EVS_TMAF	Inhouse Count (Het)	Inhouse Count (Hom)
LDB3 c.1324G>C p.(Ala442Pro)	ENST00000361373	missense	N	N	het	SIFT=deleterious(0.03)	PolyPhen=possibly_damaging(0.898)	N	0/586	0/586
EP400 c.92A>C p.(His31Pro)	ENST00000542457	missense	N	N	het	SIFT=deleterious(0)	PolyPhen=possibly_damaging(0.615)	N	0/586	0/586
EP400 c.98A>C p.(Asn33Thr)	ENST00000542457	missense	N	N	het	SIFT=deleterious(0)	PolyPhen=possibly_damaging(0.442)	N	1/586	0/586
EP400 c.109T>C p.(Ser37Pro)	ENST00000542457	missense	N	N	het	SIFT=deleterious(0)	PolyPhen=probably_damaging(0.998)	N	0/586	0/586
PTPN21 c.1967C>T p.(Thr656Ile)	ENST00000556564	missense	N	N	het	SIFT=deleterious(0.01)	PolyPhen=benign(0.349)	N	0/586	0/586
PTPN21 c.1706A>C p.(Tyr569Ser)	ENST00000556564	missense		N	het	SIFT=deleterious(0)	PolyPhen=probably_damaging(0.999)	N	0/586	0/586
RTL1 c.3836G>C p.(Arg1279Pro)	ENST00000534062	missense	N	N	het	SIFT=deleterious(0.02)	PolyPhen=benign(0.143)	N	0/586	0/586
RTL1 c.3827A>C p.(His1276Pro)	ENST00000534062	missense	N	N	het	SIFT=tolerated(0.21)	PolyPhen=benign(0.006)	N	0/586	0/586
MYO5A c.2950C>T p.(Arg984Trp)	ENST00000553916	missense	1.66E-05	N	het	SIFT=deleterious(0)	PolyPhen=benign(0.363)	A=0.0084	0/586	0/586
MYO5A c.187C>T p.(Arg63Ter)	ENST00000553916	stop_gained	N	N	het	-	-	N	0/586	0/586
CACNA1H c.70-10G>C -	ENST00000562079	splice_region:intron	N	N	het	-	-	A=0.0085	1/586	0/586
CACNA1H c.70-6A>C -	ENST00000562079	splice_region:intron	N	N	het	-	-	N	0/586	0/586
NUDT16L1 c.592C>G p.(Arg198Gly)	ENST00000405142	missense	N	N	het	SIFT=tolerated(0.35)	PolyPhen=unknown(0)	N	0/586	0/586
NUDT16L1 c.598T>G p.(Trp200Gly)	ENST00000405142	missense	N	N	het	SIFT=deleterious(0)	PolyPhen=unknown(0)	N	0/586	0/586

Supplemental Table SV.1. Filtered Variants from Exome data

Continued next page.

Variant	Transcript	Consequence	EXaC	dBSNP	Zygosity	SIFT	Polyphen2	EVS_TMAF	Inhouse Count (Het)	Inhouse Count (Hom)
CDC27 c.1864T>A p.(Cys622Ser)	ENST00000527547	missense	N	rs78525224	het	SIFT=tolerated(0.46)	PolyPhen=benign(0.024)	N	1/586	0/586
CDC27 c.*363+2T>G -	ENST00000570818	splice_donor:NMD_transcript	N	N	het	-	-	N	0/586	0/586
CDC27 c.*363+1G>T -	ENST00000570818	splice_donor:NMD_transcript	N	N	het	-	-	N	0/586	0/586
COIL c.198G>C p.(Leu66Phe)	ENST00000240316	missense	N	N	het	SIFT=deleterious(0)	PolyPhen=probably_damaging(0.996)	N	0/586	0/586
COIL c.185A>G p.(Glu62Gly)	ENST00000240316	missense	N	N	het	SIFT=deleterious(0.01)	PolyPhen=possibly_damaging(0.689)	N	0/586	0/586
TSHZ1 c.334A>C p.(Thr112Pro)	ENST00000560918	missense	N	N	het	-	-	N	0/586	0/586
TSHZ1 c.340A>C p.(Thr114Pro)	ENST00000560918	missense	N	N	het	-	-	N	0/586	0/586
MYO9B c.5258-13A>C -	ENST00000397274	splice_region:intron	N	N	het	-	-	N	0/586	0/586
MYO9B c.5258-9A>C -	ENST00000397274	splice_region:intron	N	N	het	-	-	N	0/586	0/586
ANO8 c.1797G>C p.(Glu599Asp)	ENST00000159087	missense	0.000792	rs113297737	het	SIFT=tolerated(0.2)	PolyPhen=unknown(0)	G=0.1455	0/586	0/586
ANO8 c.217+13G>C -	ENST00000159087	splice_region:intron	N	N	het	-	-	N	0/586	0/586
SCAF1 c.646G>C p.(Ala216Pro)	ENST00000360565	missense	N	N	het	-	PolyPhen=unknown(0)	N	0/586	0/586
SCAF1 c.655G>C p.(Ala219Pro)	ENST00000360565	missense	N	N	het	-	PolyPhen=unknown(0)	N	0/586	0/586
IL4I1 c.773+15T>G -	ENST00000391826	splice_region:intron	0.008794	rs62126284	het	-	-	N	0/586	0/586
IL4I1 c.773+14C>G -	ENST00000391826	splice_region:intron	N	N	het	-	-	N	0/586	0/586
IL4I1 c.773+9C>G -	ENST00000391826	splice_region:intron	N	N	het	-	-	N	0/586	0/586

Supplemental Table SV.1. Filtered Variants from Exome data. Continued next page.

Variant	Transcript	Consequence	EXaC	dBSNP	Zygosity	SIFT	Polyphen2	EVS_TM AF	Inhouse Count (Het)	Inhouse Count (Hom)
KIR2DL1 c.229C>A p.(His77Asn)	ENST00000291633	missense	1.698E-05	rs141116605	het	SIFT=deleterious(0)	PolyPhen=benign(0.135)	N	0/586	0/586
KIR2DL1 c.230A>T p.(His77Leu)	ENST00000291633	missense	1.698E-05	rs150190837	het	SIFT=deleterious(0)	PolyPhen=benign(0.018)	G=0.0157	0/586	0/586
KIR2DL1 c.895+11C>T -	ENST00000291633	splice_region:intron	N	N	het	-	-	N	1/586	0/586
SH3BP1 c.60-11A>C -	ENST00000442465	splice_region:intron	N	N	het	-	-	N	0/586	0/586
SH3BP1 c.60-9T>C -	ENST00000442465	splice_region:intron	N	N	het	-	-	N	1/586	0/586
SH3BP1 c.1852A>C p.(Thr618Pro)	ENST00000357436	missense	N	N	het	SIFT=tolerated(0.16)	PolyPhen=unknown(0)	N	0/586	0/586
PANX2 c.1486G>C p.(Ala496Pro)	ENST00000395842	missense	N	N	het	SIFT=tolerated(0.25)	PolyPhen=benign(0)	N	0/586	0/586
PANX2 c.1498G>C p.(Ala500Pro)	ENST00000395842	missense	N	N	het	SIFT=tolerated(0.3)	PolyPhen=benign(0)	N	0/586	0/586
PANX2 c.1510G>C p.(Ala504Pro)	ENST00000395842	missense	N	N	het	SIFT=deleterious(0.03)	PolyPhen=benign(0.066)	N	0/586	0/586

Supplemental Table SV.1. Filtered Variants from Exome data

The variants from exome data of the patient with Perrault syndrome due to variants in *DAP3*. Filtered as detailed in section 7.4.2.

List of variable genes excluded from exome data of the patient with Perrault syndrome due to variants in *DAP3*

The following variants were excluded as candidate Perrault syndrome genes in Chapter 7 as they are either genes known to be highly variable or they had more than 5 rare variants in the exome data;

ENSG00000198502;HLA-DRB5

ENSG00000196126;HLA-DRB1

ENSG00000196735;HLA-DQA1

ENSG00000186715;MST1P9

ENSG00000227124;ZNF717

ENSG00000204525;HLA-C

ENSG00000234745;HLA-B

ENSG00000174450;GOLGA6L2

ENSG00000256642;LINC00273

ENSG00000134504;KCTD1

Sequence for DAP3 deletion fusion product

TAGAATGATATTTTGGGAAAAAGCACTCCTTTTCCTAAGGACTGCGACTCGGTGAACAGAAAGGA
GGCTATGCGGTGTGGCCAGCCAACTCAAGGAGGACGAAGCAACCTTTGCCTCTAAACTGCCTGG
AACTAAATGTCGATTTTTCTGACCCCTCCCAGGGAGTGCTGAGTAGTGATGGTGTCTGGAGGGTC
AAATCCATTCCCAATGGCAAAGGTGAGACTTCTCCAGATACTGATGGATGGGGGCTTGGGTAGA
GCAGAAACATGGAGAAAGGTACATTTCCTCTGCTTGTCTTCAGGTTCCTCACCACTCCCCACCGCT
ACAACTCCAAAACCACTTATCCCTACAGAGGCCAGCATCAGGGTCTGGTCAGACTTCCTCAGAGT
CCATCTCCATCCCCGGAGCATCTGTATGATTCAGAAGTACAACCACGATGGGTATGGGGACCCCA
GAGGCTTTGAGGCAAGAAACATGGGTCCCCACCAATGCAGGATGAGGCTCTTGAGGCCATCTTC
CCTGCCCTTCCCCAGGACAAGAGGCTGAGGAGTTGAGGGAAGAGATGTAAGTCTTGGATCGTGT
TTACTTGTGGCAGGGAAGCAGGTCGGCTGGAGGCTTTTGGCCAAGGGGAAAGTGTCCTAAAGGA
ACCCAAGTACCAGGAAGAGCTGGAGGACAGGCTGCATTTCTACGTGGAGGAATGTGACTACTTG
CAGGTAGTGGCGTGGCAATGTGCACTCCAGGGTGGAAGCTCTTCTCATCCTGCTAACTATCTTTC
GTCACTCAC

The underlined sequence of 478 bp, identical in both copies of the segmental duplication, is where recombination occurred. The highlighted bases are the last unique bases at the distal and proximal segmental duplication respectively.

Appendix VI: Copyright agreements

A copyright agreement was not required for Chapter 4.

Copyright agreement for figure 2.1.

ELSEVIER LICENSE
TERMS AND CONDITIONS

Sep 19, 2017

This Agreement between Miss. Leigh Demain ("You") and Elsevier ("Elsevier") consists of your license details and the terms and conditions provided by Elsevier and Copyright Clearance Center.

License Number	4192660223465
License date	Sep 19, 2017
Licensed Content Publisher	Elsevier
Licensed Content Publication	Brain Research Bulletin
Licensed Content Title	Structure and innervation of the cochlea
Licensed Content Author	Yehoash Raphael,Richard A Altschuler
Licensed Content Date	Jun 15, 2003
Licensed Content Volume	60
Licensed Content Issue	5-6
Licensed Content Pages	26
Start Page	397
End Page	422
Type of Use	reuse in a thesis/dissertation
Portion	figures/tables/illustrations
Number of figures/tables/illustrations	1
Format	both print and electronic
Are you the author of this Elsevier article?	No
Will you be translating?	No
Original figure numbers	Fig. 1.
Title of your thesis/dissertation	Identifying genetic variants implicated in Perrault syndrome for improved hearing loss diagnosis and therapeutics
Expected completion date	Sep 2017
Estimated size (number of pages)	300
Requestor Location	Miss. Leigh Demain University of Manchester Oxford Road Manchester, M13 9PL United Kingdom Attn: Miss. Leigh Demain
Publisher Tax ID	GB 494 6272 12

Copyright agreement for Chapter 3

JOHN WILEY AND SONS LICENSE TERMS AND CONDITIONS

Aug 30, 2017

This Agreement between Miss. Leigh Demain ("You") and John Wiley and Sons ("John Wiley and Sons") consists of your license details and the terms and conditions provided by John Wiley and Sons and Copyright Clearance Center.

License Number	4178890737873
License date	Aug 30, 2017
Licensed Content Publisher	John Wiley and Sons
Licensed Content Publication	Clinical Genetics
Licensed Content Title	Expanding the genotypic spectrum of Perrault syndrome
Licensed Content Author	L.A.M. Demain,J.E. Urquhart,J. O'Sullivan,S.G. Williams,S.S. Bhaskar,E.M. Jenkinson,C.M. Lourenco,A. Heiberg,S.H. Pearce,S.A. Shalev,W.W. Yue,S. Mackinnon,K.J. Munro,R. Newbury-Ecob,K. Becker,M.J. Kim,R.T. O' Keefe,W.G. Newman
Licensed Content Date	Apr 1, 2016
Licensed Content Pages	11
Type of use	Dissertation/Thesis
Requestor type	Author of this Wiley article
Format	Print and electronic
Portion	Full article
Will you be translating?	No
Order reference number	GenotypicSpectrumPS
Title of your thesis / dissertation	Identifying genetic variants implicated in Perrault syndrome for improved hearing loss diagnosis and therapeutics
Expected completion date	Sep 2017
Expected size (number of pages)	300
Requestor Location	Miss. Leigh Demain University of Manchester Oxford Road Manchester, M13 9PL United Kingdom Attn: Miss. Leigh Demain
Publisher Tax ID	EU826007151
Billing Type	Invoice
Billing Address	Miss. Leigh Demain University of Manchester Oxford Road Manchester, United Kingdom M13 9PL Attn: Miss. Leigh Demain
Total	0.00 GBP
Terms and Conditions	

30/08/2017